KU Leuven
Biomedical Sciences Group
Faculty of Medicine
Department of Neuroscience

KU LEUVEN
DOCTORAL SCHOOL
BIOMEDICAL SCIENCES

Brain-computer interfacing based on time-domain EEG response detection combined with beamforming

Benjamin Wittevrongel

Jury:
Promotor: prof. Marc Van Hulle
Chair: prof. Wim Vanduffel
prof. Luc Geurts
prof. Emmanuel Lesaffre
dr. Fabien Lotte
dr. Pieter Van Mierlo

Dissertation presented in
partial fulfilment of the
requirements for the degree of
Doctor in Biomedical sciences

October 2018

A WORD OF GRATITUDE

"What do you want to become when you grow up?" "Professor!", would be the unhesitating answer of my 8-year old self. Of course, at the time, this answer was inspired by professor Gobelijn, a character from a popular Belgian comic book series (*Jommeke*), who was blowing up his lab from time to time and who had a flying sphere for transportation. While growing up, I gradually realised that real-life science (unfortunately) does not perfectly match this view. However, my interest in science never faded away, and I consider myself lucky to have received the opportunity to pursue a PhD, during which I have experienced real science and have grown as a scientist.

Even though my name is displayed at the front of this work, it should be noted that this thesis is the result of a collaborative effort of numerous people who have either directly or indirectly supported me throughout the last four years, and without whom this work would not have been possible.

First of all, I would like to thank the internal jury members prof. Emmanuel Lesaffre, prof. Maarten De Vos and prof. Luc Geurts for guiding me and sharing their expertise and insights throughout my doctoral training. I would like to thank the external jury members, dr. Fabien Lotte and dr. Pieter Van Mierlo, for agreeing to be part of the examining committee and for reviewing this thesis. It has been an honor to make your acquaintance and to share my findings with you.

I thank my promotor, prof. Marc Van Hulle, for giving me the opportunity to pursue a PhD in his group. I followed his courses on neural computing and brain-computer interfacing during the last year of my masters program, and was immediately captivated by the field that combines both artificial intelligence (my major) and biomedical applications (my life-long interest). His help and support played a big part in why I was able to obtain a grant to pursue an academic career. I would also like to thank Irma Ravkic for her guidance and enthusiasm during my master thesis project and for encouraging me to pursue an academic career.

Next, I would like to thank my colleagues at KU Leuven's Computational Neuroscience group for sharing their knowledge and ideas, and our collaborators at UZ Gent, prof. Alfred Meurs, prof. Dirk Van Roost, prof. Paul Boon, prof. Miet De Letter, prof. Patrick Santens, Evelien Carrette, Leen De Taeye, Ine Dauwe, Stefanie Gadeyne, Kim De Keyser and Ellen Lanckmans for providing me with several opportunities to perform invasive recordings and explore new frontiers. Their input has helped me expand my interests and allowed me to grow as a researcher. Our collaborations pulled me out of my engineering-bubble, which is often blind for practical aspects, and introduced me to the fascinating world of clinical neuroscience and medicine. I profoundly

believe this view will augment the quality of the work I will be able to do throughout the rest of my career.

Thanks to my family for their continued support and for allowing me to pursue my dreams, even in times when it was unclear what those dreams were or when they seemed unachievable. Without them, I would not be where I am now and I will be eternally grateful.

Finally, I would like to thank my wonderful girlfriend for her continued support and comfort. She has been my rock during the ups and downs of the last four years. She encourages me to challenge myself, which has made me a better scientist and a better person.



Figure 0.1: Excerpt from Jommeke (no 229). "Just implant this thing on your forehead and connect some wires on the inside"

Thanks to Flickr user _DJ_ for providing the base image used to design the cover.

CONTENTS

1 INTRODUCTION 1
- 1.1 Assistive devices 1
- 1.2 Brain-computer Interfacing 2
  - 1.2.1 Visual BCI 4
  - 1.2.2 Recording from the brain 5
  - 1.2.3 Visual stimulation paradigms 7
  - 1.2.4 Alternative applications 11
- 1.3 Spatiotemporal Beamforming 12
- 1.4 Classifiers 13
  - 1.4.1 Support Vector Machines 13
  - 1.4.2 Canonical correlation analysis 14
- 1.5 Goals 14

2 FASTER P300 CLASSIFIER TRAINING USING SPATIOTEMPORAL BEAMFORMING 15
- 2.1 Introduction 16
- 2.2 Methods 17
  - 2.2.1 Subjects 17
  - 2.2.2 Experimental procedure 17
  - 2.2.3 Recording 18
  - 2.2.4 Processing 18
  - 2.2.5 Analysis 19
- 2.3 Results 23
  - 2.3.1 Individual Activation Patterns 23
  - 2.3.2 Population Activation Patterns 24
- 2.4 Discussion 28
- 2.5 Conclusion 33

3 FREQUENCY- AND PHASE ENCODED SSVEP USING SPATIOTEMPORAL BEAMFORMING 35
- 3.1 Introduction 36
- 3.2 Methods 37
  - 3.2.1 Subjects 37
  - 3.2.2 Interface 37
  - 3.2.3 Recording 38
  - 3.2.4 Processing 38
  - 3.2.5 Analysis 38
- 3.3 Results 43
  - 3.3.1 Activation Patterns 43

3.3.2 Classification 45
3.4 Discussion 46
3.4.1 Effect of combining frequency and phase encoding on SSVEP 46
3.4.2 Activation Patterns 48
3.4.3 Frequency resolution 50
3.5 Conclusion 50
4 CODE-MODULATED VISUAL EVOKED POTENTIALS USING FAST STIMULUS PRESENTATION 53
4.1 Introduction 54
4.2 Methods 55
4.2.1 Subjects 55
4.2.2 Experimental design 55
4.2.3 Recording 56
4.2.4 Preprocessing 56
4.2.5 Classification 57
4.2.6 Channel selection 60
4.2.7 Transition effect 61
4.2.8 Performance evaluation 61
4.2.9 Statistics 62
4.3 Results 62
4.4 Discussion 65
4.5 Conclusion 66
5 TRANSPARENT AND UNIFIED APPROACH TO SYNCHRONOUS VISUAL BCI 67
5.1 Introduction 68
5.2 Methods 70
5.2.1 Data acquisition and processing 70
5.2.2 Spatiotemporal beamforming 71
5.2.3 Beamformer construction and feature extraction 73
5.2.4 Target Identification 75
5.2.5 Performance estimation 75
5.2.6 Statistics 77
5.3 Results 77
5.4 Discussion 79
5.5 Conclusion 81
6 REPRESENTATION OF SSVEP IN HUMAN OCCIPITAL CORTEX 83
6.1 Introduction 84
6.2 Materials and Methods 85
6.2.1 Participants 85
6.2.2 Scalp-EEG and ECoG acquisition 85
6.2.3 Localization of ECoG electrodes 86
6.2.4 Experimental procedure 86

6.2.5 Pre-processing 87
6.2.6 Spectral Power and Phase Estimation 87
6.2.7 Time-Frequency Analysis 88
6.2.8 Statistics 89
6.3 Results 89
6.3.1 Spectral bands 90
6.3.2 Fundamental and harmonic frequencies 95
6.3.3 Peripheral targets 96
6.4 Discussion 99
6.4.1 Peripheral activations are consistent with retinotopic maps 100
6.4.2 SSVEP elicits localized activations in the alpha band 100
6.4.3 SSVEP stimulation elicits transient changes in theta band 101
6.4.4 Limitations of this study 102
6.4.5 Outlook 103
6.5 Conclusion 103
7 DECODING SSVEP FROM ELECTROCORTICOGRAPHY 105
7.1 Introduction 106
7.2 Methods 107
7.2.1 Participants 107
7.2.2 Experimental procedure 108
7.2.3 Scalp-EEG and ECoG acquisition 108
7.2.4 Localization of ECoG electrodes 109
7.2.5 Processing 109
7.2.6 Classifiers 110
7.2.7 Performance Evaluation 113
7.2.8 Statistical estimation of the patient's scalp-EEG performance 113
7.2.9 Electrode Selection 113
7.2.10 Statistics 114
7.3 Results 114
7.3.1 Single-electrode performance 114
7.3.2 Multi-electrode performance 118
7.4 Discussion 119
7.4.1 High-quality ECoG signals allow for accurate single-electrode SSVEP decoding 120
7.4.2 ECoG-based SSVEP decoding does not benefit from a multi-electrode approach 121
7.4.3 Comparison with other visual BCI paradigms 122
7.4.4 Practical considerations and future work 122
7.4.5 Limitations 123
7.5 Conclusion 123
8 GENERAL DISCUSSION 125

8.1 P300 125
8.2 SSVEP 125
8.3 cVEP 126
8.4 Limitations 127
8.5 Future of visual BCI 127

BIBLIOGRAPHY 130

9 ADDENDUM 163
9.1 Summary 163
9.2 Samenvatting 164
9.3 Acknowledgements 165
9.4 Personal contribution 165
9.5 Conflict of interest 165
9.6 Curriculum Vitae 166

ACRONYMS

ALS Amyotrophic Lateral Sclerosis

BA Brodmann Area

BCI Brain-Computer Interface

CCA Canonical Correlation Analysis

CHBF Chained Beamformer

CMS Common Mode Sense

CSP Common Spatial Pattern

CT Computed Tomography

CVEP code-modulated Visual Evoked Potential

ECOG Electrocorticography

EEG Electroencephalography

EMG Electromyography

EOG Electro-oculogram

ERP Event-Related Potential

ERS Event-Related Synchronisation

FBCCA Filterbank Canonical Correlation Analysis

FMRI Functional Magnetic Resonance Imaging

ITR Information Transfer Rate

LGN Lateral Geniculate Nucleus

LCD Liquid Crystal Display

LCMV Linearly-Constrained Minimum Variance

LDA Linear Discriminant Analysis

LIS Locked-In Syndrome

MEG Magnetoencephalography

NIRS Near-Infrared Spectroscopy

NN Nearest Neighbour

MS Multiple Sclerosis

MVEP motion-onset Visual Evoked Potential

PET Positron Emission Tomography

PSD Power Spectral Density

ROC Receiver Operating Characteristic

SNR Signal-to-Noise Ratio

SSVEP Steady-State Visual Evoked Potential

STBF Spatiotemporal Beamformer

SVM Support Vector Machine

VEP Visual Evoked Potential

1 INTRODUCTION

Communication is a crucial aspect of our daily activities as it allows us to share experiences, thoughts, wishes and desires. It enabled humans to evolve, learn and develop, and our mastery of verbal communication sets us apart from other socially interacting species although we often take it for granted. Gestures can replace to some extent verbal communication, and sign language is well-established among those devoid of speech facilities, but a conversation between two individuals that do not speak the same language can already be challenging. However, these are only moderate issues compared to those faced by individuals that have lost all speech and muscular control. In approximately 30% of cases of acute cerebrovascular disorder, also known as stroke, the patient is permanently disabled and about 1% of cases lead to Locked-In Syndrome (LIS), in which case the patient loses all muscular control although the cognitive abilities remain intact. They are "trapped" in their own body as it were. Besides stroke, also neurodegenerative diseases such as Amyotrophic Lateral Sclerosis (ALS) [198] or Multiple Sclerosis (MS) [87, 147] can lead to a decline in communication facilities and eventually to LIS. And certain brain trauma patients can suffer the same fate.

Given that the vast majority of these patients have relatively preserved cognitive abilities [260], and are thus fully aware of their disability, depression often co-occurs with these pathologies [167], and it affects also their caregivers as higher levels of depression and burden are reported as the disease progresses [96]. Providing these patients with an alternative communication channel that bypasses the affected ones could therefore not only increase their quality of life [278] but also decrease the burden on their caregivers.

1.1 ASSISTIVE DEVICES

Patients still capable of some form of muscular control can be served by a caregiver to communicate their intentions. Using vocalisation or with the help of a physical board with icons (figure 1.1), the caregiver can iterate over the options individually (i.e., actions, letters) and the patient can confirm the intended one by timely flexing the muscle (s)he has control over. In this manner, with the help of a caregiver, who recited the alphabet and the patient, by blinking with his left eye, French author Jean-Dominique Bauby was able to dictate his famous book *Le Scaphandre et le Papillon* (*The diving bell and the butterfly*), in which he described his life before and after the onset of locked-in syndrome (LIS) which was caused by a stroke. With the advent of computational power, continued miniaturization and algorithmic advancements, the

caregiver can be replaced by a display that shows these iterations over the options and a device that detects muscle reaction, e.g. using infrared or electromyography (EMG) [241], to record the intended selection. Note that the former approach was used by astrophysicist Stephen Hawking to interact with his speech computer.

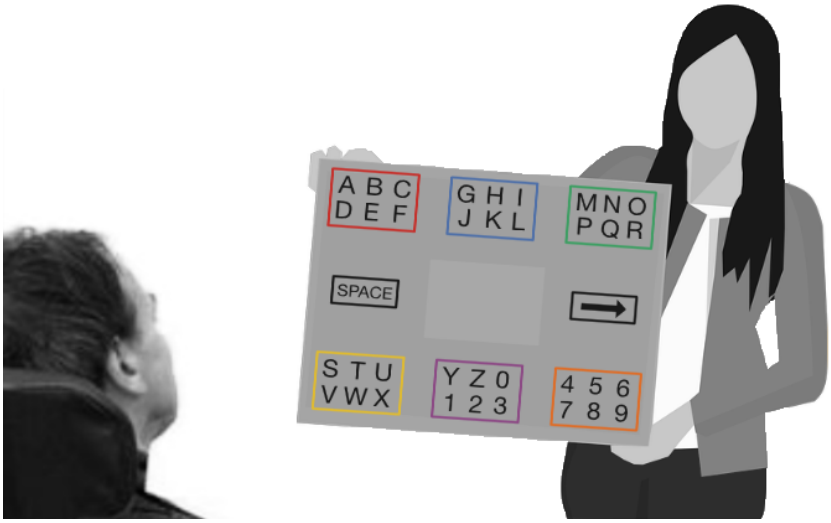

Figure 1.1: An example of a low-tech solution for assistive communication (E-Tran frame). A (typically transparent) frame with letters or icons is displayed to the patient. A caregiver iterates over the options by indicating them consecutively and visually inspects the patient for a signal (e.g., muscle contraction or blinking) that indicates that the intended box/letter/icon is reached. In this example, the characters are grouped into colored boxes, which reduces the number of options the caregiver should iterate over, thereby speeding up communication.

One promising assistive technology for automatic target selection is offered by eye-tracking devices: when the patient is fixating one of several targets on the screen (e.g., letter or action), an eye-tracker can track his/her gaze and a computer can interpret the intended selection, evidently assuming the patient is able to fixate. However, many neurodegenerative diseases result in nystagmus or another type of involuntary eye movements, impeding voluntary fixation and thus eye-tracking-based solutions. Furthermore, accurate eye-tracking devices are relatively expensive and require tailored setups.

1.2 BRAIN-COMPUTER INTERFACING

In contrast to aforementioned technologies, a brain-computer interface establishes a direct communication channel between the brain and an external device (machine or computer) without involving mechanical input devices (i.e., keyboard, mouse, joystick,

etc.) or muscular activity. Instead, brain signals are recorded and analysed for activity that provides information about the user's intentions.

Several paradigms exists to build a BCI, ranging from requiring very high to low mental demand from the user. One of the most demanding paradigms is based on voluntary modulation of certain brain activity. In this paradigm, the subject is required to increase his/her brain activity in a certain frequency band, which is monitored by an algorithm. Given that this is not a trivial or intuitive task, considerable subject training is needed. As the experimenter knows exactly which properties of the brain signal are modulated, little computational resources are required, and the BCI performance mainly depends on the proficiency of the subject [338, 339].

A more intuitive BCI paradigm is based on the detection of imagined movements. When performing or imagining a movement, characteristic changes in the mu (8-12 Hz) and beta (13-28 Hz) frequency bands are elicited [239]. As each limb is represented at a different brain location in accordance with the topography of the corresponding muscle group in the body (homunculus), when using precise brain recordings, one can in principle resolve individual limb movements. While this paradigm is raising great hopes to eventually achieve intuitive control over prosthetic limbs, currently, instead of continuous only discrete control can be achieved[1] as the extraction of limb trajectory information is still largely beyond reach. In a similar vein, also the decoding of performed and imagined speech has been attempted [114, 215, 235] in an effort to obtain intuitive language-based communication.

The two paradigms mentioned above are asynchronous paradigms: the subject decides when to engage in the paradigm. Hence, the decoding algorithm has no information about whether and when relevant brain activity will be present in the recordings, and the issue becomes considerably challenging as many irrelevant brain processes also generate (possibly similar) brain activities (e.g., a change in alpha band power due to fatigue), demoting the possibility to single out the activity trace of interest. With synchronous BCI paradigms, a stereotypical brain potential in response to well-timed sensory stimulus is elicited As this does not require the subject to actively modulate brain activity, the term *evoked potential* is adopted to characterize this response. Most studies, including the ones described in the current thesis, focus on visual stimulation since the visual sense is the primary source of information for humans [76]. However, also auditory [224], tactile [322], olfactory [191] and gustatory [125] stimulation have been shown to elicit synchronous brain responses, and can therefore also be used as a basis for brain-computer interfacing, albeit that the latter two have hardly even been investigated, likely due to difficulties with stimulus timing and the requirement of unconventional stimulation equipment.

1 For example, imagining moving the left hand selects the first option, while the imagining of the right hand movement selects the second option

1.2.1 *Visual BCI*

Figure 1.2 shows a conceptual representation of a visual BCI, and displays the steps involved in building such a system. Next, we will discuss each step separately.

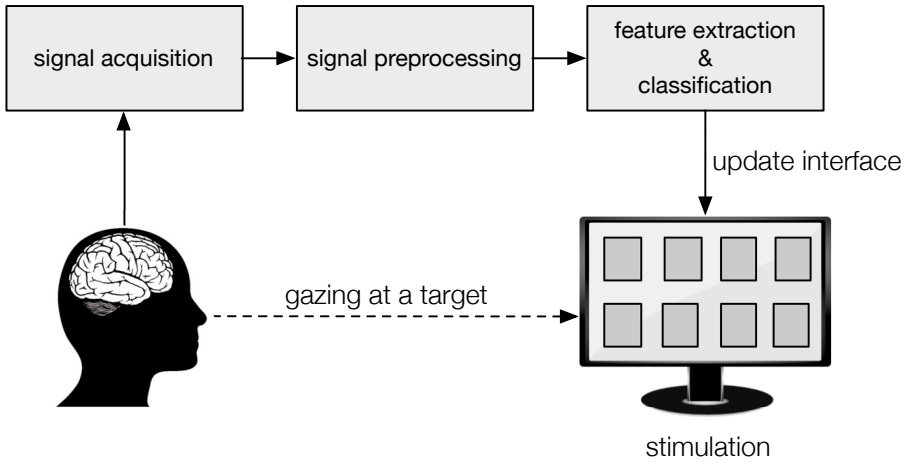

Figure 1.2: Graphical representation of a visual BCI. The subject gazes at the target on a display('interface'), to which the desired action is associated, while his/her brain activity is being recorded. Each target is stimulated visually, in a specific manner, which leaves a trace in the recorded brain activity. From the preprocessed recordings, signal features are extracted and the classification algorithm predicts the intended target, after which the display is updated accordingly or the corresponding action performed (visual feedback).

INTERFACE In a visual BCI, the subject is typically presented with a number of selectable targets (displayed on a computer monitor or with light sources), each of which represents a certain action. The targets are visually stimulated, either in a one-by-one (serial) or simultaneous (parallel) way, and the subject is typically asked to gaze at the target (s)he wants to select. While this task requires voluntary control over eye movements, visual BCIs have also been shown successful in a gaze-independent setup [6], and can thus also serve those that are not able to control their gaze.

SIGNAL ACQUISITION While the subject is gazing at the intended target, his/her brain activity is recorded from the scalp (non-invasively) using electroencephalography (EEG), from the cortical surface using electrocorticography (ECoG), from the superficial cortical tissue using micro-electrode arrays, or from subcortical structures using depth electrodes. Each of the recording modalities has its specific properties, advantages and disadvantages [48].

SIGNAL PREPROCESSING In order to isolate the signal-of-interest, the first step of the analysis is data pre-processing. Typically, this includes removal of physiological- (e.g., ocular movements, heart beats, pulmonary activity, etc) and recording (e.g., power line interference, electrodes with bad contact) artifacts, (temporal) filtering within a specific frequency band and cutting the signal into epochs in sync with the stimulus onset. Often epochs are further downsampled to reduce the dimensionality of the subsequent features and classifier.

FEATURE EXTRACTION AND CLASSIFICATION While it is possible to directly use the pre-processed epochs for classification, it is often beneficial to first extract relevant features.

CLOSING THE LOOP Based on the target predicted by the classifier, the action is executed by the external device, thereby allowing the subject to interact and possibly making additional corrections.

1.2.2 *Recording from the brain*

Neurons in the brain process information from the senses and transfer information between each other using electrical potentials. Measuring these potentials provides insight into the functioning of the brain, and can be achieved in different ways.

Single cell recordings capture action potentials from single neurons and is achieved by inserting one or more electrodes (multi-electrode array) into the cortical tissue in close proximity to the neuron(s) of interest (figure 1.3). While this approach results in the most accurate measurements of single-neuron activity, the procedure inherently damages the brain tissue leading to the buildup of scar-tissue [271], eventually affecting the signal quality and limiting the recording window [279]. Despite these disadvantages, BCI based on multi-electrode arrays, such as the Utah array, have been successful in patients suffering from severe motor disabilities [64, 118]. Similarly, using depth electrodes, it is possible to measure activity of deeper brain areas, including the limbic system (i.e., hippocampus, amygdala) and other subcortical structures (e.g., subthalamic nucleus). Typically, a strip of 8 to 10 electrodes is inserted (often perpendicularly) into the cortical surface. Depth electrodes are routinely being used for clinical purposes, such as long-term deep brain stimulation as treatment for several neurological conditions [237] (e.g., to alleviate the tremor of drug-resistant Parkinson's disease [27]) or for the localisation of epileptic foci [24]. While many studies investigating the fundamental functions of deeper brain structures have benefited from this type of recording, very little BCI studies have considered the use of such recordings for communication or control [160, 280, 348].

A less invasive recording approach is given by electrocorticography (ECoG), in which electrodes are placed on the cortical tissue, without penetrating the brain's surface (figure 1.3). Even though the subdural implantation of electrodes requires surgical

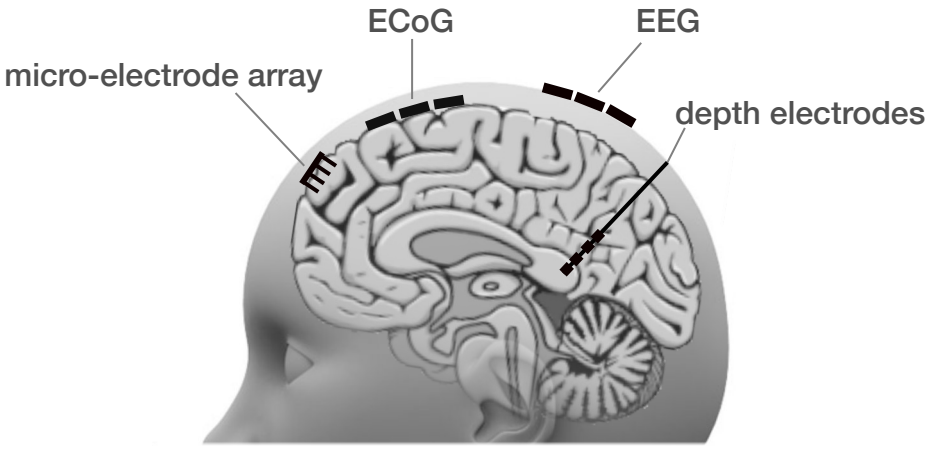

Figure 1.3: Graphical representation of the different recording modalities that measure direct electrical activations in the brain.

intervention (craniotomy or burr holes, depending on the size of the electrode grid), ECoG does not damage the brain's tissue, and the signal quality has shown to be stable for prolonged recording sessions [53, 326], with reports up to 262 days [312], proving its feasibility for prolonged invasive BCI use. ECoG has a good spatial resolution (< 5 mm^2 [48]) and typically covers a larger part of the cortex compared to micro-electrode arrays. ECoG is not able to capture individual neuronal activity, but rather reflects synchronized activations of a small population of neurons (i.e., a few thousand) directly below each electrode of the implanted grid or strip. At the time of writing, ECoG is almost exclusively implanted for medical reasons, most prominently in patients with intractable epilepsy, for whom the implanted grid is used to localize the epileptic foci and to perform functional mapping of eloquent cortex prior to resective surgery. These clinical cases provide researchers with the opportunity to study BCI based on cortical activity [43, 102, 127, 270, 325, 358]. Note that, as with ECoG one can only record from the cortical surface, electrical activity from subcortical areas is not readily accessible.

The most widespread brain recording technique for BCI purposes is based on electroencephalography (EEG), recorded from the scalp (figure 1.3). As EEG is non-invasive, it is considered the most suitable for BCI applications aimed at a broader population, beyond the clinical one. Indeed, invasive methods, which require surgical intervention, can only be considered for patients suffering from severe communication disabilities. While EEG has the benefit of being relatively cheap and easy to set up, the cortical signal has to travel through several organic layers, including the cerebrospinal fluid, dura mater, skull, skin and hair, all of which disperse and attenuate the cortical activations over a larger scalp area (≥ 10 cm^2 [48]). This process, known as volume conduction, considerably reduces the spatial resolution and signal-to-noise ratio (SNR) of EEG com-

pared to intracranial recordings. Despite these disadvantages, EEG is the most widely adopted recording modality for visual BCI studies, and several advanced algorithms have been developed that successfully counter the inferior SNR.

As the brain's inner working is based on electrical potentials, it is most obvious to measure electrical activity. However, other techniques, not based on direct measurements of electrical activity, are also available. For instance, magnetoencephalography (MEG) measures fluctuations in the magnetic fields generated by electrical potentials. As the magnetic field is perpendicular to the electric current, MEG mainly detects activity in the sulci, and can be considered complementary to EEG, as the latter is more sensitive for activity originating from the gyri. The temporal resolution of MEG is similar to EEG, but as magnetic fields do not suffer from volume conduction, its spatial resolution is higher. However, as current MEG sensors are extremely sensitive, MEG experiments typically are performed in a magnetically shielded room, which renders the adoption of present-day MEG devices infeasible for use in a real-world environment. Active research is being done to improve the usability of MEG systems, and recently a mobile version has been described, albeit it still requires the experiments to be performed in a magnetically shielded room [35]. Near-infrared spectroscopy (NIRS) gauges the increase in blood flow to activated brain areas. As oxygenated and deoxygenated blood have different reflective properties, NIRS measures the amount of reflection of a near-infrared light beam that non-invasively penetrates the skin and skull. The spatial resolution of NIRS is similar to EEG, but because the hemodynamic system does not instantaneously reflect current brain activity (i.e., the blood flow to an active brain area peaks several seconds after the onset of a stimulus [71]), the temporal resolution of NIRS is relatively low, making this recording modality suboptimal for brain-computer interfacing.

1.2.3 *Visual stimulation paradigms*

One of the main prerequisites for a visual BCI is a consistent brain response to a visual stimulus. Over the years, several stimulation paradigms have been developed. In the next section, we will introduce and discuss the three most widely adopted paradigms.

1.2.3.1 *P300 Event-Related Potential*

An Event-Related Potential (ERP) is a stereotypical amplitude deflection in response to and in synchrony with an external stimulus. While the signal-to-noise ratio is low, averaging responses over multiple stimulus repetitions reveals the individual ERP components by averaging out uncorrelated noise and responses that are not time-locked to the stimulation. ERP components are identified by the polarity and peak latency of the amplitude deflection. For example, the P300 component is a positive EEG deflection which reaches its peak around 300 ms after the stimulus onset, while the N400 com-

ponent is characterised by a negative deflection peaking around 400 ms post-stimulus onset [194].

ERPs have been used to study many brain processes in both healthy individuals and patients, including visual processing (P100, N170) [116], attention (P300) [104] and language processing (N400 and P600) [150, 151]. Among the ERP components described in the literature, the relatively strong P300 component was the first to be utilized in the context of a BCI [84]. The P300 ERP is typically elicited by an infrequently presented stimulus-of-interest, and can be characterized as a cognitive ERP as it can only be elicited when the subject is paying attention to the stimulus (in contrast to sensory potentials which are elicited regardless of the subject's attention). On the scalp, the P300 can most strongly be measured over the centro-parietal area (Figure 1.4), albeit that the scalp distribution can vary across subjects [82] and has been shown to experience an anterior shift with increasing age [89, 258, 328].

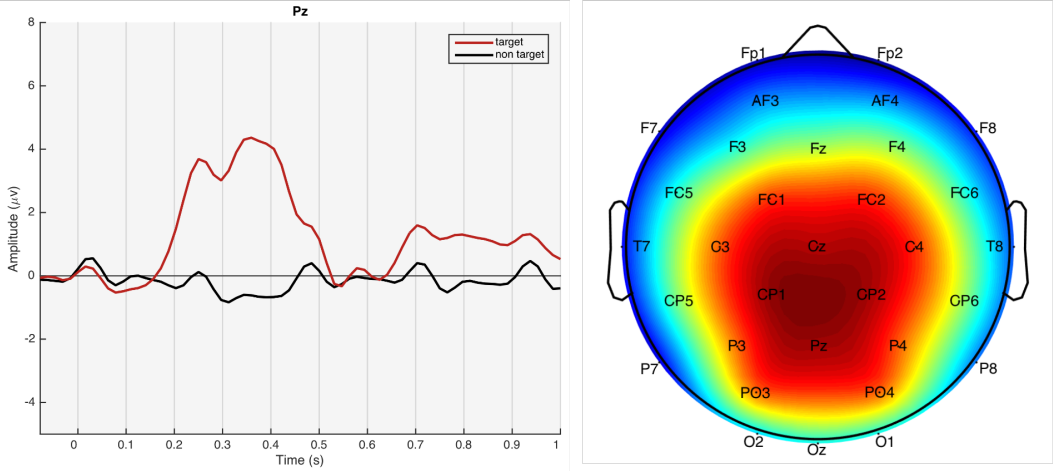

Figure 1.4: The P300 ERP is characterised by a positive deflection that reaches its peak around 300 ms after stimulus onset (left panel), and is most strongly present over centro-parietal scalp areas (right panel).

By taking advantage of the fact that the P300 potential is only elicited for a stimulus-of-interest, Farwell and Donchin [84] have shown that the P300 ERP can be used to build an EEG-based BCI for communication. In their original study, they described an interface with 36 targets presented in a matrix (6 rows and 6 columns). Here, the intended target can be identified using the P300 response which was elicited when the row and column of the gazed target was highlighted. When another row or column was highlighted, no P300 response was expected (figure 1.5). To account for the relatively low signal-to-noise ratio, each row and column was highlighted several times and the responses averaged per row and column.

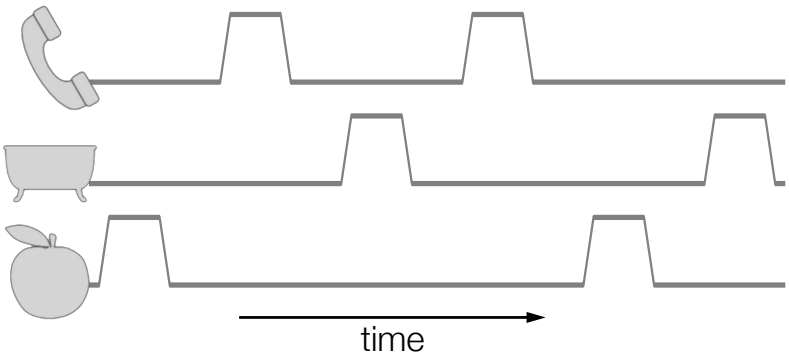

Figure 1.5: The targets in a P300-based BCI are being highlighted (e.g., change in color or luminance intensity) in a pseudorandom, consecutive and non-overlapping fashion. The EEG responses time-locked to each target stimulation are averaged and the P300 ERP is only expected for the gazed target.

1.2.3.2 *Steady-State Visual Evoked Potential*

The steady-state visual evoked potential (SSVEP) is an electrophysiological response elicited by oscillatory flickering stimulation and is, unlike the P300 ERP, a sensory (visual) potential. The signals are recorded over the occipital pole, where the visual input is processed by the brain, and exhibit similar frequency characteristics as the gazed stimulation. In addition to the fundamental frequency component (i.e., the stimulation frequency) also several harmonics are present (figure 1.6).

By encoding each selectable target in a BCI with a different flickering frequency (figure 1.7) and by examining the frequencies present in the SSVEP, one can infer the gazed target. While with the P300 paradigm, different gazed targets elicit the same response (i.e., the P300 ERP), with the SSVEP paradigm different targets elicit different frequency responses. This enables one to stimulate all targets simultaneously, which considerably reduces the time required to reliably select a target. However, as the SSVEP stimulation is often displayed on a monitor whose refresh rate is limited, and since each frequency also elicits harmonic responses, only a limited amount of frequencies can be adopted for target encoding. As an alternative to frequency encoding, also phase-encoding of targets has been proposed. Instead of assigning a unique frequency to each target, all targets adopt the same frequency but differ in phase [181, 206]. While this paradigm is able to re-use stimulation frequencies, the correct decoding of phase-encoded targets is considerably more difficult due to the inter-trial variability of the phase responses [202]. Finally, frequency-and phase decoding can be combined such that each selectable target adopts a unique combination of frequency and phase [55, 126, 221].

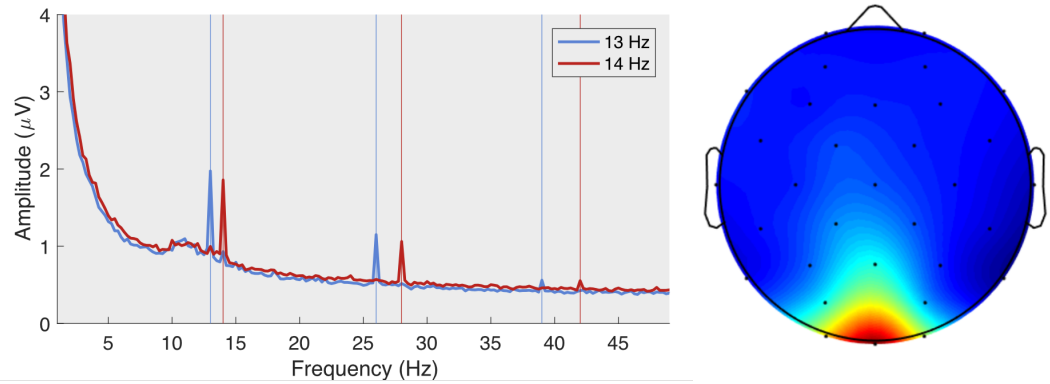

Figure 1.6: The SSVEP is characterised by frequency components that follow the stimulation of the gazed target (left panel). Next to the fundamental component, also the harmonic components of the EEG signal exhibit an increased amplitude. In the figure, when gazing at a target flickering at 13 Hz (blue line), a strong amplitude increase is measured at the 13 Hz component of the EEG signal, as well as additional peaks at 26 and 39 Hz, while the 14 Hz target (red line) has peaks at 14, 28 and 42 Hz. Spatially, the SSVEP, as least as adopted in BCI settings, is exclusively present over the occipital scalp area (right panel).

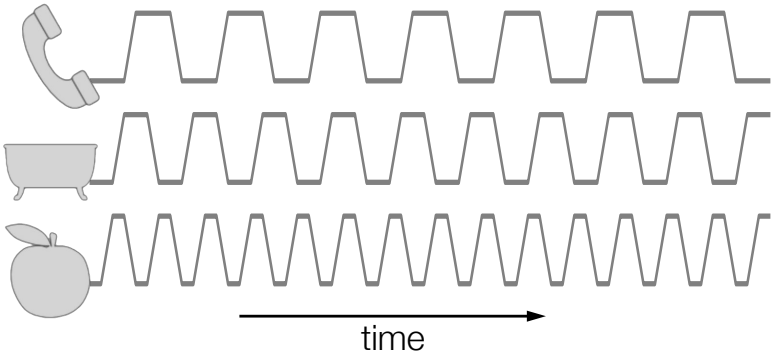

Figure 1.7: In an SSVEP-based BCI, each selectable target is traditionally encoded with different frequencies. By measuring the frequency components of the occipital EEG response, the gazed target can be decoded.

1.2.3.3 *Code-modulated Visual Evoked Potential*

The code-modulated visual evoked potential (cVEP) is elicited by a pseudo-random binary sequence of stimulus intensities with unequal duty cycles (unlike the SSVEP, which adopts equal duty cycles). Targets are encoded using the same sequence, but shifted with a number of places (figure 1.8). As pseudo-random stimulus sequence, an m-sequence is often used, as it has favourable autocorrelation properties. The shifted versions of an m-sequence have a low correlation, making them more easily distinguishable (i.e., different shifted versions of the same sequence are not very similar). Despite the reported high transfer rates, which are mainly due to the fact that they scale up easily to a larger number of targets (e.g., one m-sequence of 64 bits can encode up to 32 targets, when adopting a two-bit shift between targets), the cVEP paradigm is not as widely studied as the P300 or SSVEP paradigms.

While the cVEP paradigm does not have a clear spatial and temporal consistent response across subjects, studies mainly focus on the parieto-occipital scalp electrodes [33] as these have shown good performance. The decoding of cVEP-encoded targets has furthermore also been shown to be feasible from ECoG recordings [139].

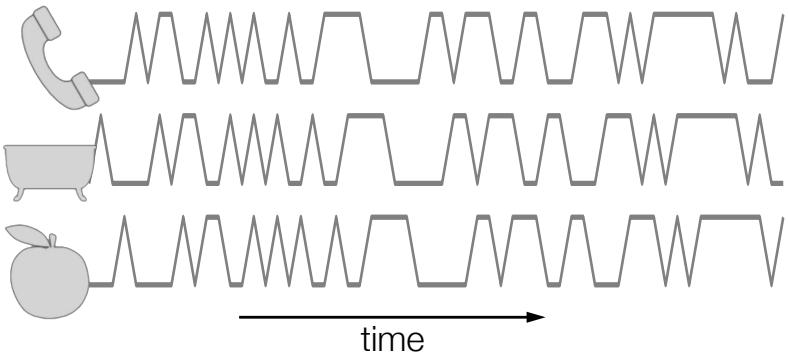

Figure 1.8: In a cVEP-based BCI, targets are encoded with lagged versions of a unique pseudo-random sequence of high and low stimulus intensities. While only a single stimulus sequence is defined, the lagged versions each elicit a unique response as they are time-locked to the stimulation onset.

1.2.4 *Alternative applications*

While the main aim of the BCI community is to provide an alternative communication channel for severely impaired patients, also other types of applications have been developed and the rapidly evolving BCI technology has recently sparked interest of commercial companies[2] in recent years. One important prospect is gaming [4, 34]

2 e.g., Facebook and Neuralink

and several research groups have developed and tested proof-of-concept BCI games, including adaptations of popular games like Pinball [157] and Tetris [244], and custom-developed games in which characters can be guided through a virtual world (e.g., a maze [60]) using a BCI or in which the interaction with the game is based on evoked potentials [174], (imagined) motor commands [171] or the mental state of the subject [152].

Other promising BCI applications include the natural, intuitive control of a prosthetic limb [209, 276] and the development of more efficient motor rehabilitation procedures [72]. For example, visual [143] (e.g., the movement is performed by an avatar displayed on a monitor) or somatosensory [228] feedback during the rehabilitation session has been used as a way to improve the efficiency of rehabilitation of the targeted movement, even if the subject was not able to actually perform it.

1.3 SPATIOTEMPORAL BEAMFORMING

In this thesis, we will assess the feasibility of the spatiotemporal beamformer algorithm for decoding several BCI paradigms. Originally, the beamforming algorithm was developed as a spatial filter for radar-, sonar- and seismic technology [309].

To illustrate the principle, consider the following example[3] of a room filled people engaged in conversations (figure 1.9a). While an observing human in this situation is typically able to isolate the conversation-of-interest from the surrounding noise [23], this is not the case with sensor technology. Assume there are several audio recording devices at a different locations in the room, each one picking up a unique mixture of all conversations. From individual recordings, it is very difficult to isolate one particular conversation. The beamforming principle will make a linear combination of all recordings (i.e., at different locations in the room) to optimally extract the information from a conversation-of-interest. Using this principle, a recording that mainly captures a noise source (i.e., a conversation not of interest) could be used to 'clean' a recording that captures the target conversation as well as the previously mentioned noise source.

This example can be 'translated' to electrophysiological recordings by assuming that each conversation is a dipole in the brain and the recording devices are electrodes placed on the scalp (figure 1.9b). Each electrode measures a unique mixture of ongoing activity at the dipoles, and their recorded activities are combined to optimally isolate the activity originating in a dipole-of-interest. The beamforming principle has shown successful with EEG for the localisation of electrical sources [135, 310], for ERP analysis [306], as well as for the decoding of motor imagery for BCI [105].

In practice, a weight is assigned to each sensor (e.g., electrode), and the vector containing these weights is called the beamformer. Among the many algorithms proposed to obtain these weights, the linearly-constrained minimum variance (LCMV) variant seems most promising for the task at hand (i.e., target decoding in a BCI context). Min-

3 this example is also known as the cocktail party problem

imum variance beamformers have reported higher gains than their minimum norm variants [135], and the linear constraint furthermore allows for a convenient measure of the contribution of the activity-of-interest.

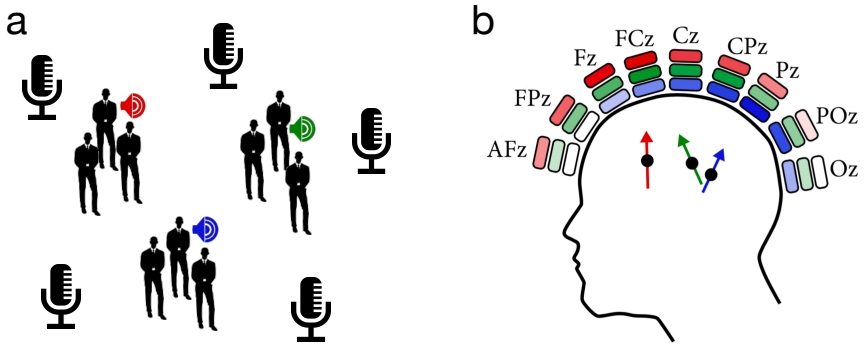

Figure 1.9: Visual rendition of the beamforming principle to isolate (a) a conversation-of-interest in the context of the cocktail party problem (b) the activity at a dipole-of-interest in the context of EEG. All sensors measure a unique combination of activity at the sources, and the activity of the blue source in (b) could, for example, be estimated by subtracting the measurement at FPz from the measurements of Pz, essentially eliminating the contribution of the red and green source at measured at Pz.

While originally formulated as a spatial filter, also a spatiotemporal extension of the beamforming principle has been described [319] and shown to be successful for single-trial ERP (N400) analysis in the context of semantic processing [319].

1.4 CLASSIFIERS

In the following chapters, we will compare the performance of the spatiotemporal beamformer with existing algorithms for target detection in the context of visual BCI. In this section, we briefly introduce two algorithms being used.

1.4.1 *Support Vector Machines*

A support vector machine (SVM) [313] aims to define a hyperplane that maximally separates the training samples belonging to two classes. The hyperplane is constructed to have a maximal margin to the both classes and takes into account a regularization parameter that penalizes those samples that fall on the wrong side of the hyperplane, and the obtained hyperplane minimizes the total penalty. While SVMs can also split the data non-linearly, linear solutions have shown more accurate in the BCI literature [162].

An example of a linear separation of training samples as done by a SVM is shown in Figure 1.10a.

1.4.2 *Canonical correlation analysis*

The canonical correlation analysis (CCA) algorithm finds linear combinations $\mathbf{w}_x$ and $\mathbf{w}_y$ for two multivariate sets $\mathbf{X}$ and $\mathbf{Y}$, such that their linear combinations $\mathbf{x} = \mathbf{X}\mathbf{w}_x^T$ and $\mathbf{y} = \mathbf{Y}\mathbf{w}_y^T$ are maximally correlated [111]. For BCI studies, CCA is mainly used to find spatial filters that maximize the correlation between the measured signals and a group of target signals (i.e., signals-of-interest). A graphical depiction of the CCA principle is shown in Figure 1.10b.

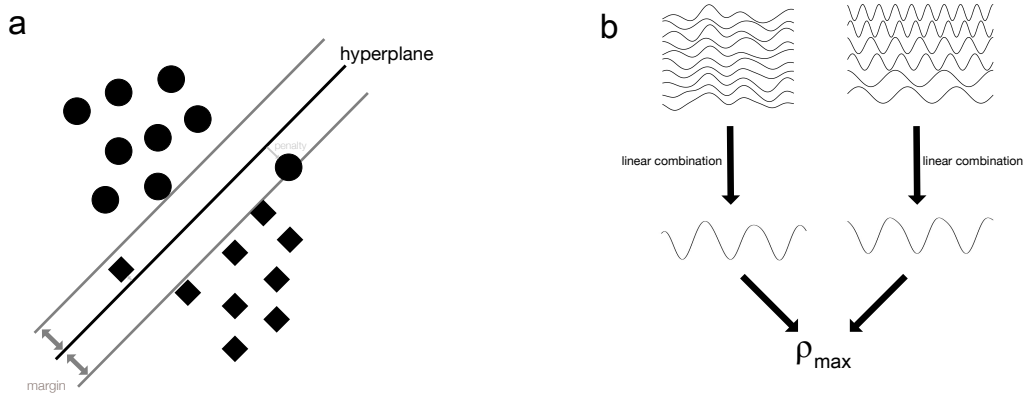

Figure 1.10: Graphical representation of two classification algorithms used throughout this work: (a) Support Vector Machine (b) Canonical Correlation Analysis

1.5 GOALS

The aim of this thesis is to contribute to the development of visual brain-computer interfaces. To this end, we will assess the feasibility of the spatiotemporal beamforming algorithm for the three most widely-studied visual BCI paradigms. The performance of the proposed approach is compared with those of the state-of-the-art classifiers (at the time of writing) of each paradigm, both in terms of accuracy and training time. The P300 paradigm is investigated in chapter 2, the SSVEP paradigm in chapter 3, and the cVEP paradigm in chapter 4. Chapter 5 describes the spatiotemporal beamformer in a common framework for the three paradigms, and investigates whether interaction between the beamformer outputs of different selectable targets can be used to improve the decoding performance. In chapter 6, we investigate the cortical activations elicited by SSVEP stimulation in detail using ECoG recordings covering the entire right occipital cortex. Finally, in chapter 7, the target decoding performance of state-of-the-art SSVEP classifiers are assessed with ECoG recordings and compared with traditional scalp-EEG for which they were originally developed.

2

FASTER P300 CLASSIFIER TRAINING USING SPATIOTEMPORAL BEAMFORMING

This chapter has been published as:
B. Wittevrongel and M.M. Van Hulle (2016) *Faster P300 Classifier Training Using Spatiotemporal Beamforming.* International journal of Neural Systems 26,1650014.

The Linearly-Constrained Minimum-Variance (LCMV) beamformer is traditionally used as a spatial filter for source localization, but here we consider its spatiotemporal extension for P300 classification. We compare two variants and show that the spatiotemporal LCMV beamformer is at par with state-of-the-art P300 classifiers, but several orders of magnitude faster in training the classifier.

2.1 INTRODUCTION

A brain-computer interface (BCI) is a direct communication channel between the brain and a computer and is of particular interest for people suffering from motor-[45] and communication disabilities, as it allows issuing commands without requiring any muscular activity [1, 84, 221, 230, 316, 317, 351, 353]. Among the gamut of possible electroencephalography (EEG) paradigms considered for non-invasive BCI [32, 37, 190, 219], the P300 event-related potential (ERP) is one of the most widely studied, also in patients [68, 201]. The P300 ERP is evoked in response to an infrequent but attended stimulus ("oddball") and characterized by a positive amplitude deflection peaking around 300 ms post-stimulus onset and recorded over central and parietal regions of the scalp. However, the exact scalp topography, amplitude and latency of the P300 are subject-dependent and also the subject's age [234] and environmental factors [247] were shown to play a role. A popular way to address the limited signal-to-noise ratio of EEG, is to average P300 responses of multiple trials (referred to as epochs) thereby cancelling components unrelated to stimulus onset [194]. The downside is that the same stimulus needs to be shown multiple times, reducing BCI communication speed [341].

Several approaches have been suggested to improve P300 detection. Some investigated the use of motion-onset- [128] and face stimuli [131, 142], and the mismatch negativity paradigm [132]. These stimulation paradigms elicit additional EEG components (N170 and N400f ERPs, M-VEP, and N200 and N400 ERPs, respectively), providing additional information for detecting the EEG response to the stimulus of interest. Also variations in luminosity contrast and stimulus duration have been considered (e.g., [183]). Other studies focus on machine learning algorithms for P300 detection, including a convolutional neural network [51], an ensemble of support vector machines (SVMs) combined with a genetic algorithm [98], and a single-layer feed-forward neural network [347]. When separating the P300 component, some supervised learning approaches have been shown to yield spatial- or spatiotemporal filters. For example, linear SVM and linear discriminant analysis (LDA) can be considered spatiotemporal filters. Such data-driven filters take advantage of labeled (training) data to maximize discriminability between experimental conditions based on a chosen criterion. Other filters used for P300 detection include extensions of the common spatial pattern (CSP) [66, 159] and xDAWN [262]. Another category of filters are the beamformers. While originally conceived as a multivariate spatial filter for source localization of radar, sonar and seismic data [309], spatial beamformers have also been employed in EEG to isolate the signal originating from a predefined brain location [310], to perform imagined movement detection [105],to perform P300 detection [243], and to estimate the amplitude of the N400 ERP [319]. In this study, we investigate a spatiotemporal extension of the original spatial beamformer for P300 detection, and assess its performance for use in P300-based BCI.

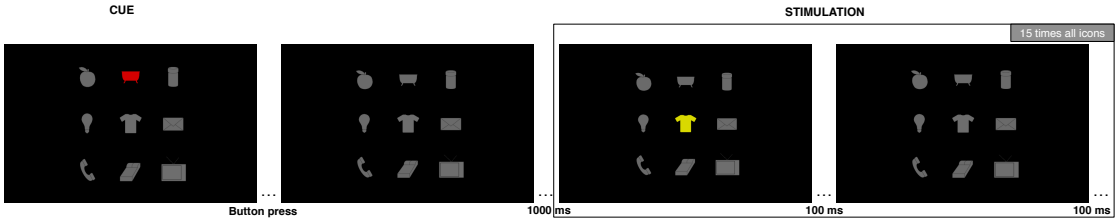

Figure 2.1: The interface used in the experiment and the time course of one stimulation sequence, preceded by a cue.

2.2 METHODS

2.2.1 *Subjects*

We recruited 21 healthy subjects for our experiment (13 female, avg. 22.9 years, std. 1.93 years) of which 16 never participated in any EEG experiment before. Prior to the experiment, subjects read and, when they agreed, signed an informed consent form approved by the ethical committee of our university hospital UZLeuven. All subjects had normal or corrected to normal vision, and were paid for their participation.

2.2.2 *Experimental procedure*

The interface consisted of 9 icons, arranged in a 3×3 design, projected on an LCD computer display (sized 24.1 inch, resolution 1920×1200, 60 Hz refresh rate). The icons were approximately 2 cm wide and high, and their centers 4 cm apart. Subjects were seated in a comfortable arm chair at a distance of approximately 70 cm from the display. All experiments were done in a sound-attenuated, air-conditioned room.

Figure 2.1 shows the interface. An individual stimulation sequence was preceded by a cue, i.e., one of the icons highlighted in red, after which the subject had to press a key to start the stimulation sequence during which the icons were flashed individually (thus, not in the traditional way of flashing an entire row or column) by changing their color from gray to yellow for 100 ms. The interstimulus interval was 100 ms during which all icons adopted a gray color. An individual stimulation sequence consisted of 15 random permutations of the 9 icons. We ensured that between two stimulations of the cued icon at least three other icons were flashed (to avoid a contamination of P300 responses). In order to keep subjects attentive, they were asked to mentally count how many times the cue was flashed in the stimulation sequence. Prior to start each sequence, the subject had to press a key on the keyboard, immediately after which the cued icon disappeared and the sequence started. This was done to reduce the chance that (s)he missed the cue due to distraction or temporary concentration loss. Each icon was used as a cue four times, leading to a total of 36 sequences, each one having a

length of 28 seconds. In between sequences, the subject was allowed to take a break. A recording session lasted approximately 25 minutes, and was preceded by 2.5 minutes of EOG calibration (see further).

2.2.3 *Recording*

EEG was recorded continuously (sampling speed 2048 Hz, CMS[1] referencing) using a BioSemi ActiveTwo system (BioSemi, Amsterdam, the Netherlands) and 32 active Ag/AgCl electrodes, evenly distributed over the entire scalp[2]. All 32 electrodes are listed along the vertical axis of Figure 2.6c. Additionally, six external electrodes were placed: two on both mastoids, for off-line re-referencing, and four around the eyes, on the upper and lower side of the left eye (vertical) and near the external canthus of each eye (horizontal), for electro-oculogram recording (EOG, bi-polar recording). Except for the external ones, all electrodes were mounted in an electrode cap placed on the subject's head. Conductive gel was applied in each of the electrode holes, as well as on the surface of the external electrodes to reduce electrode impedance. Prior to the main experiment, an EOG calibration session was performed to capture eye movements and blinks using the method described in Croft & Barry [70]. During the recording of eye movements, a white circle on a black background was moving vertically and horizontally starting from the center of the screen. Subjects were instructed to follow the circle with their eyes, without moving their head or blinking. During the recording of eye blinks, the same circle was coming down from the upper edge of the screen and was hitting the line in the middle of the screen. Subjects were instructed to focus on the center of the screen and blink every time the circle hit the line. They were specifically cautioned not to track the circle.

2.2.4 *Processing*

The EEG signal was re-referenced offline from the original CMS reference to the average of both mastoid signals, and EOG correction was performed using Croft's method. The corrected recordings were then bandpass filtered between 0.5 and 15 Hz using a 4th order Butterworth filter, and cut into 1.1-second epochs, from 100 ms pre-stimulus onset to 1000 ms post-stimulus onset. Baseline correction was performed by subtracting the average of the 100 ms pre-onset activity. Finally, the epochs were downsampled to 64 Hz and stored for further analysis, together with the indices of the corresponding icon and the cue of the corresponding sequence. In total, 4860 epochs were extracted for each subject with 540 marked as target epochs, i.e. for which a P300 component is expected. These correspond to the epochs whose stimulated icon was equal to the cue of the sequence. Two subjects reported to have forgotten the cue of a particular

1 Common Mode Sense[308], positioned next to electrode Pz

2 positioning and naming convention following a subset of the international extended 10-20 system

sequence. The corresponding sequences were removed from further analysis, hence, for these subjects, we had 4725 epochs (35 sequences).

2.2.5 *Analysis*

2.2.5.1 *Beamforming*

The beamforming approach requires an explicit activation pattern (i.e., a template) of the component-of-interest, in our case the P300 ERP. Let matrix $\mathbf{A} \in \mathbb{R}^{m \times n}$ be the spatiotemporal activation pattern of the P300 ERP, where m represents the number of electrodes and n the number of samples.

While the beamformer was originally formulated as a spatial filter (i.e., a weight vector), we extend this idea to a spatiotemporal filter. We adopt the formulation of van Vliet et al. [319]. A Linearly-Constrained Minimum-Variance (LCMV) spatial beamformer $\mathbf{w}_{sp} \in \mathbb{R}^{m \times 1}$ minimizes the variance of the beamformer output $\mathbf{w}_{sp}^{\intercal}\mathbf{S}$:

$$\arg\min_{\mathbf{w}_{sp}} \mathbf{w}_{sp}^{\intercal}\mathbf{S}(\mathbf{w}_{sp}^{\intercal}\mathbf{S})^{\intercal} = \arg\min_{\mathbf{w}_{sp}} \mathbf{w}_{sp}^{\intercal}\mathbf{\Sigma}_{sp}\mathbf{w}_{sp}, \tag{2.1}$$

where $\mathbf{\Sigma}_{sp} \in \mathbb{R}^{m \times m}$ is the spatial covariance matrix of the EEG signal $\mathbf{S} \in \mathbb{R}^{m \times n}$. By adding the linear constraint:

$$\mathbf{a}_{sp}^{\intercal}\mathbf{w}_{sp} = 1, \tag{2.2}$$

where $\mathbf{a}_{sp} \in \mathbb{R}^{m \times 1}$ is the spatial activation pattern, we avoid trivial solutions of (2.1), and signals that are similar to $\mathbf{a}_{sp}$ will be mapped to a value close to 1, allowing for an easy measure of similarity. The solution of (2.1) under constraint (2.2) can be found using the method of Lagrange multipliers [310]:

$$\mathbf{w}_{sp} = \frac{\mathbf{\Sigma}_{sp}^{-1}\mathbf{a}_{sp}}{\mathbf{a}_{sp}^{\intercal}\mathbf{\Sigma}_{sp}^{-1}\mathbf{a}_{sp}}. \tag{2.3}$$

The spatial beamformer can be expanded to a spatiotemporal variant as follows. Let $\mathbf{X} \in \mathbb{R}^{r \times (mn)}$ be a matrix where each row is obtained by concatenating the rows of the corresponding epoch $\mathbf{S}_i$ ($i = 1..r$), $\mathbf{\Sigma} \in \mathbb{R}^{(mn) \times (mn)}$ the covariance matrix of $\mathbf{X}$, and $\mathbf{a}^{\intercal} \in \mathbb{R}^{1 \times (mn)}$ a vector containing the concatenated rows of $\mathbf{A}$. The spatiotemporal LCMV beamformer $\mathbf{w} \in \mathbb{R}^{(mn) \times 1}$ with the linear constraint $\mathbf{a}^{\intercal}\mathbf{w} = 1$ can now be calculated as:

$$\mathbf{w} = \frac{\mathbf{\Sigma}^{-1}\mathbf{a}}{\mathbf{a}^{\intercal}\mathbf{\Sigma}^{-1}\mathbf{a}}, \tag{2.4}$$

and applied to the data as a simple weighted sum:

$$y = \mathbf{s}\mathbf{w}, \tag{2.5}$$

where $\mathbf{s} \in \mathbb{R}^{1 \times (mn)}$ indicates the concatenated rows of a signal $\mathbf{S}$.

Another way to obtain a spatiotemporal filter is to apply a spatial beamformer $\mathbf{w}_{sp} \in \mathbb{R}^{m\times 1}$ followed by a temporal beamformer $\mathbf{w}_{tmp} \in \mathbb{R}^{n\times 1}$. Let $\mathbf{B} \in \mathbb{R}^{r\times n}$ be the matrix containing the results of applying spatial filter $\mathbf{w}_{sp}$ to the EEG epochs $\mathbf{S}_i$:

$$\mathbf{B} = \begin{pmatrix} \mathbf{w}_{sp}^{\mathsf{T}}\mathbf{S}_1 \\ \mathbf{w}_{sp}^{\mathsf{T}}\mathbf{S}_2 \\ \vdots \\ \mathbf{w}_{sp}^{\mathsf{T}}\mathbf{S}_r \end{pmatrix}. \tag{2.6}$$

$\mathbf{\Sigma}_{tmp} \in \mathbb{R}^{n\times n}$, the covariance matrix of $\mathbf{B}^{\mathsf{T}}$, together with a temporal activation pattern $\mathbf{a}_{tmp} \in \mathbb{R}^{n\times 1}$, allows for a temporal beamformer to be obtained as follows:

$$\mathbf{w}_{tmp} = \frac{\mathbf{\Sigma}_{tmp}^{-1}\mathbf{a}_{tmp}}{\mathbf{a}_{tmp}^{\mathsf{T}}\mathbf{\Sigma}_{tmp}^{-1}\mathbf{a}_{tmp}}. \tag{2.7}$$

By consecutively applying the beamformers constructed in (2.3) and (2.7) to the epoch under consideration, a spatiotemporal beamformer is obtained:

$$y = \mathbf{w}_{sp}^{\mathsf{T}}\mathbf{S}\mathbf{w}_{tmp}. \tag{2.8}$$

We further refer to (2.5) as the spatiotemporal beamformer (stBF) and to (2.8) as the chained beamformer (chBF).

2.2.5.2 *Activation Patterns*

Generated by a network of brain regions [285] the P300 ERP could be modeled by simulating activities in these regions and their propagation throughout the brain towards the scalp using a head model. However, for our study it is not important to know where the P300 is generated. We are only interested in how it is distributed over the scalp and how it develops over time. Therefore, we will base our estimation on actual scalp recordings. For the stBF, we estimate the spatiotemporal activation pattern $\mathbf{A}_{st} \in \mathbb{R}^{m\times n}$ as the difference between the grand averaged target epochs and grand averaged non-target epochs:

$$\mathbf{A}_{st} = \frac{\sum\limits_{i\in N_t}\mathbf{S}_i}{|N_t|} - \frac{\sum\limits_{j\in N_{nt}}\mathbf{S}_j}{|N_{nt}|}, \tag{2.9}$$

where N_t and N_{nt} refer to the sets of indices of the target and non-target epochs, respectively. Note that by subtracting the averaged non-target response from the target one, we also remove any ERPs that are in common.

The chained beamformer needs both spatial and temporal activation patterns. As a spatial activation pattern, we select the column of $\mathbf{A}_{st}$ that maximizes the sum of the samples:

$$\mathbf{a}_{sp} = \mathbf{A}_{st}[*, t] \in \mathbb{R}^{m\times 1}, \tag{2.10}$$

where

$$t = \arg\max_{t \in [1..n]} \sum_{c=1}^{m} \mathbf{A}_{st}[c, t]. \tag{2.11}$$

For the temporal activation pattern, we first build k spatial beamformers $\mathbf{w}_{sp}^{k}$, one for each subject whose epochs make up the data set, where beamformer $\mathbf{w}_{sp}^{k}$ is constructed using only the data of subject k. Then, each epoch is filtered with the beamformer of the corresponding subject, leading to a data set of single-channel epochs (cfr. **B**). From this, we construct the temporal activation pattern $\mathbf{a}_{tmp} \in \mathbb{R}^{n \times 1}$ as the difference between the averaged (filtered) target- and non-target epochs:

$$\mathbf{a}_{tmp} = \frac{\sum_{i \in N_t} \mathbf{B}[i, *]}{|N_t|} - \frac{\sum_{j \in N_{nt}} \mathbf{B}[j, *]}{|N_{nt}|}. \tag{2.12}$$

We consider two approaches in our study. First, using only data of individual subjects, we build subject-specific activation patterns. This approach is able to capture individual variations in the P300 waveform, and yields a beamformer that is tailored to each subject. Second, instead of tailoring activation patterns to individual subjects, we also investigate whether one, more general, activation pattern could be used for all subjects. To do so, the data of multiple subjects is used, and we will refer to it as the population activation pattern. However, to build a beamformer, the covariance matrix still needs to be estimated individually, as it captures current noise sources.

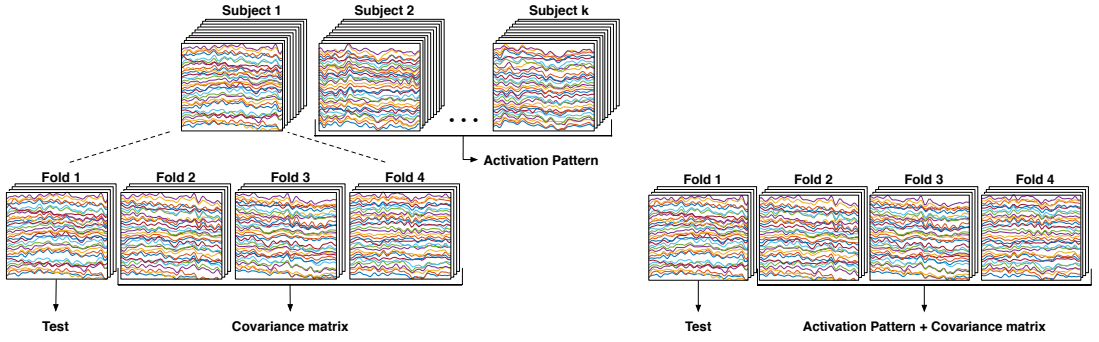

(a) (b)

Figure 2.2: Cross-validation setup to test the performance of the beamformer. (a) Population activation patterns. (b) Individual activation patterns.

2.2.5.3 *Classifiers*

Training the classifier starts with the estimation of the activation pattern(s) and the construction of the beamformer. From all training epochs, depending on the beamforming

type used, either the spatial- and temporal covariance matrices or the spatiotemporal covariance matrix is estimated and used (together with the activation pattern(s)) in the beamformer construction.

We then apply the beamformer to the averaged response of each icon of a given sequence with the number responses used for averaging (i.e., $[1..15]$) a parameter in the classifier assessment (see further). To arrive at an icon prediction for a given sequence, the icon with the highest beamformer output y, for all 9 icons is taken ("winner").

We apply a cross-validation scheme to assess the performance of the beamformer-based classifier. For the individual activation patterns, we apply stratified four-fold cross-validation. The folds are constructed such that all epochs in a fold are in response to each one of the nine possible cues. Each fold thus contains the epochs of nine sequences. Both the activation pattern and covariance matrix are estimated from all epochs in the training folds.

To test the population activation pattern, we apply a leave-one-subject-out cross-validation. The activation patterns are estimated using the epochs from all subjects, except the subject under consideration. For the latter, we apply four-fold cross-validation but this time the epochs in the training folds are only used to estimate the covariance matrix. Both setups are shown in figure 2.2.

For each sequence in the testing fold, we average the first l $(\in [1..15])$ occurrences of each icon, apply the beamformer to these averages, and mark the winning icon.

We also compare our spatiotemporal beamformer approach with a support vector machine (SVM) [313]. SVMs have proven to be among the best classifiers for P300 detection [193] and linear approaches have shown to outperform non-linear ones [162]. We therefore also consider a linear SVM and optimize its regularization parameter using a line-search algorithm and 10-fold cross-validation as suggested in Hsu et al. [122]. To train the SVM we use the modified finite Newton method proposed in Keerthi & DeCoste. [144]. This method was successfully applied to P300 detection in patients with incomplete Locked-In Syndrome (LIS) [68] and the detection of error-related potentials (ErrPs) in healthy subjects [67]. A similar decision strategy is used as for the beamformers, i.e., for each sequence we average the first $l \in [1..15]$ occurrences of each icon and indicate the most positive of the nine predictions as winner.

We evaluate the SVM for an individual subject by using the same cross-validation scheme as for our beamformers. In order to estimate the performance of an SVM trained on population data, we apply leave-one-subject-out cross-validation. We use all data of the subject under consideration as test data, unlike for the beamformers where we use an additional four-fold cross-validation to estimate the covariance matrix.

In addition to comparing accuracies, we also compare stBF and SVM based on the similarity of their activation patterns (i.e., the pattern used for discriminating between targets and non-targets). Since SVMs learn a weight vector, we can transform the latter into an activation pattern [112]. To assess the similarity of the two classifiers, we

Table 2.1: Configurations

REF	TIME WINDOW	NB CHANNELS
(C1)	0.0 - 1.0 sec	32
(C2)	0.0 - 1.0 sec	10
(C3)	0.1 - 0.6 sec	32
(C4)	0.1 - 0.6 sec	10

compute the stBF and SVM activation patterns for each subject, using all data of this subject, and calculate the Pearson correlation coefficient.

2.2.5.4 *Procedure for parameter sensitivity testing*

The P300 component should have its peak around 300 ms post-onset. In addition to the one-second window described above, we also run the analysis using a 500 millisecond-window from 100 to 600 ms post-stimulus onset. This window focusses on the P300 component (including its rise and fall) and has some margin to account for differences in latency between subjects.

We also assess the effect of number of electrodes. Instead of using all 32 electrodes, we selected electrodes that more closely correspond to the centro-parietal scalp distribution of the P300 [12, 163] (*Fz, Cz, Pz, Oz, O1, O2, PO3, PO4, P3* and *P4*) and repeated our analysis. The reduced electrode set has the advantage to reduce the dimensionality of the covariance matrix, leading to a more reliable estimate given a limited amount of data. However, excluding channels from the analysis also excludes potential useful information about noise sources that can be employed for building a more reliable filter [112].

Table 2.1 provides an overview of all setups used in our analysis, labeled for easy reference.

2.2.5.5 *Statistics*

Significance levels are calculated using a two-sided Wilcoxon Rank Sum Test. P-values below 0.05 are considered as significant.

2.3 RESULTS

2.3.1 *Individual Activation Patterns*

Figure 2.3 shows the performance of the spatiotemporal- and chained beamformers, for the different configurations. The chained beamformer is not affected by the smaller

window size or the reduced electrode set. For the spatiotemporal beamformer, configuration (C1) has a lower accuracy than the other configurations. This could be due to the larger amount of parameters that need to be estimated during the construction of the covariance matrix. Tables 2.2 and 2.3 show the significance levels for the two beamformers. There are no significant differences for the chained beamformer. For the spatiotemporal beamformer, there is a significant difference between (C1) and (C3) when less than 8 epochs are used for averaging. Also (C1) is significantly different from (C4) when less than 7 epochs are averaged, and (C1) and (C2) are significantly different when averaging 4, 5 or 6 epochs.

In order to compare both beamformers with SVM, we use the minimal configuration (C4). The accuracies with respect to the number of averaged trials are shown in figure 2.4. The difference in performance between the spatiotemporal beamformer and the SVM is not significant (table 2.4). The chained beamformer performs significantly worse, even when more epochs are used for averaging.

2.3.1.1 *Training time*

Next to assessing accuracy, we also measure the average time needed to train the P300 classifiers. Three classifiers (chBF, stBF & SVM) were trained for each subject, using all epochs (32 channels) of the subject under consideration. The timings are taken on a quad-core 2.3 GHz Intel i7 machine. Table 2.5 summarizes the results. Both beamformers need only a fraction of the time needed to train the SVM. One factor that explains the larger computational cost of the SVM is the cross-validation used to optimize the regularization parameter. This step requires a lot of classifiers to be built, increasing the time needed to finish training.

2.3.1.2 *Correlation*

The correlations between the stBF and SVM activation patterns are shown in figure 2.5. Except for subjects 11 and 20, the SVM learns a very similar activation pattern as the beamformer approach. However, as pointed out before, the SVM takes a lot more time to train.

2.3.2 *Population Activation Patterns*

Figure 2.6 shows the population activation patterns obtained when using all epochs from all subjects. The spatial activation pattern has, as expected, a clear centro-parietal distribution, and the temporal pattern shows a peak amplitude around 350 ms. The spatiotemporal activation pattern additionally has some negativity at occipital areas around 200 ms post-stimulus onset.

Using a population activation pattern in combination with an individual covariance matrix for building the beamformer does not provide an acceptable performance. Fig-

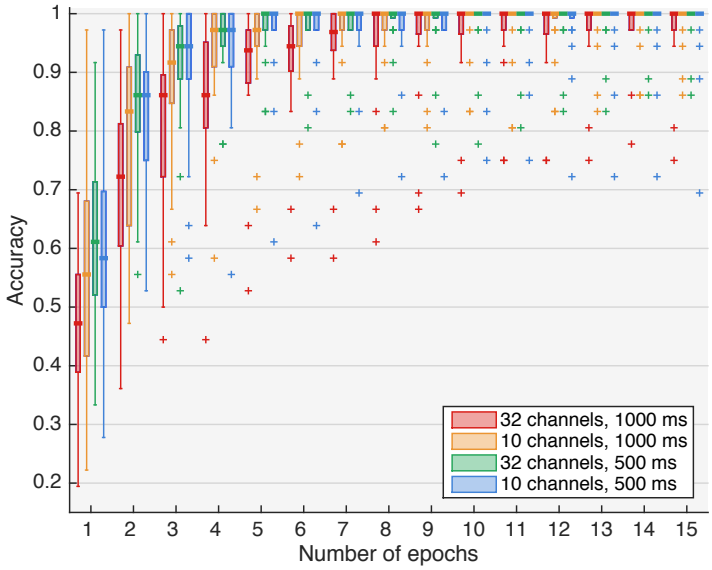

(a) Spatiotemporal Beamformer

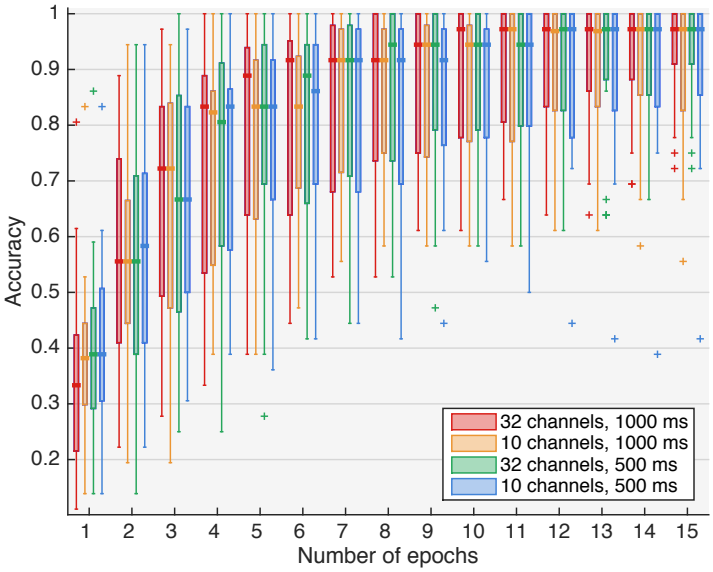

(b) Chained Beamformer

Figure 2.3: Influence of time window and number of electrodes on both beamformers.

	Number of averaged epochs														
	1	2	3	4	5	6	7	8	9	10	11	12	13	14	15
(C1) - (C2)	0.077	0.063	0.100	0.012	0.043	0.045	0.096	0.210	0.281	0.153	0.375	0.498	0.386	0.624	0.548
(C1) - (C3)	0.001	0.002	0.003	0.001	0.001	0.007	0.031	0.070	0.108	0.118	0.302	0.278	0.331	0.342	0.323
(C1) - (C4)	0.011	0.015	0.008	0.009	0.002	0.014	0.061	0.152	0.290	0.156	0.399	0.515	0.430	0.645	0.620
(C2) - (C3)	0.279	0.442	0.281	0.426	0.132	0.660	0.623	0.597	0.686	0.974	0.922	0.727	0.974	0.663	0.747
(C2) - (C4)	0.554	0.847	0.293	0.762	0.161	0.791	0.936	0.931	0.919	0.991	1.0	1.0	1.0	0.991	0.991
(C3) - (C4)	0.504	0.537	0.914	0.739	0.865	0.915	0.675	0.709	0.548	0.896	0.974	0.753	0.896	0.663	0.747

Table 2.2: Significance levels for stBF using individual activation patterns. p-values are calculated using a two-sided Wilcoxon Rank Sum Test; darker cells indicate significant differences.

	Number of averaged epochs														
	1	2	3	4	5	6	7	8	9	10	11	12	13	14	15
(C1) - (C2)	0.579	0.847	0.779	0.658	0.613	0.666	0.788	0.915	0.835	0.589	0.974	0.541	0.892	0.800	0.800
(C1) - (C3)	0.480	0.985	0.945	0.995	0.876	0.693	0.945	0.825	0.964	0.934	0.955	0.741	1.0	0.901	0.860
(C1) - (C4)	0.222	0.975	0.916	0.631	0.658	0.808	0.875	0.845	0.835	0.443	0.854	0.525	0.913	0.781	0.742
(C2) - (C3)	0.695	0.779	0.896	0.649	0.528	0.965	0.846	0.719	0.825	0.708	0.913	0.813	0.861	0.719	0.679
(C2) - (C4)	0.435	0.906	0.945	0.866	0.985	0.798	0.856	0.995	0.965	0.786	0.894	0.864	0.943	0.923	0.943
(C3) - (C4)	0.676	0.945	0.995	0.695	0.520	0.876	0.955	0.682	0.719	0.548	0.834	0.706	0.892	0.682	0.635

Table 2.3: Significance levels for chBF using individual activation patterns. Other conventions as in Table 2.2.

	Number of averaged epochs														
	1	2	3	4	5	6	7	8	9	10	11	12	13	14	15
spBF - chBF	0.002	<0.001	<0.001	<0.001	<0.001	<0.001	<0.001	<0.001	<0.001	<0.001	<0.001	0.002	0.005	0.006	0.005
chBF - SVM	<0.001	<0.001	<0.001	<0.001	<0.001	<0.001	<0.001	<0.001	<0.001	<0.001	<0.001	<0.001	0.004	0.004	0.004
spBF - SVM	0.965	0.398	0.874	0.891	0.996	0.865	0.796	0.686	0.784	0.892	0.926	0.675	0.922	0.922	0.896

Table 2.4: Significance levels for comparison between classifiers based on individual activation patterns. Other conventions as in Table 2.2.

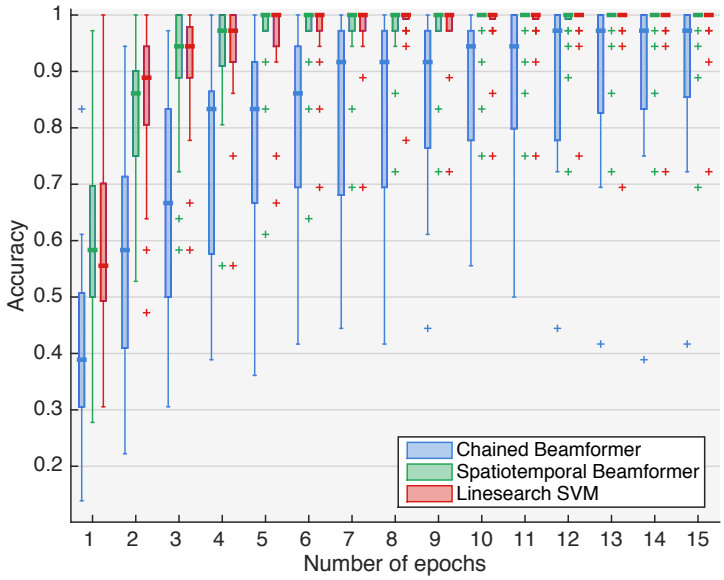

Figure 2.4: Accuracy of beamformer classifiers and SVM, using configuration (C4) and plotted as a function of number of epochs used in averaging.

	Time Window	
	[0.0, 1.0]	**[0.1, 0.6]**
chBF	0.60 (std 0.01)	0.49 (std 0.01)
stBF	4.64 (std 0.06)	0.76 (std 0.01)
SVM	498.74 (std 122.67)	147.16 (std 47.73)

Table 2.5: Average time needed (in seconds) to train the classifiers on all epochs of one subject.

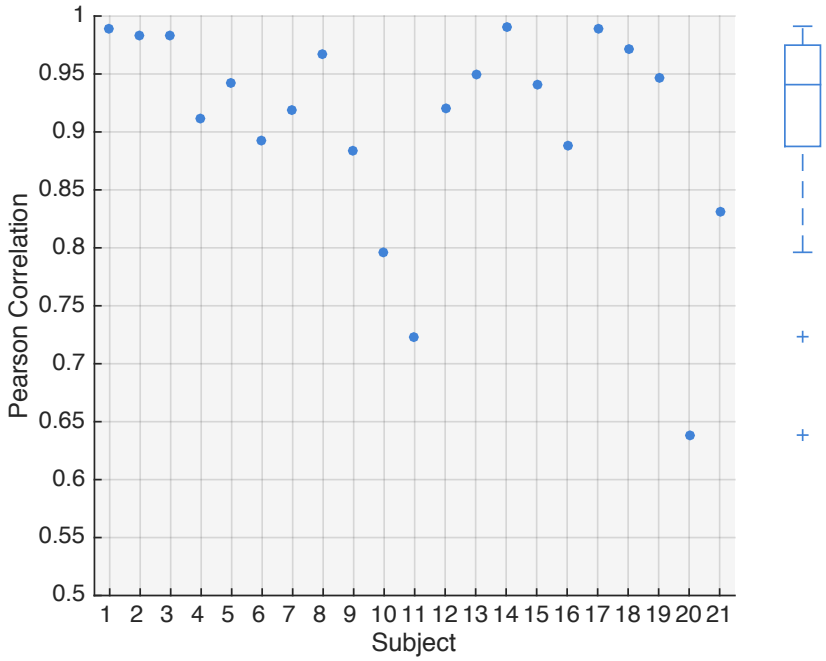

Figure 2.5: Correlations between stBF and SVM activation patterns for configuration (C4)

ure 2.7 shows the accuracies of both beamformers and the SVM with a 10 electrode setup and a one-second time window.

Similar to the case of individual activation patterns, the spatiotemporal beamformer yields a better performance than the chained variant. Even by averaging 15 epochs, the maximum considered in this study, the chained beamformer is not able to reach a median accuracy of 70%, which is often assumed to be required for reliable communication [42, 68, 165, 166]. While the spatiotemporal beamformer is able to reach this threshold for 8 epochs, its performance is significantly lower compared to when individual activation patterns are used (2 epochs to reach 70%). The SVM outperforms both beamformers on the population level (Figure 2.7) but at the individual level it is at par with the spatiotemporal beamformer (Figure 2.4). Note that the SVM performs significantly worse on population level compared to individual level (Figure 2.8).

2.4 DISCUSSION

In this study, we applied two variants of the spatiotemporal LCMV beamformer for P300 potential detection, and assessed their performance in view of a BCI implementation, but actually they could be applied to other ERP types as long as the corresponding activation patterns can be captured.

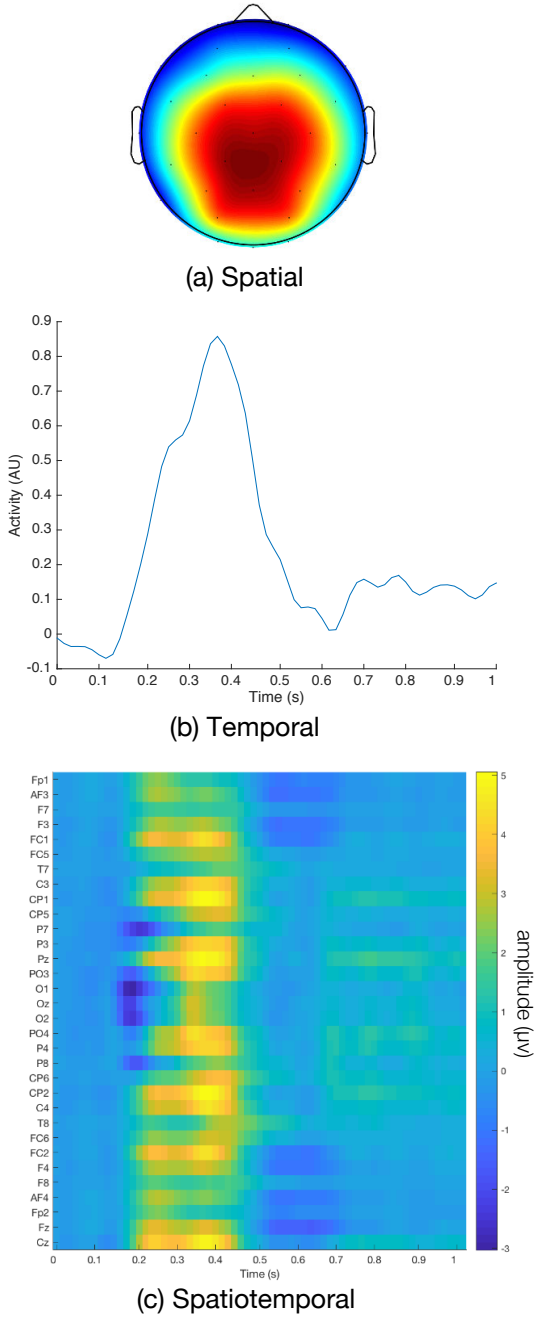

(a) Spatial

(b) Temporal

(c) Spatiotemporal

Figure 2.6: Population activation patterns built on all epochs of all subjects.

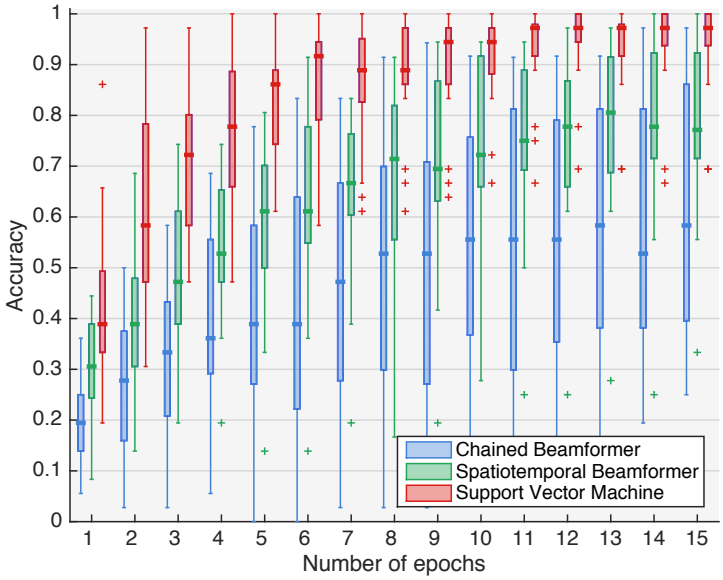

Figure 2.7: Performance of beamforming based on population activation pattern using configuration (C2).

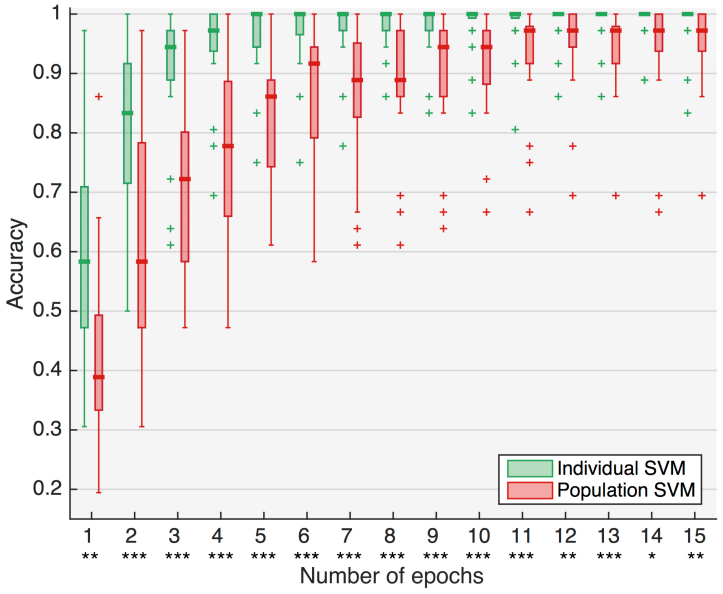

Figure 2.8: Comparison of SVMs built on individual- and population data. Stars indicate the significance levels based on a two-sided Wilcoxon Rank Sum testing:
*($p < 0.05$), **($p < 0.01$), ***($p < 0.001$)

In all configurations, the spatiotemporal beamformer achieves a better performance than its chained variant. This indicates that the chained variant loses valuable (spatiotemporal) information by performing the spatial and temporal filtering separately. An example of this can be seen in the population activation pattern (figure 2.6c). The spatiotemporal pattern clearly has a negative component in the occipital region around 200 ms post-stimulus onset. This N200[3] component is expected, as it is associated with orienting attention to a task-relevant stimulus [196], and it is known to contribute to P300 classification [141]. However, in the temporal pattern, the N200 is not present. The spatial filtering in the first step eliminates this component as this filtering is tailored to the peak of the P300. While the spatiotemporal filter is able to capture this information, it requires the estimation of more parameters during its construction. Figure 2.9 summarizes the results of the singular value decompositions of the individual spatiotemporal activation patterns of each subject. This shows that there are multiple singular values significantly different from zero, and indicates that a single spatial and temporal pattern are not sufficient to accurately capture the spatiotemporal P300 response. Only when only one large singular value is present can the spatiotemporal activation pattern be decomposed as the outer product of a single spatial and temporal component.

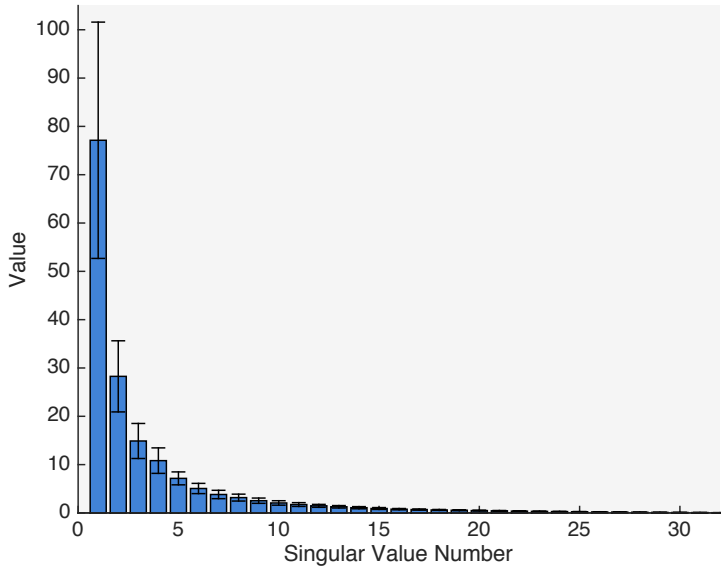

Figure 2.9: Average singular values (and standard deviations) of the spatiotemporal activation pattern. Singular value decomposition was applied to the individual spatiotemporal activation pattern of each subject separately.

Reducing the number of channels and the window length shows an improvement in the spatiotemporal beamformer to the point where it competes with SVM. This could

3 also called N1 in visual stimulation settings

be due to the reduction in the number of (covariance) parameters to estimate given the same number of training samples.

The P300 population activation pattern has, as expected, a clear central-parietal distribution and peaks around 300 ms post-stimulus onset. However, using this template for the beamformer does not result in an acceptable performance, probably due to the inter-subject variability of the P300 response. However, not being able to use a population template is not a noteworthy disadvantage. Since noise sources are subject dependent, a training session for each subject is needed to obtain the covariance matrix, which in turn can be used to optimize the beamformer for that particular subject. The same training data can also be used to obtain a subject-specific activation pattern, rendering the population activation pattern obsolete.

The amplitude and latency of the P300 response is linked to the level of attention of the subject [155, 246, 305]. Real-world P300 BCIs, where prolonged use is an issue, could benefit from retraining the classifier multiple times on most recent data. In order to provide a non-disruptive user experience, it is important that the retraining of the classifier can be done in a timely manner. For SVMs, instead of training a completely new model, which is computationally expensive, especially for large data sets, the 'incumbent' SVM can be updated to better fit the new data. This is the area of incremental (and decremental) learning [178, 245] of SVMs where the model is adapted when new samples become available (and old samples become obsolete). While efficient algorithms have been developed for updating the support vectors [140], the parameters of the SVM, including the regularization parameter C, remain fixed, which might lead to suboptimal models.

The spatiotemporal beamformer described in this study does not share this issue as there are no parameters to be optimized. Additionally, the y-values of the winning icons could be a trigger for retraining. As the P300 response evolves throughout the use of the BCI, it can be expected that the y-values increasingly migrate away from 1 towards 0.

Another consideration for real-world BCI applications is that the user will not constantly employ the interface, and that the algorithm needs to be asynchronous (i.e., be able to discriminate between a use state and an idle state). The present study developed a synchronous algorithm in which one icon is always identified as winner. To extend this algorithm to an asynchronous variant, a threshold on the y-values (after beamforming) could be introduced and the y-value of the winner would be required to surpass that threshold to decide that the user is actively attempting to employ the interface. One could also use a threshold to achieve a data-dependent trade-off between stimulus repetition and detection accuracy (early or dynamic stopping and adaptive stimulation [274]). These are directions of future exploration.

2.5 CONCLUSION

In this study, we have shown that P300 ERP detection based on spatiotemporal beamforming is feasible and that the activation pattern developed by the spatiotemporal beamformer are very similar to that of the SVM classifier, at least for most subjects, but using significantly less training time. Spatiotemporal beamforming could therefore be of particular interest to adaptive BCI applications.

Using beamformers with a single P300 activation pattern for all subjects in combination with individual noise estimation was not successful. The variability in shape and latency of the P300 response among subjects renders the population activation pattern suboptimal for reliable classification. The activation pattern should therefore be obtained from each subject individually. Further study is needed to assess whether this activation pattern could be reused by the same subject across sessions.

3

FREQUENCY- AND PHASE ENCODED SSVEP USING SPATIOTEMPORAL BEAMFORMING

This chapter has been published as:
B. Wittevrongel and M.M. Van Hulle (2016) *Frequency- and Phase Encoded SSVEP using Spatiotemporal Beamforming.* PLOS One 11, e0159988

In brain-computer interfaces (BCIs) based on steady-state visual evoked potentials (SSVEPs) the number of selectable targets is rather limited when each target has its own stimulation frequency. One way to remedy this is by combining frequency- with phase encoding. We introduce a new multivariate spatiotemporal filter, based on Linearly Constrained Minimum Variance (LCMV) beamforming, for discriminating between frequency-phase encoded targets more accurately, even when using short signal lengths than with (extended) Canonical Correlation Analysis (CCA), which is traditionally posited for this stimulation paradigm.

3.1 INTRODUCTION

The steady-state visual evoked potential (SSVEP) is a neurophysiological response to a periodic visual stimulus commonly gauged with electroencephalography (EEG) over the occipital cortex when using stimuli flickering at a frequency above 6 Hz but in practice lower than about 30 Hz (due to the usual 60 Hz screen refresh rate and the EEG bandwidth). The recorded EEG signals not only resonate at that frequency but also contain a number of harmonics. When considering a display with several disjoint, spatially delimited stimuli, each one flickering at a different frequency, the stimulus the subject is currently gazing at can be inferred from a spectral analysis of the recorded EEG signals. This is also the principle behind the SSVEP-based brain-computer interface (BCI) where those stimuli become selectable targets in a subject interaction paradigm. However, a simple frequency analysis technique based on the (fast) Fourier transform [58, 146] typically requires long (i.e., 3 seconds or more[187, 343]) signals to accurately discriminate targets flickering at nearby frequencies. Further studies have led to several SSVEP detection techniques that are able to work with shorter signals such as *Similarity of Background* (SOB)[344], *Minimum Energy Combination* (MEC)[91], time-domain analysis [199, 203], and the widely adopted *Canonical Correlation Analysis* (CCA) [31, 185, 346, 350] and its variants [56, 353].

The number of frequency-coded targets is not only limited by the harmonics of the stimulus frequency, but also by the screen refresh rate: when using a 50% duty-cycle stimulation (i.e., 'on-off' stimulation) the usable frequencies are restricted to integer dividers of the screen refresh rate. This restriction was demoted by replacing on-off stimulation with screen luminosity modulation [207].

As an alternative to frequency coding, also phase coding of the targets has been suggested [83, 181, 189, 202, 206, 207, 361]: (a subset of) targets flicker at the same frequency but with different phase 'lags'. However, discriminating phases is more challenging and, typically, the number of useable phases is also quite limited, especially when based on short signals [206].

Another attempt to increase the number of selectable targets is to consider for each target a unique combination of frequency and phase [55, 126, 221]. For the joint detection of frequency and phase, the CCA method was extended and shown to be useful for a high-speed BCI application [221]. We will also consider combined frequency/phase coded targets but propose a new decoding approach: spatiotemporal beamforming in combination with time-domain analysis of EEG signals. The beamformer was originally formulated as a spatial filter for radar, sonar and seismic data analysis [309]. It was also employed in EEG analysis to isolate the signal originating from a predefined brain location [310], to estimate the amplitude of an ERP component [319, 331], and to build a BCI application based on imagined movement detection [105]. Here we extend the beamformer to a spatiotemporal filter for combined frequency-phase SSVEP BCI.

3.2 METHODS

3.2.1 *Subjects*

We recruited 21 subjects, for our experiments, 14 female and 7 male (average age 22.7 years, between 19 to 26 years). Prior to the experiment, and after being informed of its purpose and design, our subjects read and, when they agreed, signed an informed consent form previously approved by the ethical committee of our university hospital UZLeuven. All subjects had normal or corrected to normal vision and were paid for their participation. All experiments were done in a sound-attenuated, air-conditioned room.

3.2.2 *Interface*

The targets consisted of four identical squares sized 9.5 $\times$ 9.5 cm, horizontally and vertically separated by 5.4 cm gap ($\sim$ 4.4°) and diagonally by a 7.6 cm gap ($\sim$ 6.2°), projected on an LCD computer display (sized 24.1 inch, resolution 1920$\times$1200, 60 Hz refresh rate). Each square was assigned a different combination of frequency (12 or 15 Hz) and phase (0 or π radians) (Fig 3.1). Subjects were seated in a comfortable arm chair at a distance of approximately 70 cm from the display.

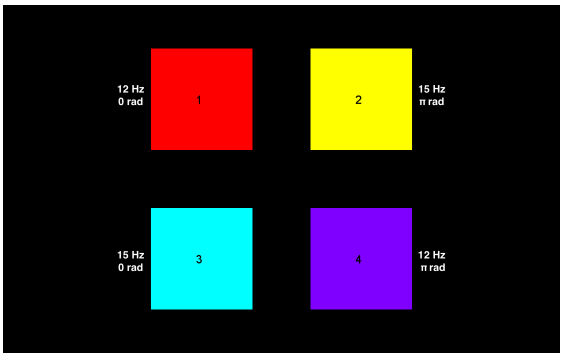

Figure 3.1: Interface used in the experiment. Each of the four squares has a unique combination of frequency and phase.

The recording session consisted of 60 trials. At the beginning of each trial, one of the squares was cued (target) with its corresponding color while the other squares were shown in gray. The subject was asked to direct his/her gaze at the cued square during the entire five-second stimulation. The trial was initiated when the subject pressed a key on the keyboard after which the all the squares regained their color. During a trial, all squares were flickering, in accordance with their frequency/phase combination, by sinusoidally modulating their luminosities using the method described in [207]. Between trials, the subject was allowed to take a break.

3.2.3 *Recording*

EEG was recorded continuously (sampling speed 2048 Hz, common mode sense (CMS) referencing) using 32 active Ag/AgCl electrodes (BioSemi Active Two) placed according to the extended international 10-20 system. Additionally, six external electrodes were placed: two on the left and right mastoids, for further off-line re-referencing, and four around the eyes, one on the upper and lower side of the left eye (vertical), and one near the external canthus of each eye (horizontal), for electro-oculogram recording (EOG, bi-polar recording). Except for these external ones, all electrodes were mounted in the electrode cap that was placed on the subject's head. Conductive gel was applied in each of the electrode holes, as well as on the surface of the external electrodes to reduce electrode impedance. Prior to the main experiment, an EOG calibration session was performed to offline remove eye movements and blinks, using the method described in Croft & Barry [70].

3.2.4 *Processing*

The recordings were re-referenced offline from a CMS reference to the average of both mastoid signals and the EOG signal used to remove eye artifacts following the method of Croft and co-workers [70]. The corrected signals were bandpass filtered between 5 and 20 Hz using a 4th order Butterworth filter and then cut into five-second epochs, time-locked to the stimulation onset. Finally, the epochs were downsampled to 512 Hz, and labeled according to the color cued square. For each subject, 60 five-second epochs were extracted and stored for further analysis.

3.2.5 *Analysis*

3.2.5.1 *Time-domain approach*

In order to discriminate between the frequency-and-phase encoded targets, we adopt a time-domain approach [199, 203]: each epoch is cut into consecutive, non-overlapping and identical segments with lengths equal to a single period of stimulus frequency f (blue traces in Fig 3.2). As we are using frequencies of 12 and 15 Hz, we have two such lengths, 83 and 67 ms, respectively. Then, we compute averages (red traces in Fig 3.2) When the stimulus frequency of the target that is gazed at matches one of the assumed stimulus periods, the corresponding average trace will be periodic, else it will be (almost) flat.

3.2.5.2 *Beamforming*

The beamformer starts from an activation pattern (i.e., a template of the signal-of-interest) that represents the EEG response to a particular frequency-phase combina-

tion (see further on how activation patterns are constructed), and transforms it into a weight vector (i.e., a multivariate filter), so as to optimally isolate the targeted response from noise and possible non-target related activity, by taking into account the information contained in the covariance matrix estimated from the entire data. As the signals-of-interest differ among targets, each target has its own template with length equal to a single period of the target's stimulus frequency and thus also its own beamformer. The latter is applied then to an averaged segment of the same length. As the templates differ among targets, each target has its own template and thus also beamformer that is applied to an averaged segment with length equal to a single period of the target's stimulus frequency. The following explanation therefore applies to each target individually. Let matrix $\mathbf{A} \in \mathbb{R}^{m \times n}$ be the spatiotemporal activation pattern of a given frequency-phase combination, where m represents the number of electrodes and n the number of samples. Note that n depends on the segment length (given the sampling rate which is fixed), and thus on the target frequency (but not its phase).

While the beamformer was originally formulated as a spatial filter, we extend it to a spatiotemporal filter. We adopt the formulation of van Vliet and coworkers [319]. A Linearly Constrained Minimum Variance (LCMV) spatial beamformer $\mathbf{w}_{sp} \in \mathbb{R}^{m \times 1}$ minimizes the variance of the beamformer output $\mathbf{w}_{sp}^{\mathsf{T}}\mathbf{S}$:

$$\arg\min_{\mathbf{w}_{sp}} \mathbf{w}_{sp}^{\mathsf{T}}\mathbf{S}(\mathbf{w}_{sp}^{\mathsf{T}}\mathbf{S})^{\mathsf{T}} \Rightarrow \arg\min_{\mathbf{w}_{sp}} \mathbf{w}_{sp}^{\mathsf{T}}\mathbf{\Sigma}_{sp}\mathbf{w}_{sp}, \tag{3.1}$$

where $\mathbf{\Sigma}_{sp} \in \mathbb{R}^{m \times m}$ is the spatial covariance matrix of the EEG segment $\mathbf{S} \in \mathbb{R}^{m \times n}$. By adding the linear constraint:

$$\mathbf{a}_{sp}^{\mathsf{T}}\mathbf{w}_{sp} = 1, \tag{3.2}$$

where $\mathbf{a}_{sp} \in \mathbb{R}^{m \times 1}$ is the spatial activation pattern, we avoid trivial solutions of (3.1), and signals that are similar to $\mathbf{a}_{sp}$ will be mapped to a value close to 1, allowing for an easy measure of similarity. The solution of (3.1) under constraint (3.2) can be found using the method of Lagrange multipliers [310]:

$$\mathbf{w}_{sp} = \frac{\mathbf{\Sigma}_{sp}^{-1}\mathbf{a}_{sp}}{\mathbf{a}_{sp}^{\mathsf{T}}\mathbf{\Sigma}_{sp}^{-1}\mathbf{a}_{sp}}. \tag{3.3}$$

The spatial beamformer can be expanded to a spatiotemporal variant as follows. Let r be the number of segments, $\mathbf{X} \in \mathbb{R}^{r \times (mn)}$ a matrix where each row is obtained by concatenating the rows of a corresponding segment $\mathbf{S}_i$ ($i = 1..r$), $\mathbf{\Sigma} \in \mathbb{R}^{(mn) \times (mn)}$ the covariance matrix of $\mathbf{X}^{\mathsf{T}}$, and $\mathbf{a}^{\mathsf{T}} \in \mathbb{R}^{1 \times (mn)}$ a vector containing the concatenated rows of $\mathbf{A}$. The spatiotemporal LCMV beamformer $\mathbf{w} \in \mathbb{R}^{(mn) \times 1}$ with the linear constraint $\mathbf{a}^{\mathsf{T}}\mathbf{w} = 1$ can now be calculated as:

$$\mathbf{w} = \frac{\mathbf{\Sigma}^{-1}\mathbf{a}}{\mathbf{a}^{\mathsf{T}}\mathbf{\Sigma}^{-1}\mathbf{a}}, \tag{3.4}$$

and applied to the data as a simple weighted sum:

$$y = \mathbf{sw}, \tag{3.5}$$

where $\mathbf{s} \in \mathbb{R}^{1\times(mn)}$ indicates the concatenated rows of a segment $\mathbf{S}$.

Another way to obtain a spatiotemporal filter is to apply a spatial beamformer $\mathbf{w}_{sp} \in \mathbb{R}^{m\times 1}$ followed by a temporal beamformer $\mathbf{w}_t \in \mathbb{R}^{n\times 1}$. Let $\mathbf{B} \in \mathbb{R}^{r\times n}$ be the matrix containing the results of the spatial filter $\mathbf{w}_{sp}$ applied to the EEG segments $\mathbf{S}_i$:

$$\mathbf{B} = \begin{pmatrix} \mathbf{w}_{sp}^\mathsf{T}\mathbf{S}_1 \\ \mathbf{w}_{sp}^\mathsf{T}\mathbf{S}_2 \\ \vdots \\ \mathbf{w}_{sp}^\mathsf{T}\mathbf{S}_r \end{pmatrix}. \tag{3.6}$$

$\mathbf{\Sigma}_t \in \mathbb{R}^{n\times n}$, the covariance matrix of $\mathbf{B}^\mathsf{T}$, together with a temporal activation pattern $\mathbf{a}_t \in \mathbb{R}^{n\times 1}$, allows for a temporal beamformer to be obtained as follows:

$$\mathbf{w}_t = \frac{\mathbf{\Sigma}_t^{-1}\mathbf{a}_t}{\mathbf{a}_t^\mathsf{T}\mathbf{\Sigma}_t^{-1}\mathbf{a}_t}. \tag{3.7}$$

By consecutively applying the beamformers constructed in (3.3) and (3.7) to the segment under consideration, a spatiotemporal beamformer is obtained:

$$y = \mathbf{w}_{sp}^\mathsf{T}\mathbf{S}\mathbf{w}_t. \tag{3.8}$$

We further refer to (3.5) as the spatiotemporal beamformer (stBF) and to (3.8) as the chained beamformer (chBF).

3.2.5.3 *Activation Patterns*

Since each frequency-phase combination is expected to evoke a different EEG response, activation patterns need to be calculated for each target i ($\in [1..4]$). Let $\boldsymbol{E}_i \in \mathbb{R}^{m\times n\times r}$ be the target epochs (i.e., the epochs during which the subject was focussing on target i). Each epoch in $\boldsymbol{E}_i$ is then cut into segments, using the time-domain approach described above, where frequency f is the stimulation frequency of target i. The spatiotemporal activation pattern $\mathbf{A}_{st[i]}$ is then calculated by averaging the obtained segments.

As spatial activation pattern for target i, the column of $\mathbf{A}_{st[i]}$ for which channel Oz reaches its maximal value is selected:

$$\mathbf{a}_{sp[i]} = \mathbf{A}_{st[i]}[*, t] \tag{3.9}$$

where

$$t = \arg\max_t \mathbf{A}_{st[i]}[Oz, t]. \tag{3.10}$$

Channel *Oz* was chosen since it can be expected that the SSVEP response is strongest at this channel.

To calculate the temporal activation pattern $\mathbf{a}_{t[i]}$ for square i, all epochs in $\boldsymbol{E}_i$ are spatially filtered using a beamformer that was constructed with $\mathbf{a}_{sp[i]}$ as activation pattern. The covariance matrix used for constructing this beamformer is also estimated on $\boldsymbol{E}_i$. The spatially filtered target epochs are then cut into segments using the time-domain approach where the frequency f is set to the stimulation frequency of target i. The temporal activation pattern is given by the average of these segments. The pseudo-code of this algorithm is shown in Algorithm 1.

Algorithm 1 Calculate Activation Patterns

for $i := 1 .. 4$ **do**
  $f_i \leftarrow$ stimulation frequency of target i
  $\boldsymbol{E}_i \leftarrow$ target epochs for target i
  Cut epochs in $\boldsymbol{E}_i$ into segments, using f_i
  $\mathbf{A}_{st[i]} \leftarrow$ average segments
  $\mathbf{a}_{sp[i]} \leftarrow$ select column of $\mathbf{A}_{st[i]}$, using equations (3.9) and (3.10)
  Build beamformer with $\mathbf{a}_{sp[i]}$ and $\boldsymbol{E}_i$
  Filter all epochs in $\boldsymbol{E}_i$ with beamformer
  Cut filtered epochs into segments, using f_i
  $\mathbf{a}_{t[i]} \leftarrow$ average segments
end for

3.2.5.4 *Classifiers*

Training the beamformer-based classifier involves the construction of four beamformers and 'training' four binary (one-vs-all) sub-classifiers, one for each target. The activation patterns and the beamformers were constructed as described earlier in this section. The feature space of the sub-classifiers is given by the output of the beamformers and is therefore one-dimensional. A threshold is applied to this output in order to discriminate between the target-(positive class) and the non-target (negative class) epochs (binary classification). Using a stratified four-fold cross-validation (i.e., in each fold, all labels occur equally frequent) for the training data, we determined for each sub-classifier the optimal threshold by using a Receiver Operating Characteristic (ROC) analysis. (An ROC curve shows the binary classification performance when varying the threshold.) Since the maximum classification performance could be reached for multiple thresholds (equal ROC points or points on the maximal iso-performance line), we took the median of those thresholds as final threshold.

Classification of an epoch is performed by independently applying each sub-classifier (and its necessary preprocessing, i.e., cutting into segments) to obtain four binary predictions and scores. (Fig 3.2) The binary prediction is based on the threshold of the

respective sub-classifier and the score is equal to the y-value after applying the respective beamformer. From the sub-classifiers that return a positive prediction, the one having the highest score is taken as winner. In case of no positive predictions, the winner is determined by the sub-classifier returning the highest score.

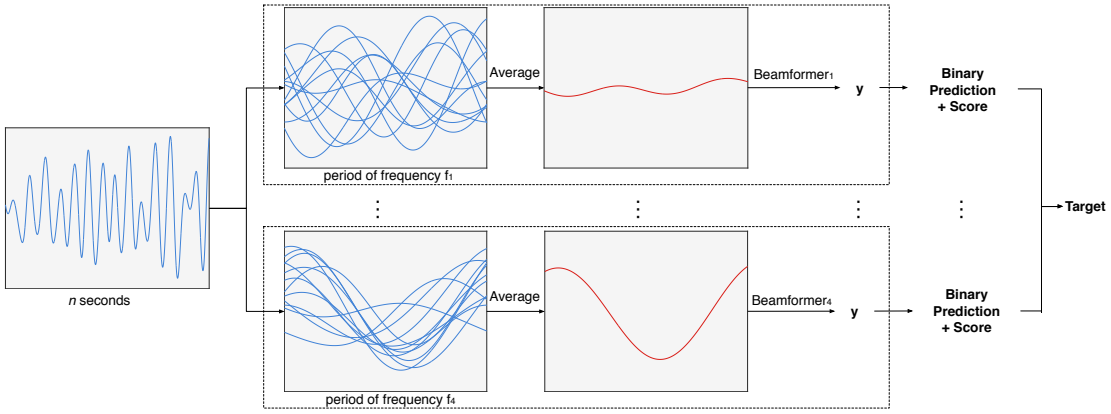

Figure 3.2: Concept behind the classification of a single epoch. Note that the actual analysis is done on a spatiotemporal epoch, involving multiple electrodes.

To estimate the performance of the beamformer-based classifier, we apply a stratified five-fold cross-validation scheme. Because of the relatively high inter-subject variability of EEG responses to SSVEP stimulation [303], the analysis is run for each subject separately.

We compare our beamformer to an extension of the popular Canonical Correlation Analysis (CCA) method [221], with the number of harmonics set to three. To the best of our knowledge, when using short time windows in a frequency-phase SSVEP setting, the most reliable classification performance has been reported for the extended CCA method.

3.2.5.5 *Parameter sensitivity*

We assess the performance of the classifiers with different epoch lengths, from 250 ms to 3 s in steps of 250 ms. For each epoch length l, we select a window from 0.120 to 0.120+l seconds from the original five-second epochs, and run the analysis with these reduced epochs. With longer epoch lengths, more segments can be extracted, leading to more reliable and easier to discriminate averages (see also the discussion section). The first 100-150 ms of each trial corresponds to the latency of the brain to SSVEP stimulation [73, 74]. Including this in our analysis might lower performance, hence, we chose to start from 120 ms post stimulus-onset. Note that this was also used in the Nakanishi study we consider in our comparison [221]

Since SSVEP is a visual stimulation paradigm, it can be expected that primarily electrodes over the occipital pole are relevant. However, including channels surrounding

the occipital cortex might provide information about noise sources and thus lead to a more accurate filter [112]. On the other hand, a smaller number of channels reduces the dimensionality of the spatiotemporal filter, which is expected to increase performance (less parameters to be estimated, cf., curse of dimensionality [248, 272]). To test the influence of the number of channels, we additionally run the analysis using a reduced electrode setup, one with 10 channels (Ch_{env} = {*Fz*, *Cz*, *Pz*, *P3*, *P4*, *PO3*, *PO4*, *O1*, *Oz* and *O2*}) and one with only three occipital channels (Ch_{occ} = {*O1*, *Oz* and *O2*}). The complete 32-channel setup will be referred to as Ch_{full}.

In addition to the sampling rate of 512 Hz, we also ran the analysis using further downsampled epochs, and assessed their influence on the prediction performance. Lower sampling rates lead to less samples per segment and, thus, also to a lower dimensionality of the covariance matrices used when constructing the beamformers. The downsampling rates tested are 256 and 128 Hz, and the number of samples per segment are summarized in table 3.1.

Table 3.1: Segment lengths (in samples) for different frequencies. T corresponds to one period of a given frequency. Segments are input to the beamformers.

Sample Rate (Hz)	**T[12Hz] (samples)**	**T[15Hz] (samples)**
512	42	34
256	21	17
128	10	8

3.2.5.6 *Statistics*

Significance levels are calculated using a two-sided Wilcoxon Rank Sum Test. P-values below 0.05 are considered as significant.

3.3 RESULTS

3.3.1 *Activation Patterns*

The activation patterns for one subject are shown in Fig 3.3. The spatial activation patterns confirm that occipital electrodes are most informative, and that parietal and parietal-occipital electrodes also can contribute to the SSVEP detection.

When comparing the temporal patterns of all subjects for a given target (Fig 3.4), it is clear that they are very subject dependent. Hence, activation patterns should be determined for each subject individually rather than for a population if one is not willing to sacrifice classification performance. Therefore, we will build subject-specific beamformers and also assess their classification performance in this way.

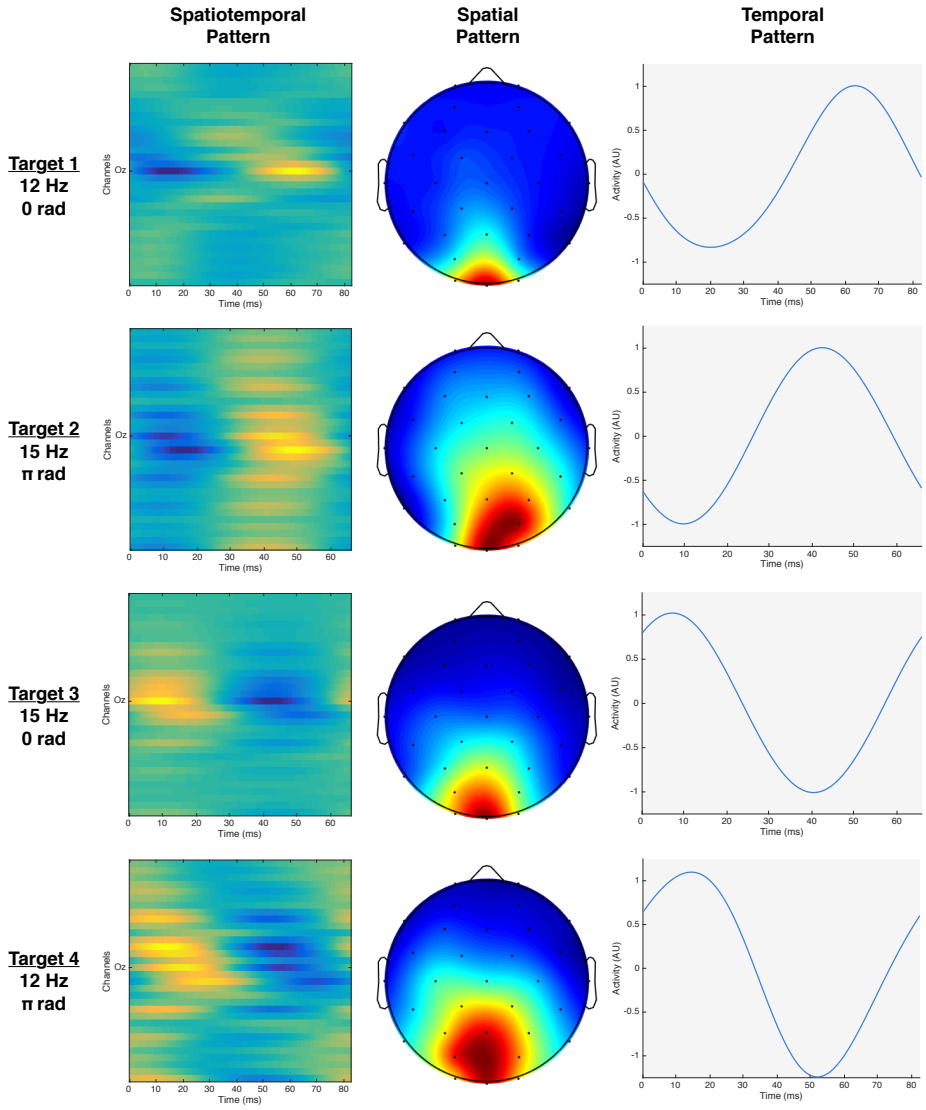

Figure 3.3: Activation patterns for subject 6. Each row corresponds to a different target. The left column shows the spatiotemporal activation patterns $\mathbf{A}_{st[i]}$ that are used for building spatiotemporal beamformers. The middle and right columns show the spatial ($\mathbf{a}_{sp[i]}$) and temporal activation patterns ($\mathbf{a}_{t[i]}$) that are employed to build the chained beamformer

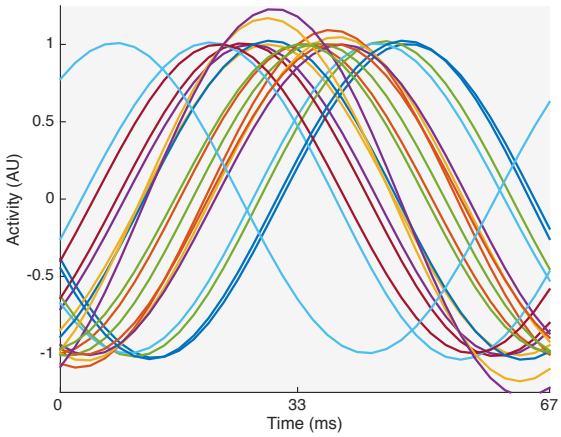

Figure 3.4: Temporal activation patterns for all subjects for target 2. Each trace corresponds to the temporal activation pattern of one subject.

3.3.2 *Classification*

Fig 3.5 shows the performance of the beamformers for the three channel sets, and supplementary material S1 and S2 Tables summarize the statistical significance. The chained beamformer performs best using Ch_{env} on short epoch lengths (max. 1 s). Even though the differences are not statistically significant, Ch_{occ} has a lower median performance for almost all trial lengths. With stBF, both reduced channel sets significantly outperform the full channel set for epochs shorter than 2.25 seconds. Ch_{env} reaches a median accuracy of 100% for 1.25 s epoch lengths, while Ch_{occ} needs an additional 0.5 seconds to achieve similar (median) performance. Only with a very small epoch length (250 ms), Ch_{env} performs significantly worse than Ch_{occ}.

For Ch_{env}, the effect of downsampling is shown in Fig 3.6 and supplementary material S3 and S4 Tables. For both beamformers, there are only minor effects. None of the differences with the chBF are significant. The only significant differences with stBF are for an epoch length of 250 ms. However, in that case the median performance does not reach 70%, which is often taken as the minimum for reliable communication [42, 68, 165, 166].

To compare the beamformers with the extended CCA method, a sampling rate of 512Hz and Ch_{env} was used. Fig 3.7 shows the prediction performances, and the statistical significance is given in supplementary material. Except for the shortest epoch length, our beamformer-based classifiers outperform the CCA alternative. The stBF-variant is significantly better than the CCA-alternative for short epoch lengths ($\leq$1.25 s). It is also clear that the variance of both beamformers is smaller than that of the CCA alternative. Note that the performance of the extended CCA method on our data is comparable to the original study.

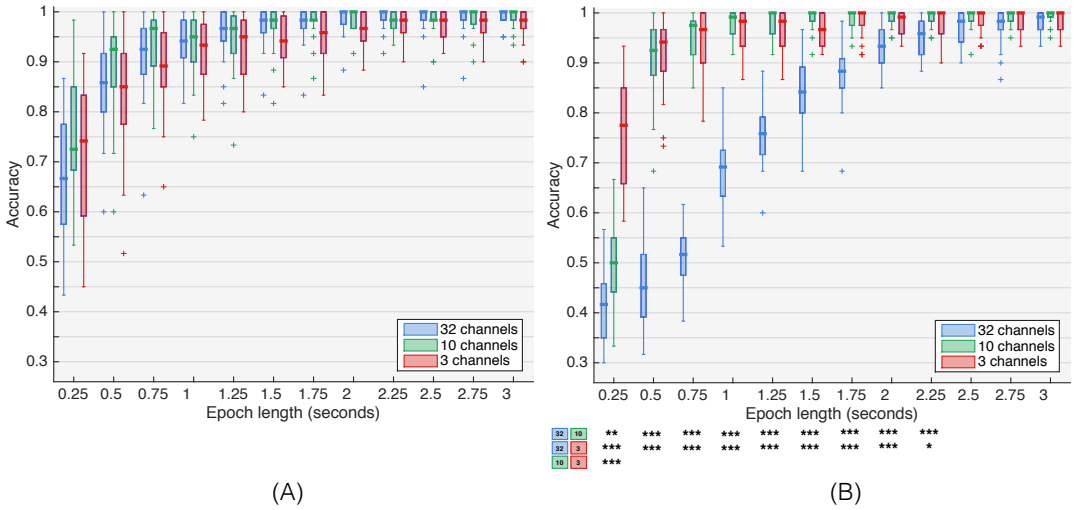

Figure 3.5: Influence of channel set on beamformer performance. (A) chained beamformer, (B) spatiotemporal beamformer. Stars indicate significance levels based on Wilcoxon Rank Sum Test: *($p < 0.05$), **($p < 0.01$), ***($p < 0.001$)

The accuracies achieved by the four sub-classifiers during the analysis of the performance reported in Fig 3.7 are shown in supplementary material S1 and S2 Figs, for the stBF- and chBF-based classifier respectively. For all targets, the sub-classifier accuracies are approximately equal. However, target 4 (i.e., 15Hz and π rad) has consistently the lowest detection accuracy for both beamformers.

Finally, Fig 3.8 shows two confusion matrices of the stBF classifier of Fig 3.7 for epoch lengths of 0.5 and 1 second. We observe that for target 4 there are more misclassifications (last column in each matrix) than for the other targets and that there are less misclassifications between targets of opposite phase than between targets of different frequencies (*e.g.*, in Fig 3.8(A), compare predicted target 1 vs. actual target 4 (1.67%) and vs. actual target 2 (2.33%)) .

3.4 DISCUSSION

3.4.1 *Effect of combining frequency and phase encoding on SSVEP*

Generally, the SSVEP signal has an oscillatory waveform with the same temporal frequency and phase as the flickering stimulus and its harmonics [257] and is considered to be evoked by the electrophysiological activity of large synchronized neuronal populations in early visual cortex [250]. The feasibility of identifying targets from spatially disparate (in visual angle or screen coordinates) flickering stimuli is supported by several lines of evidence. Firstly, as the gaze is directed, the attended stimulus is present

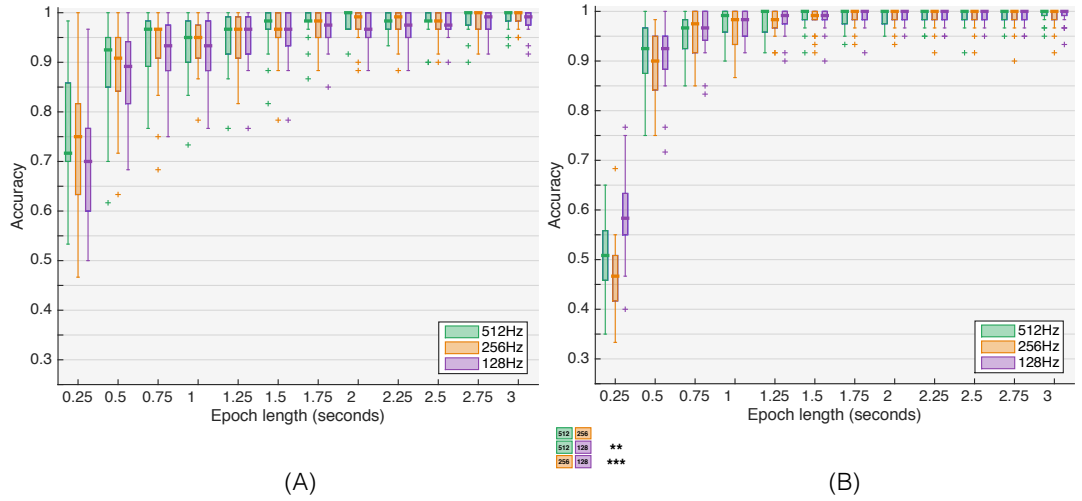

Figure 3.6: Influence of downsampling on beamformer-based classification performance. (A) chained beamformer, (B) spatiotemporal beamformer, both for channel set Ch_{env}.

in the fovea whereas the unattended targets are in the periphery of the subject's visual field. As early visual areas are retinotopically organized, disparate visual stimuli activate disparate anatomical locations and vice-versa, as clearly evidenced by several neuroimaging studies[39, 253, 311]. When using neuroimaging techniques or EEG in combination with inverse mapping techniques, it was shown that flickering stimuli at different locations in the visual field activate different SSVEP generators in the early visual system [75].

A second aspect is the cortical magnification effect: a disproportionately large amount of visual cortex is allotted to processing foveal input compared to more peripheral input [69, 294]. As a result, the electrophysiological response evoked by a stimulus increases when becoming closer to the center of the visual field [294]. This implies that the amplitude of a foveated flickering stimulus is not going to be influenced by an another flickering stimulus when the visual angle that separates them is large enough [359]. When flickering targets are in close proximity, modulatory effects in the recorded EEG signal can be expected, in addition to an effect of attention. This has been studied by Fuchs and co-workers [92]. When the subject is focusing and attending one flickering target, and ignoring the other one, and when the visual angle that separates these targets is smaller than 4°, then the SSVEP amplitude of the attended target is unaltered with a small SSVEP amplitude of the unattended target added to it (co-amplification). Hence, when the flickering frequencies of those two targets are identical, but their phases in opposition (180° phase difference), and their separating angles much smaller than 4°, then the SSVEP amplitude of the attended target will be demoted or even largely cancelled. In our case, te SSVEP responses to attended tar-

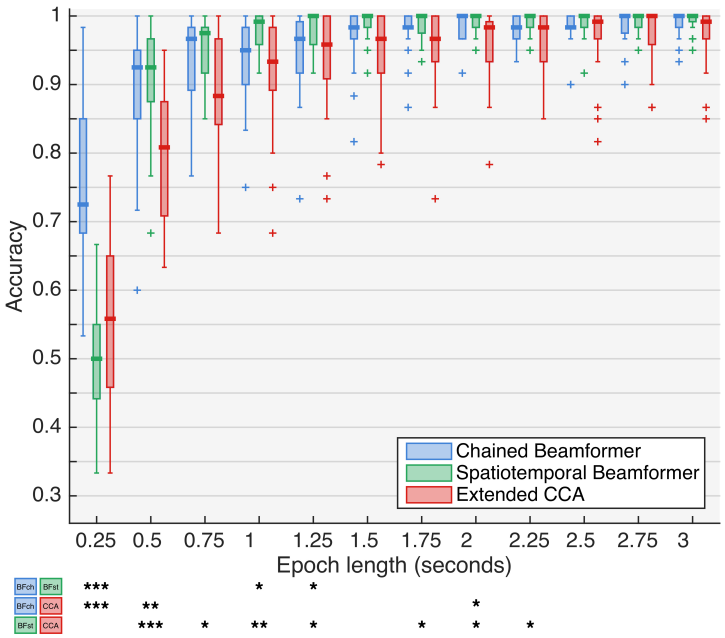

Figure 3.7: Performance of different types of classifiers. Channel set Ch_{env} and no downsampling was used. Stars indicate significance levels, based on a Wilcoxon Rank Sum Test: *($p < 0.05$), **($p < 0.01$), ***($p < 0.001$)

gets are not canceled by targets with identical frequencies but opposite phases (target 1 vs. 4 and target 2 vs. 3) because their separating angles are much larger ($\sim 6.2°$). On the other hand, as the separating angles between targets flickering with different frequencies is much smaller ($\sim 4.4°$), we observe a co-amplification effect in the EEG responses to the attended targets (Fig 3.9). This is also reflected in the confusion matrices (Fig 3.8) by a much larger degree of misclassification between targets with different flickering frequencies than with opposite phases.

3.4.2 *Activation Patterns*

The activation patterns confirm that the SSVEP response is mostly present in the occipital regions, however using only those channels does not yield maximum performance. While surrounding channels have a smaller SSVEP response, they do contain information about noise sources that might contaminate the occipital signals [112]. By taking these channels into account, performance improves. However, increasing the number of channels also increases the dimensionality of the beamformer and the size of the (training) data set needed to accurately estimate the covariance matrix. [248, 272]

The beamformer approach developed in this study constructs an activation pattern for each individual subject, which calls for a training session for each subject. Indeed,

ACTUAL \ PREDICTED	1	2	3	4
1	**92.00**	2.00	1.67	4.33
2	2.33	**92.67**	0.33	4.67
3	2.67	0.00	**92.00**	5.33
4	1.67	4.33	4.67	**89.33**

(A)

ACTUAL \ PREDICTED	1	2	3	4
1	**97.33**	0.00	1.00	1.67
2	0.67	**97.00**	0.00	2.33
3	1.00	0.00	**97.67**	1.33
4	0.33	0.33	1.33	**98.00**

(B)

Figure 3.8: Confusion matrices of the stBF from Fig 3.7. The numbers on the diagonal indicate the predictive accuracy (in %) of the stBF-classifier for each target. The values displayed are the average of the confusion matrices of all subjects. (A) For an epoch length of 0.5 seconds. (B) For an epoch length of 1 second. Targets 1 and 4 flicker at 12 Hz but with opposite phase, targets 2 and 3 flicker at 15 Hz but with opposite phase.

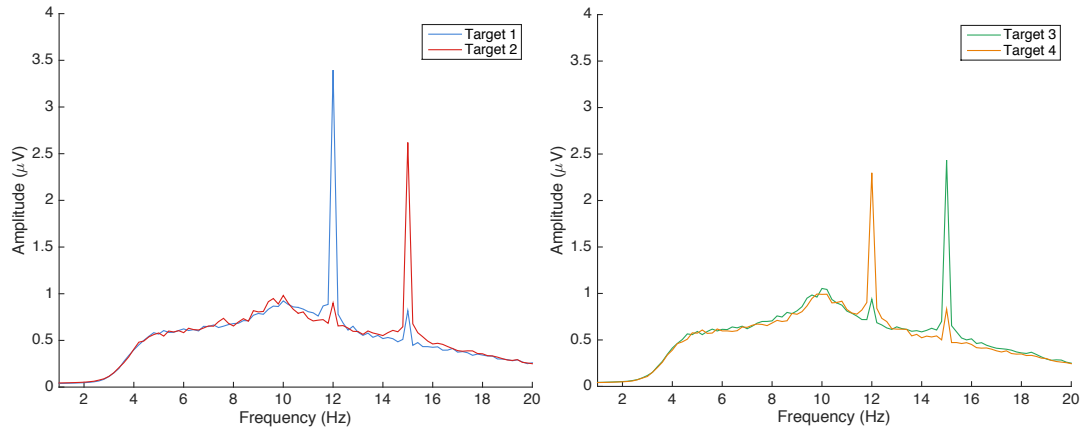

Figure 3.9: Co-amplification effect. EEG frequency spectrum, averaged over all subjects, revealing co-amplification effect: the peripheral target flickering at a different frequency ($\sim$ 4.4° separating angle) adds a small amplitude to the SSVEP signal of the attended target. (A) For targets 1 and 2, flickering at 12 and 15 Hz, respectively. (B) For targets 3 and 4, flickering at 15 and 12 Hz, respectively.

the temporal responses to phase-based SSVEP stimulation were observed to vary considerably among subjects (Fig 3.4), hindering the construction of one activation pattern for the entire population. On the other hand, when individuating the beamformer, it can take into account subject- and session-dependent noise sources, which has a positive effect on performance. In addition, when comparing our beamformers with extended CCA, we observed for the beamformer-based classifiers not only a better performance but also a smaller interquartile range (IQR) over the subject population. This indicates that, although they are developed per subject, the beamformer-based classifiers yield a more stable performance across subjects. While both the beamformer and the extended CCA approach use prior information (targets, subjects), the beamformer takes into account the possible presence of non-target activity and structured noise embedded in the trials by using the covariance matrix, whereas the CCA method only extracts target trials to estimate canonical correlations. We therefore advocate that the beamformer is more efficient in extracting relevant information, leading to a better performance.

3.4.3 *Frequency resolution*

Our time-domain analysis of SSVEP signals is influenced by the frequencies used for stimulating the targets. If the difference in segment lengths between targets increases then less segments will be needed to accurately discriminate between a waveform and a 'flat' response. Fig 3.10 shows the effect of epoch lengths for a 15 Hz SSVEP response at channel *Oz* when assuming targets with frequencies (12, 13, 14, and 15 Hz). It is clear that longer epoch lengths are needed when discriminating targets with similar stimulation frequencies. Indeed, for 250 ms, one can easily exclude the 12 Hz response from the list of possible target responses, but longer segments are needed to discriminate between the 14 and 15 Hz responses.

3.5 CONCLUSION

In this study, we have introduced beamforming as a new method for simultaneous frequency and phase detection in SSVEP-based BCI application. We have shown that our method outperforms an extension of CCA which has been touted as the best method for targets encoded by individual frequency-phase combinations, even for 1.25 sec epoch lengths.

SUPPLEMENTARY MATERIAL

Supplementary material available at https://doi.org/10.1371/journal.pone.0159988

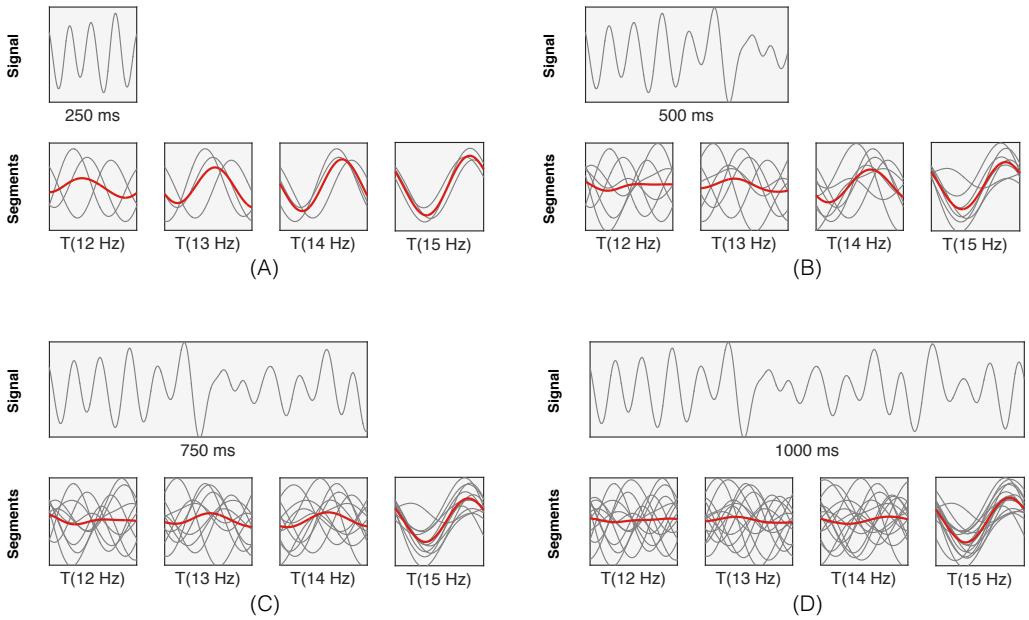

Figure 3.10: Frequency resolution of the time-domain analysis. A signal from channel Oz in response to a 15 Hz stimulus, and its segments with lengths corresponding to one period (T) of 12, 13, 14 and 15 Hz. Signal length are (A) 250 ms, (B) 500 ms, (C) 750 ms and (D) 1000 ms.

4

CODE-MODULATED VISUAL EVOKED POTENTIALS USING FAST STIMULUS PRESENTATION AND SPATIOTEMPORAL BEAMFORMER DECODING

This chapter has been published as:
B. Wittevrongel, E. Van Wolputte and M.M. Van Hulle (2017) *Code-modulated visual evoked potentials using fast stimulus presentation and spatiotemporal beamformer decoding.* Scientific Reports 7, 15037

When encoding visual targets using various lagged versions of a pseudorandom binary sequence of luminance changes, the EEG signal recorded over the viewer's occipital pole exhibits so-called code-modulated visual evoked potentials (cVEPs), the phase lags of which can be tied to these targets. The cVEP paradigm has enjoyed interest in the brain-computer interfacing (BCI) community for the reported high information transfer rates (ITR, in bits/min). In this study, we introduce a novel decoding algorithm based on spatiotemporal beamforming, and show that this algorithm is able to accurately identify the gazed target. Especially for a small number of repetitions of the coding sequence, our beamforming approach significantly outperforms an optimised support vector machine (SVM)-based classifier, which is considered state-of-the-art in cVEP-based BCI. In addition to the traditional 60 Hz stimulus presentation rate for the coding sequence, we also explore the 120 Hz rate, and show that the latter enables faster communication, with a maximal median ITR of 172.87 bits/min. Finally, we also report on a transition effect in the EEG signal following the onset of the stimulus sequence, and recommend to exclude the first 150 ms of the trials from decoding when relying on a single presentation of the stimulus sequence.

4.1 INTRODUCTION

Among the gamut of brain-computer interfacing (BCI) paradigms [223], the code-modulated visual evoked potential (cVEP) has been reported to yield one of the highest information transfer rates (ITRs) [32]. The cVEP paradigm defines a binary sequence of high and low stimulus intensities with unequal duty cycles, called the 'code', and uses for each selectable target a unique lagged version of this code [32, 110, 294]. As coding sequence, the m-sequence [362] is often chosen because of its favourable autocorrelation properties [32], amongst other properties [100]. M-sequences have also been applied in other fields such as fMRI [44] and sensor technology [265]. Albeit rarely adopted, as an alternative to m-sequences, a periodic pseudorandom binary code has been described for cVEP [220].

As far as we are aware, only one group previously investigated the application of a faster stimulus presentation for cVEP (i.e., higher than the traditional 60 Hz) [8–11]. The encoding sequence was presented to the subject by LEDs at a carrier frequency of 40 Hz controlled by an Arduino micro-controller, which would compare to a 80 Hz screen refresh rate. The authors investigated the effect of stimulation colour [8, 9], classifier kernels [11] and filter bands [10], but could not achieve a higher decoding performance for the faster stimulus rate. In one of their studies [11], they report on the decoding performance with an increasing number of m-sequence repetitions, but did not consider the implication on the performance in terms of ITR.

Although cVEP has achieved among the highest ITR, the paradigm is considerably less studied compared to other visual BCI paradigms such as the P300 event-related potential (ERP) and the steady-state visual evoked potential (SSVEP) (see the review of Gao and coworkers [94] for reference). Traditionally, cVEPs are decoded from electroencephalography (EEG) using a template matching algorithm [32], canonical correlation analysis (CCA) [8] or a combination [33, 327]. BCIs adopting these algorithms have been proven successful in online settings, including EEG-based spelling applications [289] and robot control [138, 259], and have also been applied in an intracranial EEG (iEEG) setting [139]. In recent research, the support vector machine (SVM) has been shown to identify targets more accurately than the traditional decoding algorithms [9], with a linear kernel achieving in the highest accuracy [11].

Recently, a spatiotemporal extension of the beamforming algorithm has been introduced in EEG-BCI and shown to yield promising results with EEG signals that have consistent spatial and temporal characteristics, such as the N400- [319] and P300 [331] ERPs. With SSVEP, the combination of the spatiotemporal beamformer with a time-domain analysis [199, 203] proved successful in both offline [332] and online [333] settings.

The goal of this study is to assess the performance of the spatiotemporal beamforming algorithm for target identification when using cVEP-based encoding, and to com-

pare the performance for both traditional (60 Hz) and high-speed (120 Hz) stimulus presentations.

4.2 METHODS

4.2.1 *Subjects*

Seventeen subjects with normal or corrected-to-normal vision participated in the experiment (14 female, 13 right handed, aged 22.35 $\pm$ 2.9, ranging from 18 to 30 years old). Prior to the experiment, the subjects read and, when they agreed, signed an informed consent form approved by the ethical committee of our university hospital UZ Leuven. All subjects received a monetary reward for their participation. This study was carried out in accordance with the relevant guidelines and regulations.

4.2.2 *Experimental design*

The interface consisted of 32 circular white targets (4 cm diameter, 2 cm vertical and horizontal inter-target distance) that follow an m-sequence stimulation paradigm (see further) and that were overlaid with static (i.e., non-flickering) grey letters or numbers arranged in a matrix (Figure 4.1).

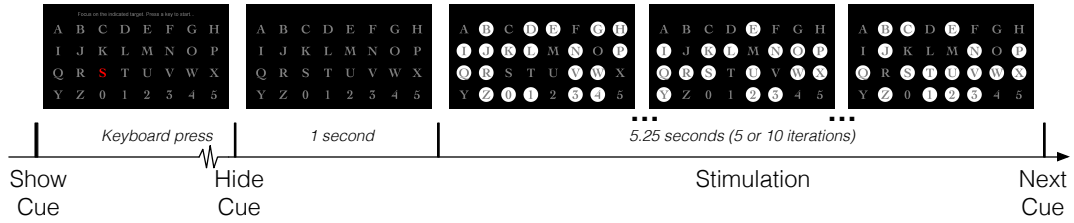

Figure 4.1: Time-course of one trial during the experiment.

The interface was presented on a ViewPixx-EEG monitor (24 inch, native 120 Hz refresh rate, resolution of 1920 $\times$ 1080, VPixx Technologies, Canada). The subjects were seated approximately 60 cm from the monitor. At this distance, the circular targets spanned a visual angle of approximately 3.8°, with an inter-target angle of 1.9°. The experiment was implemented in Matlab, using the Psychophysics Toolbox extensions [38, 154, 236].

The following m-sequence of length of 63 was used to encode the targets:

000100001011001010100100111100000110111001100011101011111101101

whereby targets were lagged by integer multiples of two frames. We adopted the equivalent-neighbours strategy used in other studies [33, 289], but decided not to implement the additional outer border in order to reduce visual demand.

Figure 4.1 visualises the experimental interface during one trial. A trial started with the presentation of a cue (i.e., one target shown in red). Subjects were asked to redirect their gaze to the cued target and to press a button to start the stimulation. After that, all targets were hidden (with the characters still shown in grey) for one second, followed by the stimulation phase during which all targets adopted their unique lagged m-sequence and repeated this sequence either 5 or 10 times (depending on the session, see further). To avoid visual fatigue and boredom, subjects were allowed to take breaks between trials.

Unlike traditional 60 Hz monitors, the monitor used in our experiment had a refresh rate of 120 Hz, which allowed us to experiment with high-speed presentations of the coding sequence. The full experiment consisted of two sessions. In one session, S_{120}, the stimulus presentation followed the screen refresh rate. In the other session, S_{60}, we simulated the stimulation as it would be presented on a 60 Hz screen by presenting each entry of the m-sequence for two frames before moving to the next entry. In each trial of S_{120} and S_{60}, the m-sequence was repeated 10 and 5 times, respectively. In both sessions, the stimulation duration per trial was 5.25 seconds, and all targets were cued 5 times in pseudorandom order, leading to a total of 160 ($= 32 \times 5$) trials per session.

The two sessions were counterbalanced across subjects: 9 of the 17 subjects started with S_{60}, while the other 8 performed S_{120} first. Table 4.1 summarises the details of the two sessions.

4.2.3 *Recording*

EEG was recorded continuously using a SynampsRT device (Compumedics Neuroscan, Australia) operating at a sampling rate of 2000 Hz with 32 active Ag/AgCl electrodes covering the parietal and occipital poles, where consistent activations in response to cVEP stimulation are expected [9, 33]. The ground (GND) and reference (REF) electrodes were located at FPz and AFz, respectively (Figure 4.2). Conductive gel was applied at each electrode site and impedances were kept below 2 kΩ.

4.2.4 *Preprocessing*

The raw signal was re-referenced offline to the average of both mastoids signals (TP9 and TP10) and filtered between 4 and 31 Hz using a 4th order Butterworth filter, in order to attenuate the presence of artefacts such as slow drifts due to electrode gel expiration and sweat, low frequency oscillations due to electrode movements, high-frequency extraphysiologic noise, and powerline interference. The EEG was then cut into 5.25-second epochs starting from the onset of the stimulation, and labeled with the corresponding cued target. Finally, the epochs of S_{60} and S_{120} were downsampled to 100 Hz and 200 Hz, respectively, and stored for further analysis. The difference in downsampling rate was included to obtain a fair comparison between the classification

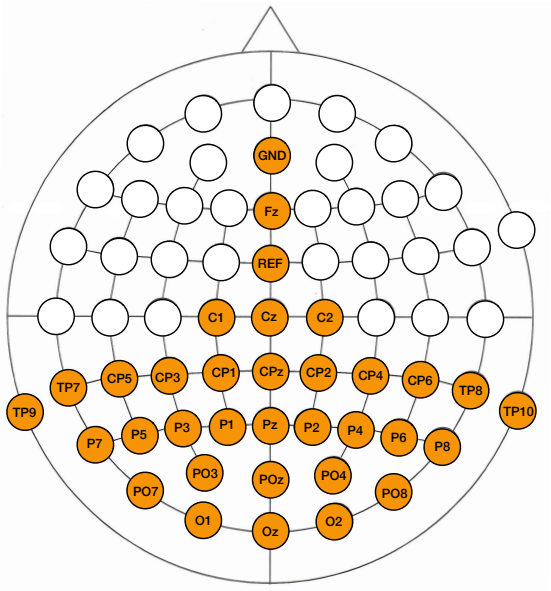

Figure 4.2: Locations of the 32 electrodes used during the experiment.

results (each repetition of the m-sequence at both the traditional and faster stimulus rate has an equal number of samples, see Table 4.1). For each subject and session, 160 labeled epochs were extracted and saved.

Session	Stimulation			Analysis	
	stimulus presentation rate	m-sequence repetitions per trial	trial duration	downsampling	samples per segment
S_{60}	60 Hz	5	5.25 s	100 Hz	105
S_{120}	120 Hz	10	5.25 s	200 Hz	105

Table 4.1: Stimulation and analysis details of both sessions. For the faster stimulation rate, the downsampling rate is doubled, leading to an equal number of samples in the segments of both sessions. Note that a segment corresponds to the EEG response elicited by one full presentation of the m-sequence.

4.2.5 *Classification*

Target identification was achieved using a classifier based on the linearly-constrained minimum-variance (LCMV) spatiotemporal beamformer [319]. This recent extension of the original spatial beamformer estimates the contribution of an a-priori specified activation pattern (i.e., a template, a signal of interest) to the current input. It has been shown that LCMV beamforming is a special case of Minimum Variance Distortionless Response (MVDR) beamforming [287], introduced to improve the robustness of the

latter [218]. The EEG responses to the stimuli of interest are not only confluenced by ongoing brain activity but can also be modulated by the subject's attention level, motivation and fatigue. The LCMV beamformer in an EEG context has shown to be effective as spatial filter for ERP detection [306] and source localisation for studying source connectivity [25, 121, 307], and its spatiotemporal extension has shown effective for ERP analysis [319] and as target identification algorithm in BCI settings [331–333].

Since each target elicits a different brain response (cf. unique lags of the m-sequence), each target evokes an unique EEG activation pattern, and training the classifier thus involves the estimation of 32 activation patterns, each used to construct a beamformer tailored to a specific target. The training and classification procedures for both the beamformer- and SVM-based classifier are depicted in Figure 4.3.

4.2.5.1 *Beamforming*

The activation patterns and the beamformers (one for each target) were calculated from the training data $\boldsymbol{T}_{training} \in \mathbb{R}^{m \times t \times l}$, where m is the number of channels, t is the number of samples and l is the number of epochs, as follows. For each epoch in $\boldsymbol{T}_{training}$, a maximal number of c-second consecutive non-overlapping segments were extracted, where c represents the time needed to display one complete m-sequence. Let $\boldsymbol{S} \in \mathbb{R}^{m \times n \times r}$ be all r segments extracted and $\boldsymbol{S}_i \in \mathbb{R}^{m \times n \times k}$ be the segments from $\boldsymbol{S}$ in response to the cued target $i \in [1..32]$, with n the number of samples per segment and k the total number of segments extracted for target i. Note that, while the m-sequences of S_{120} only span half the time ($c = 0.525$ s) compared to S_{60} ($c = 1.05$ s), their sampling rate is doubled so that the segments obtained from epochs of both S_{60} and S_{120} have the same number of samples.

The spatiotemporal activation pattern $\mathbf{A}_i \in \mathbb{R}^{m \times n}$ for target i was then obtained as the average of all k segments from $\boldsymbol{S}_i$. The spatiotemporal beamformer $\mathbf{w}_i \in \mathbb{R}^{(mn) \times 1}$ for target i was calculated as an LCMV beamformer as follows: let $\mathbf{E} \in \mathbb{R}^{r \times (mn)}$ be the matrix where each row is obtained by concatenating the rows of a corresponding sequence $\boldsymbol{S}[*, *, r]$, $\boldsymbol{\Sigma} \in \mathbb{R}^{(mn) \times (mn)}$ the covariance matrix of $\mathbf{E}$, and $\mathbf{a}_i^\intercal \in \mathbb{R}^{1 \times (mn)}$ a vector containing the concatenated rows of $\mathbf{A}_i$. The LCMV beamformer under constraint $\mathbf{a}_i^\intercal \mathbf{w}_i = 1$ can be calculated using the method of Langrage multipliers [310]:

$$\mathbf{w}_i = \frac{\boldsymbol{\Sigma}^{-1} \mathbf{a}_i}{\mathbf{a}_i^\intercal \boldsymbol{\Sigma}^{-1} \mathbf{a}_i}, \tag{4.1}$$

and applied to the data as a simple weighted sum: $y_i = \mathbf{s}\mathbf{w}_i$, where $\mathbf{s} \in \mathbb{R}^{1 \times (mn)}$ indicates the concatenated rows of an input segment $\mathbf{S}_{in} \in \mathbb{R}^{m \times n}$.

In our study, the covariance matrix $\boldsymbol{\Sigma}$ was estimated using Matlab's (2015a) *cov* function and was inverted using the *pinv* function, which calculates the Moore-Penrose pseudoinverse, to account for possible singularity of $\boldsymbol{\Sigma}$.

In some studies, a single activation pattern $\mathbf{A}_1$ was calculated based on the EEG response to target 1, and the activation pattern $\mathbf{A}_i$ of target i was constructed as a

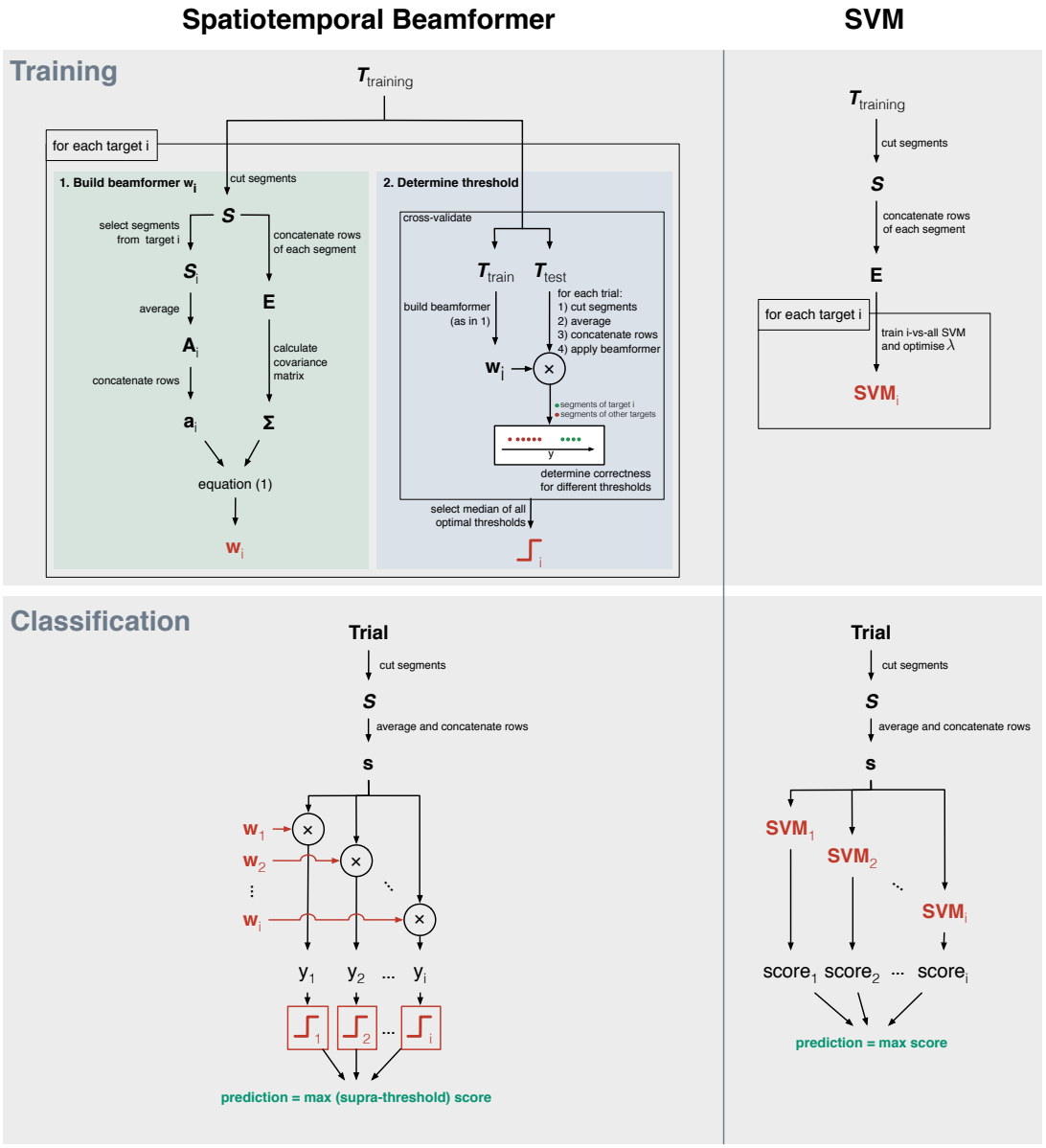

Figure 4.3: Visual representation of the training and classification procedure for the beamformer- and SVM-based classifier.

circular-shifted version of $\mathbf{A}_1$ (following the phase difference between the m-sequences of targets 1 and i) [32, 33]. However, given the availability of training data for each target, we opted to calculate the activation patterns for each target independently. In this way, discontinuities introduced by the circular shift were avoided and minor variations between templates were taken into account, leading to more accurate beamformers.

4.2.5.2 *Classifier*

In addition to building a beamformer for each target, a threshold was determined for each target in order to classify segments (in a one-vs-all fashion) into target-(positive class) and non-target (negative class). The threshold for each target was optimised via a Receiver Operating Characteristic (ROC) analysis [29, 177], using an additional 4-fold cross-validation on the training data (3 folds were used to train the beamformer, the remaining fold to test its performance). The ROC curve plots binary classification performance as a function of threshold value. Since the maximum classification performance could be reached for multiple thresholds (equal ROC points or points on the maximal iso-performance line), we selected the median of these.

Classification of a new epoch involved the extraction of the segments $\boldsymbol{S}_{test}$, using an identical procedure as for the training epochs. The segments were averaged and concatenated and then independently filtered by each beamformer to obtain a score y_i for each target i. Among the scores that exceeded the corresponding threshold, the one with the highest score was taken as winner. In case of none of the scores exceeded their threshold, the winner was determined by the highest (sub-threshold) score.

We compared our classifier based on spatiotemporal beamforming (stBF) with a SVM-based classifier. Similar to before, segments are extracted from the training epochs and concatenated to form feature vectors (cfr. $\boldsymbol{E}$). Then, for each target, a one-vs-all linear SVM [313] was trained, whose regularisation parameter λ was optimised using a line-search strategy and 4-fold cross validation [122]. All SVMs were trained using the modified finite Newton method [144]. This procedure was successfully applied before to detect the P300 event-related potential (ERP) in patients with incomplete locked-in syndrome (LIS) [68], to detect error-related potentials (ErrPs) in healthy subjects [67], and served as a comparison for the spatiotemporal beamformer for P300 detection [331]. SVMs have been shown to outperform the traditional CCA classifier for cVEP detection [9, 11], and we opted for an optimised version of the SVMs in order to maximise accuracy. Prediction of a given (concatenated) input segment (cfr. $\mathbf{s}$) was given by the SVM returning the highest (i.e., most positive) score.

4.2.6 *Channel selection*

For each subject, the channels included in the analysis were obtained using a greedy approach, in which we iteratively added the channel that improved the accuracy the

most until it did no longer improve or until 100% accuracy was reached. As optimisation criterion, we used the classification accuracy obtained with the beamformer-based classifier when averaging two repetitions of the m-sequence (i.e., signal length of 2.10 and 1.05 sec for S_{60} and S_{120}, respectively).

4.2.7 *Transition effect*

It has been shown that the brain exhibits a latency of 100 to 150 ms in response to SSVEP stimulation[73, 74]. During this time, the SSVEP is not stable, and in SSVEP-BCI research, the initial 100 to 150 ms of the epochs (time-locked to the onset of the flickering stimulation) is often excluded from analysis as it leads to increased accuracies[221, 332]. Similar to SSVEP, cVEP is a visual paradigm adopting flickering stimulation (albeit not periodic), and we tested whether performance could be improved by excluding the initial 150 ms of each epoch. Note that, when excluding the first 150 ms of each epoch, an additional 150 ms is required at the end of the epoch to obtain the same number of complete m-sequences. For example, when excluding the initial signal, the first full m-sequence requires 0.150+1.05 = 1.2 seconds, compared to just 1.05 second without the exclusion.

In this study, we ran the analysis both with and without the exclusion of the initial 150 ms of each epoch.

4.2.8 *Performance evaluation*

The performance of the classifiers was estimated offline using a stratified 5-fold cross-validation strategy. Since each target was cued 5 times, each fold contained one 5.25-second epoch for each target. We obtained the target identification accuracy for different signal lengths, corresponding to multiples of the time needed to present one repetition of the m-sequence.

As the two stimulus presentation rates as well as the possible exclusion of the initial signal lead to differences in stimulation time, one should be careful in interpreting the accuracies obtained by the different conditions. The ITR, however, takes into account the stimulation length and therefore provides a fair comparison between the conditions. Hence, next to target identification accuracy, we also measure ITR (in bits/min) as follows:[340, 341]

$$ITR = \frac{\log_2 N + p.\log_2 p + (1-p).\log_2(\frac{1-p}{N-1})}{t/60}, \tag{4.2}$$

where N is the number of selectable targets, p is the accuracy of the target identification, and t is the time needed to make a selection (in seconds). In our study, N was equal to 32 and t was set to the stimulation length plus an additional 500 ms to account for the time the subject would need to switch their gaze to the next target. In the

literature, studies investigating BCI spelling interfaces often adopt a gaze-switching interval in the range from 300 to 1000 ms[54, 184, 221, 289, 320], and a 500 ms interval has been shown feasible in an online setting[57], albeit with the SSVEP paradigm.

In addition to accuracy and ITR, we also measured the time needed to train the spatiotemporal beamformer- and SVM-based classifiers on all data for each subject. Timings were collected on a quad-core 2.3 GHz Intel i7 machine.

4.2.9 *Statistics*

Since the distributions do not consistently follow a Gaussian distribution, we adopted the non-parametric (two-tailed) Wilcoxon signed rank test. We used this test to compare the accuracy of both classifiers and to compare the influence of excluding the first 150 ms of each epoch. The significance threshold was set to 0.05.

4.3 RESULTS

All results of S_{60} and S_{120} are summarised in Figure 4.4 and Figure 4.5, respectively.

For both sessions, the optimal channel set was obtained using a greedy approach. For S_{60}, all subjects reached convergence with three or less channels (Figure 4.4b), while between 3 and 6 channels were selected for S_{120} (Figure 4.5b) before convergence was reached. The occipital channels Oz and O1 were selected most often (Figure 4.4a and Figure 4.5a), and several parietal channels were selected by a smaller number of subjects, indicating considerable inter-subject variability.

Using the individually optimised channel sets, the target identification accuracy for both the spatiotemporal beamformer- and the SVM-based classifier are shown in Figure 4.4c for S_{60} and Figure 4.5c for S_{120}, both with and without the exclusion of the initial 150 ms of the stimulation. As expected, longer stimulation times (i.e., more repetitions of the m-sequence) increases performance. For the same stimulation lengths, the faster stimulus presentation (S_{120}) is able to present twice the amount of m-sequences compared to S_{60}, which results in a higher accuracy for equal-length stimulation. Only the faster stimulus presentation in combination with the exclusion of the initial signal is able to surpass the accuracy threshold of 70% with a single repetition of the m-sequence. All other conditions require at least two repetitions to reach this threshold, which is deemed minimal for establishing reliable communication [42, 68, 165, 166].

Using the full signal, the accuracies of both classifiers differ significantly when averaging up to four (S_{60}, Figure 4.4c,) ($p = 0.033$; $p = 0.012$; $p = 0.0017$ and $p = 0.030$) and two (S_{120}, Figure 4.5c) ($p = 0.016$ and $p = 0.020$) repetitions of the m-sequence, respectively. With the exclusion of the initial 150 ms, the two classifiers are not significantly different. However, within stBF, the accuracies with and without the exclusion of the initial signal significantly differ for 2 to 4 repetitions (S_{60}) ($p < 0.001$, $p = 0.003$ and $p = 0.004$) and 1 repetition (S_{120}) ($p < 0.001$) of the m-sequence, respectively. Sim-

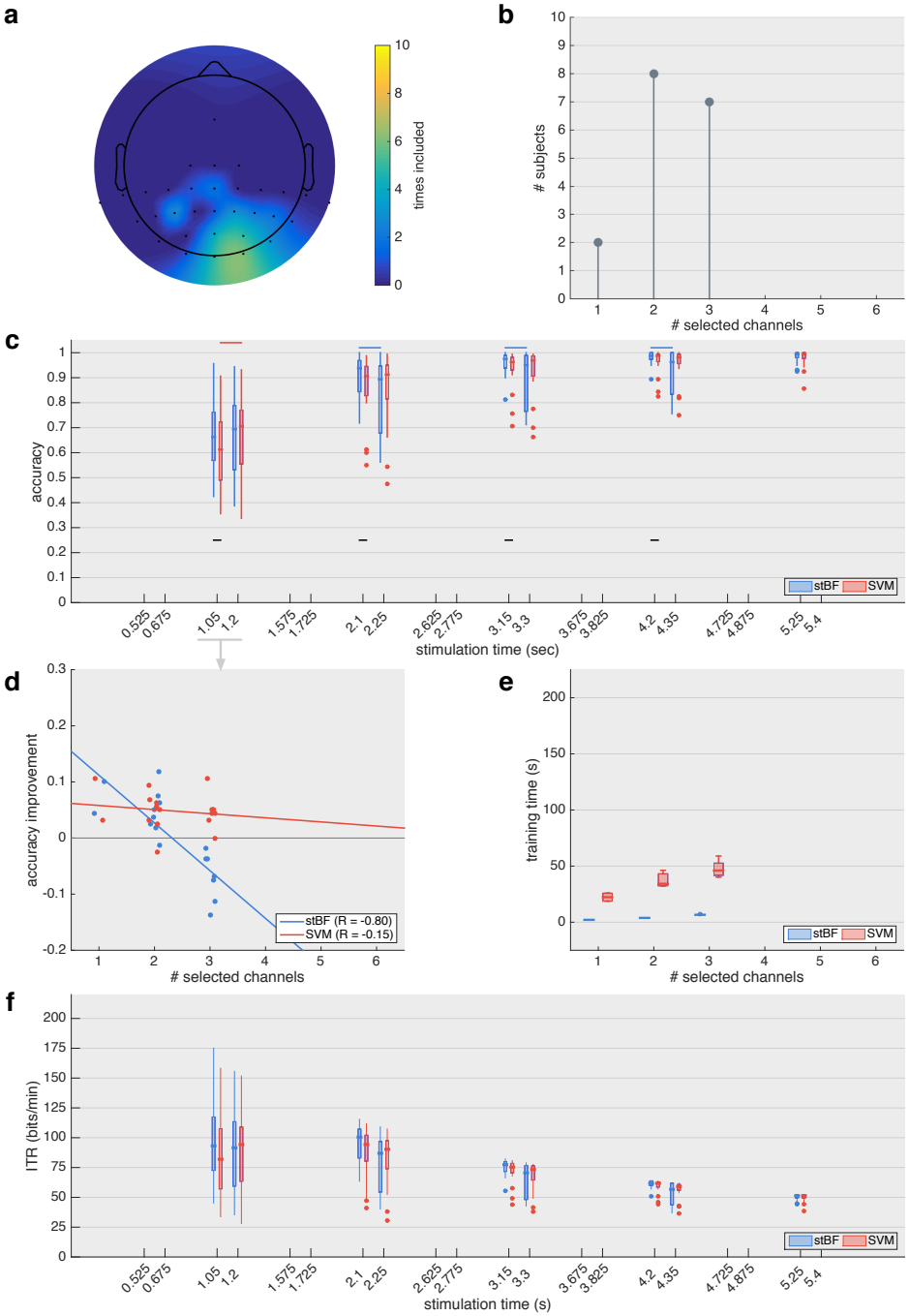

Figure 4.4: Results for the session adopting the traditional 60 Hz stimulus rate. (a) Scalp plot indicating how many times each channel was selected by the greedy channel-selection algorithm across subjects. Note that most of the frontal and temporal area was not recorded during the experiment. (b) Summary of the total number of channels selected by the greedy channel-selection algorithm before convergence. (c) Target identification accuracy for both classifiers with an increasing number of repetitions of the stimulation sequence (1 m-sequence = 1.05 sec), with and without the initial 150 ms of each epoch. Black horizontal lines indicate significant differences between the classifiers. Blue and red horizontal lines indicate significant differences when excluding the first 150 ms. (d) Regression analysis of the increase in target identification accuracy based on one repetition of the m-sequence when excluding the first 150 ms. (e) Time needed to train the classifiers on all data of each subject. (f) Virtual ITR achieved when factoring in 0.5 seconds for gaze shifting.

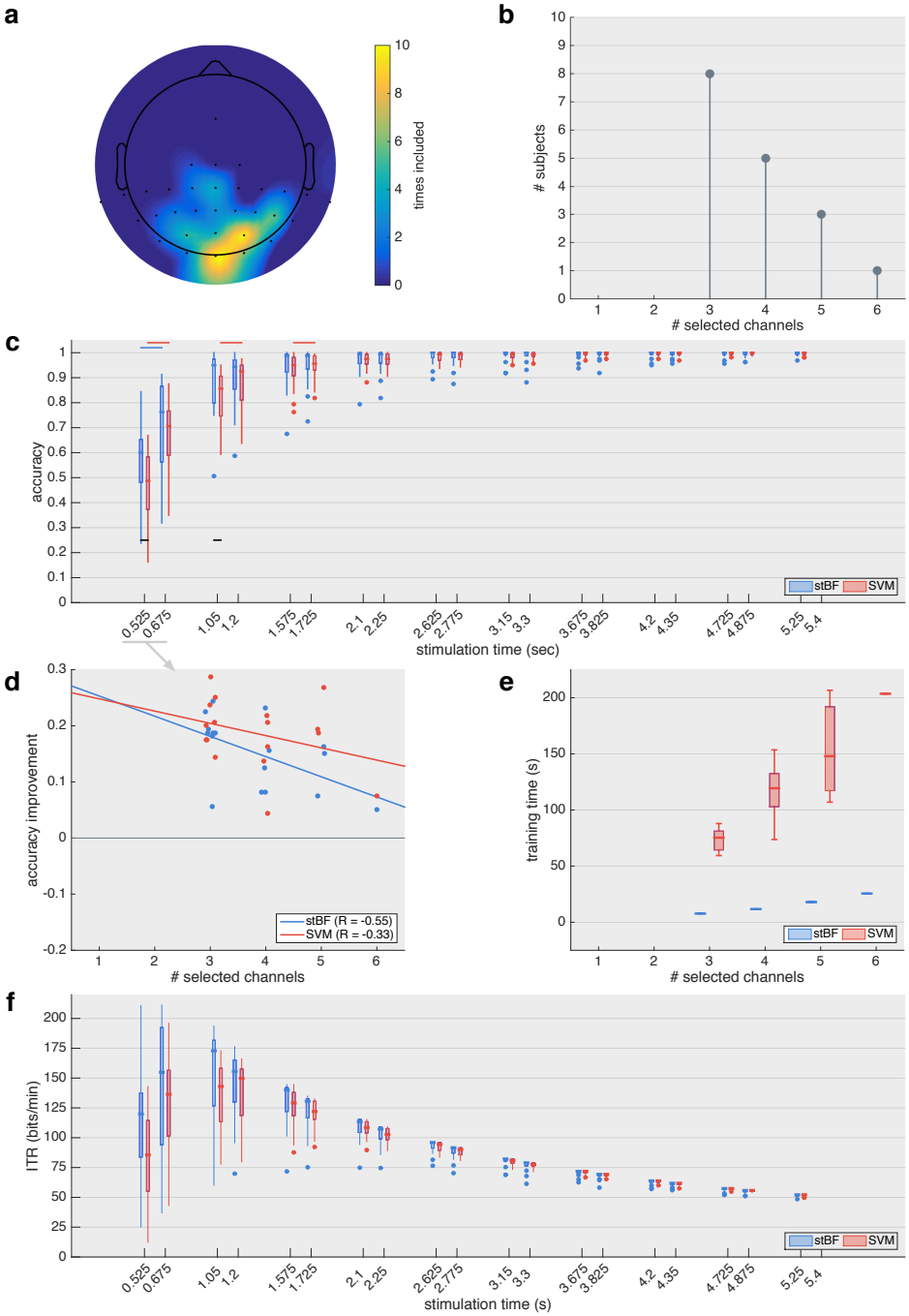

Figure 4.5: Results for the session adopting the 120 Hz stimulus rate. (a) Scalp plot indicating how many times each channel was selected by the greedy channel-selection algorithm across subjects. Note that most of the frontal and temporal area was not recorded during the experiment. (b) Summary of the total number of channels selected by the greedy channel-selection algorithm before convergence. (c) Target identification accuracy for both classifiers with an increasing number of repetitions of the stimulation m-sequence (1 sequence = 0.525 sec), with and without the exclusion of the initial 150 ms of each epoch. Black horizontal lines indicate significant differences between the classifiers. Blue and red horizontal lines indicate significant differences when excluding the first 150 ms. (d) Regression analysis of the increase in target identification accuracy based on one repetition of the m-sequence when excluding the first 150 ms. (e) Time needed to train the classifiers on all data of each subject. (f) Virtual ITR achieved when factoring in 0.5 seconds for gaze shifting.

ilarly, within the SVM-based classifier, the accuracies with and without the exclusion of the initial signal significantly differ for one repetition (S_{60}) ($p < 0.001$) and 1 to 3 repetitions (S_{120}) ($p < 0.001$, $p < 0.001$ and $p = 0.008$) of the m-sequence, respectively.

A detailed inspection of the accuracy increase with one repetition of the m-sequence (Figure 4.4d for S_{60} and Figure 4.5d for S_{120}) shows a negative relation between the increase in accuracy and the number of selected channels. This effect is most prominent for stBF at the traditional 60 Hz stimulus rate (Figure 4.4d). All subjects requiring three channels have a reduction in accuracy by removing the first 150 ms of the epochs, while the other subjects have an increased accuracy. The SVM is less influenced by the number of channels, and removing the initial 150 ms signal only decreases its accuracy for two subjects. While this negative trend can also be detected for the faster stimulation rate, all subjects have an increased accuracy compared to when the initial 150 ms signal is included in the analysis.

For both sessions, the time needed to train stBF on all data of each subject is significantly lower compared to SVM (Figure 4.4e for S_{60} and Figure 4.5e for S_{120}), and for both classifiers, the training time increases when more channels are included in the analysis.

For both the traditional and faster stimulus presentation rates, the median ITR reaches its maximal value of 100.46 and 172.87 bits/min, respectively, using the beamformer-based classifier, two repetitions of the m-sequence and the full signal (stimulation time = 2.1 and 1.05 seconds, respectively).

4.4 DISCUSSION

In this study, we assessed the feasibility of spatiotemporal beamforming for resolving m-sequence encoded targets in a cVEP setting, and investigated the influence of stimulus presentation rate on target identification accuracy and ITR.

We showed that the proposed classifier is able to accurately discriminate targets, and that it is able to compete with a classifier based on optimised linear SVMs. We additionally show that a faster stimulus presentation rate is beneficial for the communication speed, as more iterations of the m-sequence can be presented in an equal amount of time. Both stimulation rates have similar performance in terms of number of m-sequence repetitions, and at least two repetitions are necessary to obtain a performance over 70%, which is deemed minimal for establishing reliable communication [42, 68, 165, 166]. With two repetitions of the m-sequence, the median ITR is maximal and reaches 100.46 bits/min for the traditional 60 Hz and 172.87 bits/min for the faster 120 Hz stimulus presentation, respectively. As far as we are aware, no other cVEP study has reported a higher ITR. As commercial monitors with high frame rates are becoming increasingly more accessible at affordable prices, they are recommended for cVEP-BCI applications.

Compared to the SVM, the spatiotemporal beamformer can be trained considerably faster, as there are no parameters to be optimised. This could be important to achieve fast, online retraining of the beamformer-based classifier without causing the interface to be temporarily unavailable or to interfere with stimulation. The shorter training time would also allow for other optimisation algorithms to be executed (eg., channel selection, downsampling rate, filtering range, etc.) that would otherwise not be able to complete within a reasonable time.

We present evidence that the cVEP response exhibits a transition effect following the onset of a stimulation sequence. Previously, a response latency of 100 to 150 ms has been described for SSVEP [74], and in recent SSVEP-BCI research, the initial signal was excluded from the analysis to improve target identification [221, 332]. In this study, excluding the initial 150 ms of each epoch improves classification accuracy of both classifiers when using merely one repetition of the m-sequence. The performance increase is negatively correlated with the number of selected channels and mostly affects the spatiotemporal beamformer, even causing a performance decrease when adopting three channels at the traditional 60 Hz stimulus presentation rate. For the 120 Hz case, all accuracies increase despite larger channels sets. The discrepancy between these results could be due to the fact that, when excluding the initial signal from each epoch, the last m-sequence of each epoch is not complete, and the number of complete training segments is reduced by 20% for S_{60} compared to only 10% for S_{120}. In order to maintain the same number of training segments, one could extend the stimulation of the training session by 150 ms. Additionally, the negative correlation between increase in accuracy and number of selected channels can be explained by the fact that the dimensions of the spatiotemporal beamformer increase linearly with the number of channels, thereby requiring more data to accurately estimate the covariance matrix [248, 272] (cf., the curse of dimensionality).

4.5 CONCLUSION

In this study, we have shown that a classifier based on spatiotemporal beamforming is able to accurately discriminate targets encoded by an m-sequence, and could be employed in the context of cVEP BCI. We compared the traditional 60 Hz and the faster 120 Hz stimulus presentation rates, and found that the latter yields more accurate results for equal stimulation lengths, as the encoding sequence can be presented twice as many times as with the 60 Hz case. The maximal median ITR for both stimulus presentation rates and for two iterations of the m-sequence was 100.46 bits/min for the 60 Hz (stimulation time = 2.1 seconds) and 172.87 bits/min for the 120 Hz case rate (stimulation time = 1.05 seconds). We additionally described a transition effect following the onset of the stimulation, similar to SSVEP, and showed that removing the initial 150 ms of the epochs significantly improves classification accuracy when relying on only one repetition of the encoding sequence.

5

SPATIOTEMPORAL BEAMFORMING: A TRANSPARENT AND UNIFIED DECODING APPROACH TO SYNCHRONOUS VISUAL BRAIN-COMPUTER INTERFACING

This chapter has been published as:
B. Wittevrongel and M.M. Van Hulle (2017) *Spatiotemporal beamforming: a transparent and unified decoding approach to synchronous visual Brain-Computer Interfacing.* Frontiers in Neuroscience 11, 630

Brain-Computer Interfaces (BCIs) decode brain activity with the aim to establish a direct communication channel with an external device. Albeit they have been hailed to (re-)establish communication in persons suffering from severe motor- and/or communication disabilities, only recently BCI applications have been challenging other assistive technologies. Owing to their considerably increased performance and the advent of affordable technological solutions, BCI technology is expected to trigger a paradigm shift not only in assistive technology but also in the way we will interface with technology. However, the flipside of the quest for accuracy and speed is most evident in EEG-based visual BCI where it has led to a gamut of increasingly complex classifiers, tailored to the needs of specific stimulation paradigms and use contexts. In this contribution, we argue that spatiotemporal beamforming can serve several synchronous visual BCI paradigms. We demonstrate this for three popular visual paradigms even without attempting to optimizing their electrode sets. For each selectable target, a spatiotemporal beamformer is applied to assess whether the corresponding signal-of-interest is present in the preprocessed multichannel EEG signals. The target with the highest beamformer output is then selected by the decoder (maximum selection). In addition to this simple selection rule, we also investigated whether interactions between beamformer outputs could be employed to increase accuracy by combining the outputs for all targets into a feature vector and applying three common classification algorithms. The results show that the accuracy of spatiotemporal beamforming with maximum selection is at par with that of the classification algorithms and interactions between beamformer outputs do not further improve that accuracy.

5.1 INTRODUCTION

In a Brain-Computer Interface (BCI), signals are recorded from the brain with the aim to enable users to interact with an external device, without the need for muscular, vocal or other means of communication [316]. Typically, the subject is presented with a number of targets, each one representing a specific action (e.g., a letter in a spelling interface, a movement of a prosthetic limb or a wheelchair, etc.) that can be selected either by redirecting gaze or attention to the intended target (Figure 5.1) or by performing a mental action (e.g., imagined movement [240]).

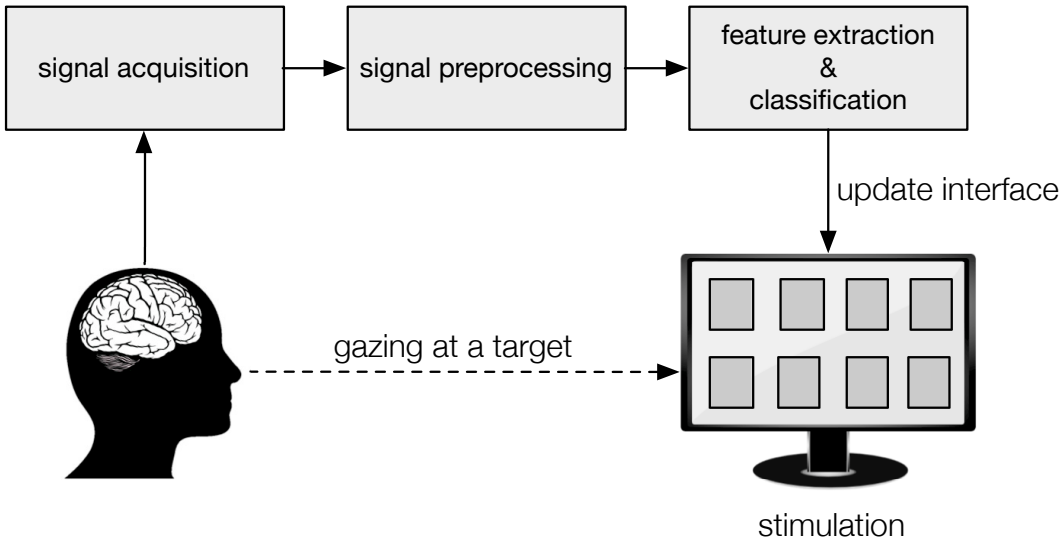

Figure 5.1: Graphical representation of a visual BCI. The subject gazes at the target on a display ('interface'), to which the desired action is associated, while his/her brain activity is being recorded. Each target is stimulated visually, in a specific manner, which leaves a trace in the recorded brain activity. From the preprocessed recordings, signal features are extracted and the classification algorithm predicts the intended target, after which the display is updated accordingly (visual feedback) and the corresponding action performed.

Among the most performant BCI paradigms, in terms of accuracy and speed, are the ones where targets are visually stimulated and the user directs his/her gaze to target to be selected (for review, see [32, 223]). Each stimulation paradigm elicits specific brain potentials, which are recorded from the scalp using electroencephalography (EEG) [193], from the cortical surface using electrocorticography (ECoG) [271] or from implants such as microelectrode arrays and depth electrodes [149, 208]. For each paradigm, analysis- and decoding techniques have been proposed tailored to maximise target prediction speed and accuracy.

One popular paradigm is based on the P300 event-related potential (ERP), an EEG component recorded over the centro-parietal region that exhibits a positive deflection in amplitude, peaking around 300 ms (whence its name), in sync with the onset of an infrequent stimulus (called oddball) to which the subject pays attention. In a P300-based BCI, the targets are overlaid with the oddball stimulus in a non-overlapping fashion (serial stimulation). The P300 can be elicited in response to a variety of sensory stimuli, including visual- [84, 204, 277], auditory- [93, 273, 277], and tactile stimuli [40]. EEG recordings are typically cut into epochs, in sync with possible oddball events. However, in order to address the relatively low signal-to-noise ratio (SNR), several oddball events need to be generated and epochs averaged before P300 responses can be detected in them, resulting in a reduction in communication speed. P300-based BCIs have been most extensively studied, resulting in a wide range of techniques for EEG feature extraction and classification [193]. The most simple ones consider template matching in which a (spatio)temporal template is first learned from P300-labeled responses and then used to identify the intended target as the one with the highest correlation coefficient [162] or consider peak picking in which the target having the largest difference between the lowest amplitude prior to and the highest amplitude in the P300 time window is selected as winner [84]. The Linear Discriminant Analysis (LDA) [130] and its variants, including Fisher LDA [162, 205], Bayesian LDA [119, 205] and Stepwise LDA [84, 162, 205], have been applied to pre-processed epochs or after feature extraction by Common Spatio-Temporal Pattern [159], xDAWN [262] and linear predictive coding [216]. More complex methods include multilayer feed-forward neural networks [106, 205], Nuclear Norm on tensor representation [124], Bayesian statistical classifiers [242], ensemble methods with SVMs and a genetic algorithm [98], and a fuzzy fusion of the outcome of template matching and peak picking [266, 267]. As far as we are aware, state-of-the-art P300 classification for BCI is achieved by the linear Support Vector Machine (SVM) [66, 68, 162, 205] as it outperforms its non-linear [162, 205] counterparts. The recently introduced spatiotemporal beamforming filter has been shown to be at par with an optimized linear SVM for P300 detection [331].

Unlike the P300 paradigm, which is inherently serial in nature, the SSVEP paradigm encodes the targets using periodically and simultaneously flickering stimuli, and in which each target adopts a unique frequency [211, 256], unique phase [181, 189, 202] or unique frequency-phase combination [126]. EEG signals are recorded over the occipital cortex and are expected to carry the same signal characteristics as the target being gazed at. Hence, SSVEP decoding methods are traditional relying on frequency domain methods such as the Fourier transform [95] and the Continuous Wavelet Transform [357]. Other frequency-detection algorithms include the Minimum Energy Combination [61, 68, 91], the Multivariate Synchronization Index (MSI) [354, 355] and time-domain analysis [199, 203]. Among the machine learning algorithms that have been used for SSVEP target identification are Bayesian LDA [52], SVM [284], k-Nearest Neighbor (kNN) [168], and several neural network architectures [169, 206, 207, 284].

However, the most accurate SSVEP decoding methods are based on the Canonical Correlation Analysis (CCA) [186], and its numerous extensions [55, 56, 221, 231, 321, 353, 356], and spatiotemporal beamforming [332, 333].

Whereas the P300 paradigm encodes targets in terms of ERP responses and SSVEP in terms of frequency and/or phase combinations, the code-modulated VEP (cVEP) paradigm encodes the targets using lagged versions of a binary coding sequence. While record-breaking communication speed was achieved when it was introduced, it has been considerably less studied [94], and fewer decoding algorithms have been proposed for this paradigm. Originally, template matching [32] was used to identify the gazed target from averaged epochs, but also the CCA algorithm has been applied [9, 33, 327] as well as SVMs [10, 11] and spatiotemporal beamforming [335]. The latter two have shown state-of-the-art performance with shorter stimulation times.

Importantly, what the majority of the reported decoding algorithms have in common is that they have been construed to maximize performance of a given paradigm, even when used in a particular context. We argue that one of these algorithms, the spatiotemporal beamformer, can achieve state-of-the-art performance in all three paradigms. The beamformer is a filter that estimates the contribution of an a-priori defined activation pattern (i.e., a template, a signal-of-interest) into new data. It can appear as a spatial, temporal or spatiotemporal filter. Unlike in our previous work [331, 332, 335], which was aimed at investigating the beamformer in the context of a specific paradigm, the first goal of this chapter is to describe a generalized and unified approach to spatiotemporal beamforming for decoding synchronous EEG responses by demonstrating its versatility in the context of synchronous visual BCI. Secondly, in addition to a simple maximum-beamformer output classification, we also investigate whether interactions between beamformer outputs can increase decoder accuracies. We end by indicating future directions for spatiotemporal beamforming in BCI.

5.2 METHODS

5.2.1 *Data acquisition and processing*

The data used in this study has been collected in previous offline BCI studies. For more details about the experimental setting, interface and recordings, we refer the reader to the corresponding chapters. All three studies were carried out in accordance with the recommendations and approval of the ethics committee of our university hospital UZ Leuven with written informed consent from all subjects. All subjects gave written informed consent in accordance with the Declaration of Helsinki.

Data for the P300 paradigm was collected using an interface consisting of 9 targets [331]. In each trial, subjects were asked to direct their gaze to a cued target and continue to focus as all targets were individually highlighted 15 times for 100 ms (with 100 ms inter-stimulus interval) in pseudorandom order. In response to the cued tar-

get, when highlighted, a P300 response will be elicited. All targets were used as cue 4 times, leading to a total of 36 trials, each consisting of 15 'P300 epochs' (i.e., where the cued target was highlighted) and 120 epochs where another target was highlighted. Data from 21 subjects was collected using an ActiveTwo system (BioSemi, The Netherlands) with 32 active Ag/AgCl electrodes (and 4 additional electrodes around the eyes) at a sampling rate of 2048 Hz. The raw data was offline referenced from the Common-Mode Sense (CMS) reference to average of the mastoid signals, corrected for eye artifacts using the RAAA-method [70], filtered between 0.5 and 15 Hz and cut in 0.6-second epochs time-locked to the onset of the stimulation. Each epoch was baselined by subtracting the average of the 100 ms pre-onset activity and downsampled to 64 Hz.

SSVEP data was obtained from an interface consisting of 4 targets, each adopting an unique frequency-phase combination of 12 or 15 Hz and 0 or π radians [332]. During a trial, subject were asked to direct their gaze to a cued target and continue to focus when all targets were simultaneously flickering at their unique frequency-phase combinations for 5 seconds. All targets were cued 15 times, leading to a total of 60 5-second trials. Data from 20 subjects was recorded using an ActiveTwo system (BioSemi, The Netherlands) with 32 active Ag/AgCl electrodes (and 4 additional electrodes around the eyes) at a sampling rate of 2048 Hz. The raw data was offline referenced from the CMS reference to the average of the mastoid signals, corrected for eye artifacts using the RAAA-method [70], filtered between 4 and 20 Hz, cut in 5-second trials time-locked to the onset of the flickering, and downsampled to 512 Hz.

For the cVEP study, a 32-target interface was used [335]. Targets were encoded using lagged versions of a binary m-sequence of length 63, presented at a stimulation rate of 120 Hz (1 m-sequence = 0.525 second). Each trial started with a cue, to which the subjects need to direct their gaze and to continue focusing while all targets were simultaneously presented with their unique lagged m-sequences. The sequences were repeated 10 times. Each target was cued 5 times, leading to a total of 160 trials. Data from 17 subjects was recorded using a Neuroscan SynampsRT device (Compumedics, Australia) with 32 active Ag/AgCl electrodes at a sampling rate of 1000 Hz with ground and reference electrodes at FPz and AFz, respectively. The data was offline referenced to the average of the mastoid signals, filtered between 4 and 31 Hz, cut into trials that are time-locked to the onset of the stimulation, and finally downsampled to 120 Hz. Since no ocular electrodes were included in the recording, the data was not corrected for eye artifacts.

5.2.2 *Spatiotemporal beamforming*

The beamforming principle was originally introduced as a spatial filter for radar, sonar and seismic data analysis [309], but has also been employed in EEG analysis to isolate

the signal originating from a predefined brain location [310], for ERP analysis [306], and to build a BCI application based on imagined movement detection [105].

Van Vliet and coworkers [319] introduced a spatiotemporal extension to beamforming for single-trial N400 ERP detection in the context of processing semantic stimuli. To calculate the spatiotemporal filter, a spatiotemporal activation pattern $\mathbf{A} \in \mathbb{R}^{m \times n}$ needs to be defined, where m represents the number of channels (here, EEG electrodes) and n the number of samples. This activation pattern represents the signal-of-interest (or template) and can be obtained a-priori [319] or based on actual training data [331, 332, 335]. The resulting beamformer $\mathbf{w} \in \mathbb{R}^{1 \times mn}$ is a multivariate filter that optimally isolates the targeted response from noise and possible other unrelated activity, by taking into account the information contained in the covariance matrix $\mathbf{\Sigma} \in \mathbb{R}^{(mn) \times (mn)}$ estimated from the available (training) data.

The original formulation of the Linearly Constrained Minimum Variance (LCMV) spatial beamformer $\mathbf{w}_{sp} \in \mathbb{R}^{m \times 1}$ minimizes the variance of the beamformer output $\mathbf{w}_{sp}^{\intercal}\mathbf{S}$:

$$\arg\min_{\mathbf{w}_{sp}} \mathbf{w}_{sp}^{\intercal}\mathbf{S}(\mathbf{w}_{sp}^{\intercal}\mathbf{S})^{\intercal} \Rightarrow \arg\min_{\mathbf{w}_{sp}} \mathbf{w}_{sp}^{\intercal}\mathbf{\Sigma}_{sp}\mathbf{w}_{sp}, \tag{5.1}$$

where $\mathbf{\Sigma}_{sp} \in \mathbb{R}^{m \times m}$ is the spatial covariance matrix of an EEG trial $\mathbf{S} \in \mathbb{R}^{m \times n}$. By adding the linear constraint:

$$\mathbf{a}_{sp}^{\intercal}\mathbf{w}_{sp} = 1, \tag{5.2}$$

where $\mathbf{a}_{sp} \in \mathbb{R}^{m \times 1}$ is the spatial activation pattern, trivial solutions of (5.1) are avoided, and signals that are similar to $\mathbf{a}_{sp}$ will be mapped to a value close to 1, allowing for an easy measure of similarity. The solution of (5.1) under constraint (5.2) can be found using the method of Lagrange multipliers [310]:

$$\mathbf{w}_{sp} = \frac{\mathbf{\Sigma}_{sp}^{-1}\mathbf{a}_{sp}}{\mathbf{a}_{sp}^{\intercal}\mathbf{\Sigma}_{sp}^{-1}\mathbf{a}_{sp}}. \tag{5.3}$$

The spatial beamformer can be expanded to a spatiotemporal variant as follows. Let $\boldsymbol{S} \in \mathbb{R}^{m \times n \times r}$ be r trials, $\mathbf{X} \in \mathbb{R}^{r \times (mn)}$ a matrix where each row l is obtained by concatenating the rows of a corresponding trial $\boldsymbol{S}[*, *, l]$ with $l \in [1..r]$, $\mathbf{\Sigma} \in \mathbb{R}^{(mn) \times (mn)}$ the covariance matrix of $\mathbf{X}^{\intercal}$, and $\mathbf{a}^{\intercal} \in \mathbb{R}^{1 \times (mn)}$ a vector containing the concatenated rows of the spatiotemporal activation pattern $\mathbf{A}$. The spatiotemporal LCMV beamformer $\mathbf{w} \in \mathbb{R}^{(mn) \times 1}$ with the linear constraint $\mathbf{a}^{\intercal}\mathbf{w} = 1$ can now be calculated as:

$$\mathbf{w} = \frac{\mathbf{\Sigma}^{-1}\mathbf{a}}{\mathbf{a}^{\intercal}\mathbf{\Sigma}^{-1}\mathbf{a}}, \tag{5.4}$$

and applied to the data as a simple weighted sum:

$$y = \mathbf{s}\mathbf{w}, \tag{5.5}$$

where $\mathbf{s} \in \mathbb{R}^{1 \times (mn)}$ indicates the concatenated rows of a segment $\mathbf{S}$ and y represents the contribution of the activation pattern $\mathbf{A}$ in $\mathbf{S}$.

5.2.3 *Beamformer construction and feature extraction*

As the activation pattern captures the signal-of-interest, each paradigm (P300, SSVEP, cVEP) will have unique activation patterns, and since EEG responses might different across subjects, beamformers should be constructed for each subject individually [331]. In the next few sections, we will describe for each paradigm how one or more beamformers (BF) are constructed and used to extract feature vectors. A visual depiction of this process is given in Figure 5.2.

5.2.3.1 *P300*

For a P300-based BCI the activation pattern $\mathbf{A}$ represents the P300 ERP. One trial $\mathbf{T}$ in the P300 paradigm consists of k stimulations (i.e., highlights) of all targets. To obtain the activation pattern $\mathbf{A}$, all training trials are first cut into time-locked epochs $\boldsymbol{S}$ from 0 to 600 ms post-stimulus onset and their baseline subtracted. The activation pattern $\mathbf{A}$ can then be obtained as the difference between the average ($\mathbf{S}_t$) of the P300 epochs (i.e., when the target being gazed at is highlighted) and the average ($\mathbf{S}_{nt}$) of the non-P300 epochs. The covariance matrix $\boldsymbol{\Sigma}$ is calculated from $\boldsymbol{S}$ (using the concatenation approach described above), and a single beamformer $\mathbf{w}$ constructed.

To obtain the feature vector for a trial $\mathbf{T}$, the trial is first cut into time-locked epochs and all epochs corresponding to the same target are averaged. Each averaged epoch $\mathbf{S}_i \in \mathbb{R}^{m \times n}$ is then filtered by the beamformer $\mathbf{w}$ to obtain an value y_i, which represents the P300 contribution for target i.

5.2.3.2 *SSVEP*

Targets in the SSVEP paradigm are encoded with unique frequency-phase combinations, and one trial T consists of k seconds of SSVEP stimulation, during which all targets are simultaneously flickering at their assigned frequency-phase combinations. Unlike for the P300 case, each target elicits a specific frequency and phase response, and it is therefore not possible to define a single activation pattern to discriminate targets, but rather multiple activation patterns, each one tailored to one target, are needed. To capture the frequency-phase response to target i, a time-domain analysis [199, 203] is adopted: each training trial $\mathbf{T}$ is cut into consecutive, non-overlapping segments $\boldsymbol{S}_i$ with a length n equal to a single period of stimulus frequency f_i. The activation pattern $\mathbf{A}_i$ for target i is then given by averaging the segments ($\overline{\boldsymbol{S}}_i \subset \boldsymbol{S}_i$) extracted from the trials during which target i was cued. The covariance matrix $\boldsymbol{\Sigma}$ was calculated from $\boldsymbol{S}_i$ and beamformer $\mathbf{w}_i$ from equation 5.4.

The feature vector for a trial $\mathbf{T}$ contains the beamformer outputs y_i for each target i. To obtain y_i, the trial is cut into segments of length one period of frequency f_i, the segments are averaged and filtered using the corresponding beamformer $\mathbf{w}_i$.

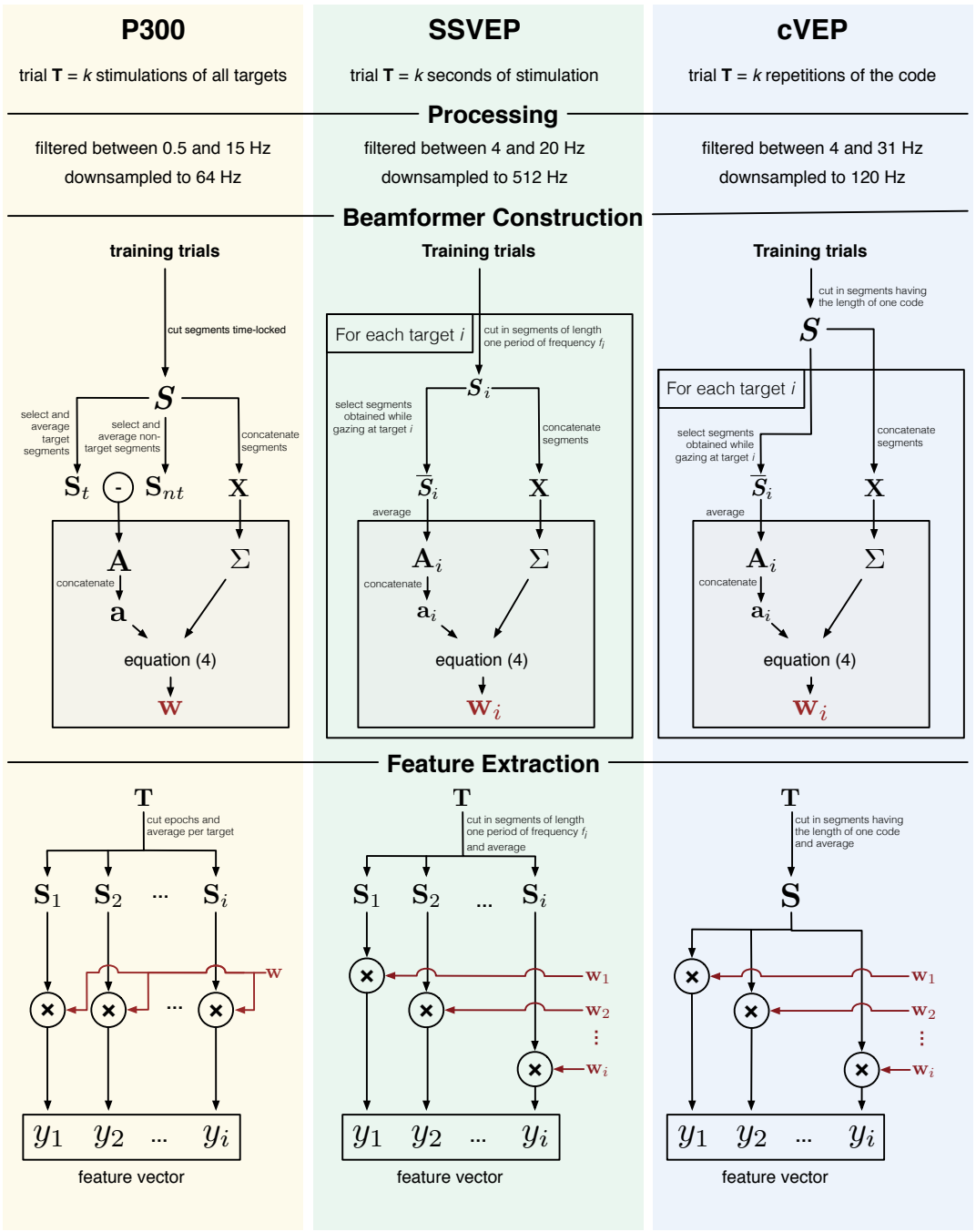

Figure 5.2: Graphical representation of feature extraction and beamformer construction for three paradigms.

To improve classification accuracy, the first 120 ms of each trial were removed prior to cutting the segments, as the SSVEP response is not stable during this time. [221, 332]

5.2.3.3 *cVEP*

In the cVEP paradigm, targets were encoded using lagged versions of a binary m-sequence, which was repeated k times over the course of one trial $\mathbf{T}$. Similar to the SSVEP paradigm, each target elicited a unique response and several activation patterns (one for each target) were defined. Each training trial T was cut into a maximal number of 0.525-second consecutive, non-overlapping segments $\boldsymbol{S}$. Note that the 0.525 seconds corresponds to the time needed to display one full m-sequence. The activation pattern $\mathbf{A}_i$ for target i was then obtained as the average of the segments $\overline{\boldsymbol{S}}_i \subset \boldsymbol{S}$ in response to target i. As for SSVEP, the covariance matrix $\boldsymbol{\Sigma}$ was calculated from $\boldsymbol{S}$, and beamformer $\mathbf{w}_i$ from equation 5.4.

The feature vector for a trial is constructed by cutting the trial into segments (using the same method as above), averaging the segments ($\mathbf{S}$) and independently applying the beamformer $\mathbf{w}_i$ to obtain the corresponding y_i for each target i.

5.2.4 *Target Identification*

Based on the feature vector, a prediction for the intended target was made. We compared several prediction strategies. As the feature vectors contain estimates of the degree to which the activation pattern of each target is present in the trial, the most naive prediction is to select the target with the highest score (i.e., prediction $= \max(y_i)$). However, as alternatives, we also applied three common classifiers (Nearest Neighbor (NN), LDA and a linear SVM) to the features vectors. These classifiers can take into account possible interactions between beamformer outputs of different targets (i.e., features in the feature vector). The feature vectors of the training trials were used to train these classifiers. The complete procedure is depicted in Figure 5.3. The three classifiers were implemented by using the corresponding built-in functions in Matlab (2015a) (*fitcdiscr*, *fitcknn*, *fitcecoc*).

5.2.5 *Performance estimation*

Classification accuracy was estimated using cross-validation (4-fold for the P300 data and 5-fold for SSVEP and cVEP data), for increasing signal lengths (i.e., stimulus repetitions for P300 and cVEP and stimulation length for SSVEP).

For all paradigms, the same electrode set was included in the analysis, consisting of *Fz*, *Cz*, *Pz*, *Oz*, *O1*, *O2*, *PO3*, *PO4*, *P3* and *P4*. The locations of the included electrodes (Figure 5.4) cover the scalp areas where routinely P300 (centro-parietal), SSVEP (occip-

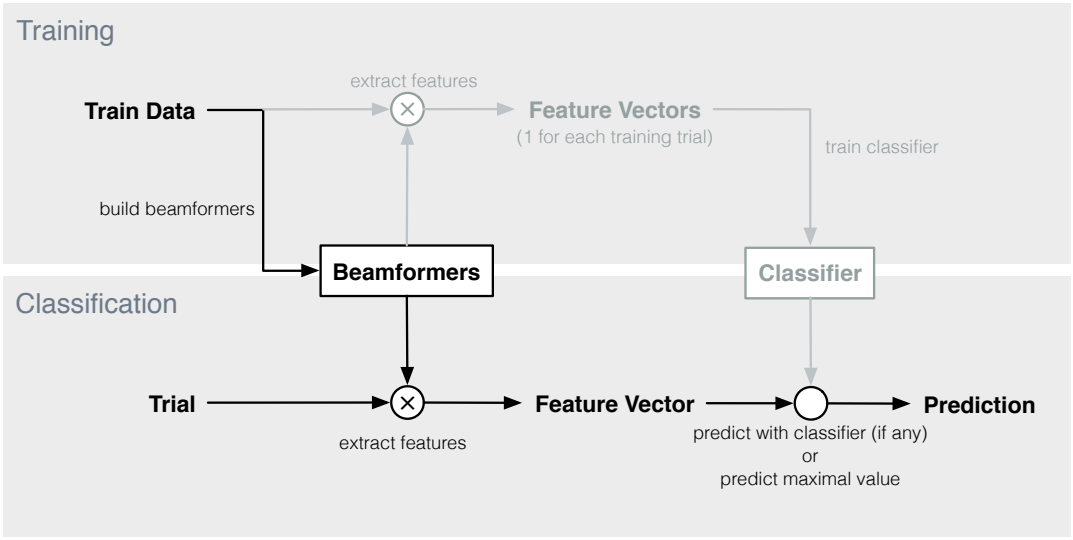

Figure 5.3: Overview of training and classification procedure. Elements indicated in lighter color are not used in maximum-based target prediction. The feature vectors consist of the scores (i.e., y-values) of each individual beamformer.

ital) and cVEP (parieto-occipital) responses are detected. Note that we do not attempt to optimize the electrode sets of the paradigms, but rather consider the same assembly for all three paradigms, which adds to the genericness of our approach.

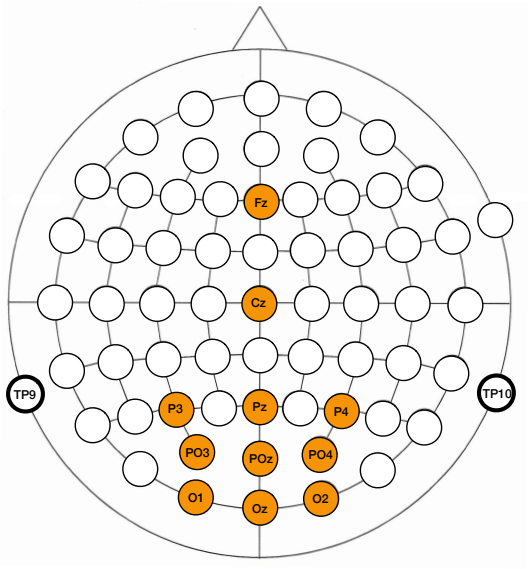

Figure 5.4: Scalp locations of electrodes used in the EEG analysis of the three paradigms.

5.2.6 *Statistics*

Since the distributions do not consistently follow a Gaussian distribution, we adopted the non-parametric (two-tailed) Wilcoxon signed rank test. We used this test to compare the accuracies of the different classifiers. The significance threshold was set to 0.0083 ($= \frac{0.05}{6}$) after applying the Bonferroni correction for multiple comparisons.

5.3 RESULTS

Figure 5.5a shows the classification accuracies of the four classifiers for the P300 paradigm with increasing stimulus repetitions (1 repetition = 1.8 seconds). For all stimulus repetitions in the P300 case, there is no significant difference between maximal beamformer output prediction and NN- or SVM-based classification. LDA-based prediction consistently has the lowest median accuracy and is significantly different up to 5 (compared to SVM, $p < 0.003$) and 10 (compared to max and NN, $p < 0.008$) stimulus repetitions. All four prediction approaches require at least two stimulus repetitions to surpass the 70% accuracy threshold (median accuracy of 86.1% for maximum-, 83.3% for kNN- and SVM- and 75.0% for LDA-based prediction) deemed necessary for establishing reliable communication [42, 68, 165, 166].

With the SSVEP paradigm (Figure 5.5b), the target identification accuracies of the four classification approaches are not significantly different for any of the stimulation lengths. The accuracies of all classifiers increase considerably up until 1.12 second of stimulation, after which the maximal median accuracy of 100% is reached (for maximum-, kNN- and SVM-based prediction) and remains consistent for longer stimulation lengths. Note that the interquartile ranges (as well as the number of outliers) are considerably smaller compared to the P300 paradigm, indicating a higher consistency across subjects, which may be due to the fact that SSVEP is an automatic visual (sensory) response while P300 is a cognitive potential and thus more influenced by ongoing mental activity (e.g., attention).

Similar to the P300-case, for the cVEP paradigm (Figure 5.5c), LDA-based prediction consistently exhibits the lowest median accuracy for all signal lengths. While the maximal-based prediction is significantly different from NN for a stimulation length of 1.05 seconds ($p = 0.006$, two-tailed Wilcoxon signed rank test) and from SVM for 1.625 second stimulation ($p = 0.002$, two-tailed Wilcoxon signed rank test), maximal-, NN- and SVM-based predictions are not significantly different for any other stimulation lengths. Two repetitions of the m-sequence (i.e., stimulation length of 1.05 seconds) are necessary for the median to surpass the 70% accuracy threshold (median accuracy of 81.3% for maximum-, 81.9% for kNN-, 80.6% SVM- and 73.7% for LDA-based prediction). For all classifiers, the accuracies steadily increase with increasing stimulation length.

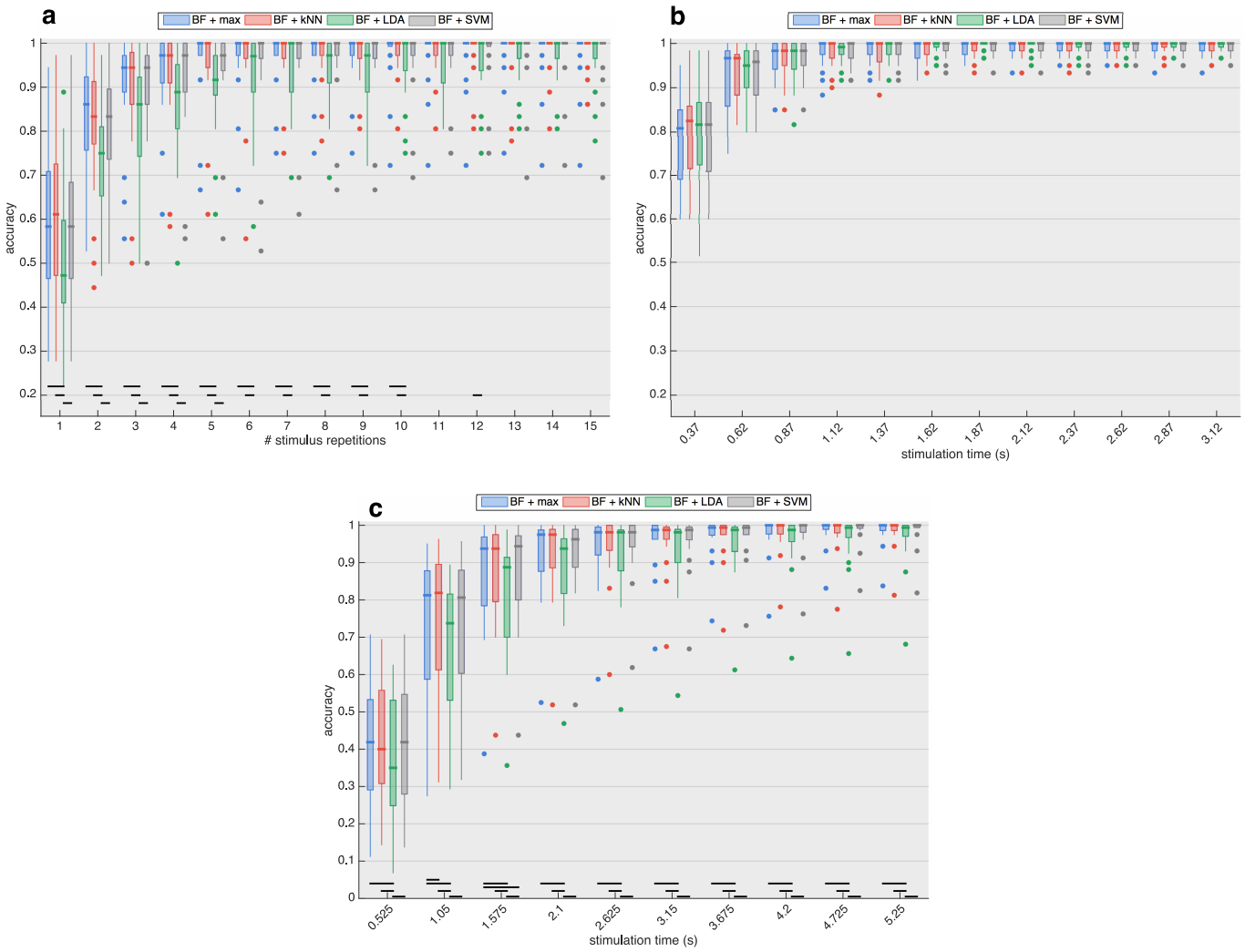

Figure 5.5: Accuracy of target identification for the (a) P300, (b) SSVEP and (c) cVEP paradigms with increasing stimulation lengths, and with target prediction based on the maximal beamformer (BF + max) output, as well as the prediction based on the k-Nearest Neighbour (kNN), Linear Discriminant Analysis (LDA) and Support Vector Machine (SVM) algorithms, using the beamformer outputs of all targets as feature vector. The results show that classification algorithms do not outperform maximum-based prediction, indicating that interactions between beamformer outputs do not increase target prediction accuracy. The black horizontal lines indicate significant differences based on the paired two-tailed Wilcoxon signed rank test with Bonferroni correction. Accuracies of all subjects are summarized using boxplots: the thick horizontal line indicates the median accuracy, the box stretches from the 1st to the 3rd quartile, the lines extending from the box indicate the minimum and maximum value within 1.5 times the interquartile range from the 1st and 3rd quartile, respectively, and the dots represent outliers.

5.4 DISCUSSION

In this manuscript, we described a transparent and unified decoding approach to synchronous visual BCI, and showed its feasibility for three popular paradigms: P300, SSVEP and cVEP. The feature vector of a trial was determined as the output of spatiotemporal beamformer(s), and we compared four methods for predicting the intended target.

The accuracies obtained by the NN- and SVM-based predictions are, with two exceptions for the cVEP paradigm, not significantly different from maximum-based prediction. The additional information given by the interaction between the beamformer outputs is not beneficial for target identification, and is even detrimental when adopting an LDA-based classifier. Furthermore, maximum-based prediction has a computational advantage as no feature extraction and classifier training is required after building the spatiotemporal beamformer(s) (see Figure 5.3).

For all three tested paradigms, an identical electrode set was included in the analysis to demonstrate the versatility and robustness of the spatiotemporal beamforming approach. As the aim of this study was to describe a unified methodology for synchronous BCI, the accuracies reported in this manuscript are likely not optimal and could be improved by optimizing the electrode set [15, 17, 173, 200, 275, 335] or the filtering range [204, 286] for each subject individually. In our previous work [331, 332, 335], we have shown that the accuracies obtained by the spatiotemporal beamforming approach are at par of even outperform the state-of-the-art classifiers of the respective paradigms, and that training beamformers is often faster than alternative classification methods such as SVM, which would allow experimenters to explore the aforementioned optimizations within a reasonable amount of time.

Both spatial and spatiotemporal filtering serve to improve the signal-to-noise ratio (SNR), which allows for more accurate ERP analysis or classification performance. While the LCMV beamformer approach with a data-driven activation pattern has also been applied to spatial filtering [306], the spatiotemporal filter used in this study has the advantage to jointly model both the spatial and temporal characteristics of the signal-of-interest. For the P300 ERP, for example, it has been shown that target prediction is more accurate when the early visual ERP components (e.g., N200 elicited over the occipital cortex) are included in the analysis [30, 141], and many studies have therefore investigated stimulation paradigms that elicit additional ERP components [129, 132, 142]. A spatial filter tuned to the centro-parietal P300 component would filter out these additional components, causing a reduction in prediction accuracy.

In recent years, various complex algorithms have been proposed that often rely on (multiple) extensions of an existing algorithm and that are tailored to a specific paradigm (eg., the extensions for MSI [355] and CCA [55, 56, 186, 221, 231, 321, 353, 356] for SSVEP detection). Other proposed approaches apply a black-box classification algorithm (SVM, Neural Networks), where the experimenter does not have control

over the pattern on which target discrimination is based. However, in the context of BCI, this pattern is in most cases well known, and in previous work we have shown that for example the pattern learned by a state-of-the-art black-box SVM in the context of a P300-BCI is very similar to the activation pattern obtained by simple averaging such as in the spatiotemporal beamformer approach [331]. Unlike these algorithms, the beamforming approach described in this manuscript is less complex (as desired, cfr. Occam's razor), fully transparent and applicable to various synchronous stimulation paradigms.

In future work, we will further develop the spatiotemporal beamformer. At this point, the main bottleneck is to estimate the high-dimensional covariance matrix, which, to be accurate, requires a significant amount of training data (cfr. the curse of dimensionality [248, 272]). Compared to the spatial beamformer, the covariance matrices in the spatiotemporal variant consider the complete temporal dimension of the signal-of-interest for each evaluated channel (hence its dimension of $(mn) \times (mn)$, with m the number of channel and n the number of (time) samples). For the 10 channels selected in our study, the covariance matrices had the following dimensions: 380 (= 10 channels x 38 samples) for P300; 420 or 340 (depending on the frequency) for SSVEP; and 630 for cVEP. Furthermore, since our approach requires spatiotemporal samples, training data is considerably harder to obtain. For a spatial beamformer, one typically can collect hundreds of samples in one second, while for the spatiotemporal variant the number of samples that can be collected per second depends on the temporal characteristics of the signal-of-interest. In our study, the P300 epochs were 0.6 s long (albeit that they are partially overlapping), SSVEP segments required 1/12 or 1/15 seconds of stimulation (depending on the frequency), and one signal-of-interest in the cVEP paradigm was 0.525 seconds long, leading to a mere 3 (= 0.6 s with 0.2 s stimulus onset asynchrony), 12 or 15, and 1.9 samples extracted from the first second of stimulation for P300, SSVEP and cVEP, respectively. In addition to reducing the number of channels included, alternative methods for the estimation of the covariance matrix can be considered. In this and previous studies, we estimated a pooled covariance matrix by including non-targeted segments for the covariance matrix estimation, which is often used in cases when the amount of samples is smaller than the dimensions of the covariance matrix (e.g., facial recognition [78], BCI [318]). However, several methods for covariance matrix estimation with a small number of samples have been described (e.g., shrinkage [179], regularization [90], among others) and can be assessed in terms of improving the estimation of the covariance matrix.

At this time, we applied the beamformer for synchronous signals, but it can likely be extended for asynchronous detection of spatiotemporal signals of interest. As the beamformer outputs can be interpreted, the spatiotemporal beamformer in combination with a sliding window could be used as transformation of multi-electrode EEG to a single-trace estimate of the contribution of a spatiotemporal template in ongoing

EEG recordings. An important aspect of this development will be to limit to amount of false positive detections.

5.5 CONCLUSION

In this study, we described spatiotemporal beamforming as a unified approach for target identification in BCI applications that rely on EEG responses synchronized to the stimulation onset. We have shown the versatility of our approach by applying it to three popular visual stimulation paradigms (P300, SSVEP and cVEP), and demonstrated its robustness since high accuracies were reached with an identical (thus, non-optimized) electrode set for all paradigms. Unlike other classification algorithms, the spatiotemporal beamformer is fairly straightforward and fully transparent as the experimenter has full control over the activation pattern used for target discrimination. Finally, we showed that selecting the target with the highest beamformer output suffices to achieve a competitive accuracy, and that by accounting for possible interactions between beamformer outputs, accuracy does not further improve.

6

REPRESENTATION OF STEADY-STATE VISUAL EVOKED POTENTIALS ELICITED BY LUMINANCE FLICKER IN HUMAN OCCIPITAL CORTEX: AN ELECTROCORTICOGRAPHY STUDY

This chapter has been published as:
B. Wittevrongel, E. Khachatryan, M. Fahimi Hnazaee, E. Carrette, L. De Taeye, A. Meurs, P. Boon, D. Van Roost and M.M. Van Hulle (2018) *Representation of steady-state visual evoked potentials elicited by luminance flicker in human occipital cortex: an electrocorticography study.* NeuroImage 175, 315-326.

Despite the widespread use of steady-state visual evoked potentials (SSVEPs) elicited by luminance flicker in clinical and research settings, their spatial and temporal representation in the occipital cortex largely remain elusive. We performed intracranial-EEG recordings in response to targets flickering at frequencies from 11 to 15 Hz using a subdural electrode grid covering the entire right occipital cortex of a human subject, and we were able to consistently locate the gazed stimulus frequency at the posterior side of the primary visual cortex (V1). Peripheral flickering, undetectable in scalp-EEG, elicited activations in the interhemispheric fissure at locations consistent with retinotopic maps. Both foveal and peripheral activations spatially coincided with activations in the high gamma band. We detected localized alpha synchronization at the lateral edge of V2 during stimulation and transient post-stimulation theta band activations at the posterior part of the occipital cortex. Scalp-EEG exhibited only a minor occipital post-stimulation theta activation, but a strong transient frontal activation.

6.1 INTRODUCTION

Steady-State Visual Evoked Potentials (SSVEPs) are electrophysiological responses to visual stimulation at particular frequencies. Originally studied in the context of scalp-recorded EEG [254, 255], it has also been considered in fMRI [22], MEG [302] and PET [232, 233], in both animal [222, 250] and human subjects. It has been used to study a wide range of pathological (eg., schizophrenia [63], autism [26], etc.) and physiological (eg., aging [249], attention [217], etc.) phenomena, and is widely adopted in human visual psychophysics (eg., binocular rivalry [352], visual perception [7, 133, 225, 263], etc.), and brain-computer interfacing (BCI) [32, 187, 332–334] (for review, see [315]).

By taking advantage of so-called "frequency tagging" of stimuli, the involvement of different cortical areas in a given task (e.g., frontal [80, 148], occipito-temporal [13, 133, 145], parietal areas [145]) can be differentially investigated in terms of their spatial and temporal response dynamics [80, 281, 282] and attentional deployment [304]. Even though the used stimuli can activate a number of cortical areas depending on the employed task and stimulus complexity, there is general consensus that it always activates the primary visual cortex (V1). However, only very few studies [137, 158, 330] provide direct electrophysiological evidence by using electrodes placed on or into the cortical tissue. Previous studies [88, 170, 210, 283, 291, 301] mainly rely on hemodynamic techniques such as fMRI and PET that provide a higher spatial resolution than EEG but lack the temporal resolution needed to monitor the temporal dynamics of SSVEP responses.

In an attempt to reconcile their spatial and temporal resolutions, hemodynamic neuroimaging techniques have also been combined with scalp-recorded EEG [22, 75, 232], although they actually reflect different aspects of neuronal activity [22, 330]. By combining PET and scalp-EEG with stroboscopic stimulation between 5 and 40 Hz, Pastor and coworkers concluded that the representation of the fundamental frequency is located in V1 [232] and the representation of the second harmonic component mainly in occipito-parietal regions [233]. Another study, based on simultaneous fMRI-EEG recordings, confirmed that the primary activation is located in the primary visual cortex (V1) but with additional activations in area MT/V5 [75], albeit that the latter was most likely due to the perceived motion evoked by pattern-reversal stimulation.

In an early study by Kamp and coworkers [137], one human subject was implanted with multiple depth electrodes and engaged in an experiment with periodically flickering stimuli. Although some electrodes extended into the occipital cortex, these recordings were not reported in their manuscript. Furthermore, the results were mainly qualitative, with no statistical assessment, and no insights were provided into their anatomical distribution. Krolak-Salmon and coworkers [158] studied the effect of high-frequency flickering (60-70 Hz) in the lateral geniculate nucleus (LGN) and primary visual cortex in three patients with refractory epilepsy, two of which were implanted with depth electrodes along the superior bank of the calcarine sulcus. They measured

spectral power and found a strong, highly localized activation, corresponding to the stimulation frequency, in LGN and around the posterior side of the calcarine sulcus, and weaker activations along the parietal-occipital sulcus. Additionally, their study showed that the upper bank of the right calcarine sulcus is most active when stimulating the left inferior quadrant of the visual field, which is in line with retinotopic mapping studies [81, 251, 324].

In this study, we investigate occipital SSVEP responses evoked by luminance flickering with electrocorticography (ECoG) covering the entire occipital cortex of a patient's right hemisphere. We investigate these responses not only in terms of stimulation frequencies, but also explore activations in theta, alpha and (high) gamma bands.

6.2 MATERIALS AND METHODS

6.2.1 *Participants*

A 38-year old male patient (right-handed, corrected-to-normal vision) with refractory non-photosensitive epilepsy participated in the study. He was admitted to the hospital (UZ Gent) for monitoring seizure activity and functional mapping of eloquent cortex (visual, language, etc.). A subdural grid was implanted over the right occipital cortex (Figure 6.2a). The study was conducted according to the current version of the Declaration of Helsinki (2013) following ethical approval from the ethical committee from Ghent University Hospital. Prior to participating, we informed the patient about the aim of our study, the experimental procedure, and what would be done with the recorded data, after which he gave his written consent.

Additionally, five healthy subjects (4 male, 1 female, mean age 23.6 years, ranging from 19 to 28 years, 1 left-handed) with normal or corrected-to-normal vision participated in the experiment as a control group while continuously recording their scalp EEG. Prior to their participation, all control subjects were informed about the aim, setup and data use, after which they read and signed a consent form approved by the ethical committee of Leuven University Hospital (UZ Leuven). The control subjects received a monetary reward.

6.2.2 *Scalp-EEG and ECoG acquisition*

For the patient, 48-channel ECoG and 27-channel scalp-EEG data were recorded simultaneously at a sampling rate of 1024 Hz using an SD LTM 64 Express (Micromed, Italy) medically certified device. The ECoG signal was acquired using subdural platinum electrodes embedded in silastic (Ad-Tech, USA). Each electrode had a 4.0 mm diameter with 2.3 mm exposure and 10 mm contact spacing. The subdural grid (6×8 contacts) was covering the right occipital cortex: convexity and mesial interhemispheric cortex. Functional mapping confirmed that a large part of the grid was located over the visual

cortex. Due to insufficient quality of the simultaneously recorded scalp-EEG (dried conductive gel, as well as the influence of scarred and swollen tissue), the patient's scalp-EEG was excluded from further analysis.

The scalp recorded EEG from healthy control subjects was acquired with a Synamps RT device (Neuroscan, Australia), using 128 active Ag/AgCl electrodes evenly distributed over the scalp (Figure 6.5b) and a sampling rate of 2 kHz. Conductive gel was applied at each electrode, and the impedance between the skin and the electrodes was kept below 2 kΩ.

6.2.3 *Localization of ECoG electrodes*

Based on the pre-implantation MRI scan of the patient, cortical reconstruction and volumetric segmentation was performed with the Freesurfer image analysis suite (version 5.3.0) [85]. The Freesurfer output was then loaded into Brainstorm [296] and co-registered with the post-implant CT. The coordinates of the implanted electrodes were then manually obtained and mapped on the cortical surface.

6.2.4 *Experimental procedure*

The experimental interface consisted of six identical rectangular targets (8.8×5.8 cm) presented on a 60 Hz LCD monitor. A number (from 1 to 6) was displayed in the center of each target, which served as fixation point for the corresponding rectangle. The targets adopted a green color to reduce the visual demand [49, 300] and the risk of inducing an epileptic seizure [136]. All subjects were seated approximately 60 cm from the screen. At this distance, the visual angle spanned by the rectangles was $8.4^\circ \times 5.5^\circ$, and the distance from the fixation point to the edge of the neighbouring target is 5.5° horizontally and 4.1° vertically.

The experiment consisted of four sessions. In each session, all rectangles were assigned an unique combination of frequency and phase (Table 6.1).

Session	Target					
	1	2	3	4	5	6
1	12/0	$14/\frac{2\pi}{3}$	$12/\frac{4\pi}{3}$	$14/\frac{4\pi}{3}$	$12/\frac{2\pi}{3}$	14/0
2	13/0	$14/\frac{2\pi}{3}$	$13/\frac{4\pi}{3}$	$14/\frac{4\pi}{3}$	$13/\frac{2\pi}{3}$	14/0
3	11/0	$15/\pi$	13/0	$13/\pi$	$11/\pi$	15/0
4	13/0	$15/\pi$	14/0	$14/\pi$	$13/\pi$	15/0

Table 6.1: Target frequency-phase combinations for each session, represented as [frequency (Hz)/phase (radians)].

Each session consisted of 90 trials. At the beginning of each trial, one of the targets was cued by maintaining its green color while the other rectangles were shown in grey (Figure 6.1). The subject was instructed to direct his/her gaze at the cued target during the subsequent stimulation. When the subject pressed a key on the keyboard, the rectangles all regained their green color, and one second later, the four-second stimulation was initiated, during which all targets were flickering in accordance with their frequency/phase combination, achieved by sinusoidally modulating their luminosities [207]. Between trials, the subject was allowed to take a break, with a longer break (± 5 min) between sessions. In each session, all targets were cued 15 times in pseudorandom order. An example (video) of the stimulation of the first session is provided in the supplementary material.

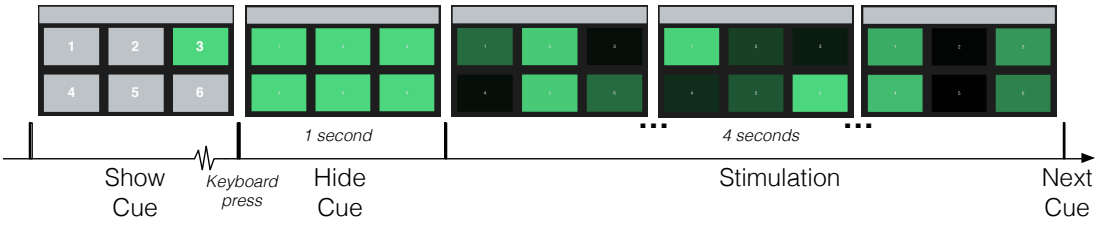

Figure 6.1: The time-course of one trial, with representation of the interface at several moments. Note that the target numbers on the left interface are enlarged for better visualization, and do not correspond to the actual size.

6.2.5 *Pre-processing*

The raw ECoG data was re-referenced offline to the grid's average, and cut into four-second epochs, time-locked to the onset of the stimulation. Additionally, for each trial, two extra epochs were extracted corresponding to one second before and one second after stimulation. These pre-and post-stimulation epochs were used for the time-frequency analysis (see further). The number of the cued target was used to label to the epoch (and the corresponding pre- and post-stimulation epochs), and all epochs were stored for further analysis. In total, 90 labeled epochs were extracted per session.

The scalp-EEG recordings of the control group were re-referenced offline to the average of the mastoid signals (TP9 & TP10), and subjected to an identical epoching procedure.

6.2.6 *Spectral Power and Phase Estimation*

The power spectral density (PSD) of an epoch was estimated using Welch' method with a hamming window of two seconds and a 50% overlap between successive windows.

The hamming window minimises spectral leakage in neighbouring frequencies, which is important since the maximal stimulation-frequency resolution in our experiment was 1 Hz. The power at frequency f was obtained directly from the PSD function, and the average power in the theta (4-8 Hz), alpha (8-12 Hz), and high gamma (80-120 Hz) bands were obtained from Matlab's (2015a) *bandpower* function.

For concise visualization, we used contourplots of a cubic interpolated activation map, and only plotted the activations that exceeded a threshold th:

$$th = median(\mathbf{X}) + 2 * std(\mathbf{X}), \tag{6.1}$$

where $\mathbf{X} \in \mathbb{R}^{n \times tr}$ contains the power values for all n channels of tr trials. As activations on the cortex are very localized [48], one can expect them to be outliers compared to the other channels.

The phase φ_c of the signal $\mathbf{s}_c(t)$ in channel c is estimated as [126, 207, 323]:

$$\begin{aligned} \varphi_c &= \text{Arg}\Big(\mathcal{F}(\mathbf{s}_c)(f)\Big) \\ &= \text{Arg}\Big(\sum_t \mathbf{s}_c(t)\,\cos(2\pi f t) + j\sum_t \mathbf{s}_c(t)\,\sin(2\pi f t)\Big) \\ &= \text{atan2}\Big(\sum_t \mathbf{s}_c(t)\,\cos(2\pi f t), \sum_t \mathbf{s}_c(t)\,\sin(2\pi f t)\Big), \end{aligned} \tag{6.2}$$

where f is the frequency under consideration, $\mathcal{F}(\mathbf{s}_c)$ is the discrete Fourier transform of $\mathbf{s}_c(t)$, and $j = \sqrt{-1}$.

6.2.7 *Time-Frequency Analysis*

The excellent temporal resolution of ECoG allows us to perform a time-frequency analysis of the trials to detect Event-Related Synchronization (ERS) [238, 239].

To detect the ERS of a session, first, all trials of said session were extended by prepending and appending the corresponding pre- and post-stimulation epoch (see section about preprocessing). Then, all extended trials were filtered in a given frequency range and for each sample, the average value across all trials was subtracted in order to remove evoked effects (cfr. Event-Related Potentials, ERPs) that might interfere with the induced effects, especially in the lower frequency bands (theta and alpha band) [102, 103, 239]. This was followed by the squaring of the values, averaging across trials and subtraction of the baseline value. As baseline, we used the median activity in the (filtered, subtracted, squared and averaged) one-second pre-stimulation epoch. To avoid overestimating ERS [123], we did not normalize by dividing the baseline and, to account for spurious activity during the pre-stimulation epoch, we used the median rather than the average to obtain the baseline. Finally, the baselined curve was smoothened using a centered 50 ms sliding average (i.e. [-25, 25] ms) to obtain the final ERS curve. 95% confidence intervals were calculated by a bootstrapping procedure with 1000 iterations, following the procedure described by Graimann and coworkers

[102, 103]. In each iteration, 360 datapoints were randomly selected (with replacement) for each sample, and used to ascertain the confidence interval.

Unlike for frequency bands, to obtain ERS at the stimulation frequency, not all trials were filtered in the same range. Each trial t was filtered between $f_t - 1$ and $f_t + 1$ Hz, where f_t is the stimulation frequency of the foveal target of trial t, followed by the same subtraction, squaring, averaging, baselining and smoothing procedure described above.

For the control group, the ERS for a particular session was obtained as the average ERS of all subjects for that session.

6.2.8 *Statistics*

Since the Shapiro-Wilk normality test did not show consistent Gaussian distributions (i.e., normality rejected), we adopted nonparametric tests for measuring statistical significance. We compared several factors:

1) Differences in spectral band powers with respect to the location of the gazed target was assessed using the Kruskal-Wallis test and pairwise comparisons with the two-tailed Wilcoxon rank-sum test.

2) The spectral band powers were compared with respect to foveal frequency. However, unlike for the target locations, the number of trials (observations) for each foveal frequency were not equal, hence, to account for the unequal number of observations, we adopted a bootstrapping procedure with 100 iterations. In each iteration, all 30 trials for the 11 Hz frequency (which had the least trials) were included and joined by 30 randomly chosen (with replacement) trials for every other frequency. For each iteration, a Kruskal-Wallis test was adopted to assess differences between frequencies, and a two-tailed Wilcoxon rank-sum test was applied to asses pairwise comparison. For both the initial and pairwise statistical measures, the final p-value was given by the median p-value of 100 iterations.

3) The powers at the fundamental and harmonic frequency were compared using a paired two-tailed Wilcoxon signed-rank test.

Results that had a p-value lower than 0.05 were considered statistically significant. For multiple comparisons, a Bonferroni correction was applied to the significance threshold.

6.3 RESULTS

We presented six flickering targets and asked the patient and control subjects to gaze at an indicated target (see Figure 6.1 for a visual rendition of a single trial). All subjects performed four sessions, in which targets adopted a unique frequency/phase combination (see Table 6.1).

6.3.1 *Spectral bands*

Figure 6.2 shows the average spatial activations of the spectral bands (theta, alpha and high gamma band) for each of the targets for the first session.

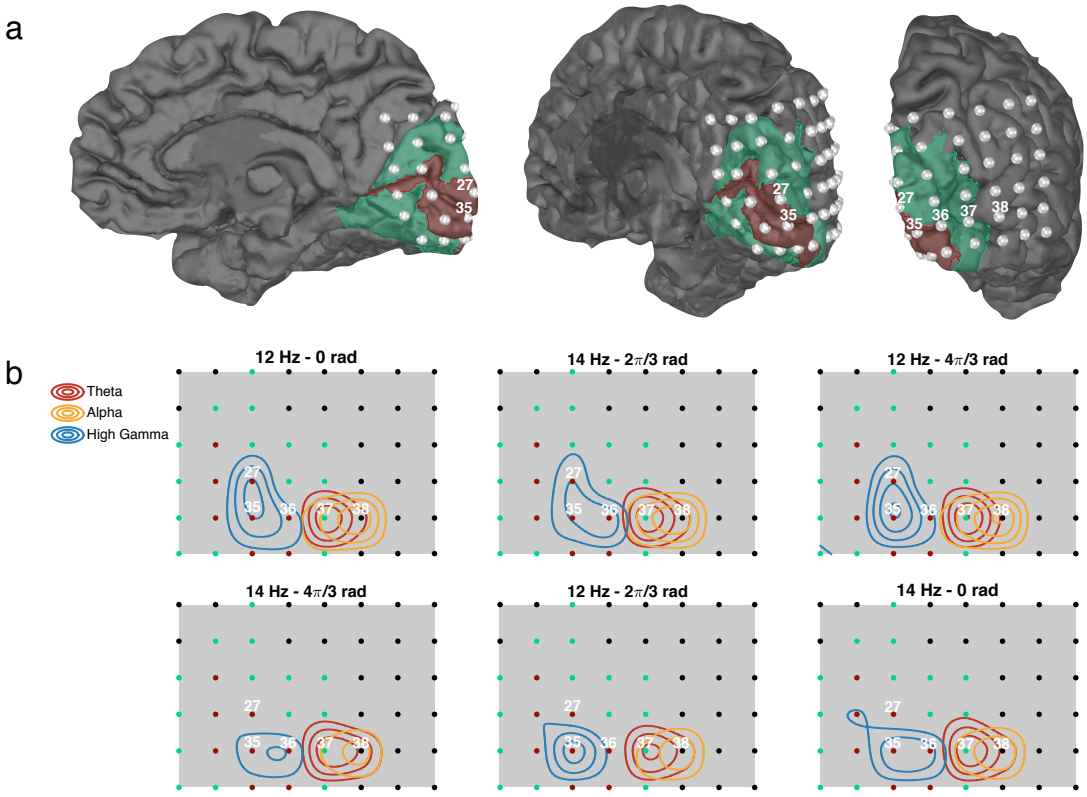

Figure 6.2: Spatial activations in theta, alpha and high gamma band. (a) Visualisation of the patient's right hemisphere with the location of the implanted electrodes. The red and green areas represent V1 and V2, respectively, and were extracted by Freesurfer. (b) Average activations in theta, alpha and gamma bands for each of the six targets for the first session. Red and green electrodes correspond to V1 and V2, respectively.

For all targets, theta activations are consistently located at the lateral side of V2 (superior occipital sulcus, electrode 37). The activations are consistent across sessions (see supplementary figure S1), and their locations invariant to the stimulation frequency and position of the gazed target. A Kruskal-Wallis test revealed a significant effect of foveal target on the spectral power in the theta band ($\chi^2(5) = 17.04$, $p = 0.0044$) as well as a significant effect of foveal frequency ($p = 0.0002$, bootstrapped Kruskal-Wallis test with 100 iterations). There is a tendency towards an increased theta response with increasing frequency (Figure 6.3a, bottom panel), albeit only significantly for most extremal frequencies (11 vs 15 Hz, $p = 0.0001$ and 12 vs 15 Hz, $p = 0.0008$). With

respect to the location of the gazed target, there is a significant difference in theta power between targets 2 and 5 (top center versus bottom center target, $p = 0.0006$) and targets 3 and 5 (top right versus bottom center target, $p = 0.0007$). A temporal analysis (Figure 6.5a) confirms that activity in the theta band only increases at electrode 37 during stimulation and returns to its baseline when flickering ends. However, an exploratory analysis revealed that, while other locations are not activated during stimulation, strong transient activations are exhibited at several posterior electrodes (electrode 35, 36 and 38) following stimulation offset. In scalp-EEG (Figure 6.5b), minor post-stimulation activations can be detected over central to occipital areas and a very strong theta activation over the frontal pole. The post-stimulation activity at Pz is similar to the lateral cortical activity at electrode 38, while the medial short-latency activation at cortical electrode 35 has no obvious counterpart on the scalp. Finally, at electrodes 38 (middle occipital gyrus) and 37 (superior occipital sulcus), we observe a small increase and decrease in theta band activity during the pre-stimulation interval.

Similar to the theta band, activations in the alpha band are consistently located at the lateral edge of V2 (Figure 6.2b), and most strongly in the middle occipital gyrus (electrode 38). A Kruskal-Wallis test revealed a significant effect of foveal target on alpha power ($\chi^2(5) = 74.18, p \ll 0.001$), as well as a significant effect of foveal frequency ($p = 0.0023$, bootstrapped Kruskal-Wallis test with 100 iterations). The alpha power at this location is significantly higher when gazing at one of the upper targets compared to the lower targets (Figure 6.3b), but not significantly different across frequencies, except when gazing at a 12 Hz frequency target compared to a target flickering at 13 ($p = 0.0025$) or 15 Hz ($p = 0.0022$). An ERS analysis (Figure 6.5) confirms that the alpha power at the lateral edge of V2 (electrodes 37 and 38) increases during stimulation, and returns to baseline after stimulation, and that electrode 35 has a transient post-offset activation in the alpha band. Similar to the theta band, electrodes 37 and 38 also exhibit a small transient activation in the pre-stimulation interval. On the scalp, the alpha activation increases over occipital and parietal areas, and a transient response is observed over the frontal area, albeit considerably smaller in amplitude compared to the theta band. Also in the alpha band, the post-stimulus transient activation at medial cortical electrode 35 cannot be detected in occipital scalp-recorded EEG.

Activations in the high gamma band are localized at the posterior side of the primary visual cortex (electrodes 35 and 36, Figure 6.2b). While gazing at the upper targets, the activation includes electrode 27.

A Kruskal-Wallis test on high gamma band power revealed a significant effect of foveal target at electrodes 26 ($\chi^2(5) = 279.43, p \ll 0.001$), 27 ($\chi^2(5) = 290.9, p \ll 0.001$), 35 ($\chi^2(5) = 109.92, p \ll 0.001$) and 36 ($\chi^2(5) = 84.39, p \ll 0.001$), and a significant effect of stimulation frequency (bootstrapped Kruskal-Wallis with 100 iterations) at electrodes 27 ($p = 0.0037$), 35 ($p \ll 0.001$) and 36 ($p \ll 0.001$).

Figure 6.4a confirms that both electrode 26 and 27 are location selective and significantly different (upper vs. lower targets) in the high gamma band. While a significant

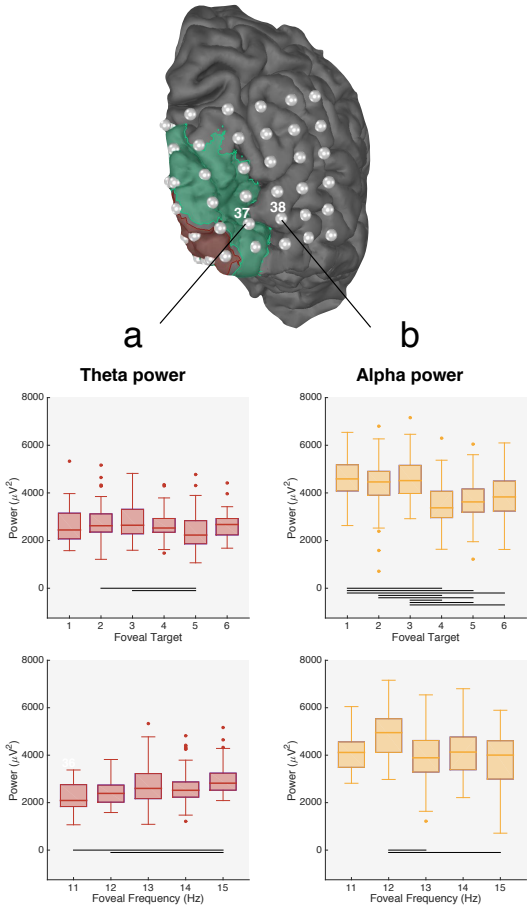

Figure 6.3: Spectral power as function of foveal target (upper panels) and foveal frequency (lower panels). (a) Average power in the theta band at electrode 37. (b) Average power in the alpha band at electrode 38. Horizontal lines indicate significant differences based on a two-tailed pairwise Wilcoxon ranksum test with Bonferroni correction. The spectral powers of all four sessions are summarized in boxplots: the thick horizontal line indicates the median value, the box stretches from the 1st to the 3rd quartile, the lines extending from the box indicate the minimum and maximum value within 1.5 times the interquartile range from the 1st and 3rd quartile, respectively, and the dots represent outliers.

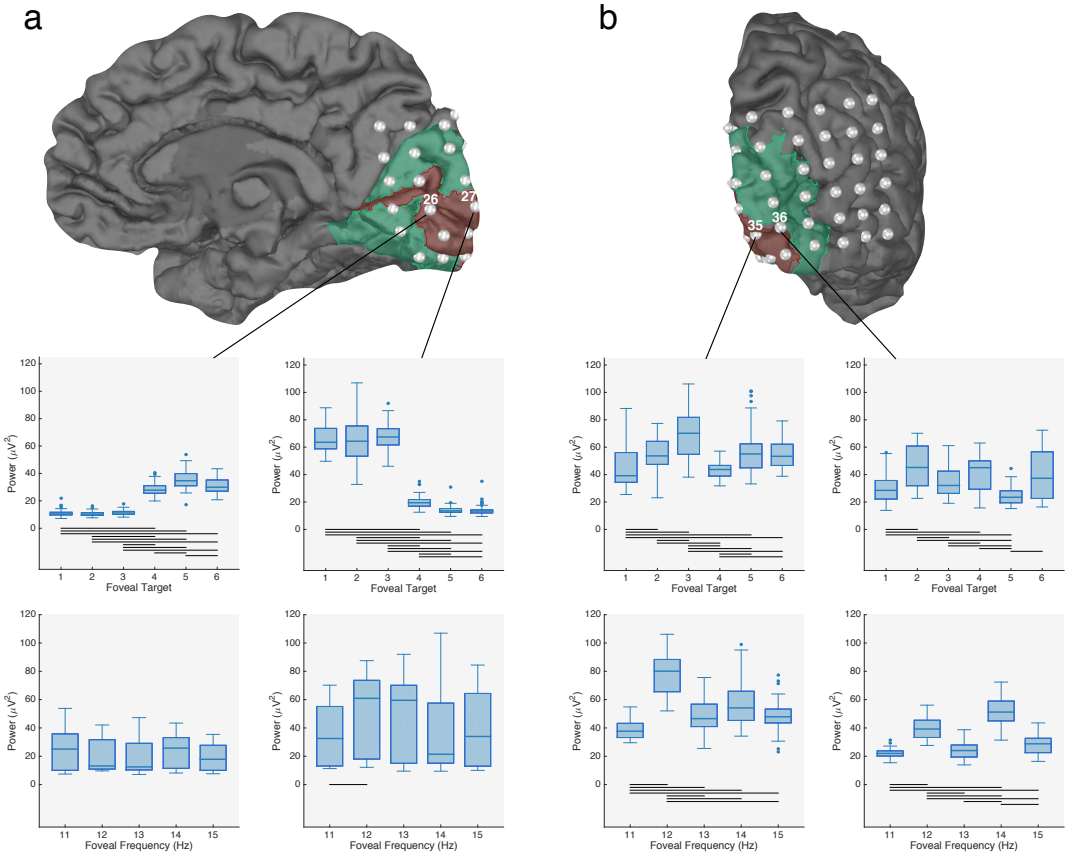

Figure 6.4: Average power in the high gamma band as function of foveal target (top panels) and foveal frequency (bottom panels). (a) electrodes 26 (left) and 27 (right), (b) electrodes 35 (left) and 36 (right). Horizontal lines indicate significant differences based on a two-tailed pairwise Wilcoxon ranksum test with Bonferroni correction. The spectral powers of all four sessions are summarized in boxplots using the same convention as in Figure 6.3

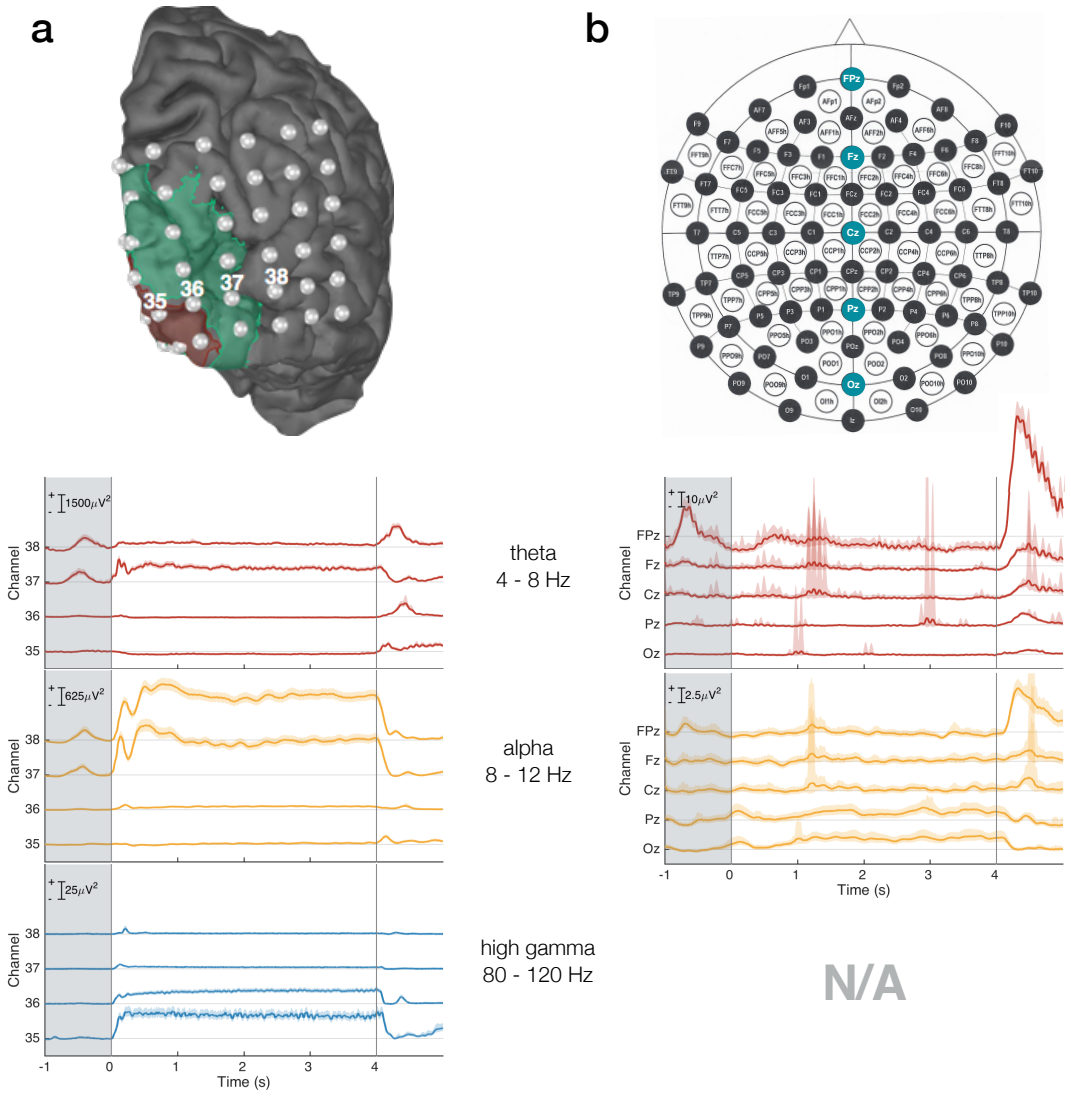

Figure 6.5: ERS analysis in different frequency bands. (a) at several locations on the cortex, revealing transient pre-and post-stimulation activations, and (b) along the midline of the scalp EEG (calculated using all control subjects), revealing a strong frontal peak in the theta band. Since the spatial activations of the alpha, theta and gamma band are stable across all frequencies and foveal targets (Figure 6.2b), all trials were used to calculate the ERS curve. Note that the ERS plots have different scales. The solid curve and shaded area represent the mean and 95% confidence interval across all four sessions, respectively. The baseline window is indicated in grey, and the vertical line at 4 seconds marks the offset of the visual stimulation. N/A (not available) signifies that high gamma activity was not detectable in the scalp EEG.

difference was found at electrode 27 between the high gamma powers for a stimulation frequency of 11 and 12 Hz ($p = 0.0006$, bootstrapped Wilcoxon rank-sum test), this is most likely due to the imbalance in the experimental design (i.e., not all frequencies were adopted as many times nor at all target locations) and the considerable difference in power between the upper and lower targets at this electrode.

At electrode 35, the power in the high gamma band is considerably higher for a stimulation frequency of 12 Hz, and is significantly different from all other frequencies. In addition, there is a tendency for an increased gamma response when gazing at a target located at the right side of the interface (i.e., when there is a target in the left hemifield, Figure 6.4b (top left panel)). In contrast, at electrode 36, the 14 Hz stimulation frequency evokes the highest high gamma activation, followed by the 12 Hz stimulation, and both are significantly different from the activations evoked by the other stimulation frequencies. Despite several statistical differences between the high gamma responses to the six foveal targets, no clear pattern could be observed.

ERS analysis (Figure 6.5, lower panel) reveals that the gamma response rises quickly at electrodes 35 and 36 following stimulation onset and remains stable until shortly after stimulation offset.

6.3.2 *Fundamental and harmonic frequencies*

To assess foveal activation for each stimulation frequency, we averaged the activations of all targets sharing the same stimulation frequency across all sessions. This averaging filters out the activations that are not consistent across equal-frequency targets, including the activations elicited by peripheral targets.

Figure 6.6a shows the average spatial activations at the fundamental frequency of the foveal target and its second harmonic for each of the stimulation frequencies. The fundamental activations are located around the posterior side of the occipital cortex, most strongly in V1 (electrode 35, 36) and reaching laterally to V2 (electrode 37). For the 11 Hz stimulation frequency, there seems to be two localised activations, one in V1 (electrode 35 and 36) and one lateral from V2 (electrode 38). However, since electrode 38 is also the location where the alpha band is most prominent for all stimulation frequencies (see above), and since the 11 Hz frequency falls within the alpha band, this lateral activation could be an artifact of the alpha band activation. When excluding this lateral activation, the fundamental SSVEP component is consistently represented in V1 (electrodes 35 and 36) for all stimulation frequencies used in this study.

The spatial overlap between the fundamental and harmonic activations is maximal for the 15 Hz stimulation, and there is increasingly less overlap for the lower frequencies. This pattern is consistent across sessions (see supplementary figure S2). The 15 Hz frequency has the lowest median fundamental power, and the difference with its harmonic power is not significant ($p = 0.067$, paired signed rank, Figure 6.6b), while for the other frequencies the difference is significant. Note that, since the spatial ac-

tivations are not stable across frequencies and harmonics, both the fundamental and second harmonic power are obtained as the maximum value over all channels. While the measured fundamental powers are not significantly different across foveal frequencies (except between 14 and 15 Hz, $p < 0.005$ (corrected), ranksum test with bootstrapping), there is a tendency for a stronger second harmonic power when gazing at higher frequencies.

In contrast with ECoG, the scalp-EEG power of the second harmonic frequency is significantly decreasing for higher frequencies (Figure 6.6c). This is most probably due to the volume conduction effect, and the low-pass filter properties of the skull [290]. As there is a considerable amount of inter-subject variability in the SSVEP response for each subject [113, 293], the group-level average exhibits many outliers (represented by dots in Figure 6.6c). The power of the fundamental and second harmonic components for each individual subject are shown in supplementary figure S3. For most subjects, the difference between the fundamental powers is not significant, and the second harmonic powers significantly decrease for higher frequencies.

The temporal analysis (Figure 6.6d) confirms that the activation at the stimulation frequency is only present during flickering, and that some time is required to reach maximal levels. Also in scalp EEG (Figure 6.6e, channel Oz), a similar increase in activation is present. Similar to the theta and alpha band, a transient activation is elicited following the stimulation offset at electrode 35 on the cortex, which is not detectable on the scalp.

6.3.3 *Peripheral targets*

Figure 6.7 shows activations elicited by peripheral targets during the second and fourth sessions. The peripheral activations of the other sessions are consistent with these and are shown in supplementary figure S4.

When the subject is gazing at one of the three top targets, the stimulation frequency of the respective lower target is consistently located at electrode 27. Similarly, when gazing at one of the lower targets, the stimulation frequency of the corresponding upper target is consistently located at electrode 26. As electrodes 26 and 27 are located on opposite sides of the calcarine sulcus, these observations are in line with the retinotopic mapping described in other studies [81, 251, 324]. Additionally, these electrodes correspond to locations where high gamma band power significantly differs between upper and lower targets.

All attended targets that have a peripheral flickering target in the left visual field (i.e., targets 2, 3, 5 and 6) display an activation in the medial inferior electrodes of the grid, embedded in the interhemispheric fissure (electrodes 41 and 42), consistent with the stimulation frequency of the said peripheral target. We do not observe any activations from the right peripheral target, as these signals should be processed by the left hemisphere (contralateral processing of visual field).

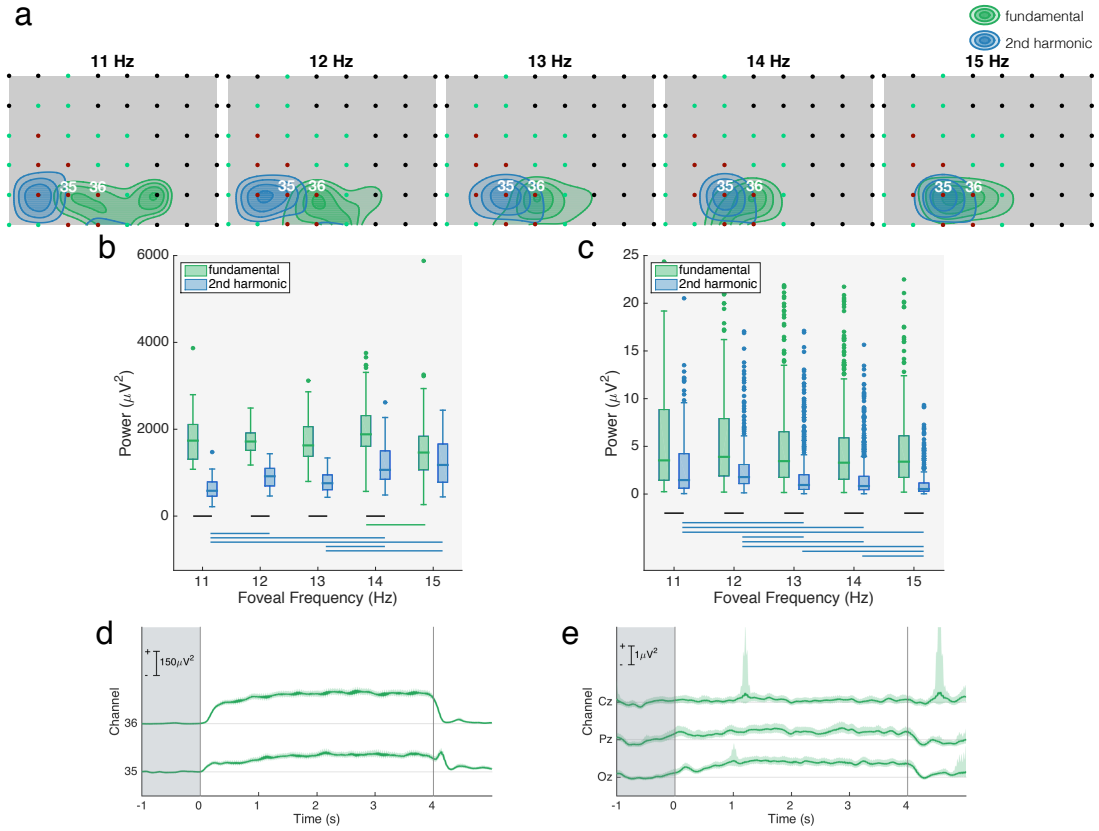

Figure 6.6: Fundamental and second harmonic components. (a) Spatial distribution of fundamental frequency and second harmonic power for each foveal frequency. (b,c) Maximal power of the fundamental and second harmonic component for each stimulation frequency for the implanted patient (ECoG, maximum over all channels, panel b) and the control subjects (scalp EEG at channel Oz, panel c) (for individual control subjects, see supplementary figure S3). The power values are represented as boxplots (same convention as in Figure 6.3). Black, green and blue horizontal lines indicate significant differences between fundamental and harmonic power within each frequency, fundamental power between frequencies, and harmonic power between frequencies. (d,e) Temporal analysis of the SSVEP at the foveal frequency for the implanted patient (ECoG, panel d) and the control group (scalp EEG, panel e). The solid line and shaded curves indicate the mean and 95% confidence interval across the four sessions.

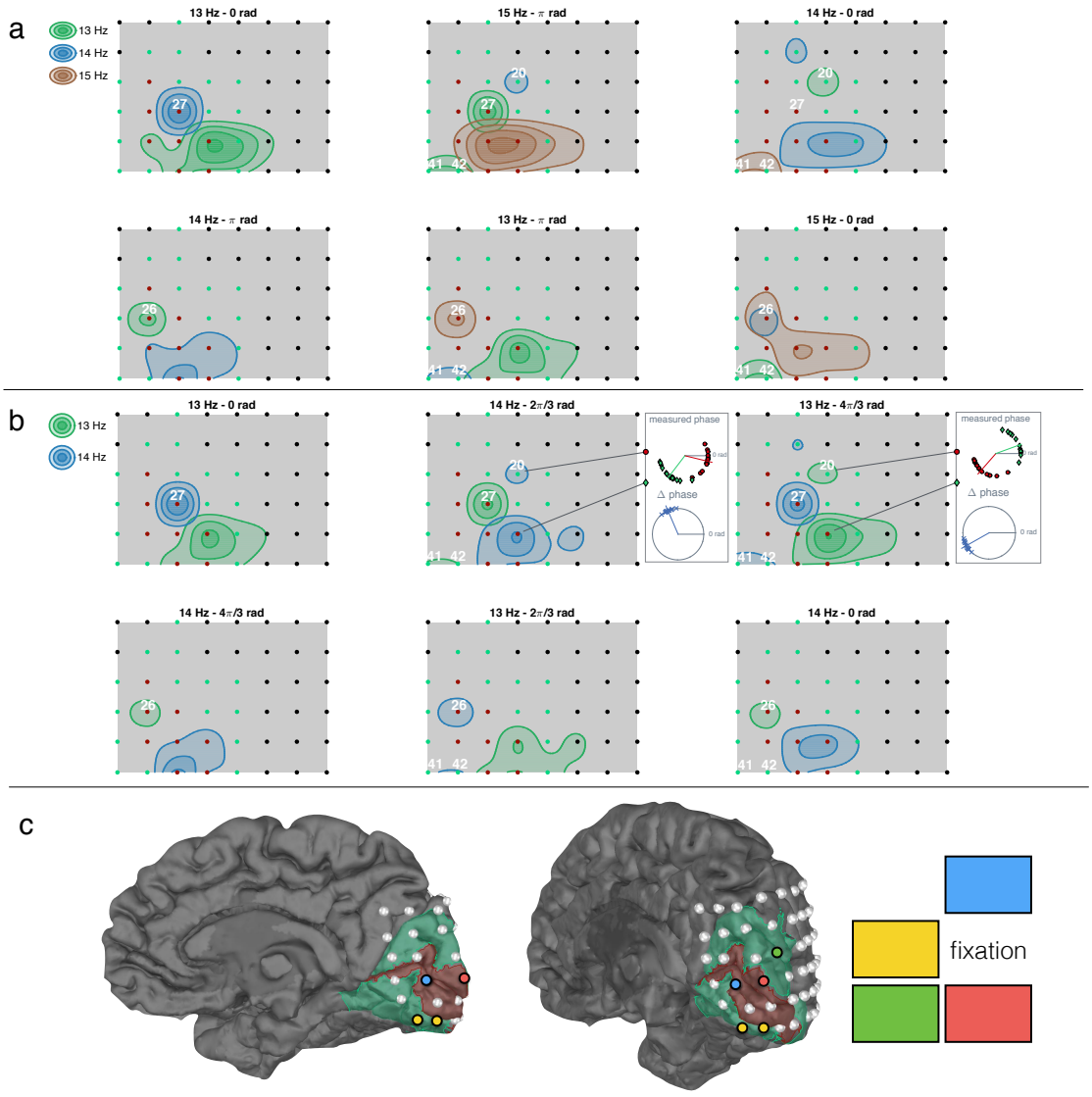

Figure 6.7: Spatial activations elicited by peripheral flickering. (a,b) Spatial frequency activations while gazing at each of the six foveal targets in session 4 and 2, respectively. (c) Summary indicating the cortical electrodes activated by flickering in different peripheral visual fields (color coded).

Finally, for targets 2 and 3, there is an activation along the superior occipital sulcus (electrode 20) that is consistent with the stimulation frequency of the lower left peripheral target. In sessions 1 and 2, the foveal and lower left peripheral targets share the same stimulation frequency, but different phases, hence the question about their phase difference. As shown in Figure 6.7b, the phase differences are consistent with the phase difference between the foveal- and the lower left peripheral stimulation. It is additionally worth noting that the phase responses deviate from trial to trial, but the difference between the phases at different electrodes (Δ) has considerable less variation, indicating a high level of synchronicity.

Figure 6.7c shows a summary of the findings obtained by analysing the peripheral activations. Note that all these findings are consistent with retinotopic mapping [81, 251, 324].

6.4 DISCUSSION

With the current study, we aim to advance our insights into the cortical representation of SSVEPs elicited by luminance flickering in the human occipital cortex.

Using direct electrophysiological evidence, we identified the fundamental component of all used stimulation frequencies (11 to 15 Hz) at the posterior side of the primary visual cortex (pericalcarine cortex, electrode 35-36). Our results are in line with the findings of Krolak-Salmon and coworkers [158], who identified the strongest frequency power (using 70 Hz visual stimulation) at the posterior site of the calcarine sulcus. Our study extends their findings, as we show that also lower-frequency stimulation elicits activations at the posterior side of V1. We additionally refine the observations of previous studies based on indirect measurements (fMRI [22], PET [232]) by showing that only a small part of the primary visual cortex is activated by foveal flickering.

Similar to the fundamental frequency component, the second harmonic component is also located in the primary visual cortex, but the exact location is frequency-dependent. When gazing at an 11 Hz target, the overlap between fundamental and harmonic activations is minimal, while for the 15 Hz target, the overlap is maximal. The PET study by Pastor and coworkers located the source of the second harmonic component at the inferior half of the parieto-occipital sulcus (and to a lesser extend at the rostral portion of the calcarine sulcus), but found no overlap in the representation of the fundamental component for any of the frequencies they considered (5, 10, 15, 25 and 40 Hz) [233]. This is not in line with our results. Moreover, the implanted electrode grid used in our study covered the parieto-occipital sulcus and, while hemodynamic activity may increase at those locations, we could not find any electrophysiological evidence that these areas are involved in the representation of the fundamental and second harmonic component of our target stimulus frequencies. It should however be noted that, contrary to our study, more distant frequencies were tested in Pastor's

study, hence, we are not in a position to comment on the representation of the fundamental and second harmonic components in response to higher or lower stimulus frequencies.

6.4.1 *Peripheral activations are consistent with retinotopic maps*

The activations elicited by peripheral stimulation are located in the interhemispheric fissure and are independent of the peripheral stimulation frequency. Flickering in the upper visual field elicits activations at the corresponding frequency around the lower bank of the calcarine sulcus. Similarly, flickering in the lower peripheral field elicits activations around the upper bank of the calcarine sulcus. These findings are consistent with retinotopic mapping studies [81, 251, 324].

EEG studies have shown that, when flickering targets are spatially separated by a visual angle of four degrees or less, co-amplification occurs (i.e., the frequency spectrum shows increased power at both foveal and peripheral frequency), and an additional intermodulation frequency appears in the frequency spectrum measured from the scalp [92]. In our study, the visual angle between targets always exceeds the four degrees threshold, hence, we are not able to shed light on this issue. However, despite their absence in the scalp-EEG frequency spectrum, our ECoG results show that peripheral targets are represented in the primary or associative visual cortex, even at visual angles exceeding four degrees. Based on our observations, retinotopic mapping, and the fact that the amplitude of the attended frequency is not affected by the distance to the distractor frequency [92], we believe that it is unlikely that both attended and distractor frequencies have a common representation at close proximities in the visual field. Rather, we hypothesize that with decreasing visual distance between foveal and peripheral targets, the peripheral activations originate closer to the foveal activations, and thus increase in strength (following the cortical magnification effect [69]).

6.4.2 *SSVEP elicits localized activations in the alpha band*

During SSVEP stimulation, the power in the alpha band increases at the lateral edge of the associative visual cortex (extrastriate cortex, with strongest power at the middle occipital gyrus, electrode 38), with a significantly higher power when gazing at the upper targets (i.e., when there are peripheral targets in the lower visual field). A time-frequency analysis of the scalp EEG of the control group also revealed an increased alpha activity during stimulation, albeit to a smaller extent.

These results provide an explanation for the alpha band resonance phenomenon observed by Herrmann [115]. While subjecting the human brain to SSVEP stimulation ranging from 1 to 100 Hz, Herrmann consistently measured activation of the alpha band in scalp-EEG. Our results now suggest that these alpha observations originate from the area lateral to V2. Given the minor influence of target location on the alpha

power described in this study, and the absence of peripheral distractors in the Herrmann's study, one can conclude that the alpha response is inherently linked to the SSVEP paradigm, at least with non-complex stimuli.

In an invasive study by Rager and Singer [250] in the cat visual cortex, the resonance in the alpha band was not detected by the electrodes implanted in the primary and associative visual cortices (Brodmann area (BA) 17 and 18 respectively). While Herrmann explained this contradiction by hypothesising that the generators responsible for the alpha oscillations consisted of larger networks of neurons, and could thus not be captured by the local recordings performed by Rager and Singer, our study shows that the alpha activations are highly localized and originate more lateral from BA 17 and 18, in the middle occipital gyrus.

6.4.3 *SSVEP stimulation elicits transient changes in theta band*

As far as we are aware, theta band activations in human visual cortex has never been reported in SSVEP studies. However, a number of (invasive) studies did investigate theta band activations in relation to memory function, most extensively in the hippocampus [47, 101], but also in other areas it has been assumed to play a role in memory function (e.g., macaque extrastriate cortex during a working memory task [180]). With event-related potentials (ERPs), theta oscillations have been correlated with selective attention [18], expectancy [20] and 'orienting' (i.e., alertness, arousal or readiness to process information) [19, 20] (for review, see [21]).

While only one implanted electrode showed clear theta synchronisation during stimulation, the offset of the stimulation elicited a clear transient activity at multiple posterior implanted electrodes. On the scalp, only a minute post-offset theta synchronisation could be detected over the occipital pole, whereas prominent theta activation over frontal areas was observed, which might result from sustained attention to the stimulus [62] or indicate a link to memory function [134].

Prior to the stimulation, the theta (and alpha) band exhibits a transient synchronisation around the superior occipital sulcus (electrodes 37 and 38), most likely representing the anticipation of the upcoming event (i.e., flickering stimulation in this study) [36, 41]. The anticipation of a sensory event (i.e., pre-stimulus) has been linked to a reset of the phase of delta-theta (2-8 Hz) activity, which speeds up the rate at which a stimulus can be detected [14], and the phase of slow spectral components (theta and alpha band) in frontal regions has been shown to play a role in the successful detection of subtle (i.e., low constrasting) stimulation [46]. Our results suggest that anticipatory slow-wave activity is present not only in complex (e.g., working memory and cognitive) tasks, but also in a basic, sensory task that does not involve higher cognitive functions (basic visual processing, as in our case).

Although that strong theta synchronization was detected over the frontal pole in our scalp-EEG, the transient theta activations observed on the cortical surface do not have

a counterpart on the scalp. It is known that scalp-EEG mainly reflects electric current in pyramidal cells perpendicular to the cortical surface [99, 153, 195, 345], rendering the orientation of the activations located at the edge of the interhemispheric fissure suboptimal for detection on the scalp. Epilepsy studies have reported that scalp-EEG is less sensitive for loci in the interhemispheric fissure [77], and bilateral activations facing the interhemispheric fissure even result in partial cancellation [3, 176]. While it seems likely that the left hemisphere has similar activity in the theta band, we are not able to confirm or reject this hypothesis, as our implanted electrodes only covered the right hemisphere. While the suboptimal orientation provides a reason for the absence of medial activations on the scalp, also no scalp-counterparts were found for the theta activations at lateral locations (electrodes 36, 37 and 38) despite of their tangential orientation. Source localisation studies have found that at least 6 cm^2 of cortical surface needs to be activated for it to be detectable on the scalp [226, 227]. Given that the transient theta activations cannot even be observed in neighbouring cortical electrodes (which are just 1 cm apart), it is likely that the surface area of the activation is not large enough to survive volume conduction. In contrast, alpha activations during stimulation span a larger area (electrode 37 and 38), and these are consequently visible over the occipital pole on the scalp.

6.4.4 *Limitations of this study*

The stimulation frequencies used in this study were limited to the range from 11 to 15 Hz, as higher frequencies (i.e., 15 to 25 Hz) generally have a higher chance to evoke a generalized epileptic seizure [86, 298] (especially since we adopted high contrast stimuli [86, 117, 120], and since our patient suffered from occipital lobe epilepsy [197, 299]), and lower frequencies might induce increased discomfort and visual fatigue [97, 349, 360]. Since the focus of this study was to explore the physiological dynamics of SSVEPs evoked in response to simple visual stimulation (flickering stimulus), at this point, the exploration of additional frequencies was not taken up in our study. Despite the partial overlap between the stimulation frequencies and the alpha band, which might slightly complicate the results, we were able to clearly distinguish alpha activations from those at the stimulation frequency (i.e., fundamental component) by averaging activations across all stimulation frequencies.

We reported on the activations of the complete right occipital cortex, including the interhemispheric fissure. As there was no grid located over the left hemisphere -the implant served a clinical purpose- we were not able to investigate activations in the left hemisphere.

6.4.5 *Outlook*

This study has shown that SSVEP stimulation elicits transient theta band activity over the posterior primary visual cortex in ECoG. While this activity was hardly detectable over the occipital pole in scalp EEG, it was strongly present over the frontal scalp area. More research is needed to determine to what extent these activations are stimulus dependent (stimulation properties such stimulation length and frequency, target location in visual field, etc.) or even pathology dependent.

6.5 CONCLUSION

Despite of its widespread use, the spatial and temporal characteristics of the electrophysiological representation of SSVEPs elicited by luminance flickering in the occipital cortex is still not resolved. Using direct evidence from intracranial EEG recordings covering the entire occipital lobe of the right hemisphere, we have shown that the fundamental component of foveal flickering is represented at the posterior side of the primary visual cortex, with little variation across stimulation frequencies (from 11 to 15 Hz), whereas peripheral flickering elicited activations in the interhemispheric fissure. The exact location of the peripheral activation is in line with evidence from retinotopic mapping studies. Both foveal and peripheral activations are accompanied by activations in the high gamma band at invariably the same locations, indicating independent processing. Additionally, this study showed that the alpha band synchronizes at the lateral edge of V2 (middle occipital gyrus) and the theta band lateral to V1 (superior occipital sulcus) during flickering stimulation. Moreover, following the offset of the stimulation, activity in the theta band peaks at several posterior locations in the visual cortex. While these transient activations are hardly detectable in occipital scalp EEG, a large post-stimulus transient activation is observed over the frontal area.

SUPPLEMENTARY MATERIAL

Supplementary material available at
https://doi.org/10.1016/j.neuroimage.2018.04.006

7

DECODING STEADY-STATE VISUAL EVOKED POTENTIALS FROM ELECTROCORTICOGRAPHY

This chapter has been published as:
B. Wittevrongel, E. Khachatryan, M. Fahimi Hnazaee, F. Camarrone, E. Carrette, L. De Taeye, A. Meurs, P. Boon, D. Van Roost and M.M. Van Hulle. *Decoding Steady-State Visual Evoked Potentials from Electrocorticography.* Frontiers in Neuroinformatics 12, 65

We report on a unique electrocorticography (ECoG) experiment in which Steady-State Visual Evoked Potentials (SSVEPs) to frequency- and phase-tagged stimuli were recorded from a large subdural grid covering the entire right occipital cortex of a human subject. The paradigm is popular in EEG-based Brain Computer Interfacing where selectable targets are encoded by different frequency- and/or phase-tagged stimuli. We compare the performance of two state-of-the-art SSVEP decoders on both ECoG- and scalp-recorded EEG signals, and show that ECoG-based decoding is more accurate for very short stimulation lengths (i.e., less than 1 second). Furthermore, whereas the accuracy of scalp-EEG decoding benefits from a multi-electrode approach, to address interfering EEG responses and noise, ECoG decoding enjoys only a marginal improvement as even a single electrode, placed over the posterior part of the primary visual cortex, seems to suffice. This study shows, for the first time, that EEG-based SSVEP decoders can in principle be applied to ECoG, and can be expected to yield faster decoding speeds using less electrodes.

7.1 INTRODUCTION

Electrocorticography (ECoG) records electrophysiological signals from the cortical surface, without the electrodes penetrating the cortical tissue, unlike multi-electrode arrays and deep brain electrodes. This recording modality has led to new opportunities for Brain-Computer Interfacing (BCI). While scalp-EEG avoids surgical interventions, it comes with inferior signal quality and spatial resolution, due to volume conduction, which challenges the speed/accuracy ratio when judging decoding performance [270, 271]. Additionally, success in EEG-based BCI applications depends on alleviating eye and head motion artifacts [70], including those causing minute electrode displacements, the drying out of the conductive gel that ensures low impedance contact with the subject's scalp, and the time-consuming electrode set-up and the ensuing retraining of the BCI prior to each use (for review, see [172]). When relying on micro-electrode arrays such as the Utah array [64, 118] one is facing permanent damage to the cortical tissue and its vasculature leading to histological processes and fibrous scar tissue formation [271] and brain plasticity processes that deteriorate the signal quality and whence BCI performance [279]. Compared to scalp-recorded EEG, ECoG signals are less contaminated by eye and motion artifacts [16], have higher amplitudes [271], a broader bandwidth [292], and higher spatial resolution [213]. Several studies were able to discriminate fine real (i.e., performed) movements from ECoG recordings such as hand extension and flexion [127], hand movement direction [182] and individual finger movements [212], all of which are not be feasible from EEG recordings. ECoG-based BCI have furthermore shown great promise for long-term recording sessions [53, 326] with reports of 262 days BCI-use without signal degradation [312].

While motor paradigms are raising great hopes to eventually achieve intuitive control over prosthetic limbs, currently, instead of continuous, only discrete control can be achieved (i.e., discrimination between distinct imagined motor tasks) [229, 312] as the extraction of reliable limb trajectory information is still largely beyond reach [156]. In the discrete setting, visual paradigms vastly outperform sensorimotor paradigms in terms of accuracy, number of selectable targets and information transfer rate (ITR) [223]. Several studies have investigated the feasibility of ECoG for visual BCI paradigms, such as the P300 Event-Related Potential [43, 161, 288] and the code-modulated Visual Evoked potential [138]. The implanted electrodes were mainly located over frontal, temporal, parietal and occipital areas, albeit not reaching to the primary visual cortex (V1) and merely a few electrodes to the secondary visual cortex (V2) [288]. However, to the best of our knowledge, the Steady-State Visual Evoked Potential (SSVEP), the most performant visual BCI paradigm [57], has not yet been assessed in terms of ECoG (or even intracranially recorded signals in general). Subdural electrode implants primordially serve a clinical purpose such as to localize epileptogenic foci of drug-resistant epilepsy and the mapping of eloquent cortex prior to resective surgery. Of all epilepsy cases, only 5 to 10% have an occipital lobe origin [295]. Foci in the first

visual layers (V1, V2) are, moreover, considered inoperable, as resection would leave the patient blinded, thereby normally not warranting electrode implantation. As, in general, only intractable cases of epilepsy are considered for implantation and given the above-mentioned precautions, patients with ECoG grids over primary visual areas are extremely rare. Furthermore, as the SSVEP paradigm relies on periodically flickering stimuli, photo-sensitive epilepsy patients are excluded from participation in an SSVEP study, further limiting the opportunities to study SSVEP responses over (primary) visual areas in human subjects. There are very few SSVEP-based studies with implanted electrodes in the occipital cortex, which are all limited to electrode strips [137, 158, 330], thereby not providing a wider view of the cortical activations, and none of these studies investigated SSVEP decoding performance. We report on a single case study where a large subdural grid was covering the entire right occipital cortex of a human subject.

When used in BCI, SSVEP-selectable targets are traditionally encoded with different flickering frequencies [211, 256] or phases [181, 189, 202], but in order to maximize the number of selectable targets, a joint frequency-phase encoding has been suggested [126]. Many SSVEP decoding algorithms have been described (for overviews, see [187, 192, 334]), but the more advanced ones are based on adapted versions of canonical correlation analysis (CCA) [2, 31, 55, 185, 221, 231, 321, 350, 353, 356], with the filterbank CCA [56] yielding the highest decoding accuracy, and on a spatiotemporal extension of the beamforming algorithm [334], successfully used for SSVEP [333] as well as several other visual BCI paradigms [331, 332, 336]. While both filterbank CCA (fbCCA) and spatiotemporal beamformer (stBF) yield state-of-the-art decoding performance on scalp-recorded EEG, it is unclear how well they perform on ECoG as the signal properties are different [48, 261]. This study aims to investigate SSVEP decoding from the cortical surface and to compare the obtained accuracies to the ones from traditional scalp-recorded signals.

7.2 METHODS

7.2.1 *Participants*

A 38-year old male patient (right-handed) with refractory, non-photosensitive epilepsy participated in the study. He was admitted to the hospital (UZ Gent) for monitoring seizure activity and functional mapping of eloquent cortex (visual, language, etc.). A subdural grid of 48 platinum electrodes embedded in silastic (Ad-Tech, USA) was implanted over the right occipital cortex. Additionally, a control group of eight healthy subjects (5 male, mean age 24.5 years, ranging from 19 to 30 years, 1 left-handed) were recruited for scalp-EEG recording. Previous studies have shown that BCI accuracy is not affected by age [5], thereby not requiring age-matched controls. All recruited participants, including the patient, had normal or corrected-to-normal vision and were

informed, prior to participating, about the aim of the study, the experimental procedure, and what would be done with the recorded data, after which they signed the informed consent form. The study was conducted according to the latest version of the Declaration of Helsinki (2013) following prior approval from the ethical committee of Ghent University Hospital (ECoG study) and Leuven University Hospital (UZ Leuven) (EEG study).

7.2.2 *Experimental procedure*

The experimental interface consisted of six identical rectangular targets (8.8×5.8 cm) presented on a 60 Hz LCD monitor. A number (from 1 to 6) was displayed in the center of each target, serving as a fixation point for the corresponding rectangle. The targets adopted a green color to reduce the visual demand [49, 300] and the risk of inducing an epileptic seizure [136]. All subjects were seated approximately 60 cm from the screen. At this distance, the visual angle spanned by the rectangles was $8.4^\circ \times 5.5^\circ$, and the distance from the fixation point to the edge of the neighboring target was 5.5° horizontally and 4.1° vertically. The fixation numbers spanned a visual angle of approximately $0.35^\circ \times 0.70^\circ$.

In order to investigate the decoding performance for different stimulus settings, the experiment consisted of four sessions, in each of which all rectangles were assigned a unique combination of frequency and phase (Table 7.1). Each session consisted of 90 trials. At the beginning of each trial, one of the targets was cued by maintaining its green color while the other rectangles were shown in grey (figure 7.1a). The subject was asked to direct his/her gaze at the cued target and maintain focus. When the subject pressed a key on the keyboard, all rectangles regained their green color, and one second later, the four-second stimulation was initiated, during which all targets were flickering in accordance with their frequency-phase combination, achieved by sinusoidally modulating their luminosities [207]. Between trials, the subject was allowed to take a short break, and a longer one (around 5 min) between sessions. In each session, all targets were cued 15 times in pseudorandom order. The experiment was implemented in Matlab, using the Psychophysics Toolbox extensions [38, 154, 236].

7.2.3 *Scalp-EEG and ECoG acquisition*

For the patient, 48-channel ECoG and 27-channel scalp-EEG (following the international 10-20 system) data were recorded simultaneously at a sampling rate of 1024 Hz using an SD LTM 64 Express (Micromed, Italy) medically certified device. Each ECoG electrode had a 4.0 mm diameter with 2.3 mm exposure and 10 mm inter-contact spacing. The subdural grid (6×8 contacts) was covering the right occipital cortex: convexity and mesial inter-hemispheric cortex (figure 7.1b). Functional mapping confirmed that a large part of the grid was located over the primary and associative visual cortex. Due

Table 7.1: Target frequency-phase combinations for each session, represented as [frequency (Hz)/phase (radians)].

Session	Target					
	1	2	3	4	5	6
1	$12/0$	$14/\frac{2\pi}{3}$	$12/\frac{4\pi}{3}$	$14/\frac{4\pi}{3}$	$12/\frac{2\pi}{3}$	$14/0$
2	$13/0$	$14/\frac{2\pi}{3}$	$13/\frac{4\pi}{3}$	$14/\frac{4\pi}{3}$	$13/\frac{2\pi}{3}$	$14/0$
3	$11/0$	$15/\pi$	$13/0$	$13/\pi$	$11/\pi$	$15/0$
4	$13/0$	$15/\pi$	$14/0$	$14/\pi$	$13/\pi$	$15/0$

to insufficient quality of the simultaneously recorded scalp-EEG (dried conductive gel, as well as the influence of scarred and swollen tissue), the patient's scalp-EEG was excluded from further analysis.

The scalp recorded EEGs from the control subjects were acquired with a Synamps RT device (Neuroscan, Australia), using 32 active Ag/AgCl electrodes evenly distributed over the scalp (figure 7.1c) and at a sampling rate of 2 kHz. The electrodes were placed using an electrode cap (EasyCap GmbH, Germany) with fixed holes according to the international 10/20 system. Conductive gel was applied at each electrode, and the impedance between skin and electrodes was kept below 2 kΩ. As SSVEPs are less susceptible to ocular artifacts (i.e., blinks and saccades) [257, 315], no electro-oculogram (EOG) was recorded and no artifact correction was applied in this study.

7.2.4 *Localization of ECoG electrodes*

Based on the pre-implantation MRI scan of the patient, cortical reconstruction and volumetric segmentation was performed with the Freesurfer image analysis suite (version 5.3.0) [85]. The Freesurfer output was then loaded into Brainstorm [296] and co-registered with the post-implant CT. The coordinates of the implanted electrodes were then obtained by visual inspection and mapped onto the subject's cortical surface.

Figure 7.1b shows the locations of the implanted electrodes, with indication of the primary (V1) and associative (V2) visual cortices.

7.2.5 *Processing*

The processing of the ECoG and EEG data differs only in the used re-referencing. The raw ECoG data was offline re-referenced to the grid's average (Common Average Reference, CAR), while the EEG data was offline re-referenced to the average of both mastoid electrodes (TP9 & TP10).

Since each classifier (see next section for their description) requires different filtering ranges, all recordings were stored four times, but with different filtering ranges: a fourth-order Butterworth filter between 0.5 and 40 Hz for the naive classifier, between 4 and 20 Hz for the spatiotemporal beamformer [332], and between 8 and 70 Hz and between 16 and 70 Hz for the filterbank CCA algorithm [56], respectively. The filtered EEG and ECoG recordings were then cut into four-second trials time-locked to the onset of the stimulation, downsampled to 500 Hz, labeled with the corresponding cue, and stored for further analysis.

7.2.6 *Classifiers*

In this study, we assessed the performance of two state-of-the-art classifiers, filterbank CCA (fbCCA) and spatiotemporal beamformer (stBF), and a simple (called naive) classifier based on the Fourier transform in combination with a phase estimation method.

7.2.6.1 *Naive classifier*

This classifier is the most straightforward one to identify gazed targets. First, the most prominent frequency (among the used stimulation frequencies) in a trial was determined from the signal's power spectral density (PSD), obtained after applying the Fourier transform. Then, this frequency was used to estimate the phase of the trial. Finally, the predicted target was taken as the one whose frequency and phase best corresponded to the extracted frequency and phase. This is now explained in more detail.

Training the naive classifier involved the estimation of the phase Φ_i of each target $i \in [1..6]$, obtained by applying the following equation to each training trial s of target i and averaging their values [126, 207, 323]:

$$\begin{aligned} \varphi &= \operatorname{Arg}\Big(\mathcal{F}_s(f_i)\Big) \\ &= \operatorname{Arg}\Big(\sum_t s(t)\,\cos(2\pi f_i t) + j\sum_t s(t)\,\sin(2\pi f_i t)\Big) \\ &= \operatorname{atan2}\Big(\sum_t s(t)\,\cos(2\pi f_i t), \sum_t s(t)\,\sin(2\pi f_i t)\Big), \end{aligned} \tag{7.1}$$

with t the sample in time units, f_i the frequency of target i, $\mathcal{F}_s$ the discrete Fourier transform of $s(t)$, and $j = \sqrt{-1}$.

To classify a trial, the power spectral density (PSD) was calculated using the Fourier transform with a Hamming window whose size was equal to the length of the trial.

For each of the stimulation frequencies f_i, the power was calculated as the average in a narrow (0.5 Hz) band, centered at frequency f_i:

$$p_{f_i} = \int_{f_i-0.25}^{f_i+0.25} PSD(x)\,\mathrm{d}x, \tag{7.2}$$

where x is the range of the PSD spectrum. The predicted frequency $\hat{f}$ was given by f_i with the highest power, and further used for estimating the phase $\hat{\varphi}$ of the trial, using equation 7.1. Finally, the phase difference δi between Φ_i and $\hat{\varphi}$ was calculated for all targets i that were encoded by frequency $\hat{f}$, using the *CircStat* toolbox [28]. The gazed target was predicted as the one with the closest-to-zero phase difference.

7.2.6.2 *Filterbank CCA*

The CCA algorithm was originally used in the context of SSVEP-BCI for the identification of frequency-encoded SSVEP targets [185]. The algorithm finds linear combinations $\mathbf{w}_x \in \mathbb{R}^{1\times m}$ and $\mathbf{w}_y \in \mathbb{R}^{1\times k}$ for multivariate sets $\mathbf{X} \in \mathbb{R}^{n\times m}$ and $\mathbf{Y} \in \mathbb{R}^{n\times k}$, such that their linear combinations $\mathbf{x} = \mathbf{X}\mathbf{w}_x^\mathsf{T}$ and $\mathbf{y} = \mathbf{Y}\mathbf{w}_y^\mathsf{T}$ are maximally correlated [111].

In the context of SSVEP, $\mathbf{X}$ is the measured (multi-channel) EEG and $\mathbf{Y}_i$ is a set of sine and cosine signals with the stimulation frequency of target i and a number of harmonics ($h = k/2$).

$$\mathbf{Y}_i = \begin{pmatrix} \sin(2\pi f_i t) \\ \cos(2\pi f_i t) \\ \vdots \\ \sin(2\pi h f_i t) \\ \cos(2\pi h f_i t) \end{pmatrix} \tag{7.3}$$

Since the original algorithm does not contain any phase information, an extension was proposed [221] to discriminate joint frequency-phase encoded SSVEP targets by incorporating individual calibration data. The filterbank CCA method [56] combines the aforementioned CCA extension [221] with a filterbank approach [314]. By analyzing the signals in different sub-bands, information originating from the fundamental and harmonic components are examined more efficiently and aggregated at a later stage. In this study, the number of harmonics h for the predefined signals $\mathbf{Y}_i$ was set to 3 and the sub-bands used were [8-70] Hz and [16-70] Hz as in [57].

7.2.6.3 *Spatiotemporal Beamforming*

The spatiotemporal extension [319] (termed here stBF) of the original beamforming algorithm [309] has first been proposed for the analysis of the N400 ERP in the context of semantic processing, and since then applied in the context of BCIs [334] for target identification based on the P300 ERP [331], SSVEP [332, 333] and cVEP [336] paradigms.

Spatiotemporal beamforming estimates the contribution of a predefined spatiotemporal pattern to new data. Each trial is cut into consecutive, non-overlapping segments whose length is equal to the period of the expected frequency [199, 203]. If the frequency is present in the signal, the averaged segments should resemble a sine-wave of a single period. If not, averaging the segments will cancel out any patterns and result in a 'flat' response. As the segments are time-locked, the averaged pattern also accounts for the phase of target stimulation.

Since each target elicits a different brain response (cf., the unique frequency/phase combinations), each target requires a unique activation pattern, hence training the classifier involves calculating six spatiotemporal beamformers, one for each target.

The *activation patterns* and the beamformers were calculated from the training data as follows: let $\boldsymbol{T}_i \in \mathbb{R}^{m \times t \times r}$ be the trials obtained during the training session in response to the cued target $i \in [1..6]$, where m represents the number of channels, t the number of samples and r the number of trials, and f_i be the stimulation frequency of target i. Applying the time-domain approach to all trials in $\boldsymbol{T}_i$ with f_i the returned segments $\boldsymbol{S}_i \in \mathbb{R}^{m \times n \times k}$, where n is the number of samples corresponding to one period of frequency f_i and k the total amount of segments obtained from all trials in $\boldsymbol{T}_i$. The spatiotemporal activation pattern $\mathbf{A}_i \in \mathbb{R}^{m \times n}$ for target i can now be obtained as the average of all k segments.

The *spatiotemporal beamformer* was calculated as a linearly-constrained minimum-variance (LCMV) beamformer $\mathbf{w}_i \in \mathbb{R}^{(mn) \times 1}$ for target i as follows: let $\mathbf{E}_i \in \mathbb{R}^{(mn) \times k}$ be the matrix where each row was obtained by concatenating the rows of a corresponding segment $\boldsymbol{S}_i[*, *, k]$, $\boldsymbol{\Sigma}_i \in \mathbb{R}^{(mn) \times (mn)}$ the covariance matrix of $\mathbf{E}_i$, and $\mathbf{a}^\intercal \in \mathbb{R}^{1 \times (mn)}$ a vector containing the concatenated rows of $\mathbf{A}_i$. The LCMV beamformer under constraint $\mathbf{a}_i^\intercal \mathbf{w}_i = 1$ can now be calculated using the method of Lagrange multipliers [310]:

$$\mathbf{w}_i = \frac{\boldsymbol{\Sigma}_i^{-1} \mathbf{a}_i}{\mathbf{a}_i^\intercal \boldsymbol{\Sigma}_i^{-1} \mathbf{a}_i}, \tag{7.4}$$

and applied to the data as a simple weighted sum: $y = \mathbf{s}\mathbf{w}_i$, where $\mathbf{s} \in \mathbb{R}^{1 \times (mn)}$ indicates the concatenated rows of an input segment $\mathbf{S}_{in} \in \mathbb{R}^{m \times n}$.

The feature vector for a trial $\mathbf{T}$ was given by the beamformer outputs y_i for each target i. To obtain y_i, the trial was cut into segments of length one period of frequency f_i, the segments were averaged and filtered using the corresponding beamformer $\mathbf{w}_i$.

Based on the feature vector, a prediction was made of the target gazed by the subject. As the feature vectors contain estimates of the degree to which the activation pattern of each target is present in the trial, the target having the highest score was marked as winner (i.e., prediction $= \max(y_i)$).

Note that longer trials can be cut into more segments, leading to more reliable average segment responses that can be input to the beamformers. Prior to training and classification, trials were bandpass filtered between 4 and 20 Hz.

7.2.7 *Performance Evaluation*

The decoding accuracy of all classifiers was estimated offline using a stratified 5-fold cross-validation strategy. We estimated performance for varying signal lengths, from 250 ms to 4 seconds in steps of 250 milliseconds. Note that only the testing trials were shortened, while the training trials remained 4 seconds long. Single-electrode performance was assessed for all three classifiers, while multi-electrode performance was only estimated for the two state-of-the-art classifiers (filterbank CCA and spatiotemporal beamformer).

7.2.8 *Statistical estimation of the patient's scalp-EEG performance*

As the patient's scalp-EEG was not of sufficient quality for use in our analysis, we statistically estimated his scalp-EEG accuracy for the single-electrode case using an imputation analysis based on phase variability. For each trial, the phase was calculated using equation 7.1. Albeit that the measured phase on the scalp might be different from the cortical phase measurement due to the mixing of different cortical activities, this should not affect its trial-to-trial variability. First, we verified that the phase variability (measured as the circular standard deviation [28]) of the ECoG signal (at electrode 36) is not significantly different from the scalp-recorded phase variability at channel Oz of our control subjects. To this end, the Kuiper's test was used (*CircStat* toolbox [28]). Next, for each session, an imputation analysis with 100 iterations was performed in which the patients scalp-EEG decoding accuracy was treated as missing value. The patient's trial-to-trial phase variability of the session under consideration (at electrode 36) was used, together with the phase variabilities and decoding accuracies of all sessions from the control group to estimate the patient's scalp-EEG decoding accuracy.

7.2.9 *Electrode Selection*

While many approaches have been described to recruit electrodes for multi-electrode analysis [15, 17, 173, 200, 275], we used greedy forward selection: we iteratively added the electrode that resulted in the largest accuracy increase until no further improvement could be achieved or 100% accuracy was reached. As an optimization criterion, we used the average classification accuracy across stimulation lengths (from 250 ms to 4 s in steps of 250 ms, see above). This procedure was repeated for each classifier separately, in order to maximize their individual accuracies.

While the greedy approach does not guarantee optimal performance (as it does not backtrack on the choices made), it is universal, simple and straightforward to implement compared to other selection strategies. As the main aim of this study was to compare ECoG- and EEG-based SSVEP target decoding accuracy, the selection of the optimal electrode set was not deemed important in this study. Furthermore, the greedy

selection approach takes into account the differences inherent to the classifiers (e.g., fbCCA solely aims at detecting the frequency-phase combinations while stBF estimates the contribution of a given activation pattern and takes into account information about noise sources and non-targeted patterns), and is often described as a *wrapper* approach [108].

7.2.10 *Statistics*

For the EEG subjects, the significance of the differences in classifier accuracies was assessed with the (two-tailed) Wilcoxon signed rank test. We adopted this non-parametric test since the distributions did not consistently follow a Gaussian distribution. The significance threshold was set to 0.05 for the multi-electrode case, and was corrected to 0.0167 ($= \frac{0.05}{3}$) for the single-electrode case, using the Bonferroni correction for multiple comparisons.

7.3 RESULTS

Our subjects were shown a visual interface constituting of six rectangular targets, each one periodically flickering at a unique frequency and phase (Table 7.1). All subjects performed four sessions of 90 trials. In each trial, the subject was asked to direct his/her gaze to a cued target and to maintain focus during the ensuing 4-second flickering stimulation (figure 7.1). In each session, all targets were cued 15 times in pseudorandom order.

7.3.1 *Single-electrode performance*

As this is the first study on ECoG-based SSVEP decoding, we started with an exploratory analysis of target detection accuracy of individual electrodes when using fbCCA [56] and stBF [332], and a naive classifier based on spectral analysis but extended with phase modeling. The naive classifier has been applied to scalp-EEG recordings of SSVEP responses (for review, see [187]), but now considered outdated in terms of accuracy, hence, it is interesting to see to what extend that classifier could benefit from the improved ECoG signal quality.

Figure 7.2a shows the highest single-electrode decoding accuracies obtained from the three classifiers for increasing stimulation lengths during the second session. The results of the other sessions are equivalent and are shown in Figures S1 to S3, in the supplementary material section. For ECoG, the two state-of-the-art classifiers, as well as the naive classifier, exhibit a rapid increase in accuracy with increasing stimulation lengths up to 0.75 seconds of stimulation, after which the accuracy only improves marginally or remains constant. fbCCA is the most accurate classifier with an accu-

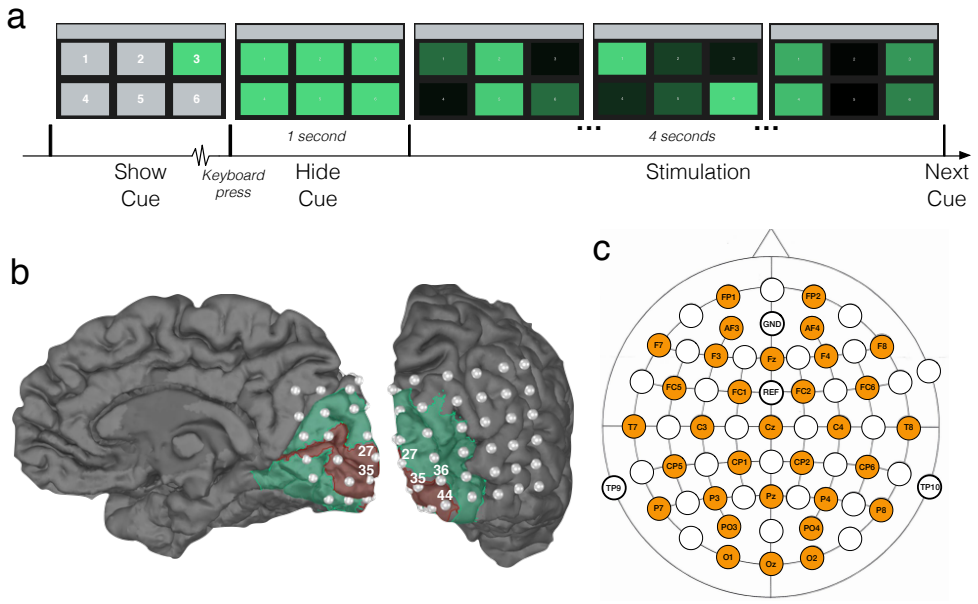

Figure 7.1: Experimental setup. (a) Time-course of one trial with characteristic displays. For the sake of exposition, target numbers in the first display are larger than those shown to our subjects. (b) Visualization of the patient's right hemisphere with location of implanted ECoG electrodes. Red and green areas correspond to V1 and V2, respectively, and were extracted with Freesurfer [85]. (c) Location of scalp-EEG electrodes for the control experiment.

racy of 96.7% for 0.75-second stimulation, compared to 91.1% and 92.2% for stBF and the naive classifier, respectively. Using long stimulation (i.e., 4 seconds), the accuracy converges to 97.8% for the fbCCA and naive classifiers, and 96.7% for stBF. For scalp-EEG, the accuracy at the best electrode of each subject steadily increases with increasing signal lengths, but remains considerably lower than the ECoG-based accuracy (e.g., $79.6 \pm 13.5\%$ for EEG compared to 97.8% for ECoG with fbCCA at a stimulation length of 2 seconds). Here, the accuracy of the naive classifier is consistently lower than that of the state-of-the-art classifiers, and is significantly different for all stimulation lengths above 0.25 seconds. At least 1.5 second of stimulation is needed for scalp-EEG to surpass the 70% accuracy threshold deemed necessary to establish reliable communication [43, 68, 165, 166]. In comparison, using ECoG, all classifiers surpass this threshold within 0.5 seconds of stimulation.

Figures 7.2b to d summarize the average decoding accuracy across all stimulation lengths for each individual electrode during the second session. The EEG electrodes over the middle occipital area (electrode Oz) yield the highest accuracies, as expected. The subdural electrodes located over the posterior part of the primary visual cortex (electrodes 36 and 44) most accurately decode the intended target. These results are

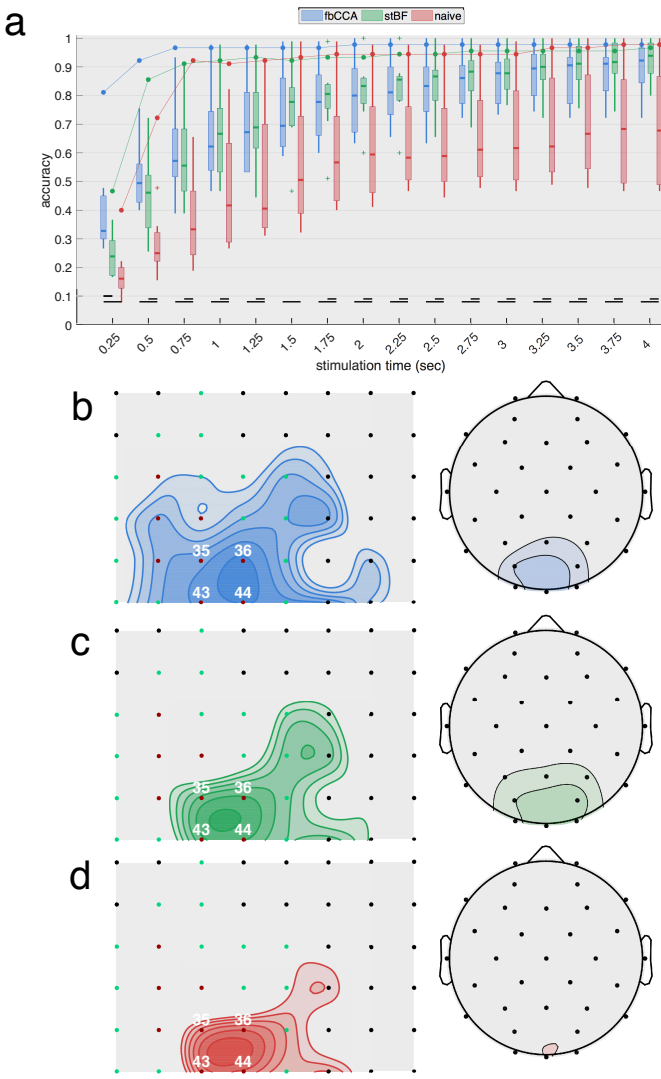

Figure 7.2: Single-electrode performance. (a) Best single-electrode accuracies obtained with the three classifiers plotted as a function of stimulation lengths during the second session. The full line indicates accuracies based on cortical recordings and the boxplots summarize accuracies based on scalp-EEG (control subjects). (b-d) Overview of accuracies (averaged across all stimulation lengths) for all cortical electrodes (left) and scalp channels (right) for (b) fbCCA, (c) stBF and (d) naive classifier. Subdural electrodes indicated in red and green indicate V1 and V2, respectively. Iso-accuracy lines on the subdural grids (left panels) start at 75% accuracy and increase in steps of 5% and on the scalp plots (right panels) start at 50% accuracy and increase in steps of 10%.

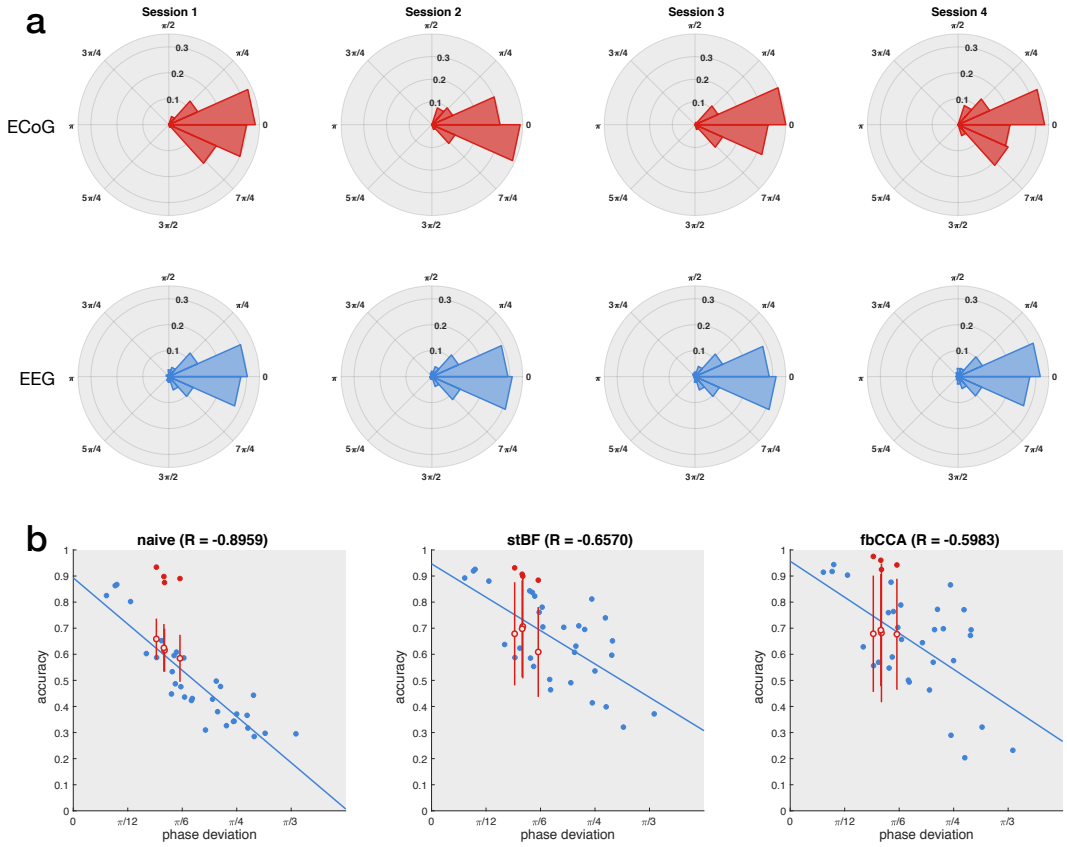

Figure 7.3: Estimation of the patient's scalp-EEG accuracy. (a) Distribution of the phase deviation at the stimulation frequency across trials of the ECoG (left column) and scalp-EEG (right column) for the four sessions (rows). Kuiper's test did not reveal any significant differences between the ECoG and scalp-EEG phase deviation distributions for any of the four sessions. (b) Regression of accuracy on phase deviation. Each dot represents one session of one subject. Blue dots the control subjects, red filled dots indicate the patient, and red open dots indicate the statistically estimated scalp-EEG accuracy of the patient with the vertical red line the corresponding standard deviation for 100 imputations.

consistent across classifiers and sessions (see supplementary material for the other sessions).

As the quality of the scalp-EEG of the patient was not sufficient, we statistically estimated his scalp-EEG decoding performance based on the measured phase of the ECoG signal. Figure 7.3a shows the distribution of the phase deviations across all targets for each session for both the ECoG (electrode 36) and EEG control group (electrode Oz). The distributions of ECoG and scalp-EEG are not statistically significant for all four sessions ($p > 0.05$, Kuiper's test), indicating that both ECoG and scalp-EEG experience similar phase deviations across trials, and that the higher classification accuracy

of ECoG does not originate from more stable phase responses. Using the phase and accuracy measurements of the control group, the accuracy of the patient's scalp-EEG was statistically estimated using an imputation-analysis [50, 264]. Figure 7.3b shows a regression analysis of the accuracy (averaged over all stimulation lengths) with respect to the phase deviation based on the control group for all classifiers. Additionally, the accuracies and phase deviations of the ECoG signal at electrode 36 are added, as well as the estimations of the patient's scalp-EEG accuracy, given the observed ECoG phase deviations. While all three classifiers exhibit a decrease in accuracy for decreasing phase stability, the naive classifier is most strongly affected, probably as it does not adopt more advanced signal processing procedures. For all classifiers, the ECoG-based accuracies clearly outperform the scalp-EEG counterparts with similar phase deviations.

7.3.2 *Multi-electrode performance*

Since several EEG studies showed that the decoding accuracy of scalp-EEG improves when using a multi-electrode approach [187], we adopted a greedy forward electrode selection strategy to determine the electrode set for each classifier and subject individually.

Figure 7.4a shows the resulting classification accuracies for the second session. While the accuracies from ECoG largely remain the same as in the single-electrode case, for EEG, the accuracies are considerably improved. The stimulation length required to reach the 70% threshold now decreases to 0.5 and 0.75 seconds for stBF and fbCCA, respectively. The spatiotemporal beamformer significantly outperforms the filterbank CCA algorithm for signal lengths from 0.5 to 3.25 seconds, but significantly underperforms for the shortest stimulation length, albeit that the accuracies of both classifiers are not satisfactory (i.e., below 70%).

Figure 7.4b shows the number of electrodes selected for each session for both classifiers, and Figure 7.4c shows the general increase in accuracy (i.e., averaged accuracy across all stimulation lengths) for the four sessions. While the accuracies with EEG increase considerably (median improvement between 14 and 23%), those with ECoG increase only marginally ($\sim$ 5% for the stBF and $\leq$ 1% for fbCCA). For sessions 2 to 4, greedy electrode selection did not come up with additional electrodes for the fbCCA method (figure 7.4b), resulting in identical accuracies as for the single-electrode case. Unlike for the fbCCA classifier, between 6 and 11 electrodes were included for the stBF in the ECoG modality, but this led to only minor improvements in decoding accuracy (figure 7.4c).

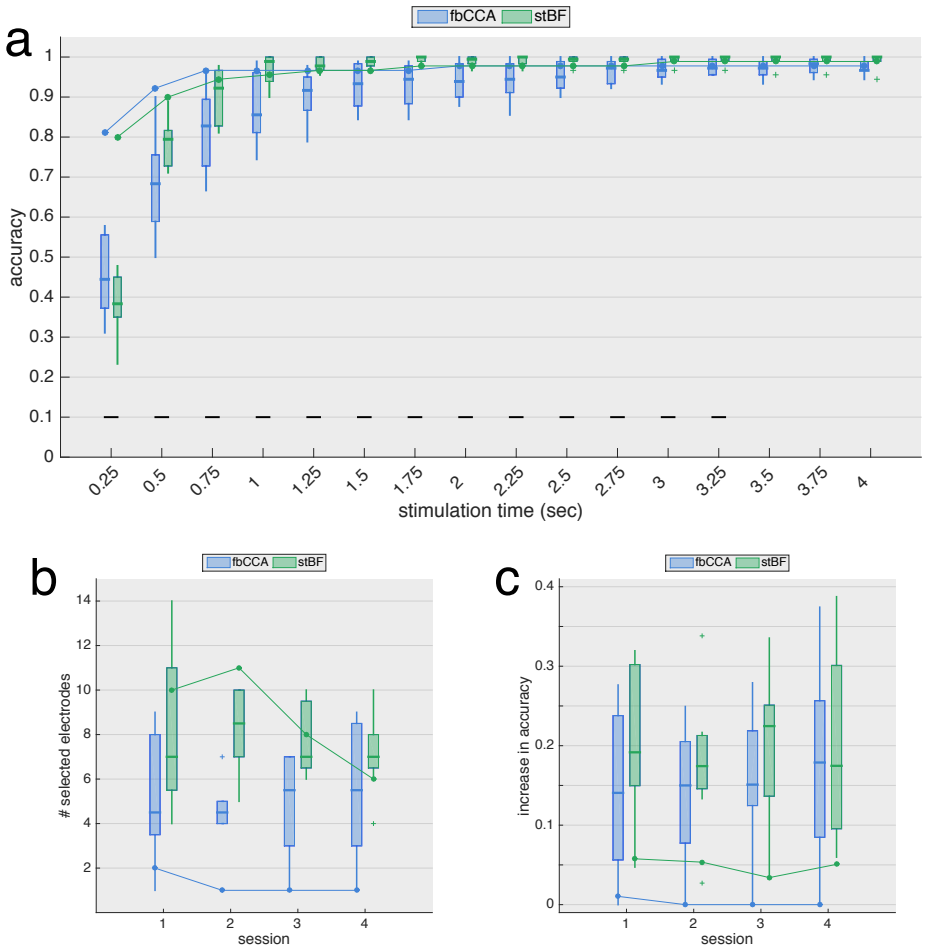

Figure 7.4: Multi-electrode performance. (a) Multi-electrode analysis of classification accuracies during the second session. (b) Number of electrodes selected by the greedy algorithm, for each session. Boxplots and solid line indicate results for EEG (control subjects) and ECoG (implanted patient), respectively. (c) Increase in accuracy (averaged over all stimulation lengths) for all sessions. Boxplots and solid line indicate results for EEG (control subjects) and ECoG (implanted patient), respectively.

7.4 DISCUSSION

We investigated the accuracy with which SSVEP-selectable targets can be decoded from ECoG recordings, obtained from a subdural electrode grid spanning the entire right occipital cortex, when using classifiers that were originally designed for scalp-EEG recordings. We considered two state-of-the-art classifiers and one naive approach, based on spectral analysis and phase detection, and assessed their accuracies for both

ECoG and scalp-EEG recordings in terms of stimulation length in single- and multi-electrode settings.

7.4.1 *High-quality ECoG signals allow for accurate single-electrode SSVEP decoding*

The superior decoding accuracy of ECoG was most striking for the single-electrode analysis, as even the naive classifier surpassed 90% classification accuracy for stimulation lengths as short as 0.75 seconds. However, when adopting even shorter stimulation length ($\leq$ 0.5 s), both state-of-the-art classifiers, and fbCCA in particular, yielded noticeably higher accuracies compared to the naive classifier, e.g., for the second session, we obtained 92.2% and 85.6% for fbCCA and stBF, respectively, compared to 72.2% for the naive classifier at a stimulation length of 0.5 seconds. In comparison, when using scalp-EEG, both state-of-the-art classifiers outperformed the naive classifier for all stimulation lengths, but required much longer stimulation times (more than 3 seconds) to reach 90% accuracy. The fact that the naive classifier attains high accuracy levels on ECoG supports the claim that subdural signals are of better quality. Figure 7.5 confirms this as the single-trial signal-to-noise ratio (SNR) of the subdural signal (at electrode 36) is considerably higher than that of its scalp-recorded counterpart (at electrode Oz).

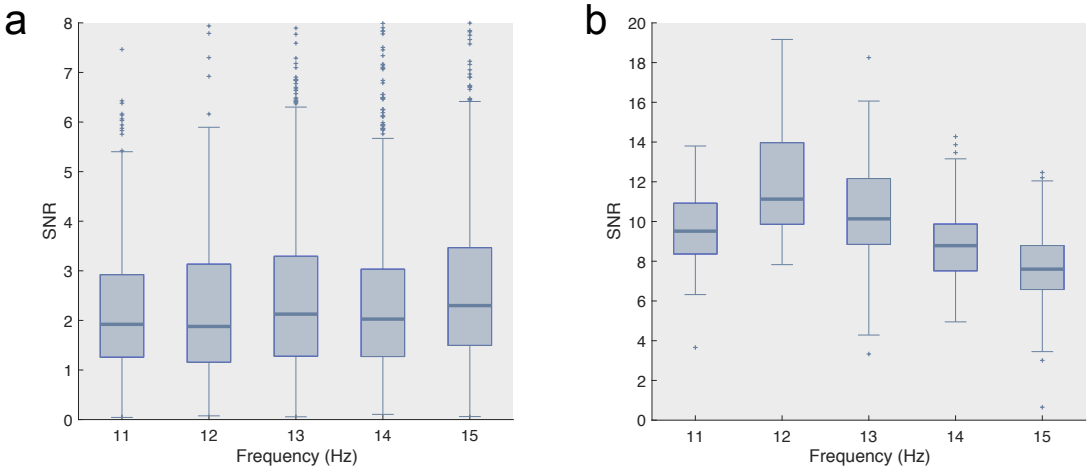

Figure 7.5: Signal-to-noise ratio's for all considered frequencies (a) scalp-recorded EEG and (b) ECoG

In order not to interfere with the patient's clinical workup, we were not able to obtain simultaneous scalp-EEG from the patient. However, even in case simultaneous scalp-EEG was obtained, it is unclear whether the decoding accuracy would be useful for comparison, as several studies have presented initial evidence that the implanted silastic layer containing the subdural electrodes considerably attenuates the scalp-recorded

potentials [175, 252, 297]: a 2-3 times attenuation for a 4×8 grid and up to 8 times for an 8×8 grid [79]. As an alternative, we estimated the patient's scalp-EEG decoding accuracy from the ECoG phase variability using a data imputation exercise based on the fact that volume conduction affects the EEG signal's amplitude, not its phase. In the same vein, the head-models used in EEG source localization studies are resistive and therefore do not account for phase information [109, 268, 342].

The high regression value for the naive classifier with respect to the scalp-EEG phase deviation (figure 7.3) indicates that this classifier is mainly influenced by the consistency of the phase responses. However, despite that the variability of the subdural phase responses are not significantly different to those of the control group, the subdural decoding accuracy is considerably higher. This discrepancy in accuracy also shows up in the imputation analysis (figure 7.3). We suggest that the higher decoding accuracy is due to the higher SNR of ECoG signals (figure 7.5).

As for the naive classifier, the decoding accuracies of stBF and fbCCA are reduced when the phase deviation increases (figure 7.3b). However, as the latter are more advanced classifiers, their regression coefficients are lower, indicating they are able to partially account for the trial-by-trial phase variability.

7.4.2 *ECoG-based SSVEP decoding does not benefit from a multi-electrode approach*

Assuming that information from other channels improves the classification accuracy, many researchers (for review [187]) developed spatial filtering and multi-electrode decoding strategies, including the ones considered in this study. When adopting a multi-electrode approach, the scalp-EEG decoding accuracies improve considerably for both classifiers, with an increased accuracy (averaged over all stimulation lengths) between 13 and 23%, depending on the considered session. In contrast, for ECoG, the decoding accuracy increased only marginally ($\sim$ 5%) with stBF, and even less for fbCCA, for which the greedy electrode selection did not include any additional electrode, as the accuracy could not be improved (with exception of the first session where 1 additional electrode was included). Overall, when opting for a multi-electrode approach, the accuracies obtained from ECoG and EEG were similar as soon as the stimulation length exceeded 1 second, demonstrating the effectiveness of current state-of-the-art SSVEP decoding algorithms.

In our previous work [337], we showed that the representation of the foveal flickering was highly localized at the posterior part of the primary visual cortex (electrodes 35 and 36), with little variation across the stimulation frequencies used. Also in the single-electrode analysis (figure 7.2), the highest accuracies were obtained with the electrodes covering the posterior part of the primary visual cortex. The inclusion of additional subdural electrodes in the analysis did not improve decoding accuracy, indicating that the electrodes over the posterior part of the primary visual cortex carry the information needed for target decoding, and that there is little overlap with the

information provided by the surrounding electrodes. This is in line with the literature that, compared to scalp-recorded potentials, cortical activations (both induced and noise) are considerably more localized [48]. As volume conduction attenuates and disperses the cortical activity over a larger scalp area, multiple scalp-electrodes carry information from the activity-of-interest. A multi-electrode analysis is therefore beneficial for decoding SSVEPs from the scalp, as it includes multiple weaker sources of information about the activity-of-interest.

7.4.3 *Comparison with other visual BCI paradigms*

ECoG has been hailed for BCI purposes for its long-term stability, superior signal quality and permanent availability of the interface (no electrode mounting required) [312, 326], but the reported applications rely on multiple electrodes, implanted as grids or strips, requiring a major surgical intervention. For instance, when pursuing a motor imagery application, one typically relies on a multi-electrode implants covering over the sensorimotor cortex to decode actions of different limbs, the activity of which is highly localized [214]. Visual Event-Related Potential (ERP) paradigms have shown high accuracies in multi-electrode ECoG settings, but the accuracy considerably drops when adopting a single-electrode analysis (100% with 4 electrodes and 3 stimulus repetitions compared to 78% with a single electrode [43]). As to the cVEP paradigm, a multi-electrode analysis using CCA as spatial filter showed an accuracy of 86.8% with a stimulation time of 1.05 seconds [138]. Compared to the paradigms mentioned above, as we have shown in this contribution, SSVEP stands out due to its high single-electrode decoding accuracy with short stimulation times (96.7% with a stimulation time of only 0.75 seconds). This could even be reached by using naive classifier based on the Fourier transform, without tailoring the frequency or phase characteristics to the subject. If the stimulus characteristics were optimized, the decoding performance could likely be further increased [57].

7.4.4 *Practical considerations and future work*

Another important point in the comparison of scalp-EEG and ECoG accuracies is the conditions in which the recording was performed. Despite the impressive stimulation length/accuracy ratio we obtained with ECoG, it is worth mentioning that in most sessions the patient was unable to reach maximal accuracy (i.e., 100%), even with longer stimulation lengths. While some EEG subjects did reach maximal accuracy, it should be noted that our control subjects performed the experiment in a dedicated experimental room without distractions (sound-attenuated, air-conditioned, black walls), while the patient performed the experiment in a hospital room where many distractions were present (e.g., the experiment was interrupted several times to ensure normal continued medical treatment, surrounding relatives and so on). Despite these suboptimal

recording conditions, our results clearly demonstrate the superiority of ECoG compared to scalp-EEG for the SSVEP paradigm, both in terms of number of electrodes and stimulation lengths.

While the patient did not have a seizure during the experimental session, interictal activity might influence the recorded signals. However, the clinical functional mapping showed that none of the electrodes over V1 overlapped with the clinically determined ictal onset zone, which was located lateral from V2, indicating that the primary visual cortex of this patient can be considered healthy, normal tissue. The fact that the variability in the measured phase responses of ECoG and scalp-EEG was not significantly different and that the imputation analysis returned accuracies in the expected range provide further confidence that our results would generalize to other subjects and that there was no influence of the epileptic tissue on our results.

Given these encouraging findings, although based on offline analysis, we believe that our results could also pertain to an online implementation: the used state-of-the-art decoding algorithms have already been shown to also yield superior online decoding accuracy when based on scalp-EEG [57, 333].

7.4.5 *Limitations*

For this study, we recorded one subject implanted with a subdural grid over the occipital cortex. While it is generally unclear whether or not the results from a single subject generalize to the population, the current study provided an unique opportunity to study the cortical activations of the widely adopted SSVEP paradigm. As mentioned before, the prevalence of occipital lobe epilepsy is low. Only 5 to 10% of epilepsy cases have an epileptic generator in the occipital cortex [295]. Of this small group, only cases of intractable (and operable) epilepsy are candidate for intracranial implantation. Furthermore, one has to exclude photosensitive epilepsy patients, as SSVEPs are elicited by periodically flickering stimulation. Finally, as an alternative to electrode implantation, more and more surgeons currently prefer awake surgery during which they can perform functional mapping, thereby removing the need for electrode implantation. Given all these restrictions, it is very rare to study cortical activations in response to SSVEP stimulation in-vivo in a human subject, even more when the primary visual cortex is completely covered, including the interhemispheric fissure.

Unfortunately, as the hospital's EEG system was not set up for communicating real-time recordings to an external system, a closed-loop SSVEP experiment could not be performed.

7.5 CONCLUSION

The recording of brain signals directly from the cortical surface using electrocorticography (ECoG) has great benefits for brain-computer interfacing (BCI). However, the most

performant visual BCI paradigm, based on the Steady-State Visual Evoked Potential (SSVEP), has never been assessed with ECoG, primarily due to the highly exceptional occurrence of subdural electrode implantation over the occipital cortex. In this work, we quantify the superior SSVEP decoding accuracies of ECoG compared to those of a control group with scalp-recorded electroencephalography (EEG), and show that, unlike with scalp-EEG, ECoG does not benefit from a multi-electrode analysis.

SUPPLEMENTARY MATERIAL

Supplementary material available at https://doi.org/10.3389/fninf.2018.00065.

8

GENERAL DISCUSSION

In this thesis, we have shown the feasibility of spatiotemporal beamforming for visual brain-computer interfacing.

8.1 P300

As to the P300 ERP, the most popular visual BCI paradigm, the gazed target identification accuracy of spatiotemporal beamforming is on par with a linear SVM which is considered state-of-the-art in P300 detection. However, contrary to the SVM, which requires optimizing its regularization parameter, the beamformer can be trained significantly faster as there are no parameters to be optimized. Both the SVM and the spatiotemporal beamformer use a highly similar spatiotemporal pattern to discriminate target (i.e., P300) and non-target responses but, as the SVM is a black-box algorithm, the latter relies on data-driven statistical inference to arrive at the spatiotemporal pattern. However, when performing traditional averaging of the target responses, a highly similar spatiotemporal pattern is obtained and this is what the beamformer relies on to achieve its accuracy at a significantly lower computational cost.

Fast classifier training is important when envisaging adaptive BCI applications, in which the decoder is regularly retrained to support long-term use. Retraining is required to maintain accuracy levels despite of fatigue and decreased attention as these affect the P300 component. A computationally inexpensive training algorithm limits the unavailability of the interface during retraining and furthermore reduces the need for high-performance hardware that could increase the cost of a real-world BCI application.

8.2 SSVEP

When discriminating selectable targets encoded in terms of a unique frequency/phase combination, multiple beamformers need to be constructed, one for each target. The linear constraint of the LCMV beamformer enforces comparability between beamformers, as for each target, the filtered/beamformed response will adopt a value closer to 1 when it resembles the activation pattern of the respective target. Compared to the state-of-the-art SSVEP decoders at the time of writing (i.e., extended CCA and filterbank CCA), classification of scalp-recorded signals based on spatiotemporal beamforming achieves higher accuracies for shorter stimulation lengths.

When relying on intracortical recordings, which have a higher signal-to-noise ratio compared to scalp-EEG, the accuracies of both the filterbank CCA- and beamforming-based classifiers are on par, and considerably higher for stimulation lengths shorter than 1 second compared to their scalp-recorded counterparts. Next to the expected increase in decoding accuracy, another important observation is that ECoG only requires one electrode to reach this high performance, while a multi-electrode approach is required for scalp-EEG. Despite that only one patient with ECoG was included in the analysis, this initial result seems promising. If our results could be confirmed with ECoG recordings from multiple patients, a highly-performant ECoG-based BCI with SSVEP encoded targets could be developed for long-term deployment. Compared to non-invasive recordings, ECoG has favorable properties for long-term use (no re-training, low maintenance, permanent availability of the interface, etc.), which was proven by reports of continued successful use with a motor-imagery paradigm [312]. Unlike the larger electrode grids required by other BCI paradigms, the small number of electrodes required for the SSVEP paradigm could be an advantage as they could be implanted using a burr-hole instead of a craniotomy, thereby limiting intra- and post-surgical risks. It should be noted that, ethically, intracranial electrode implants are a solution only for patients with severe communication disabilities and who lack other options.

Despite the widespread use of SSVEP, it is largely unclear how the responses are represented in the occipital cortex. Using intracranial recordings from one subject, we localized the foveal flickering frequency at the posterior part of the primary visual cortex, with little variation across the stimulation frequencies used (11 to 15 Hz). However, unlike the fundamental component of the foveal flickering stimulation, the location of the second harmonic component, albeit still in the primary visual cortex (V1), varied considerably with the foveal frequency, with maximal overlap between the fundamental and harmonic for the 15 Hz stimulation frequency. The flickering of the peripheral targets, which are not detectable on the scalp, are represented at cortical locations consistent with retinotopic mapping studies. Activations in response to both foveal and peripheral flickering are accompanied by high gamma activations at the same locations.

8.3 CVEP

In addition to the successful application on P300 and SSVEP target detection, spatiotemporal beamforming is also able to accurately discriminate cVEP-encoded targets (i.e., encoded by lagged versions of a pseudo-random binary sequence), as its accuracies are on par with an optimized SVM that is considered as state-of-the-art. Similar to the observations with the P300 paradigm, the beamformer can be trained considerably faster than the SVM, thus yielding similar advantages as in section 8.1.

Next to the feasibility of spatiotemporal beamforming for cVEP decoding, also the effect of stimulation speed was assessed. On traditional 60 Hz monitors, a single presentation of a binary sequence of length n requires $n/60$ seconds. However, some recent monitors adopt a faster refresh rate, allowing the sequence to be presented in less time. Our study (chapter 4) showed that, compared to the traditional 60 Hz case, a 120 Hz presentation yields a faster target selection rate with similar accuracy levels: as the screen refresh rate doubles, only half of the time is needed to present one sequence, target selection speed increases as well as the ITRs.

8.4 LIMITATIONS

The main drawback of current beamforming implementations is the required amount of training data to estimate the covariance matrix as its dimensions can be quite large in practice. Several shrinkage algorithms have been proposed to provide a more robust estimation of the covariance matrix when a limited amount of data is available. In future work, we aim to assess the influence of these shrinkage estimates on BCI performance and on the length of the training session. Alternatively, one could reduce dimensionality by reducing the number of electrodes included in the analysis. The choice of electrodes, however, should possibly be tailored to each individual, in order to maximize accuracy [65, 201, 275]. As beamformer(s) training does not require much time, an electrode selection strategy could be beneficial. While we have taken initial steps in this direction using a mutual information approach (not included in this manuscript), more work is needed to thoroughly assess its benefits.

As the aim of this work was to demonstrate the feasibility of spatiotemporal beamforming for target selection in a visual BCI, we did not test our solution on patients suffering from motor- or communication disabilities. Previous studies have reported that the patient's brain responses are considerably more noisy, resulting in lower BCI performance compared to healthy individuals. It can thus be expected that also the beamforming algorithm will face a reduction in performance when tested on patients.

We investigated and compared the accuracy of SSVEP decoders on both traditional non-invasive EEG and invasive ECoG recordings, however, as this was done on a single epilepsy patient, not suffering from one of the motor- or communication disorders targeted for BCI, it is still an open question how well the beamforming algorithm would perform on them.

8.5 FUTURE OF VISUAL BCI

Brain-computer interfaces based on visually induced brain activity have enjoyed high accuracies with short stimulation times, leading to quite performant communication systems and the ITR can most easily be increased by showing more selectable targets on the screen. While many studies are focussing on further improving the ITR, it

should be noted that user experience is probably more important for a visual BCI. When showing many simultaneous flickering targets on the screen, as is the case with the SSVEP and cVEP paradigms, visual discomfort is induced [59, 329], leading to a suboptimal user experience during long-term BCI use. As an alternative to the flashing stimuli, one could adopt other forms of visual stimulation such as a short moving stimulus as with the motion-onset visual evoked potential (mVEPs) [164]: a negative temporo-occipital deflection with a peak latency around 160 to 200 ms. As it exhibits the lowest inter- and intra-subject variability of motion-related paradigms [164], it most suited for BCI purposes. Reports of successful adoption of mVEP for BCI have been published [107, 188], and this paradigm has also been shown to work for gaze-independent interfaces [269].

To achieve the high accuracies described in the literature, also in our work, the subject needs to perform a training session prior to BCI use, as the brain's responses (e.g., latency and amplitude of the P300 ERP) often vary depending on attention level, fatigue, etc., which are unique for every session. The training session involves a cued process during which the subject has to iteratively attend a cued target, decided by the system. The duration of this training depends on the amount of data needed by the classifier, and typically ranges between 10 to 20 minutes.

One way to reduce training is to (re-)use data acquired from previous sessions of the same subject or to use data from other subjects (transfer learning). The main challenge with this approach is that the brain's responses from different subjects exhibit a non-negligible amount of variability both temporally and spatially. As shown in chapter 2, the accuracy of the beamformer with a population template, as well as the SVM trained on population data, performs considerably worse, and the variability of the phase responses (chapter 3) render averaging across subjects impossible for SSVEP. More complex statistical approaches are needed to account for this variability, for example by the inclusion of a random effect, similar to mixed model analysis.

Deep learning techniques are often hailed for their ability to account for variability. However, it has many disadvantages for BCIs. First, there is the choice of the architecture. It is often unclear which architecture to choose for a given task or paradigm. As there are endless ways to combine (sampling and convolution) layers, number of layers and neurons per layer, the architectures used vary widely across studies, with little clear motivation why a particular architecture was chosen. As deep neural networks typically exhibit many thousands of parameters, a plethora of training data is needed to accurately estimate them [192]. However, when relying on population data, then one factually restrict their application to popular BCI paradigms and even then, one will be faced with cross-subject variabilities. Also, it is unclear how well a network trained on healthy individuals would work for patients. Traditional classifiers can often easily be adapted to maximize performance of an individual (e.g., optimizing the regularization parameter or adopting an alternative implementation of the covariance matrix estimator). Training a deep neural network furthermore requires a large amount of

computational resources, demoting the possibility of online retraining. Finally, deep learning, as it is black-box approach, has only limited explanatory power - how the result is achieved is difficult to track (e.g., which spatial pattern is adopted to discriminate between targets?) -, and it renders the tweaking of parameters and fine-tuning of the architecture a cumbersome task.

A final, but not less important consideration, is the commercial viability of BCIs. Many EEG-BCI studies, including the ones reported in this thesis, rely on expensive research-grade recording equipment and carefully controlled settings. However, commercial applications typically require mobile solutions and inexpensive headsets with fixed, ready-to-go electrodes to avoid the time-consuming electrode setup of research settings, thereby compromising on signal-to-noise ratio and artifact rejection, and eventually on target selection accuracy and ITR. Further work will be needed to optimize decoding algorithms to meet the needs of consumer-grade BCI solutions.

BIBLIOGRAPHY

[1] Elias Abou Zeid and Tom Chau. "Electrode Fusion for the Prediction of Self-Initiated Fine Movements from Single-Trial Readiness Potentials." In: *International journal of neural systems* (2015), p. 1550014.

[2] Mohammad Abu-Alqumsan and Angelika Peer. "Advancing the detection of steady-state visual evoked potentials in brain–computer interfaces." In: *Journal of neural engineering* 13.3 (2016), p. 036005.

[3] Seppo P Ahlfors, Jooman Han, Fa-Hsuan Lin, Thomas Witzel, John W Belliveau, Matti S Hämäläinen, and Eric Halgren. "Cancellation of EEG and MEG signals generated by extended and distributed sources." In: *Human brain mapping* 31.1 (2010), pp. 140–149.

[4] Minkyu Ahn, Mijin Lee, Jinyoung Choi, and Sung Chan Jun. "A review of brain-computer interface games and an opinion survey from researchers, developers and users." In: *Sensors* 14.8 (2014), pp. 14601–14633.

[5] Brendan Allison, Thorsten Luth, Diana Valbuena, Amir Teymourian, Ivan Volosyak, and Axel Graser. "BCI demographics: How many (and what kinds of) people can use an SSVEP BCI?" In: *IEEE transactions on neural systems and rehabilitation engineering* 18.2 (2010), pp. 107–116.

[6] Fabio Aloise, Pietro Aricò, Francesca Schettini, Angela Riccio, Serenella Salinari, Donatella Mattia, Fabio Babiloni, and Febo Cincotti. "A covert attention P300-based brain–computer interface: Geospell." In: *Ergonomics* 55.5 (2012), pp. 538–551.

[7] Esther Alonso-Prieto, Goedele Van Belle, Joan Liu-Shuang, Anthony M Norcia, and Bruno Rossion. "The 6Hz fundamental stimulation frequency rate for individual face discrimination in the right occipito-temporal cortex." In: *Neuropsychologia* 51.13 (2013), pp. 2863–2875.

[8] Daiki Aminaka, Shoji Makino, and Tomasz M Rutkowski. "Chromatic and high-frequency cVEP-based BCI paradigm." In: *Engineering in Medicine and Biology Society (EMBC), 2015 37th Annual International Conference of the IEEE*. IEEE. 2015, pp. 1906–1909.

[9] Daiki Aminaka, Shoji Makino, and Tomasz M Rutkowski. "Classification accuracy improvement of chromatic and high–frequency code–modulated visual evoked potential–based BCI." In: *International Conference on Brain Informatics and Health*. Springer. 2015, pp. 232–241.

[10] Daiki Aminaka, Shoji Makino, and Tomasz M Rutkowski. "EEG Filtering Optimization for Code–Modulated Chromatic Visual Evoked Potential–Based Brain–Computer Interface." In: *Symbiotic Interaction*. Springer, 2015, pp. 1–6.

[11] Daiki Aminaka, Shoji Makino, and Tomasz M Rutkowski. "SVM classification study of code-modulated visual evoked potentials." In: *Signal and Information Processing Association Annual Summit and Conference (APSIPA), 2015 Asia-Pacific*. IEEE. 2015, pp. 1065–1070.

[12] Setare Amiri, Ahmed Rabbi, Leila Azinfar, and Reza Fazel-Rezai. "A review of P300, SSVEP, and hybrid P300/SSVEP brain-computer interface systems." In: *Brain-Computer Interface Systems—Recent Progress and Future Prospects* (2013).

[13] L Gregory Appelbaum, Alex R Wade, Vladimir Y Vildavski, Mark W Pettet, and Anthony M Norcia. "Cue-invariant networks for figure and background processing in human visual cortex." In: *Journal of Neuroscience* 26.45 (2006), pp. 11695–11708.

[14] Luc H Arnal and Anne-Lise Giraud. "Cortical oscillations and sensory predictions." In: *Trends in cognitive sciences* 16.7 (2012), pp. 390–398.

[15] Mahnaz Arvaneh, Cuntai Guan, Kai Keng Ang, and Chai Quek. "Optimizing the channel selection and classification accuracy in EEG-based BCI." In: *IEEE Transactions on Biomedical Engineering* 58.6 (2011), pp. 1865–1873.

[16] Tonio Ball, Markus Kern, Isabella Mutschler, Ad Aertsen, and Andreas Schulze-Bonhage. "Signal quality of simultaneously recorded invasive and non-invasive EEG." In: *Neuroimage* 46.3 (2009), pp. 708–716.

[17] Alexandre Barachant and Stephane Bonnet. "Channel selection procedure using Riemannian distance for BCI applications." In: *Neural Engineering (NER), 2011 5th International IEEE/EMBS Conference on*. IEEE. 2011, pp. 348–351.

[18] Canan Başar-Eroglu, Erol Başar, Tamer Demiralp, and Martin Schürmann. "P300-response: possible psychophysiological correlates in delta and theta frequency channels. A review." In: *International Journal of Psychophysiology* 13.2 (1992), pp. 161–179.

[19] Erol Başar. *Brain Function and Oscillations. I. Brain Oscillations: Principles and Approaches.* Springer, Berlin Heidelberg., 1998.

[20] Erol Başar. *Brain Function and Oscillations. II. Integra- tive Brain Function. Neurophysiology and Cognitive Processes.* Springer Berlin Heidelberg, 1999.

[21] Erol Başar, Canan Başar-Eroglu, Sirel Karakaş, and Martin Schürmann. "Gamma, alpha, delta, and theta oscillations govern cognitive processes." In: *International journal of psychophysiology* 39.2 (2001), pp. 241–248.

[22] Ali Bayram, Zubeyir Bayraktaroglu, Esin Karahan, Basri Erdogan, Basar Bilgic, Muge Özker, Itir Kasikci, Adil D Duru, Ahmet Ademoglu, Cengizhan Öztürk, et al. "Simultaneous EEG/fMRI analysis of the resonance phenomena in steady-state visual evoked responses." In: *Clinical EEG and neuroscience* 42.2 (2011), pp. 98–106.

[23] Mark A Bee and Christophe Micheyl. "The cocktail party problem: what is it? How can it be solved? And why should animal behaviorists study it?" In: *Journal of comparative psychology* 122.3 (2008), p. 235.

[24] Elga Behrens, Josef Zentner, Dirk Van Roost, Andreas Hufnagel, Christian E Elger, and Johannes Schramm. "Subdural and depth electrodes in the presurgical evaluation of epilepsy." In: *Acta neurochirurgica* 128.1-4 (1994), pp. 84–87.

[25] Paolo Belardinelli, Erick Ortiz, and Christoph Braun. "Source activity correlation effects on LCMV beamformers in a realistic measurement environment." In: *Computational and mathematical methods in medicine* 2012 (2012).

[26] Matthew Belmonte. "Abnormal attention in autism shown by steady-state visual evoked potentials." In: *Autism* 4.3 (2000), pp. 269–285.

[27] Alim Louis Benabid, Stephan Chabardes, John Mitrofanis, and Pierre Pollak. "Deep brain stimulation of the subthalamic nucleus for the treatment of Parkinson's disease." In: *The Lancet Neurology* 8.1 (2009), pp. 67–81.

[28] Philipp Berens et al. "CircStat: a MATLAB toolbox for circular statistics." In: *J Stat Softw* 31.10 (2009), pp. 1–21.

[29] Viv Bewick, Liz Cheek, and Jonathan Ball. "Statistics review 13: receiver operating characteristic curves." In: *Critical care* 8.6 (2004), p. 508.

[30] Luigi Bianchi, Saber Sami, Arjan Hillebrand, Ian P Fawcett, Lucia Rita Quitadamo, and Stefano Seri. "Which physiological components are more suitable for visual ERP based brain–computer interface? A preliminary MEG/EEG study." In: *Brain topography* 23.2 (2010), pp. 180–185.

[31] Guangyu Bin, Xiaorong Gao, Zheng Yan, Bo Hong, and Shangkai Gao. "An online multi-channel SSVEP-based brain–computer interface using a canonical correlation analysis method." In: *Journal of neural engineering* 6.4 (2009), p. 046002.

[32] Guangyu Bin, Xiaorong Gao, Yijun Wang, Bo Hong, and Shangkai Gao. "VEP-based brain-computer interfaces: time, frequency, and code modulations [Research Frontier." In: *IEEE Computational Intelligence Magazine* 4.4 (2009), pp. 22–26. ISSN: 1556-603X. DOI: 10.1109/mci.2009.934562.

[33] Guangyu Bin, Xiaorong Gao, Yijun Wang, Yun Li, Bo Hong, and Shangkai Gao. "A high-speed BCI based on code modulation VEP." In: *Journal of neural engineering* 8.2 (2011), p. 025015.

[34] Danny Plass-Oude Bos, Boris Reuderink, Bram van de Laar, Hayrettin Gürkök, Christian Mühl, Mannes Poel, Anton Nijholt, and Dirk Heylen. "Brain-computer interfacing and games." In: *Brain-Computer Interfaces*. Springer, 2010, pp. 149–178.

[35] Elena Boto, Niall Holmes, James Leggett, Gillian Roberts, Vishal Shah, Sofie S Meyer, Leonardo Duque Muñoz, Karen J Mullinger, Tim M Tierney, Sven Bestmann, et al. "Moving magnetoencephalography towards real-world applications with a wearable system." In: *Nature* (2018).

[36] Geert JM van Boxtel and Koen BE Böcker. "Cortical measures of anticipation." In: *Journal of psychophysiology* 18.2/3 (2004), pp. 61–76.

[37] Stevo Bozinovski, Mihail Sestakov, and Liljana Bozinovska. "Using EEG alpha rhythm to control a mobile robot." In: *Proceedings of the Annual International Conference of the IEEE Engineering in Medicine and Biology Society*. Vol. 3. IEEE, 1988, pp. 1515 –1516.

[38] David H Brainard and Spatial Vision. "The psychophysics toolbox." In: *Spatial vision* 10 (1997), pp. 433–436.

[39] H Bridge. "Mapping the visual brain: how and why." In: *Eye* 25.3 (2011), pp. 291–296.

[40] Anne-Marie Brouwer and Jan BF Van Erp. "A tactile P300 brain-computer interface." In: *Frontiers in neuroscience* 4 (2010).

[41] Cornelis HM Brunia, Geert JM van Boxtel, and Koen BE Böcker. *Negative slow waves as indices of anticipation: the Bereitschaftspotential, the contingent negative variation, and the stimulus-preceding negativity*. Ed. by Emily S. Kappenman and Steven J. Luck. The Oxford Handbook of Event-Related Potential Components. Oxford University Press, 2012.

[42] C Brunner, BZ Allison, C Altstätter, and C Neuper. "A comparison of three brain-computer interfaces based on event-related desynchronization, steady state visual evoked potentials, or a hybrid approach using both signals." In: *Journal of neural engineering* 8.2 (2011), p. 025010.

[43] Peter Brunner, Anthony L Ritaccio, Joseph F Emrich, Horst Bischof, and Gerwin Schalk. "Rapid communication with a "P300" matrix speller using electrocorticographic signals (ECoG)." In: *Frontiers in neuroscience* 5 (2011), p. 5.

[44] Giedrius T. Buračas and Geoffrey M. Boynton. "Efficient Design of Event-Related fMRI Experiments Using M-Sequences." In: *NeuroImage* 16.3 (2002), pp. 801–813. ISSN: 1053-8119. DOI: 10.1006/nimg.2002.1116.

[45] Alexis Burns, Hojjat Adeli, and John A Buford. "Brain–Computer Interface after Nervous System Injury." In: *The Neuroscientist* (2014), pp. 639–651.

[46] Niko A Busch, Julien Dubois, and Rufin VanRullen. "The phase of ongoing EEG oscillations predicts visual perception." In: *Journal of Neuroscience* 29.24 (2009), pp. 7869–7876.

[47] György Buzsáki. "Theta oscillations in the hippocampus." In: *Neuron* 33.3 (2002), pp. 325–340.

[48] György Buzsáki, Costas A Anastassiou, and Christof Koch. "The origin of extracellular fields and currents—EEG, ECoG, LFP and spikes." In: *Nature reviews neuroscience* 13.6 (2012), pp. 407–420.

[49] Teng Cao, Feng Wan, Peng Un Mak, Pui-In Mak, Mang I Vai, and Yong Hu. "Flashing color on the performance of SSVEP-based brain-computer interfaces." In: *Engineering in Medicine and Biology Society (EMBC), 2012 Annual International Conference of the IEEE*. IEEE. 2012, pp. 1819–1822.

[50] James Carpenter and Michael Kenward. *Multiple imputation and its application*. John Wiley & Sons, 2012.

[51] H. Cecotti and A. Graser. "Convolutional Neural Networks for P300 Detection with Application to Brain-Computer Interfaces." In: *Pattern Analysis and Machine Intelligence, IEEE Transactions on* 33.3 (2011), pp. 433–445. ISSN: 0162-8828. DOI: 10.1109/TPAMI.2010.125.

[52] Hubert Cecotti. "Classification of steady-state visual evoked potentials based on the visual stimuli duty cycle." In: *Applied Sciences in Biomedical and Communication Technologies (ISABEL), 2010 3rd International Symposium on*. IEEE. 2010, pp. 1–5.

[53] Zenas C Chao, Yasuo Nagasaka, and Naotaka Fujii. "Long-term asynchronous decoding of arm motion using electrocorticographic signals in monkeys." In: *Frontiers in neuroengineering* 3 (2010).

[54] Xiaogang Chen, Zhikai Chen, Shangkai Gao, and Xiaorong Gao. "A high-ITR SSVEP-based BCI speller." In: *Brain-Computer Interfaces* 1.3-4 (2014), pp. 181–191.

[55] Xiaogang Chen, Yijun Wang, Masaki Nakanishi, Tzyy-Ping Jung, and Xiaorong Gao. "Hybrid frequency and phase coding for a high-speed SSVEP-based BCI speller." In: *Engineering in Medicine and Biology Society (EMBC), 2014 36th Annual International Conference of the IEEE*. IEEE. 2014, pp. 3993–3996.

[56] Xiaogang Chen, Yijun Wang, Shangkai Gao, Tzyy-Ping Jung, and Xiaorong Gao. "Filter bank canonical correlation analysis for implementing a high-speed SSVEP-based brain–computer interface." In: *Journal of neural engineering* 12.4 (2015), p. 046008.

[57] Xiaogang Chen, Yijun Wang, Masaki Nakanishi, Xiaorong Gao, Tzyy-Ping Jung, and Shangkai Gao. "High-speed spelling with a noninvasive brain–computer interface." In: *Proceedings of the national academy of sciences* 112.44 (2015), E6058–E6067.

[58] Ming Cheng, Xiaorong Gao, Shangkai Gao, and Dingfeng Xu. "Design and implementation of a brain-computer interface with high transfer rates." In: *Biomedical Engineering, IEEE Transactions on* 49.10 (2002), pp. 1181–1186.

[59] Yu-Yi Chien, Fang-Cheng Lin, John K Zao, Ching-Chi Chou, Yi-Pai Huang, Heng-Yuan Kuo, Yijun Wang, Tzyy-Ping Jung, and Han-Ping D Shieh. "Polychromatic SSVEP stimuli with subtle flickering adapted to brain-display interactions." In: *Journal of neural engineering* 14.1 (2017), p. 016018.

[60] Nikolay Chumerin, Nikolay V Manyakov, Adrien Combaz, Arne Robben, Marijn van Vliet, and Marc M Van Hulle. "Steady State Visual Evoked Potential Based Computer Gaming-The Maze." In: *INTETAIN*. Springer. 2011, pp. 28–37.

[61] Nikolay Chumerin, Nikolay V Manyakov, Marijn van Vliet, Arne Robben, Adrien Combaz, and Marc M Van Hulle. "Steady-state visual evoked potential-based computer gaming on a consumer-grade EEG device." In: *IEEE transactions on computational intelligence and ai in games* 5.2 (2013), pp. 100–110.

[62] Michael S Clayton, Nick Yeung, and Roi Cohen Kadosh. "The roles of cortical oscillations in sustained attention." In: *Trends in cognitive sciences* 19.4 (2015), pp. 188–195.

[63] Brett A Clementz, Andreas Keil, and Johanna Kissler. "Aberrant brain dynamics in schizophrenia: delayed buildup and prolonged decay of the visual steady-state response." In: *Cognitive brain research* 18.2 (2004), pp. 121–129.

[64] Jennifer L Collinger, Brian Wodlinger, John E Downey, Wei Wang, Elizabeth C Tyler-Kabara, Douglas J Weber, Angus JC McMorland, Meel Velliste, Michael L Boninger, and Andrew B Schwartz. "High-performance neuroprosthetic control by an individual with tetraplegia." In: *The Lancet* 381.9866 (2013), pp. 557–564.

[65] KA Colwell, DB Ryan, CS Throckmorton, EW Sellers, and LM Collins. "Channel selection methods for the P300 speller." In: *Journal of neuroscience methods* 232 (2014), pp. 6–15.

[66] Adrien Combaz, Nikolay V Manyakov, Nikolay Chumerin, Johan AK Suykens, and Marc M Van Hulle. "Feature extraction and classification of EEG signals for rapid P300 mind spelling." In: *Machine Learning and Applications, 2009. ICMLA'09. International Conference on*. IEEE. 2009, pp. 386–391.

[67] Adrien Combaz, Nikolay Chumerin, Nikolay V Manyakov, Arne Robben, Johan AK Suykens, and Marc M Van Hulle. "Towards the detection of error-related potentials and its integration in the context of a P300 speller brain–computer interface." In: *Neurocomputing* 80 (2012), pp. 73–82.

[68] Adrien Combaz, Camille Chatelle, Arne Robben, Gertie Vanhoof, Ann Goeleven, Vincent Thijs, Marc M Van Hulle, and Steven Laureys. "A comparison of two spelling brain-computer interfaces based on visual P3 and SSVEP in Locked-In Syndrome." In: *PloS one* 8.9 (2013), e73691.

[69] A Cowey and ET Rolls. "Human cortical magnification factor and its relation to visual acuity." In: *Experimental Brain Research* 21.5 (1974), pp. 447–454.

[70] Rodney J Croft and Robert J Barry. "Removal of ocular artifact from the EEG: a review." In: *Neurophysiologie Clinique/Clinical Neurophysiology* 30.1 (2000), pp. 5–19.

[71] Xu Cui, Signe Bray, and Allan L Reiss. "Speeded near infrared spectroscopy (NIRS) response detection." In: *PLoS one* 5.11 (2010), e15474.

[72] Janis J Daly and Jonathan R Wolpaw. "Brain–computer interfaces in neurological rehabilitation." In: *The Lancet Neurology* 7.11 (2008), pp. 1032–1043.

[73] Francesco Di Russo and Donatella Spinelli. "Electrophysiological evidence for an early attentional mechanism in visual processing in humans." In: *Vision research* 39.18 (1999), pp. 2975–2985.

[74] Francesco Di Russo, Wolfgang A Teder-Sälejärvi, and Steven A Hillyard. "Steady-state VEP and attentional visual processing." In: *The cognitive electrophysiology of mind and brain (Zani A, Proverbio AM, eds)* (2002), pp. 259–274.

[75] Francesco Di Russo, Sabrina Pitzalis, Teresa Aprile, Grazia Spitoni, Fabiana Patria, Alessandra Stella, Donatella Spinelli, and Steven A Hillyard. "Spatiotemporal analysis of the cortical sources of the steady-state visual evoked potential." In: *Human brain mapping* 28.4 (2007), pp. 323–334.

[76] Alan Dix, Janet Finlay, Gregory D. Abowd, and Russel Beale. *Human-Computer Interaction*. 3rd. Pearson Education Limited, 2004.

[77] Katrina Ducis, Jian Guan, Michael Karsy, and Robert J Bollo. "Preoperative evaluation and surgical decision-making in pediatric epilepsy surgery." In: *Translational Pediatrics* 5.3 (2016), p. 169.

[78] Gareth J Edwards, Timothy F Cootes, and Christopher J Taylor. "Face recognition using active appearance models." In: *European conference on computer vision*. Springer. 1998, pp. 581–595.

[79] Nicolás von Ellenrieder, Leandro Beltrachini, Carlos H Muravchik, and Jean Gotman. "Extent of cortical generators visible on the scalp: effect of a subdural grid." In: *NeuroImage* 101 (2014), pp. 787–795.

[80] Kathryn A Ellis, Richard B Silberstein, and Pradeep J Nathan. "Exploring the temporal dynamics of the spatial working memory n-back task using steady state visual evoked potentials (SSVEP)." In: *Neuroimage* 31.4 (2006), pp. 1741–1751.

[81] Stephen A Engel, Gary H Glover, and Brian A Wandell. "Retinotopic organization in human visual cortex and the spatial precision of functional MRI." In: *Cerebral cortex* 7.2 (1997), pp. 181–192.

[82] Monica Fabiani, David Friedman, and Jeff C Cheng. "Individual differences in P3 scalp distribution in older adults, and their relationship to frontal lobe function." In: *Psychophysiology* 35.6 (1998), pp. 698–708.

[83] Owen Falzon, Kenneth Camilleri, and Joseph Muscat. "Complex-valued spatial filters for SSVEP-based BCIs with phase coding." In: *Biomedical Engineering, IEEE Transactions on* 59.9 (2012), pp. 2486–2495.

[84] Lawrence Ashley Farwell and Emanuel Donchin. "Talking off the top of your head: toward a mental prosthesis utilizing event-related brain potentials." In: *Electroencephalography and clinical Neurophysiology* 70.6 (1988), pp. 510–523.

[85] Bruce Fischl. "FreeSurfer." In: *Neuroimage* 62.2 (2012), pp. 774–781.

[86] Robert S Fisher, Graham Harding, Giuseppe Erba, Gregory L Barkley, and Arnold Wilkins. "Photic-and pattern-induced seizures: a review for the Epilepsy Foundation of America Working Group." In: *Epilepsia* 46.9 (2005), pp. 1426–1441.

[87] Alberto Forti, Giovanni Ambrosetto, Mario Amore, Roberto De Maria, Roberto Michelucci, Ebe Omicini, Nicola Rizzuto, F Fenzi, and Carlo Alberto Tassinari. "Locked-in syndrome in multiple sclerosis with sparing of the ventral portion of the pons." In: *Annals of neurology* 12.4 (1982), pp. 393–394.

[88] Peter T Fox and Marcus E Raichle. "Stimulus rate dependence of regional cerebral blood flow in human striate cortex, demonstrated by positron emission tomography." In: *Journal of neurophysiology* 51.5 (1984), pp. 1109–1120.

[89] David Friedman, Victoria Kazmerski, and Monica Fabiani. "An overview of age-related changes in the scalp distribution of P3b." In: *Electroencephalography and Clinical Neurophysiology/Evoked Potentials Section* 104.6 (1997), pp. 498–513.

[90] Jerome H Friedman. "Regularized discriminant analysis." In: *Journal of the American statistical association* 84.405 (1989), pp. 165–175.

[91] Ola Friman, Ivan Volosyak, and Axel Graser. "Multiple channel detection of steady-state visual evoked potentials for brain-computer interfaces." In: *IEEE transactions on biomedical engineering* 54.4 (2007), pp. 742–750.

[92] Sandra Fuchs, Søren K Andersen, Thomas Gruber, and Matthias M Müller. "Attentional bias of competitive interactions in neuronal networks of early visual processing in the human brain." In: *NeuroImage* 41.3 (2008), pp. 1086–1101.

[93] Adrian Furdea, Sebastian Halder, DJ Krusienski, Donald Bross, Femke Nijboer, Niels Birbaumer, and Andrea Kübler. "An auditory oddball (P300) spelling system for brain-computer interfaces." In: *Psychophysiology* 46.3 (2009), pp. 617–625.

[94] Shangkai Gao, Yijun Wang, Xiaorong Gao, and Bo Hong. "Visual and Auditory Brain Computer Interfaces." In: *IEEE Transactions on Biomedical Engineering* 61.5 (2014), pp. 1436–1447. ISSN: 1558-2531. DOI: 10.1109/tbme.2014.2300164.

[95] Xiaorong Gao, Dingfeng Xu, Ming Cheng, and Shangkai Gao. "A BCI-based environmental controller for the motion-disabled." In: *IEEE Transactions on neural systems and rehabilitation engineering* 11.2 (2003), pp. 137–140.

[96] A Gauthier, A Vignola, A Calvo, E Cavallo, C Moglia, L Sellitti, R Mutani, and A Chio. "A longitudinal study on quality of life and depression in ALS patient–caregiver couples." In: *Neurology* 68.12 (2007), pp. 923–926.

[97] Felix Gembler, Piotr Stawicki, and Ivan Volosyak. "Autonomous parameter adjustment for SSVEP-based BCIs with a novel BCI wizard." In: *Frontiers in neuroscience* 9 (2015).

[98] Salim Ghoggali, Mihaela Ungureanu, and Rodica Strungaru. "A genetic algorithm and ensemble of SVM approach for BCI p300 classification problem." In: *Scientific Bulleting Series C* 75.2 (2013), pp. 129–142.

[99] Pierre Gloor. "Neuronal generators and the problem of localization in electroencephalography: application of volume conductor theory to electroencephalography." In: *Journal of clinical neurophysiology* 2.4 (1985), pp. 327–354.

[100] Solomon W Golomb et al. *Shift register sequences*. Aegean Park Press, 1982.

[101] Romain Goutagny, Jesse Jackson, and Sylvain Williams. "Self-generated theta oscillations in the hippocampus." In: *Nature neuroscience* 12.12 (2009), p. 1491.

[102] B Graimann, JE Huggins, SP Levine, and G Pfurtscheller. "Visualization of significant ERD/ERS patterns in multichannel EEG and ECoG data." In: *Clinical Neurophysiology* 113.1 (2002), pp. 43–47.

[103] Bernhard Graimann and Gert Pfurtscheller. "Quantification and visualization of event-related changes in oscillatory brain activity in the time–frequency domain." In: *Progress in brain research* 159 (2006), pp. 79–97.

[104] Heather M Gray, Nalini Ambady, William T Lowenthal, and Patricia Deldin. "P300 as an index of attention to self-relevant stimuli." In: *Journal of experimental social psychology* 40.2 (2004), pp. 216–224.

[105] Moritz Grosse-Wentrup, Christian Liefhold, Klaus Gramann, and Martin Buss. "Beamforming in noninvasive brain–computer interfaces." In: *IEEE Transactions on Biomedical Engineering* 56.4 (2009), pp. 1209–1219.

[106] HO Gulcar, YK Yilmaz, and T Demiralp. "Classification of P300 component in single trial event related potentials." In: *Biomedical Engineering Days, 1998. Proceedings of the 1998 2nd International Conference*. IEEE. 1998, pp. 48–50.

[107] Fei Guo, Bo Hong, Xiaorong Gao, and Shangkai Gao. "A brain–computer interface using motion-onset visual evoked potential." In: *Journal of neural engineering* 5.4 (2008), p. 477.

[108] Isabelle Guyon and André Elisseeff. "An introduction to variable and feature selection." In: *Journal of machine learning research* 3.Mar (2003), pp. 1157–1182.

[109] Hans Hallez, Bart Vanrumste, Roberta Grech, Joseph Muscat, Wim De Clercq, Anneleen Vergult, Yves D'Asseler, Kenneth P Camilleri, Simon G Fabri, Sabine Van Huffel, et al. "Review on solving the forward problem in EEG source analysis." In: *Journal of neuroengineering and rehabilitation* 4.1 (2007), p. 46.

[110] J Hanagata and K Momose. "A method for detecting gazed target using visual evoked potentials elicited by pseudorandom stimuli." In: *Proc. 5th Asia Pacific Conf. Medical and Biological Engineering and 11th Int. Conf. Biomedical Engineering (ICBME)*. 2002.

[111] Wolfgang Härdle and Zdeněk Hlávka. "Canonical correlation analysis." In: *Multivariate Statistics: Exercises and Solutions* (2007), pp. 263–269.

[112] Stefan Haufe, Frank Meinecke, Kai Görgen, Sven Dähne, John-Dylan Haynes, Benjamin Blankertz, and Felix Bießmann. "On the interpretation of weight vectors of linear models in multivariate neuroimaging." In: *Neuroimage* 87 (2014), pp. 96–110.

[113] Sven P Heinrich and Michael Bach. "Adaptation dynamics in pattern-reversal visual evoked potentials." In: *Documenta Ophthalmologica* 102.2 (2001), pp. 141–156.

[114] Christian Herff and Tanja Schultz. "Automatic speech recognition from neural signals: a focused review." In: *Frontiers in neuroscience* 10 (2016), p. 429.

[115] Christoph S Herrmann. "Human EEG responses to 1–100 Hz flicker: resonance phenomena in visual cortex and their potential correlation to cognitive phenomena." In: *Experimental brain research* 137.3-4 (2001), pp. 346–353.

[116] MJ Herrmann, A-C Ehlis, H Ellgring, and AJ Fallgatter. "Early stages (P100) of face perception in humans as measured with event-related potentials (ERPs)." In: *Journal of neural transmission* 112.8 (2005), pp. 1073–1081.

[117] Yasuo Hishikawa, Junji Yamamoto, Eiji Furuya, Yoshihide Yamada, Kiyoshi Miyazaki, and Ziro Kaneko. "Photosensitive epilepsy: relationships between the visual evoked responses and the epileptiform discharges induced by intermittent photic stimulation." In: *Electroencephalography and clinical neurophysiology* 23.4 (1967), pp. 320–334.

[118] Leigh R Hochberg, Mijail D Serruya, Gerhard M Friehs, Jon A Mukand, Maryam Saleh, Abraham H Caplan, Almut Branner, David Chen, Richard D Penn, and John P Donoghue. "Neuronal ensemble control of prosthetic devices by a human with tetraplegia." In: *Nature* 442.7099 (2006), p. 164.

[119] Ulrich Hoffmann, Jean-Marc Vesin, Touradj Ebrahimi, and Karin Diserens. "An efficient P300-based brain–computer interface for disabled subjects." In: *Journal of Neuroscience methods* 167.1 (2008), pp. 115–125.

[120] Yoshihito Honda. "Photic Epilepsy Evoked by Square-Wave Pulses Report of a Case Studied by Changing Stimulus Intensity and Duration." In: *Journal of Pediatric Ophthalmology and Strabismus* 14.5 (1977), pp. 309–315.

[121] Jun Hee Hong, Minkyu Ahn, Kiwoong Kim, and Sung Chan Jun. "Localization of coherent sources by simultaneous MEG and EEG beamformer." In: *Medical & biological engineering & computing* 51.10 (2013), pp. 1121–1135.

[122] Chih-Wei Hsu, Chih-Chung Chang, Chih-Jen Lin, et al. *A practical guide to support vector classification*. 2003.

[123] Li Hu, P Xiao, ZG Zhang, André Mouraux, and Gian Domenico Iannetti. "Single-trial time–frequency analysis of electrocortical signals: Baseline correction and beyond." In: *Neuroimage* 84 (2014), pp. 876–887.

[124] Borbála Hunyadi, Marco Signoretto, Stefan Debener, Sabine Van Huffel, and Maarten De Vos. "Classification of structured EEG tensors using nuclear norm regularization: improving P300 classification." In: *Pattern Recognition in Neuroimaging (PRNI), 2013 International Workshop on*. IEEE. 2013, pp. 98–101.

[125] E Iannilli, N Noennig, T Hummel, and AM Schoenfeld. "Spatio-temporal correlates of taste processing in the human primary gustatory cortex." In: *Neuroscience* 273 (2014), pp. 92–99.

[126] Chuan Jia, Xiaorong Gao, Bo Hong, and Shangkai Gao. "Frequency and phase mixed coding in SSVEP-based brain–computer interface." In: *IEEE Transactions on Biomedical Engineering* 58.1 (2011), pp. 200–206.

[127] Tianxiao Jiang, Tao Jiang, Taylor Wang, Shanshan Mei, Qingzhu Liu, Yunlin Li, Xiaofei Wang, Sujit Prabhu, Zhiyi Sha, and Nuri F Ince. "Characterization and Decoding the Spatial Patterns of Hand Extension/Flexion using High-Density ECoG." In: *IEEE Transactions on Neural Systems and Rehabilitation Engineering* 25.4 (2017), pp. 370–379.

[128] Jing Jin, Brendan Z Allison, Xingyu Wang, and Christa Neuper. "A combined brain–computer interface based on P300 potentials and motion-onset visual evoked potentials." In: *Journal of neuroscience methods* 205.2 (2012), pp. 265–276.

[129] Jing Jin, Brendan Z Allison, Tobias Kaufmann, Andrea Kübler, Yu Zhang, Xingyu Wang, and Andrzej Cichocki. "The changing face of P300 BCIs: a comparison of stimulus changes in a P300 BCI involving faces, emotion, and movement." In: *PloS one* 7.11 (2012), e49688.

[130] Jing Jin, Eric W Sellers, Yu Zhang, Ian Daly, Xingyu Wang, and Andrzej Cichocki. "Whether generic model works for rapid ERP-based BCI calibration." In: *Journal of neuroscience methods* 212.1 (2013), pp. 94–99.

[131] Jing Jin, Brendan Z Allison, Yu Zhang, Xingyu Wang, and Andrzej Cichocki. "An ERP-based BCI using an oddball paradigm with different faces and reduced errors in critical functions." In: *International journal of neural systems* 24.08 (2014), p. 1450027.

[132] Jing Jin, Eric W Sellers, Sijie Zhou, Yu Zhang, Xingyu Wang, and Andrzej Cichocki. "A P300 brain–computer interface based on a modification of the mismatch negativity paradigm." In: *International journal of neural systems* 25.03 (2015), p. 1550011.

[133] Jacques Jonas, Corentin Jacques, Joan Liu-Shuang, Hélène Brissart, Sophie Colnat-Coulbois, Louis Maillard, and Bruno Rossion. "A face-selective ventral occipito-temporal map of the human brain with intracerebral potentials." In: *Proceedings of the National Academy of Sciences* 113.28 (2016), E4088–E4097.

[134] Matthew W Jones and Matthew A Wilson. "Theta rhythms coordinate hippocampal–prefrontal interactions in a spatial memory task." In: *PLoS biol* 3.12 (2005), e402.

[135] Yaqub Jonmohamadi, Govinda Poudel, Carrie Innes, Daniel Weiss, Rejko Krueger, and Richard Jones. "Comparison of beamformers for EEG source signal reconstruction." In: *Biomedical Signal Processing and Control* 14 (2014), pp. 175–188.

[136] Peter K Kaiser. "Physiological response to color: A critical review." In: *Color Research & Application* 9.1 (1984), pp. 29–36.

[137] A Kamp, CW Sem-Jacobsen, W Leeuwen, et al. "Cortical responses to modulated light in the human subject." In: *Acta Physiologica* 48.1 (1960), pp. 1–12.

[138] C. Kapeller, C. Hintermuller, M. Abu-Alqumsan, R. Pruckl, A. Peer, and C. Guger. "A BCI using VEP for continuous control of a mobile robot." In: *2013 35th Annual International Conference of the IEEE Engineering in Medicine and Biology Society (EMBC)* (2013). DOI: 10.1109/embc.2013.6610734.

[139] Christoph Kapeller, Kyousuke Kamada, Hiroshi Ogawa, Robert Prueckl, Josef Scharinger, and Christoph Guger. "An electrocorticographic BCI using code-based VEP for control in video applications: a single-subject study." In: *Frontiers in Systems Neuroscience* 8 (2014). ISSN: 1662-5137. DOI: 10.3389/fnsys.2014.00139.

[140] Masayuki Karasuyama and Ichiro Takeuchi. "Multiple Incremental Decremental Learning of Support Vector Machines." In: *Advances in Neural Information Processing Systems 22*. Ed. by Y. Bengio, D. Schuurmans, J. D. Lafferty, C. K. I. Williams, and A. Culotta. Curran Associates, Inc., 2009, pp. 907–915. URL: http://papers.nips.cc/paper/3804-multiple-incremental-decremental-learning-of-support-vector-machines.pdf.

[141] T Kaufmann, EM Hammer, and A Kübler. *ERPs contributing to classification in the P300 BCI*. na, 2011.

[142] Tobias Kaufmann, SM Schulz, Claudia Grünzinger, and Andrea Kübler. "Flashing characters with famous faces improves ERP-based brain–computer interface performance." In: *Journal of neural engineering* 8.5 (2011), p. 056016.

[143] Elaine Kearney, Sanjana Shellikeri, Rosemary Martino, and Yana Yunusova. "Augmented visual feedback-aided interventions for motor rehabilitation in Parkinson's disease: a systematic review." In: *Disability and rehabilitation* (2018), pp. 1–17.

[144] S Sathiya Keerthi and Dennis DeCoste. "A modified finite Newton method for fast solution of large scale linear SVMs." In: *Journal of Machine Learning Research*. Vol. 6. 2005, pp. 341–361.

[145] Andreas Keil, Stephan Moratti, Dean Sabatinelli, Margaret M Bradley, and Peter J Lang. "Additive effects of emotional content and spatial selective attention on electrocortical facilitation." In: *Cerebral Cortex* 15.8 (2004), pp. 1187–1197.

[146] Simon P Kelly, Edmund C Lalor, Richard B Reilly, and John J Foxe. "Visual spatial attention tracking using high-density SSVEP data for independent brain-computer communication." In: *Neural Systems and Rehabilitation Engineering, IEEE Transactions on* 13.2 (2005), pp. 172–178.

[147] Imananagha Kobina Keme-Ebi and Asindi Asindi Asindi. "Locked–in Syndrome in a Nigerian male with Multiple Sclerosis: a case report and literature review." In: *Pan African Medical Journal* 1.1 (2008).

[148] AH Kemp, MA Gray, P Eide, RB Silberstein, and PJ Nathan. "Steady-state visually evoked potential topography during processing of emotional valence in healthy subjects." In: *NeuroImage* 17.4 (2002), pp. 1684–1692.

[149] Philip R Kennedy, M Todd Kirby, Melody M Moore, Brandon King, and Adon Mallory. "Computer control using human intracortical local field potentials." In: *IEEE Transactions on Neural Systems and Rehabilitation Engineering* 12.3 (2004), pp. 339–344.

[150] Elvira Khachatryan, Mansoureh Fahimi Hnazaee, and Marc M Van Hulle. "Effect of word association on linguistic event-related potentials in moderately to mildly constraining sentences." In: *Scientific reports* 8.1 (2018), p. 7175.

[151] Elvira Khachatryan, Miet De Letter, Gertie Vanhoof, Ann Goeleven, and Marc M Van Hulle. "Sentence context prevails over word association in aphasia patients with spared comprehension: evidence from N400 event-related potential." In: *Frontiers in human neuroscience* 10 (2017), p. 684.

[152] Woongbin Kim, Minkyu Ahn, Hyunmin Moon, Yoobin Koh, Hohyun Cho, Sangtae Ahn, and Sung Chan Jun. "Application of Concentration or High Attention—Car Racing Biofeedback Game." In: *Proceedings of the ICEIC, Jeongseon Korea* (2012), pp. 496–497.

[153] Timo Kirschstein and Rüdiger Köhling. "What is the Source of the EEG?" In: *Clinical EEG and neuroscience* 40.3 (2009), pp. 146–149.

[154] Mario Kleiner, David Brainard, Denis Pelli, Allen Ingling, Richard Murray, Christopher Broussard, et al. "What's new in Psychtoolbox-3." In: *Perception* 36.14 (2007), p. 1.

[155] Albert Kok. "On the utility of P3 amplitude as a measure of processing capacity." In: *Psychophysiology* 38.3 (2001), pp. 557–577. ISSN: 1469-8986. DOI: 10.1017/S0048577201990559. URL: http://dx.doi.org/10.1017/S0048577201990559.

[156] Attila Korik, Ronen Sosnik, Nazmul Siddique, and Damien Coyle. "Decoding Imagined 3D Hand Movement Trajectories From EEG: Evidence to Support the Use of Mu, Beta, and Low Gamma Oscillations." In: *Frontiers in neuroscience* 12 (2018), p. 130.

[157] Matthias Krauledat, Konrad Grzeska, Max Sagebaum, Benjamin Blankertz, Carmen Vidaurre, Klaus-Robert Müller, and Michael Schröder. "Playing pinball with non-invasive BCI." In: *Advances in neural information processing systems*. 2009, pp. 1641–1648.

[158] Pierre Krolak-Salmon, Marie-Anne Hénaff, Catherine Tallon-Baudry, Blaise Yvert, Marc Guénot, Alain Vighetto, François Mauguière, and Olivier Bertrand. "Human lateral geniculate nucleus and visual cortex respond to screen flicker." In: *Annals of neurology* 53.1 (2003), pp. 73–80.

[159] DJ Krusienski, EW Sellers, and TM Vaughan. "Common spatio-temporal patterns for the P300 speller." In: *Neural Engineering, 2007. CNE'07. 3rd International IEEE/EMBS Conference on*. IEEE. 2007, pp. 421–424.

[160] DJ Krusienski and JJ Shih. "Control of a brain–computer interface using stereotactic depth electrodes in and adjacent to the hippocampus." In: *Journal of neural engineering* 8.2 (2011), p. 025006.

[161] Dean J Krusienski and Jerry J Shih. "Spectral components of the P300 speller response in electrocorticography." In: *Neural Engineering (NER), 2011 5th International IEEE/EMBS Conference on*. IEEE. 2011, pp. 282–285.

[162] Dean J Krusienski, Eric W Sellers, François Cabestaing, Sabri Bayoudh, Dennis J McFarland, Theresa M Vaughan, and Jonathan R Wolpaw. "A comparison of classification techniques for the P300 Speller." In: *Journal of neural engineering* 3.4 (2006), p. 299.

[163] Dean J Krusienski, Eric W Sellers, Dennis J McFarland, Theresa M Vaughan, and Jonathan R Wolpaw. "Toward enhanced P300 speller performance." In: *Journal of neuroscience methods* 167.1 (2008), pp. 15–21.

[164] Miroslav Kuba, Zuzana Kubová, Jan Kremláček, and Jana Langrová. "Motion-onset VEPs: characteristics, methods, and diagnostic use." In: *Vision Research* 47.2 (2007), pp. 189–202.

[165] Andrea Kübler and Niels Birbaumer. "Brain-computer interfaces and communication in paralysis: Extinction of goal directed thinking in completely paralysed patients?" In: *Clinical neurophysiology* 119.11 (2008), pp. 2658–2666.

[166] Andrea Kübler, Nicola Neumann, Barbara Wilhelm, Thilo Hinterberger, and Niels Birbaumer. "Predictability of brain-computer communication." In: *Journal of Psychophysiology* 18.2/3 (2004), pp. 121–129.

[167] Anja Kurt, Femke Nijboer, Tamara Matuz, and Andrea Kübler. "Depression and anxiety in individuals with amyotrophic lateral sclerosis." In: *CNS drugs* 21.4 (2007), pp. 279–291.

[168] No-Sang Kwak, Klaus-Robert Müller, and Seong-Whan Lee. "A lower limb exoskeleton control system based on steady state visual evoked potentials." In: *Journal of neural engineering* 12.5 (2015), p. 056009.

[169] No-Sang Kwak, Klaus-Robert Müller, and Seong-Whan Lee. "A convolutional neural network for steady state visual evoked potential classification under ambulatory environment." In: *PloS one* 12.2 (2017), e0172578.

[170] Kenneth K Kwong, John W Belliveau, David A Chesler, Inna E Goldberg, Robert M Weisskoff, Brigitte P Poncelet, David N Kennedy, Bernice E Hoppel, Mark S Cohen, and Robert Turner. "Dynamic magnetic resonance imaging of human brain activity during primary sensory stimulation." In: *Proceedings of the National Academy of Sciences* 89.12 (1992), pp. 5675–5679.

[171] Bram van de Laar, Danny Plass-Oude Bos, Boris Reuderink, and Dirk Heylen. "Actual and imagined movement in BCI gaming." In: *Proceedings of the International Conference on Artificial Intelligence and Simulation of Behaviour* (2009), pp. 9–16.

[172] Daniël Lacko, Jochen Vleugels, Erik Fransen, Toon Huysmans, Guido De Bruyne, Marc M Van Hulle, Jan Sijbers, and Stijn Verwulgen. "Ergonomic design of an EEG headset using 3D anthropometry." In: *Applied ergonomics* 58 (2017), pp. 128–136.

[173] Thomas Navin Lal, Michael Schroder, Thilo Hinterberger, Jason Weston, Martin Bogdan, Niels Birbaumer, and Bernhard Scholkopf. "Support vector channel selection in BCI." In: *IEEE transactions on biomedical engineering* 51.6 (2004), pp. 1003–1010.

[174] Edmund C Lalor, Simon P Kelly, Ciarán Finucane, Robert Burke, Ray Smith, Richard B Reilly, and Gary Mcdarby. "Steady-state VEP-based brain-computer interface control in an immersive 3D gaming environment." In: *EURASIP Journal on Advances in Signal Processing* 2005.19 (2005), p. 706906.

[175] Benjamin Lanfer, Christian Röer, Michael Scherg, Stefan Rampp, Christoph Kellinghaus, and Carsten Wolters. "Influence of a silastic ECoG grid on EEG/ECoG based source analysis." In: *Brain topography* 26.2 (2013), pp. 212–228.

[176] W Lang, D Cheyne, R Kristeva, R Beisteiner, G Lindinger, and L Deecke. "Three-dimensional localization of SMA activity preceding voluntary movement." In: *Experimental Brain Research* 87.3 (1991), pp. 688–695.

[177] Thomas A Lasko, Jui G Bhagwat, Kelly H Zou, and Lucila Ohno-Machado. "The use of receiver operating characteristic curves in biomedical informatics." In: *Journal of biomedical informatics* 38.5 (2005), pp. 404–415.

[178] Pavel Laskov, Christian Gehl, Stefan Krüger, and Klaus-Robert Müller. "Incremental support vector learning: Analysis, implementation and applications." In: *The Journal of Machine Learning Research* 7 (2006), pp. 1909–1936.

[179] Olivier Ledoit and Michael Wolf. "A well-conditioned estimator for large-dimensional covariance matrices." In: *Journal of multivariate analysis* 88.2 (2004), pp. 365–411.

[180] Han Lee, Gregory V Simpson, Nikos K Logothetis, and Gregor Rainer. "Phase locking of single neuron activity to theta oscillations during working memory in monkey extrastriate visual cortex." In: *Neuron* 45.1 (2005), pp. 147–156.

[181] Po-Lei Lee, Jyun-Jie Sie, Yu-Ju Liu, Chi-Hsun Wu, Ming-Huan Lee, Chih-Hung Shu, Po-Hung Li, Chia-Wei Sun, and Kuo-Kai Shyu. "An SSVEP-actuated brain computer interface using phase-tagged flickering sequences: a cursor system." In: *Annals of biomedical engineering* 38.7 (2010), pp. 2383–2397.

[182] Eric C Leuthardt, Gerwin Schalk, Jonathan R Wolpaw, Jeffrey G Ojemann, and Daniel W Moran. "A brain–computer interface using electrocorticographic signals in humans." In: *Journal of Neural Engineering* 1.2 (2004), pp. 63–71. ISSN: 1741-2552. DOI: 10.1088/1741-2560/1/2/001. URL: http://dx.doi.org/10.1088/1741-2560/1/2/001.

[183] Yueqing Li, Sangwoo Bahn, Chang S Nam, and Jungnyun Lee. "Effects of luminosity contrast and stimulus duration on user performance and preference in a P300-based brain–computer interface." In: *International Journal of Human-Computer Interaction* 30.2 (2014), pp. 151–163.

[184] Ke Lin, Xiaogang Chen, Xiaoshan Huang, Qiang Ding, and Xiaorong Gao. "A Hybrid BCI speller based on the combination of EMG envelopes and SSVEP." In: *Applied informatics*. Vol. 2. Springer Berlin Heidelberg. 2015, p. 1.

[185] Zhonglin Lin, Changshui Zhang, Wei Wu, and Xiaorong Gao. "Frequency recognition based on canonical correlation analysis for SSVEP-based BCIs." In: *Biomedical Engineering, IEEE Transactions on* 53.12 (2006), pp. 2610–2614.

[186] Zhonglin Lin, Changshui Zhang, Wei Wu, and Xiaorong Gao. "Frequency recognition based on canonical correlation analysis for SSVEP-based BCIs." In: *IEEE Transactions on Biomedical Engineering* 54.6 (2007), pp. 1172–1176.

[187] Quan Liu, Kun Chen, Qingsong Ai, and Sheng Quan Xie. "Review: recent development of signal processing algorithms for SSVEP-based brain computer interfaces." In: *J. Med. Biol. Eng* (2013).

[188] Tao Liu, Leslie Goldberg, Shangkai Gao, and Bo Hong. "An online brain–computer interface using non-flashing visual evoked potentials." In: *Journal of neural engineering* 7.3 (2010), p. 036003.

[189] MA Lopez-Gordo, Alberto Prieto, F Pelayo, and C Morillas. "Use of phase in brain–computer interfaces based on steady-state visual evoked potentials." In: *Neural processing letters* 32.1 (2010), pp. 1–9.

[190] MA Lopez-Gordo, F Pelayo, Alberto Prieto, and Eduardo Fernández. "An auditory brain-computer interface with accuracy prediction." In: *International journal of neural systems* 22.03 (2012), p. 1250009.

[191] Tyler S Lorig, Amy C Sapp, Jamie Campbell, and William S Cain. "Event-related potentials to odor stimuli." In: *Bulletin of the Psychonomic Society* 31.2 (1993), pp. 131–134.

[192] F Lotte, L Bougrain, A Cichocki, M Clerc, M Congedo, A Rakotomamonjy, and F Yger. "A review of classification algorithms for EEG-based brain–computer interfaces: a 10 year update." In: *Journal of neural engineering* 15.3 (2018), p. 031005.

[193] Fabien Lotte, Marco Congedo, Anatole Lécuyer, Fabrice Lamarche, and Bruno Arnaldi. "A review of classification algorithms for EEG-based brain–computer interfaces." In: *Journal of neural engineering* 4.2 (2007), R1.

[194] Steven J Luck. *An Introduction to the Event-Related Potential Technique (Cognitive Neuroscience)*. MIT press, 2005.

[195] Steven J Luck. *An introduction to the event-related potential technique*. MIT press, 2014.

[196] Steven J Luck, HJ Heinze, GR Mangun, and Steven A Hillyard. "Visual event-related potentials index focused attention within bilateral stimulus arrays. II. Functional dissociation of P1 and N1 components." In: *Electroencephalography and clinical neurophysiology* 75.6 (1990), pp. 528–542.

[197] Barry I Ludwig and Cosimo Ajmone Marsan. "Clinical ictal patterns in epileptic patients with occipital electroencephalographic foci." In: *Neurology* 25.5 (1975), pp. 463–463.

[198] Dorothée Lulé, Claudia Zickler, S Häcker, Marie-Aurelie Bruno, Athena Demertzi, Frederic Pellas, Steven Laureys, and A Kübler. "Life can be worth living in locked-in syndrome." In: *Progress in brain research* 177 (2009), pp. 339–351.

[199] An Luo and Thomas J Sullivan. "A user-friendly SSVEP-based brain–computer interface using a time-domain classifier." In: *Journal of neural engineering* 7.2 (2010), p. 026010.

[200] Jun Lv and Meichun Liu. "Common spatial pattern and particle swarm optimization for channel selection in BCI." In: *Innovative Computing Information and Control, 2008. ICICIC'08. 3rd International Conference on*. IEEE. 2008, pp. 457–457.

[201] JN Mak, Y Arbel, JW Minett, LM McCane, B Yuksel, D Ryan, D Thompson, L Bianchi, and D Erdogmus. "Optimizing the P300-based brain–computer interface: current status, limitations and future directions." In: *Journal of neural engineering* 8.2 (2011), p. 025003.

[202] Nikolay V Manyakov, Nikolay Chumerin, and Marc M Van Hulle. "Multichannel decoding for phase-coded SSVEP brain–computer interface." In: *International journal of neural systems* 22.05 (2012), p. 1250022.

[203] Nikolay V Manyakov, Nikolay Chumerin, Adrien Combaz, Arne Robben, and Marc M Van Hulle. "Decoding SSVEP Responses using Time Domain Classification." In: *IJCCI (ICFC-ICNC)*. 2010, pp. 376–380.

[204] Nikolay V Manyakov, Nikolay Chumerin, Adrien Combaz, and MM Hulle. "On the selection of time interval and frequency range of EEG Signal Preprocessing for P300 Brain-Computer Interfacing." In: *XII Mediterranean Conference on Medical and Biological Engineering and Computing 2010*. Springer. 2010, pp. 57–60.

[205] Nikolay V Manyakov, Nikolay Chumerin, Adrien Combaz, and Marc M Van Hulle. "Comparison of classification methods for P300 brain-computer interface on disabled subjects." In: *Computational intelligence and neuroscience* 2011 (2011), p. 2.

[206] Nikolay V Manyakov, Nikolay Chumerin, Adrien Combaz, Arne Robben, Marijn van Vliet, and Marc M Van Hulle. "Decoding phase-based information from SSVEP recordings: A comparative study." In: *Machine Learning for Signal Processing (MLSP), 2011 IEEE International Workshop on*. IEEE. 2011, pp. 1–6.

[207] Nikolay V Manyakov, Nikolay Chumerin, Arne Robben, Adrien Combaz, Marijn van Vliet, and Marc M Van Hulle. "Sampled sinusoidal stimulation profile and multichannel fuzzy logic classification for monitor-based phase-coded SSVEP brain–computer interfacing." In: *Journal of neural engineering* 10.3 (2013), p. 036011.

[208] Edwin M Maynard, Craig T Nordhausen, and Richard A Normann. "The Utah intracortical electrode array: a recording structure for potential brain-computer interfaces." In: *Electroencephalography and clinical neurophysiology* 102.3 (1997), pp. 228–239.

[209] Dennis J McFarland and Jonathan R Wolpaw. "Brain-computer interface operation of robotic and prosthetic devices." In: *Computer* 41.10 (2008).

[210] Marc J Mentis, Gene E Alexander, Cheryl L Grady, Barry Horwitz, Jack Krasuski, Pietro Pietrini, T Strassburger, Harald Hampel, Mark B Schapiro, and Stanley I Rapoport. "Frequency variation of a pattern-flash visual stimulus during PET differentially activates brain from striate through frontal cortex." In: *Neuroimage* 5.2 (1997), pp. 116–128.

[211] Matthew Middendorf, Grant McMillan, Gloria Calhoun, and Keith S Jones. "Brain-computer interfaces based on the steady-state visual-evoked response." In: *IEEE transactions on rehabilitation engineering* 8.2 (2000), pp. 211–214.

[212] KJ Miller, S Zanos, EE Fetz, M Den Nijs, and JG Ojemann. "Decoupling the cortical power spectrum reveals real-time representation of individual finger movements in humans." In: *Journal of Neuroscience* 29.10 (2009), pp. 3132–3137.

[213] Kai J Miller, Larry B Sorensen, Jeffrey G Ojemann, and Marcel Den Nijs. "Power-law scaling in the brain surface electric potential." In: *PLoS computational biology* 5.12 (2009), e1000609.

[214] Kai J Miller, Gerwin Schalk, Eberhard E Fetz, Marcel Den Nijs, Jeffrey G Ojemann, and Rajesh PN Rao. "Cortical activity during motor execution, motor imagery, and imagery-based online feedback." In: *Proceedings of the National Academy of Sciences* 107.9 (2010), pp. 4430–4435.

[215] Beomjun Min, Jongin Kim, Hyeong-jun Park, and Boreom Lee. "Vowel Imagery Decoding toward Silent Speech BCI Using Extreme Learning Machine with Electroencephalogram." In: *BioMed research international* 2016 (2016).

[216] Ali Momennezhad, Mousa Shamsi, Hossein Ebrahimnezhad, and Hamidreza Saberkari. "Classification of EEG-P300 Signals Extracted from Brain Activities in BCI Systems Using ν-SVM and BLDA Algorithms." In: *Applied Medical Informatics* 34.2 (2014), pp. 23–35.

[217] ST Morgan, JC Hansen, and SA Hillyard. "Selective attention to stimulus location modulates the steady-state visual evoked potential." In: *Proceedings of the National Academy of Sciences* 93.10 (1996), pp. 4770–4774.

[218] PengCheng Mu, Dan Li, QinYe Yin, and Wei Guo. "Robust MVDR beamforming based on covariance matrix reconstruction." In: *Science China Information Sciences* (2013), pp. 1–12.

[219] Gernot R Müller-Putz, Christoph Pokorny, Daniela S Klobassa, and Petar Horki. "A single-switch BCI based on passive and imagined movements: toward restoring communication in minimally conscious patients." In: *International journal of neural systems* 23.02 (2013), p. 1250037.

[220] Masaki Nakanishi and Yasue Mitsukura. "Periodicity detection for BCI based on periodic code modulation visual evoked potentials." In: *Acoustics, Speech and Signal Processing (ICASSP), 2012 IEEE International Conference on*. IEEE. 2012, pp. 665–668.

[221] Masaki Nakanishi, Yijun Wang, Yu-Te Wang, Yasue Mitsukura, and Tzyy-Ping Jung. "A high-speed brain speller using steady-state visual evoked potentials." In: *International journal of neural systems* 24.06 (2014), p. 1450019.

[222] Ken Nakayama and Manfred Mackeben. "Steady state visual evoked potentials in the alert primate." In: *Vision research* 22.10 (1982), pp. 1261–1271.

[223] Luis Fernando Nicolas-Alonso and Jaime Gomez-Gil. "Brain computer interfaces, a review." In: *Sensors* 12.2 (2012), pp. 1211–1279.

[224] Femke Nijboer, Adrian Furdea, Ingo Gunst, Jürgen Mellinger, Dennis J McFarland, Niels Birbaumer, and Andrea Kübler. "An auditory brain–computer interface (BCI)." In: *Journal of neuroscience methods* 167.1 (2008), pp. 43–50.

[225] Anthony M Norcia, L Gregory Appelbaum, Justin M Ales, Benoit R Cottereau, and Bruno Rossion. "The steady-state visual evoked potential in vision research: a review." In: *Journal of Vision* 15.6 (2015), pp. 4–4.

[226] Paul L Nunez and Brian A Cutillo. *Neocortical dynamics and human EEG rhythms*. Oxford University Press, USA, 1995.

[227] Paul L Nunez and Ramesh Srinivasan. *Electric fields of the brain: the neurophysics of EEG*. Oxford University Press, USA, 2006.

[228] Takashi Ono, Keiichiro Shindo, Kimiko Kawashima, Naoki Ota, Mari Ito, Tetsuo Ota, Masahiko Mukaino, Toshiyuki Fujiwara, Akio Kimura, Meigen Liu, et al. "Brain-computer interface with somatosensory feedback improves functional recovery from severe hemiplegia due to chronic stroke." In: *Frontiers in neuroengineering* 7 (2014), p. 19.

[229] G Onose, C Grozea, A Anghelescu, C Daia, CJ Sinescu, AV Ciurea, T Spircu, A Mirea, I Andone, A Spânu, et al. "On the feasibility of using motor imagery EEG-based brain–computer interface in chronic tetraplegics for assistive robotic arm control: a clinical test and long-term post-trial follow-up." In: *Spinal cord* 50.8 (2012), p. 599.

[230] Alexis Ortiz-Rosario and Hojjat Adeli. "Brain-computer interface technologies: from signal to action." In: *Reviews in the Neurosciences* 24.5 (2013), pp. 537–552.

[231] Jie Pan, Xiaorong Gao, Fang Duan, Zheng Yan, and Shangkai Gao. "Enhancing the classification accuracy of steady-state visual evoked potential-based brain–computer interfaces using phase constrained canonical correlation analysis." In: *Journal of neural engineering* 8.3 (2011), p. 036027.

[232] Maria A Pastor, Julio Artieda, Javier Arbizu, Miguel Valencia, and Jose C Masdeu. "Human cerebral activation during steady-state visual-evoked responses." In: *Journal of neuroscience* 23.37 (2003), pp. 11621–11627.

[233] María A Pastor, M Valencia, Julio Artieda, Manuel Alegre, and JC Masdeu. "Topography of cortical activation differs for fundamental and harmonic frequencies of the steady-state visual-evoked responses. An EEG and PET H215O study." In: *Cerebral Cortex* 17.8 (2007), pp. 1899–1905.

[234] Salil H Patel and Pierre N Azzam. "Characterization of N200 and P300: selected studies of the event-related potential." In: *International Journal of Medical Sciences* 2.4 (2005), p. 147.

[235] Xiaomei Pei, Eric C Leuthardt, Charles M Gaona, Peter Brunner, Jonathan R Wolpaw, and Gerwin Schalk. "Spatiotemporal dynamics of electrocorticographic high gamma activity during overt and covert word repetition." In: *Neuroimage* 54.4 (2011), pp. 2960–2972.

[236] Denis G Pelli. "The VideoToolbox software for visual psychophysics: Transforming numbers into movies." In: *Spatial vision* 10.4 (1997), pp. 437–442.

[237] Joel S Perlmutter and Jonathan W Mink. "Deep brain stimulation." In: *Annu. Rev. Neurosci.* 29 (2006), pp. 229–257.

[238] G Pfurtscheller, A Stancak, and Ch Neuper. "Event-related synchronization (ERS) in the alpha band—an electrophysiological correlate of cortical idling: a review." In: *International journal of psychophysiology* 24.1 (1996), pp. 39–46.

[239] Gert Pfurtscheller and FH Lopes Da Silva. "Event-related EEG/MEG synchronization and desynchronization: basic principles." In: *Clinical neurophysiology* 110.11 (1999), pp. 1842–1857.

[240] Gert Pfurtscheller and Christa Neuper. "Motor imagery and direct brain-computer communication." In: *Proceedings of the IEEE* 89.7 (2001), pp. 1123–1134.

[241] Carlos G Pinheiro, Eduardo LM Naves, Pierre Pino, Etienne Losson, Adriano O Andrade, and Guy Bourhis. "Alternative communication systems for people with severe motor disabilities: a survey." In: *Biomedical engineering online* 10.1 (2011), p. 31.

[242] Gabriel Pires, Miguel Castelo-Branco, and Urbano Nunes. "Visual P300-based BCI to steer a wheelchair: a Bayesian approach." In: *Engineering in Medicine and Biology Society, 2008. EMBS 2008. 30th Annual International Conference of the IEEE*. IEEE. 2008, pp. 658–661.

[243] Gabriel Pires, Urbano Nunes, and Miguel Castelo-Branco. "Statistical spatial filtering for a P300-based BCI: tests in able-bodied, and patients with cerebral palsy and amyotrophic lateral sclerosis." In: *Journal of neuroscience methods* 195.2 (2011), pp. 270–281.

[244] Gabriel Pires, Mario Torres, Nuno Casaleiro, Urbano Nunes, and Miguel Castelo-Branco. "Playing Tetris with non-invasive BCI." In: *Serious games and applications for health (segah), 2011 ieee 1st international conference on*. IEEE. 2011, pp. 1–6.

[245] T Poggio and G Cauwenberghs. "Incremental and decremental support vector machine learning." In: *Advances in neural information processing systems* 13 (2001), p. 409.

[246] John Polich. "Updating P300: an integrative theory of P3a and P3b." In: *Clinical neurophysiology* 118.10 (2007), pp. 2128–2148.

[247] John Polich and Albert Kok. "Cognitive and biological determinants of P300: an integrative review." In: *Biological psychology* 41.2 (1995), pp. 103–146.

[248] Robert M Pruzek. "High Dimensional Covariance Estimation: Avoiding the 'Curse of Dimensionality'." In: *Proceedings of the First US/Japan Conference on the Frontiers of Statistical Modeling: An Informational Approach*. Springer. 1994, pp. 233–253.

[249] Cliodhna Quigley, Søren K Andersen, Lars Schulze, Martin Grunwald, and Matthias M Müller. "Feature-selective attention: evidence for a decline in old age." In: *Neuroscience letters* 474.1 (2010), pp. 5–8.

[250] Günter Rager and Wolf Singer. "The response of cat visual cortex to flicker stimuli of variable frequency." In: *European Journal of Neuroscience* 10.5 (1998), pp. 1856–1877.

[251] Dobromir Rahnev, Peter Kok, Moniek Munneke, Linda Bahdo, Floris P de Lange, and Hakwan Lau. "Continuous theta burst transcranial magnetic stimulation reduces resting state connectivity between visual areas." In: *Journal of neurophysiology* 110.8 (2013), pp. 1811–1821.

[252] Georgia Ramantani, Matthias Dümpelmann, Laurent Koessler, Armin Brandt, Delphine Cosandier-Rimélé, Josef Zentner, Andreas Schulze-Bonhage, and Louis Georges Maillard. "Simultaneous subdural and scalp EEG correlates of frontal lobe epileptic sources." In: *Epilepsia* 55.2 (2014), pp. 278–288.

[253] Noa Raz and Netta Levin. "Cortical and white matter mapping in the visual system-more than meets the eye: on the importance of functional imaging to understand visual system pathologies." In: *Neurovision: Neural bases of binocular vision and coordination and their implications in visual training programs* (2015), p. 90.

[254] David Regan. "An effect of stimulus colour on average steady-state potentials evoked in man." In: *Nature* 210.5040 (1966), pp. 1056–1057.

[255] David Regan. "Some characteristics of average steady-state and transient responses evoked by modulated light." In: *Electroencephalography and clinical neurophysiology* 20.3 (1966), pp. 238–248.

[256] David Regan. "Electrical responses evoked from the human brain." In: *Scientific American* (1979).

[257] David Regan. *Human brain electrophysiology: evoked potentials and evoked magnetic fields in science and medicine*. Elsevier, 1989.

[258] Cassandra Richardson, Romola S Bucks, and Alexandra M Hogan. "Effects of aging on habituation to novelty: An ERP study." In: *International Journal of Psychophysiology* 79.2 (2011), pp. 97–105.

[259] Hannes Riechmann, Andrea Finke, and Helge Ritter. "Using a cVEP-Based Brain-Computer Interface to Control a Virtual Agent." In: *IEEE Transactions on Neural Systems and Rehabilitation Engineering* 24.6 (2016), pp. 692–699. ISSN: 1558-0210. DOI: 10.1109/tnsre.2015.2490621.

[260] GM Ringholz, Stanley H Appel, M Bradshaw, NA Cooke, DM Mosnik, and PE Schulz. "Prevalence and patterns of cognitive impairment in sporadic ALS." In: *Neurology* 65.4 (2005), pp. 586–590.

[261] Anthony Ritaccio, Riki Matsumoto, Martha Morrell, Kyousuke Kamada, Mohamad Koubeissi, David Poeppel, Jean-Philippe Lachaux, Yakufumi Yanagisawa, Masayuki Hirata, Christoph Guger, et al. "Proceedings of the Seventh International Workshop on Advances in Electrocorticography." In: *Epilepsy & Behavior* 51 (2015), pp. 312–320.

[262] Bertrand Rivet, Antoine Souloumiac, Virginie Attina, and Guillaume Gibert. "xDAWN algorithm to enhance evoked potentials: application to brain–computer interface." In: *IEEE Transactions on Biomedical Engineering* 56.8 (2009), pp. 2035–2043.

[263] Bruno Rossion, Katrien Torfs, Corentin Jacques, and Joan Liu-Shuang. "Fast periodic presentation of natural images reveals a robust face-selective electrophysiological response in the human brain." In: *Journal of vision* 15.1 (2015), pp. 18–18.

[264] Donald B Rubin. "Inference and missing data." In: *Biometrika* 63.3 (1976), pp. 581–592.

[265] J. Sachs, R. Herrmann, M. Kmec, M. Helbig, and K. Schilling. "Recent Advances and Applications of M-Sequence based Ultra-Wideband Sensors." In: *2007 IEEE International Conference on Ultra-Wideband* (2007). DOI: 10.1109/icuwb.2007.4380914.

[266] GR Salimi Khorshidi, Ali M Nasrabadi, and MR Hashemi Golpayegani. "Modifying the Classic Template Matching Technique Using a Fuzzy Multi Agent to Have an Accurate P300 Detection." In: *3rd Kuala Lumpur International Conference on Biomedical Engineering 2006*. Springer. 2007, pp. 410–414.

[267] Gholamreza Salimi-Khorshidi, Ali Motie Nasrabadi, and Mohammadreza Hashemi Golpayegani. "Fusion of classic P300 detection methods' inferences in a framework of fuzzy labels." In: *Artificial Intelligence in Medicine* 44.3 (2008), pp. 247–259.

[268] Jukka Sarvas. "Basic mathematical and electromagnetic concepts of the biomagnetic inverse problem." In: *Physics in Medicine & Biology* 32.1 (1987), p. 11.

[269] Sulamith Schaeff, Matthias Sebastian Treder, Bastian Venthur, and Benjamin Blankertz. "Exploring motion VEPs for gaze-independent communication." In: *Journal of neural engineering* 9.4 (2012), p. 045006.

[270] Gerwin Schalk. "Can electrocorticography (ECoG) support robust and powerful brain-computer interfaces?" In: *Frontiers in neuroengineering* 3 (2010), p. 9.

[271] Gerwin Schalk and Eric C. Leuthardt. "Brain-Computer Interfaces Using Electrocorticographic Signals." In: *IEEE Reviews in Biomedical Engineering* 4 (2011), pp. 140–154. ISSN: 1941-1189. DOI: 10.1109/rbme.2011.2172408. URL: http://dx.doi.org/10.1109/RBME.2011.2172408.

[272] Johan Schoukens and Rik Pintelon. *Identification of linear systems: a practical guideline to accurate modeling*. Elsevier, 2014.

[273] Martijn Schreuder, Benjamin Blankertz, and Michael Tangermann. "A new auditory multi-class brain-computer interface paradigm: spatial hearing as an informative cue." In: *PloS one* 5.4 (2010), e9813.

[274] Martijn Schreuder, Johannes Höhne, Benjamin Blankertz, Stefan Haufe, Thorsten Dickhaus, and Michael Tangermann. "Optimizing event-related potential based brain–computer interfaces: a systematic evaluation of dynamic stopping methods." In: *Journal of Neural Engineering* 10.3 (2013), p. 036025.

[275] Michael Schröder, Thomas Navin Lal, Thilo Hinterberger, Martin Bogdan, N Jeremy Hill, Niels Birbaumer, Wolfgang Rosenstiel, and Bernhard Schölkopf. "Robust EEG channel selection across subjects for brain-computer interfaces." In: *EURASIP Journal on Applied Signal Processing* 2005 (2005), pp. 3103–3112.

[276] Andrew B Schwartz, X Tracy Cui, Douglas J Weber, and Daniel W Moran. "Brain-controlled interfaces: movement restoration with neural prosthetics." In: *Neuron* 52.1 (2006), pp. 205–220.

[277] Eric W Sellers and Emanuel Donchin. "A P300-based brain–computer interface: initial tests by ALS patients." In: *Clinical neurophysiology* 117.3 (2006), pp. 538–548.

[278] Eric W Sellers, Theresa M Vaughan, and Jonathan R Wolpaw. "A brain-computer interface for long-term independent home use." In: *Amyotrophic lateral sclerosis* 11.5 (2010), pp. 449–455.

[279] William Shain, Leah Spataro, Jonathan Dilgen, Kraig Haverstick, Scott Retterer, Michael Isaacson, Mark Saltzman, and James N Turner. "Controlling cellular reactive responses around neural prosthetic devices using peripheral and local intervention strategies." In: *IEEE transactions on neural systems and rehabilitation engineering* 11.2 (2003), pp. 186–188.

[280] Jerry J Shih and Dean J Krusienski. "Signals from intraventricular depth electrodes can control a brain–computer interface." In: *Journal of neuroscience methods* 203.2 (2012), pp. 311–314.

[281] Richard B Silberstein, A Pipingas, et al. "Steady-state visually evoked potential topography during the Wisconsin card sorting test." In: *Electroencephalography and Clinical Neurophysiology/Evoked Potentials Section* 96.1 (1995), pp. 24–35.

[282] Richard B Silberstein, Mark A Schier, Andrew Pipingas, Joseph Ciorciari, Stephen R Wood, and David G Simpson. "Steady-state visually evoked potential topography associated with a visual vigilance task." In: *Brain topography* 3.2 (1990), pp. 337–347.

[283] Manbir Singh, Sungheon Kim, and Tae-Seong Kim. "Correlation between BOLD-fMRI and EEG signal changes in response to visual stimulus frequency in humans." In: *Magnetic resonance in medicine* 49.1 (2003), pp. 108–114.

[284] Rajesh Singla and BA Haseena. "Comparison of ssvep signal classification techniques using svm and ann models for bci applications." In: *International Journal of Information and Electronics Engineering* 4.1 (2014), p. 6.

[285] Maryam Soltani and Robert T Knight. "Neural origins of the P300." In: *Critical Reviews™ in Neurobiology* 14.3-4 (2000).

[286] Le Song and Julien Epps. "Classifying EEG for brain-computer interface: Learning optimal filters for dynamical system features." In: *Computational intelligence and neuroscience* 2007 (2008).

[287] Mehrez Souden, Jacob Benesty, and Sofiène Affes. "A study of the LCMV and MVDR noise reduction filters." In: *IEEE Transactions on Signal Processing* 58.9 (2010), pp. 4925–4935.

[288] William Speier, Itzhak Fried, and Nader Pouratian. "Improved P300 speller performance using electrocorticography, spectral features, and natural language processing." In: *Clinical Neurophysiology* 124.7 (2013), pp. 1321–1328.

[289] Martin Spüler, Wolfgang Rosenstiel, and Martin Bogdan. "Online Adaptation of a c-VEP Brain-Computer Interface(BCI) Based on Error-Related Potentials and Unsupervised Learning." In: *PLoS ONE* 7.12 (2012). Ed. by MathiasEditor Baumert, e51077. ISSN: 1932-6203. DOI: 10.1371/journal.pone.0051077.

[290] Ramesh Srinivasan, Paul L Nunez, and Richard B Silberstein. "Spatial filtering and neocortical dynamics: estimates of EEG coherence." In: *IEEE Transactions on Biomedical Engineering* 45.7 (1998), pp. 814–826.

[291] Ramesh Srinivasan, Eleonora Fornari, Maria G Knyazeva, Reto Meuli, and Philippe Maeder. "fMRI responses in medial frontal cortex that depend on the temporal frequency of visual input." In: *Experimental brain research* 180.4 (2007), pp. 677–691.

[292] Richard J Staba, Charles L Wilson, Anatol Bragin, Itzhak Fried, and Jerome Engel. "Quantitative analysis of high-frequency oscillations (80–500 Hz) recorded in human epileptic hippocampus and entorhinal cortex." In: *Journal of neurophysiology* 88.4 (2002), pp. 1743–1752.

[293] Hans Strasburger, Wolfgang Scheidler, and Ingo Rentschler. "Amplitude and phase characteristics of the steady-state visual evoked potential." In: *Applied optics* 27.6 (1988), pp. 1069–1088.

[294] Erich E. Sutter. "The brain response interface: communication through visually-induced electrical brain responses." In: *Journal of Microcomputer Applications* 15.1 (1992), pp. 31–45. ISSN: 0745-7138. DOI: 10.1016/0745-7138(92)90045-7.

[295] S Sveinbjornsdottir and JS Duncan. "Parietal and occipital lobe epilepsy: a review." In: *Epilepsia* 34.3 (1993), pp. 493–521.

[296] François Tadel, Sylvain Baillet, John C Mosher, Dimitrios Pantazis, and Richard M Leahy. "Brainstorm: a user-friendly application for MEG/EEG analysis." In: *Computational intelligence and neuroscience* 2011 (2011), p. 8.

[297] James X Tao, Amit Ray, Susan Hawes-Ebersole, and John S Ebersole. "Intracranial EEG substrates of scalp EEG interictal spikes." In: *Epilepsia* 46.5 (2005), pp. 669–676.

[298] Fatima Zahra Taoufiqi, Jamal Mounach, Amal Satte, Hamid Ouhabi, and Aboubaker El Hessni. "IPS Interest in the EEG of Patients after a Single Epileptic Seizure." In: *Neuroscience journal* 2016 (2016).

[299] Isabella Taylor, Ingrid E Scheffer, and Samuel F Berkovic. "Occipital epilepsies: identification of specific and newly recognized syndromes." In: *Brain* 126.4 (2003), pp. 753–769.

[300] Richard Junior Manuel Godinez Tello, Sandra Mara Torres Müller, André Ferreira, and Teodiano Freire Bastos. "Comparison of the influence of stimuli color on steady-state visual evoked potentials." In: *Research on Biomedical Engineering* 31.3 (2015), pp. 218–231.

[301] Christopher G Thomas and Ravi S Menon. "Amplitude response and stimulus presentation frequency response of human primary visual cortex using BOLD EPI at 4 T." In: *Magnetic resonance in medicine* 40.2 (1998), pp. 203–209.

[302] Samuel Garrett Thorpe, Paul L Nunez, and Ramesh Srinivasan. "Identification of wave-like spatial structure in the SSVEP: Comparison of simultaneous EEG and MEG." In: *Statistics in medicine* 26.21 (2007), pp. 3911–3926.

[303] Shozo Tobimatsu, Hiroyuki Tomoda, and Motohiro Kato. "Normal variability of the amplitude and phase of steady-state VEPs." In: *Electroencephalography and Clinical Neurophysiology/Evoked Potentials Section* 100.3 (1996), pp. 171–176.

[304] Paolo Toffanin, Ritske de Jong, Addie Johnson, and Sander Martens. "Using frequency tagging to quantify attentional deployment in a visual divided attention task." In: *International Journal of Psychophysiology* 72.3 (2009), pp. 289–298.

[305] Matthias S Treder and Benjamin Blankertz. "Research (C) overt attention and visual speller design in an ERP-based brain-computer interface." In: *Behavioral & Brain Functions* 6 (2010).

[306] Matthias S Treder, Anne K Porbadnigk, Forooz Shahbazi Avarvand, Klaus-Robert Müller, and Benjamin Blankertz. "The LDA beamformer: Optimal estimation of ERP source time series using linear discriminant analysis." In: *NeuroImage* 129 (2016), pp. 279–291.

[307] G Van Hoey, R Van de Walle, Bart Vanrumste, M D'Havse, I Lemahieu, and P Boon. "Beamforming techniques applied in EEG source analysis." In: *Proc. ProRISC99* 10 (1999), pp. 545–549.

[308] AC Metting Van Rijn, A Peper, and CA Grimbergen. "High-quality recording of bioelectric events." In: *Medical and Biological Engineering and Computing* 28.5 (1990), pp. 389–397.

[309] Barry D Van Veen and Kevin M Buckley. "Beamforming: A versatile approach to spatial filtering." In: *IEEE assp magazine* 5.2 (1988), pp. 4–24.

[310] Barry D Van Veen, Wim Van Drongelen, Moshe Yuchtman, and Akifumi Suzuki. "Localization of brain electrical activity via linearly constrained minimum variance spatial filtering." In: *IEEE Transactions on biomedical engineering* 44.9 (1997), pp. 867–880.

[311] M Isabel Vanegas, Annabelle Blangero, and Simon P Kelly. "Exploiting individual primary visual cortex geometry to boost steady state visual evoked potentials." In: *Journal of neural engineering* 10.3 (2013), p. 036003.

[312] Mariska J Vansteensel, Elmar GM Pels, Martin G Bleichner, Mariana P Branco, Timothy Denison, Zachary V Freudenburg, Peter Gosselaar, Sacha Leinders, Thomas H Ottens, Max A Van Den Boom, et al. "Fully implanted brain–computer interface in a locked-in patient with ALS." In: *N Engl J Med* 2016.375 (2016), pp. 2060–2066.

[313] Vladimir Naumovich Vapnik and Vlamimir Vapnik. *Statistical learning theory*. Vol. 1. Wiley New York, 1998.

[314] Martin Vetterli and Cormac Herley. "Wavelets and filter banks: Theory and design." In: *IEEE transactions on signal processing* 40.9 (1992), pp. 2207–2232.

[315] François-Benoît Vialatte, Monique Maurice, Justin Dauwels, and Andrzej Cichocki. "Steady-state visually evoked potentials: focus on essential paradigms and future perspectives." In: *Progress in neurobiology* 90.4 (2010), pp. 418–438.

[316] Jacques J Vidal. "Toward direct brain-computer communication." In: *Annual review of Biophysics and Bioengineering* 2.1 (1973), pp. 157–180.

[317] Jacques J Vidal. "Real-time detection of brain events in EEG." In: *Proceedings of the IEEE* 65.5 (1977), pp. 633–641.

[318] Carmen Vidaurre and Benjamin Blankertz. "Towards a cure for BCI illiteracy." In: *Brain topography* 23.2 (2010), pp. 194–198.

[319] Marijn van Vliet, Nikolay Chumerin, Simon De Deyne, Jan Roelf Wiersema, Wim Fias, Gerrit Storms, and Marc M. Van Hulle. "Single-Trial ERP Component Analysis Using a Spatiotemporal LCMV Beamformer." In: *IEEE Transactions on Biomedical Engineering* 63.1 (2016), pp. 55–66. ISSN: 1558-2531. DOI: 10.1109/tbme.2015.2468588.

[320] Ivan Volosyak, Diana Valbuena, T Luth, and Axel Gräser. "Towards an SSVEP based BCI with High ITR." In: *IEEE Trans. Biomed. Eng.* (2010).

[321] Hanh Vu, Bonkon Koo, and Seungjin Choi. "Frequency detection for SSVEP-based BCI using deep canonical correlation analysis." In: *Systems, Man, and Cybernetics (SMC), 2016 IEEE International Conference on*. IEEE. 2016, pp. 001983–001987.

[322] Marjolein van der Waal, Marianne Severens, Jeroen Geuze, and Peter Desain. "Introducing the tactile speller: an ERP-based brain–computer interface for communication." In: *Journal of Neural Engineering* 9.4 (2012), p. 045002.

[323] James S Walker. *Fourier analysis*. Oxford University Press, 1988.

[324] Brian A Wandell, Alyssa A Brewer, and Robert F Dougherty. "Visual field map clusters in human cortex." In: *Philosophical Transactions of the Royal Society of London B: Biological Sciences* 360.1456 (2005), pp. 693–707.

[325] Wei Wang, Alan D Degenhart, Jennifer L Collinger, Ramana Vinjamuri, Gustavo P Sudre, P David Adelson, Deborah L Holder, Eric C Leuthardt, Daniel W Moran, Michael L Boninger, et al. "Human motor cortical activity recorded with Micro-ECoG electrodes, during individual finger movements." In: *Engineering in Medicine and Biology Society, 2009. EMBC 2009. Annual International Conference of the IEEE*. IEEE. 2009, pp. 586–589.

[326] Wei Wang et al. "An Electrocorticographic Brain Interface in an Individual with Tetraplegia." In: *PLoS ONE* 8.2 (2013). Ed. by ShawnEditor Hochman, e55344. ISSN: 1932-6203. DOI: 10.1371/journal.pone.0055344. URL: http://dx.doi.org/10.1371/journal.pone.0055344.

[327] Qingguo Wei, Siwei Feng, and Zongwu Lu. "Stimulus specificity of brain-computer interfaces based on code modulation visual evoked potentials." In: *PloS one* 11.5 (2016), e0156416.

[328] Robert West, Hillary Schwarb, and Brandy N Johnson. "The influence of age and individual differences in executive function on stimulus processing in the oddball task." In: *cortex* 46.4 (2010), pp. 550–563.

[329] Arnold J Wilkins. *Visual stress.* Oxford University Press, 1995.

[330] Jonathan Winawer, Kendrick N Kay, Brett L Foster, Andreas M Rauschecker, Josef Parvizi, and Brian A Wandell. "Asynchronous broadband signals are the principal source of the BOLD response in human visual cortex." In: *Current Biology* 23.13 (2013), pp. 1145–1153.

[331] Benjamin Wittevrongel and Marc M. Van Hulle. "Faster P300 Classifier Training Using Spatiotemporal Beamforming." In: *International Journal of Neural Systems* 26.03 (2016), p. 1650014. ISSN: 1793-6462. DOI: 10.1142/s0129065716500143.

[332] Benjamin Wittevrongel and Marc M. Van Hulle. "Frequency- and Phase Encoded SSVEP Using Spatiotemporal Beamforming." In: *PLOS ONE* 11.8 (2016). Ed. by Mikhail A.Editor Lebedev, e0159988. ISSN: 1932-6203. DOI: 10.1371/journal.pone.0159988.

[333] Benjamin Wittevrongel and Marc M. Van Hulle. "Hierarchical online SSVEP spelling achieved with spatiotemporal beamforming." In: *2016 IEEE Statistical Signal Processing Workshop (SSP)* (2016). DOI: 10.1109/ssp.2016.7551800.

[334] Benjamin Wittevrongel and Marc M Van Hulle. "Spatiotemporal beamforming: a transparent and unified decoding approach to synchronous visual Brain-Computer Interfacing." In: *Frontiers in Neuroscience* 11 (2017), p. 630.

[335] Benjamin Wittevrongel, Elia Van Wolputte, and Marc M Van Hulle. "Code-modulated visual evoked potentials using fast stimulus presentation and spatiotemporal beamformer decoding." In: *Scientific reports* 7.1 (2017), p. 15037.

[336] Benjamin Wittevrongel, Elia Van Wolputte, and Marc M Van Hulle. "Code-modulated visual evoked potentials using fast stimulus presentation and spatiotemporal beamformer decoding." In: *Scientific reports* 7.1 (2017), p. 15037.

[337] Benjamin Wittevrongel, Elvira Khachatryan, Mansoureh Fahimi Hnazaee, Evelien Carrette, Leen De Taeye, Alfred Meurs, Paul Boon, Dirk Van Roost, and Marc M Van Hulle. "Representation of steady-state visual evoked potentials elicited by luminance flicker in human occipital cortex: An electrocorticography study." In: *NeuroImage* 175 (2018), pp. 315–326.

[338] Jonathan R Wolpaw and Dennis J McFarland. "Control of a two-dimensional movement signal by a noninvasive brain-computer interface in humans." In: *Proceedings of the National Academy of Sciences of the United States of America* 101.51 (2004), pp. 17849–17854.

[339] Jonathan R Wolpaw, Dennis J McFarland, and Theresa M Vaughan. "Brain-computer interface research at the Wadsworth Center." In: *IEEE Transactions on Rehabilitation Engineering* 8.2 (2000), pp. 222–226.

[340] Jonathan R Wolpaw, Herbert Ramoser, Dennis J McFarland, and Gert Pfurtscheller. "EEG-based communication: improved accuracy by response verification." In: *IEEE transactions on Rehabilitation Engineering* 6.3 (1998), pp. 326–333.

[341] Jonathan R Wolpaw, Niels Birbaumer, Dennis J McFarland, Gert Pfurtscheller, and Theresa M Vaughan. "Brain–computer interfaces for communication and control." In: *Clinical neurophysiology* 113.6 (2002), pp. 767–791.

[342] Carsten Wolters and Jan C de Munck. "Volume conduction." In: *Scholarpedia* 2.3 (2007), p. 1738.

[343] Chi-Hsun Wu, Hsiang-Chih Chang, Po-Lei Lee, Kuen-Shing Li, Jyun-Jie Sie, Chia-Wei Sun, Chia-Yen Yang, Po-Hung Li, Hua-Ting Deng, and Kuo-Kai Shyu. "Frequency recognition in an SSVEP-based brain computer interface using empirical mode decomposition and refined generalized zero-crossing." In: *Journal of Neuroscience Methods* 196.1 (2011), pp. 170 –181. ISSN: 0165-0270. DOI: http://dx.doi.org/10.1016/j.jneumeth.2010.12.014. URL: http://www.sciencedirect.com/science/article/pii/S0165027010007028.

[344] Zhenghua Wu. "SSVEP Extraction Based on the Similarity of Background EEG." In: *PloS one* 9.4 (2014), e93884.

[345] Elaine Wyllie, Gregory D Cascino, Barry E Gidal, and Howard P Goodkin. *Wyllie's treatment of epilepsy: principles and practice*. Lippincott Williams & Wilkins, 2012.

[346] Jun Xie, Guanghua Xu, Jing Wang, Feng Zhang, and Yizhuo Zhang. "Steady-State Motion Visual Evoked Potentials Produced by Oscillating Newton's Rings: Implications for Brain-Computer Interfaces." In: *PLoS ONE* 7.6 (June 2012), e39707. DOI: 10.1371/journal.pone.0039707. URL: http://dx.doi.org/10.1371%2Fjournal.pone.0039707.

[347] Songyun Xie, You Wu, Yunpeng Zhang, Juanli Zhang, and Chang Liu. "Single channel single trial P300 detection using extreme learning machine: Compared with BPNN and SVM." In: *Neural Networks (IJCNN), 2014 International Joint Conference on*. IEEE. 2014, pp. 544–549.

[348] Hagar Grazya Yamin, Tomer Gazit, Natalia Tchemodanov, Gal Raz, Gilan Jackont, Fred Charles, Itzhak Fried, Talma Hendler, and Marc Cavazza. "Depth electrode neurofeedback with a virtual reality interface." In: *Brain-Computer Interfaces* 4.4 (2017), pp. 201–213.

[349] Wang Yijun, Wang Ruiping, Gao Xiaorong, and Gao Shangkai. "Brain-computer interface based on the high-frequency steady-state visual evoked potential." In: *Neural Interface and Control, 2005. Proceedings. 2005 First International Conference on*. IEEE. 2005, pp. 37–39.

[350] Erwei Yin, Zongtan Zhou, Jun Jiang, Yang Yu, and Dewen Hu. "A Dynamically Optimized SSVEP Brain-Computer Interface (BCI) Speller." In: *Biomedical Engineering, IEEE Transactions on* 62.6 (2015), pp. 1447–1456. ISSN: 0018-9294. DOI: 10.1109/TBME.2014.2320948.

[351] Dan Zhang, Bisheng Huang, Wei Wu, and Siliang Li. "An Idle-State Detection Algorithm for SSVEP-Based Brain–Computer Interfaces Using a Maximum Evoked Response Spatial Filter." In: *International Journal of Neural Systems* 25.07 (2015), p. 1550030.

[352] Peng Zhang, Keith Jamison, Stephen Engel, Bin He, and Sheng He. "Binocular rivalry requires visual attention." In: *Neuron* 71.2 (2011), pp. 362–369.

[353] YU Zhang, Guoxu Zhou, Jing Jin, Xingyu Wang, and Andrzej Cichocki. "Frequency recognition in SSVEP-based BCI using multiset canonical correlation analysis." In: *International journal of neural systems* 24.04 (2014), p. 1450013.

[354] Yangsong Zhang, Peng Xu, Kaiwen Cheng, and Dezhong Yao. "Multivariate synchronization index for frequency recognition of SSVEP-based brain–computer interface." In: *Journal of neuroscience methods* 221 (2014), pp. 32–40.

[355] Yangsong Zhang, Daqing Guo, Dezhong Yao, and Peng Xu. "The Extension of Multivariate Synchronization Index Method for SSVEP-based BCI." In: *Neurocomputing* (2017).

[356] Yu Zhang, Guoxu Zhou, Qibin Zhao, Akinari Onishi, Jing Jin, Xingyu Wang, and Andrzej Cichocki. "Multiway canonical correlation analysis for frequency components recognition in SSVEP-based BCIs." In: *Neural Information Processing*. Springer. 2011, pp. 287–295.

[357] Zimu Zhang, Xiuquan Li, and Zhidong Deng. "A CWT-based SSVEP classification method for brain-computer interface system." In: *Intelligent Control and Information Processing (ICICIP), 2010 International Conference on*. IEEE. 2010, pp. 43–48.

[358] Hai-bin Zhao, Chun-yang Yu, Chong Liu, and Hong Wang. "ECoG-based brain-computer interface using relative wavelet energy and probabilistic neural network." In: *2010 3rd International Conference on Biomedical Engineering and Informatics* (2010). DOI: 10.1109/bmei.2010.5639897. URL: http://dx.doi.org/10.1109/BMEI.2010.5639897.

[359] JunBang Zhao, ZhiJun Zhang, Chen Zhang, Yi Tang, and ZhiFang Liu. "Neural suppression of distractors surrounding the spotlight: Evidence from steady-state visual evoked potentials." In: *Chinese Science Bulletin* 57.14 (2012), pp. 1680–1684.

[360] Danhua Zhu, Jordi Bieger, Gary Garcia Molina, and Ronald M Aarts. "A survey of stimulation methods used in SSVEP-based BCIs." In: *Computational intelligence and neuroscience* 2010 (2010), p. 1.

[361] Danhua Zhu, Gary Garcia-Molina, Vojkan Mihajlović, and Ronald M Aarts. "Online BCI implementation of high-frequency phase modulated visual stimuli." In: *Universal Access in Human-Computer Interaction. Users Diversity*. Springer, 2011, pp. 645–654.

[362] Neal Zierler. "Linear recurring sequences." In: *Journal of the Society for Industrial and Applied Mathematics* 7.1 (1959), pp. 31–48.

9

ADDENDUM

9.1 SUMMARY

Patients suffering from severe motor- and communication disorders are no longer able to interact with their surroundings, and even communication with their families becomes nearly impossible. Due to this disability, they highly depend on caregivers with whom the communication is often troublesome or laborious. Therefore, modern technology that would be able to re-establish a reliable communication channel could considerably improve their quality-of-life and decrease the burden on the caregiver. Brain-computer interfaces (BCIs) are one of such communication channels. They rely on the analysis of brain activity to decode a subject's intention, which can subsequently be performed by a computer. At the time of writing, the BCIs that provide the best results in terms of accuracy, speed and convenience are based on visual stimulation (i.e., flashes, often displayed a computer screen) of a number of selectable targets (e.g., words, letters, symbols) which elicits well-known brain signals that can be used to deduce the intended target.

In this thesis, we investigated the feasibility of the spatiotemporal beamforming principle for target selection (decoding) in the context of BCI, and assessed its performance for three widely-adopted visual paradigms. For all three paradigms, the classifier based on spatiotemporal beamforming either outperformed or performed on par with the respective state-of-the-art classifiers. Furthermore, the proposed decoding algorithm is in most cases computationally more efficient, thus requiring less expensive resources (i.e., hardware), making it well suited for retraining during the use of the BCI.

In addition to the investigation of the decoding performance of the spatiotemporal beamformer, we investigated the cortical representation of the steady-state visual evoked potential (SSVEP), a widely-adopted paradigm in different fields, including BCI. Using a subdural grid located over the occipital cortex, we showed that the foveal flickering stimulus is represented at the posterior part of the primary visual cortex (V1), with little variation across the stimulation frequencies used (11 to 15 Hz). The peripheral flickering was represented at locations consistent with retinotopic mapping studies. These results give new insights into the possible alternative interpretations of the previous SSVEP-based studies.

9.2 SAMENVATTING

Patiënten met ernstige bewegings- en communicatiestoornissen zijn niet meer in staat om interacties uit te voeren met hun omgeving. Communicatie met hun familieleden wordt daardoor bijna onmogelijk. Deze patiënten worden bijgevolg erg afhankelijk van zorgverleners en een heel arbeidsintensief communicatieproces. Met behulp van moderne technologie die als doel heeft om een betrouwbaar communicatiekanaal op te bouwen kan dus niet alleen de levenskwaliteit van de patiënt verbeterd worden, maar kan ook de last op de zorgverlener en de familie verminderen.

Eén van deze technologieën is de Brain Computer Interface (BCI). Hierbij wordt gebruik gemaakt van de cerebrale activiteit om de intentie van het subject te decoderen, waarna een computer of extern toestel deze intentie kan uitvoeren. De BCI's die in termen van accuraatheid, snelheid en bruikbaarheid op dit moment het best werken zijn gebaseerd op visuele stimulatie (i.e., het oplichten of flikkeren) van een aantal selecteerbare targets (bv. woorden, letters, symbolen). Daardoor wordt een gekende hersenactiviteit opgewekt die op haar beurt kan gebruikt worden om het bedoelde target te achterhalen.

In deze thesis onderzochten we de mogelijkheid om het principe van spatiotemporele beamforming te gebruiken voor het selecteren (decoderen) van targets in de context van een BCI waarvan we de performantie getest hebben voor drie vaak gebruikte visuele paradigma's. Voor elk van de drie paradigma's is de spatiotemporele beamformer in staat het correcte target ten minste even accuraat te decoderen als de state-of-the-art decoder voor de respectievelijke paradigma's. Daarnaast is de voorgestelde methode in de meeste gevallen computationeel efficiënter waardoor er minder middelen (bv. tijd, dure hardware) nodig zijn. Het algoritme is hierdoor erg geschikt om een hertraining van het model uit te voeren tijdens het gebruik van de BCI.

Naast het onderzoek van de decoderings-performantie van de spatiotemporele beamformer hebben we ook de cerebrale representatie van steady-state visual evoked potentials (SSVEP) onderzocht. Deze vorm van stimulatie wordt gebruikt in veel verschillende onderzoeksdomeinen, inclusief BCI. Met behulp van een subduraal electrode grid over de occipitale cortex toonden we aan dat een foveale flikkerende stimulus gerepresenteerd wordt in het posterior deel van de primaire visuele cortex (V1) en dat er weinig variatie is tussen de gebruikte stimulatie frequenties (van 11 tot 15 Hz). De perifere flikkering werd gedetecteerd op locaties die overeenkomen met de resultaten van retinotopische maps. Gebaseerd op deze resultaten kan er een diepere analyse van SSVEP-gebaseerde studies worden gemaakt.

9.3 ACKNOWLEDGEMENTS

The candidate was supported by a Strategic Basic Research (SBO) grant, funded by VLAIO (Flemish Agency for Innovation and Entrepreneurship). Additional support was provided by research grants received from the Financing program (PFV/10/008), an interdisciplinary research project (IDO/12/007), and an industrial research fund project (IOF/HB/12/021) of the KU Leuven, the Belgian Fund for Scientific Research – Flanders (G088314N, G0A0914N, G0A4118N), the Interuniversity Attraction Poles Programme – Belgian Science Policy (IUAP P7/11), the Flemish Regional Ministry of Education (Belgium) (GOA 10/019), and the Hercules Foundation (AKUL 043).

9.4 PERSONAL CONTRIBUTION

All work for this project was done by the candidate, except the following:

- E. Van Wolputte contributed in the analysis of the cVEP data for chapter 4.
- E. Khachatryan, M. Fahimi Hnazaee and F. Camarrone contributed their expertise for the analysis and interpretation of the results for the studies described in chapter 6 and 7.
- E. Carrette, L. De Taeye, A. Meurs, P. Boon, D. Van Roost recruited the patient who participated in the study from chapter 6 and 7.
- All co-authors reviewed the manuscripts.

9.5 CONFLICT OF INTEREST

All co-authors declare no conflict-of-interest for any of the studies described in this work.

9.6 CURRICULUM VITAE



Benjamin Wittevrongel

engineer ◆ scientist ◆ design enthusiast ◆ techie

date of birth	September 4, 1991
place of birth	Izegem, Belgium
email	benjamin.wittevrongel@gmail.com
phone	+32 496 74 01 88
address	Brouwersstraat 5 3000 Leuven Belgium



education

2003 — **Math and sciences** — *Roeselare, Belgium*
Klein Seminarie Roeselare
cum laude

2009 — **Bachelor of Science in Informatics** — *Leuven, Belgium*
Catholic University Leuven (KU Leuven)
cum laude

2012 — **Master of Engineering : Computer Science** — *Leuven, Belgium*
Catholic University Leuven (KU Leuven)
cum laude

master thesis
Development of an Automatic System for Detecting Quality of Movement for Prevention and Rehabilitation
promotor *prof J. Davis*, *prof B. Vanwanseele* — supervisor *dr I. Ravkic*, *dr W. Meert*

2014 — **Doctoral Training in Biomedical Sciences** — *Leuven, Belgium*
Catholic University Leuven (KU Leuven)

doctoral thesis
Brain-Computer Interfacing based on Time-Domain EEG Response Detection combined with Beamforming
promotor *prof M.M. Van Hulle*



strategic basic research (SBO) grant
Flanders Innovation and Entrepreneurschip (VLAIO)

current



publications

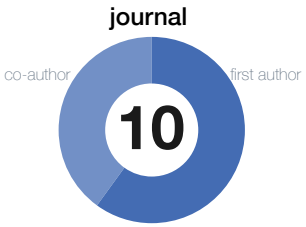



2015

B. Wittevrongel, I. Ravkic, W. Meert, J. Davis, T. Gerbrands, B. Vanwanseele
Predicting Gait Retraining Strategies for Knee Osteoarthritis
Workshop on Machine Learning in Life Sciences, ECML PKDD 2015
Porto, 7-11 September 2015

2016

B. Wittevrongel, M.M. Van Hulle
Faster P300 classifier training using LCMV beamforming
International journal of Neural Systems 26, 1650014

B. Wittevrongel, M.M. Van Hulle
Frequency- and phase encoded SSVEP using spatiotemporal beamforming
PLOS One 11, e0159988

B. Wittevrongel, M.M. Van Hulle
Hierarchical Online SSVEP Spelling Achieved With Spatiotemporal Beamforming
2016 IEEE Statistical Signal Processing Workshop (SSP)
Palma de Mallorca, 26-29 June 2016, p.482-486

B. Wittevrongel, M.M. Van Hulle
Rapid SSVEP mindspelling achieved with spatiotemporal beamforming
Opera Medica et Physiologica 1(S2) p.86-86
Volga Neuroscience Meeting, Nizhny Novgorod, Russia, 24-30 July 2016

V. Pergher, **B. Wittevrongel**, E. Khachatryan, J. Tournoy, M.M Van Hulle
P300 and n-back task: mental workload or behavioral response?
Leuven Neuropsychology Workshop, Advances in rehabilitation of neuropsychological deficits, Leuven, 16-17 September 216

V. Pergher, **B. Wittevrongel**, E. Khachatryan, J. Tournoy, M.M Van Hulle
P300 response magnitude modulated by n-back task level
VasCog 2016
Amsterdam, 13-15 July 2016

2017

B. Wittevrongel, E. Van Wolputte, M.M. Van Hulle
Code-modulated visual evoked potentials using fast stimulus presentation and spatiotemporal beamformer decoding
Scientific Reports 7, 15037

B. Wittevrongel, M.M. Van Hulle
Spatiotemporal Beamforming: A Transparent and Unified Decoding Approach to Synchronous Visual Brain-Computer Interfacing
Frontiers in Neuroscience 11, 630

V. Pergher, **B. Wittevrongel**, B. Schoenmakers, J. Tournoy, J. Arsenault, M.M Van Hulle
N-Back Training and Transfer Effects in Healthy Young Subjects Using EEG
Braininfo 2017 : The second international conference on Neuroscience and Cognitive Brain Information, p.1-7, ISBN 978-1--61208-579-1

2018

B. Wittevrongel, E. Khachatryan, M. Fahimi-Hnazaee, E. Carrette, L. De Taeye, A. Meurs, P. Boon, D. Van Roost, M.M. Van Hulle
Representation of steady-state visual evoked potentials in human occipital cortex: an electrocorticography study
NeuroImage 175, 315-326

B. Wittevrongel, E. Khachatryan, M. Fahimi Hnazaee, F. Camarrone, E. Carrette, L. De Taeye, A. Meurs, P. Boon, D. Van Roost, M.M Van Hulle
Decoding steady-state visual evoked potentials from Electrocorticography
Frontiers in Neuroinformatics 12, 65

E. Khachatryan, B. Wittevrongel, K. De Keyser, M. De Letter, M.M. Van Hulle
Event Related Potential Study of Language Interaction in Bilingual Aphasia Patients
Frontiers in Human Neuroscience 12, 81

A.Y. Ali Amer, B. Wittevrongel, M.M. Van Hulle
Accurate decoding of short, phase-encoded SSVEPs
Sensors, 18 (3), 794

V.Pergher, B. Wittevrongel, J. Tournoy, B. Schoenmakers, J. Arsenault, M.M. Van Hulle
N-back training and transfer effects in healthy young and older subjects gauged using EEG: a preliminary study
International Journal on Advances in Life Sciences, 10

V.Pergher, B. Wittevrongel, J. Tournoy, B. Schoenmakers, M.M. Van Hulle
N-back training and transfer effects revealed by behavioral responses and EEG
Brain and Behavior (in press)

B. Wittevrongel, E. Khachatryan, K. De Keyser, E. Lanckmans, M .De Letter, P. Santens, D. Van Roost, M.M. Van Hulle
Simultaneous scalp- and subcortical EEG recordings during a visual oddball paradigm
Salzburg Mind-Brain Annual Meeting (SAMBA)
Salzburg, 12-13 July 2018 (Abstract)

B. Wittevrongel, E. Khachatryan, M. Fahimi Hnazaee, E. Carrette, I. Dauwe, S. Gadeyne, A. Meurs, P. Boon, D. Van Roost, M.M Van Hulle
Towards asynchronous speech decoding
Belgian Brain Congress 2018 -Belgian Brain Council
Liège, 19 October 2018 (Abstract)
Frontiers in Neuroscience

M. Fahimi Hnazaee, B. Wittevrongel, E. Carrette, I. Dauwe, A. Meurs, P. Boon, D. Van Roost, M.M Van Hulle
Comparing Measures of Active and Passive Field Spread between non-, partially, and fully invasive human brain recordings
Belgian Brain Congress 2018 -Belgian Brain Council
Liège, 19 October 2018 (Abstract)
Frontiers in Neuroscience

A. Libert, B. Wittevrongel, M.M. Van Hulle
Evaluation of hybrid motion-onset and P300 target encoding for Brain-Computer Interfacing
Salzburg Mind-Brain Annual Meeting (SAMBA)
Salzburg, 12-13 July 2018 (Abstract)

N. Vanbilsen, V.Pergher, B. Wittevrongel, J. Tournoy, B. Schoenmakers, M.M. Van Hulle
Is cognitive training an effective tool for healthy adults and patients with cognitive decline?
Leuven Symposium, Games for Mental Health in the Lowlands
Leuven, 26 February 2018